Dissertation

submitted to the

Combined Faculty of Natural Sciences and Mathematics

of Heidelberg University, Germany

for the degree of

Doctor of Natural Sciences

Put forward by

Ingolf Franz Bischer

born in Worms

Oral examination: 16 June 2021

Effective Neutrino Interactions: Origins and Phenomenology

Referees:

Dr. Werner Rodejohann

Prof. Dr. Tilman Plehn

Zusammenfassung

Effektive Neutrinowechselwirkungen: Ursprünge und Phänomenologie

Diese Arbeit beschäftigt sich mit Neutrinowechselwirkungen jenseits des Standardmodells der Teilchenphysik im modellunabhängigen Formalismus der effektiven Feldtheorien. Hierbei werden allgemeine eich- und Lorentz-invariante Operatoren verwendet, die aus den Fundamentalteilchen des Standardmodells und hypothetischen sterilen Neutrinos zusammengesetzt werden können, wobei der Schwerpunkt auf Neutrinowechselwirkungen gelegt wird. Die Operatoren werden hierbei abhängig von der Energieskala konstruiert, entweder oberhalb oder unterhalb der elektroschwachen Skala. Weiterhin werden mögliche theoretische Ursprünge dieser Wechselwirkungen identifiziert, wobei Erweiterungen der Eichgruppe, Leptoquarks, sowie geladene und ungeladene Skalare betrachtet werden. Diese können anhand ihrer Auswirkungen in Neutrinoexperimenten und durch die Erzeugung der Teilchen, die die neue Wechselwirkung vermitteln, am Teilchenbeschleuniger getestet und eingeschränkt werden. In der Folge wird untersucht, wie verschiedene Experimente bei Energien unterhalb der elektroschwachen Skala die effektiven Neutrinowechselwirkungen einschränken. Hierbei werden insbesondere die Sensitivitäten der Experimente DUNE und KATRIN auf neue Wechselwirkungen, die die Neutrino-Elektron-Streuung beziehungsweise den Betazerfall von Tritium beeinflussen, evaluiert. Es wird aufgezeigt, wie die derzeitigen Schranken der Wechselwirkungsstärke davon abhängen, ob die neuen Wechselwirkungen von hohen Energieskalen ausgehen und in der Form von eichinvarianten Operatoren oberhalb der elektroschwachen Skala dargestellt werden können. Als eine zusätzliche Anwendung der vorgestellten effektiven Feldtheorie werden sterile Neutrinos mit einer Masse im Bereich von zehn bis einigen tausend Gigaelektronenvolt als mögliche Form der dunklen Materie diskutiert, wobei diese mittels effektiver Operatoren an die Standardmodell-Fermionen der dritten Generation gekoppelt sind. Es wird gezeigt, dass dieses Szenario konsistent mit der beobachteten Menge dunkler Materie im Universum und den Ergebnissen der Experimente zu ihrem direkten und indirekten Nachweis sind. Drei verschiedene Modelle, die die betrachteten Operatoren erzeugen können, werden vorgestellt. Ein wirkungsvoller Weg, diese zu unterscheiden, ist ihre Wechselwirkungsträger am Large Hadron Collider zu erzeugen und zu identifizieren.

Abstract

Effective neutrino interactions: Origins and phenomenology

We investigate neutrino interactions beyond the Standard Model of particle physics in a model-independent framework. Considering general gauge- and Lorentz-invariant operators composed of the known fundamental particles and hypothetical sterile neutrinos, we review the effective field theory descriptions of interactions above and below the weak scale with particular emphasis on neutrino interactions. Furthermore, we identify gauge extensions, leptoquarks, as well as charged and neutral scalars as potential origins of such new interactions which are consistent with our current observations and can be tested through their traces in neutrino experiments or the direct production of mediators at particle colliders. We survey experimental constraints on effective neutrino interactions at energies below the weak scale, including an analysis of the sensitivity of the DUNE and KATRIN experiments towards new interactions in neutrino-electron scattering and tritium beta decay, respectively. We find that if the new interactions are generated by gauge-invariant operators above the weak scale, which would be expected if they originate from new physics at high energies, neutrino interactions are more strongly constrained. The reason is that in this case they are accompanied by additional interactions involving charged leptons which are tested to greater precision. As an additional application of the framework, we show that sterile neutrinos are phenomenologically viable candidates for dark matter when identified as weakly interacting massive particles interacting through effective operators with Standard Model fermions of the third generation. As we show for three examples, explicit models generating these effective interactions can be distinguished by producing the mediator particles at the Large Hadron Collider.

Acknowledgments

I would like to express my gratitude to a number of people who have contributed to my PhD journey.

Most importantly, I am grateful to my advisor Dr. Werner Rodejohann for his guidance, encouragement and support. I had the chance to develop in many respects thanks to the freedom to explore new ideas and places while our discussions kept me from getting lost and helped me figure out the next steps to take.

Moreover, I would like to thank some collaborators. In particular Dr. Xun-Jie Xu, who through his patient explanations helped me starting smoothly into the topic of neutrino interactions. Even though results of our shared work are not being discussed in this thesis, I would like to thank Christian Döring and Dr. Andreas Trautner. The vivid discussions we had certainly energized also some of my work presented here.

Furthermore, I thank Prof. Dr. Tilman Plehn for our rewarding collaboration on dark matter and for agreeing to be the second referee. I thank also my other two examiners, Jun.-Prof. Dr. Loredana Gastaldo and Prof. Dr. Björn Malte Schäfer.

This thesis has greatly benefited from the proofreading by and valuable comments of Christian Döring, Dr. Thomas Hugle, Carlos Jaramillo, Dr. Moritz Platscher, Thomas Rink, and Oliver Scholer, to whom I express my deep gratitude.

A special thanks for on-demand IT and programming support which likely saved me weeks of desperation is addressed to Thomas Rink, Thomas Hugle, and Moritz Platscher.

An essential part of my PhD experience is the people I shared it with, which I was made painfully aware of during my final year spent mostly at home amidst a global pandemic. I warmly thank my present and former office mates—and those who felt to me like they almost were—for all the discussions about and beyond physics, the laughs about and beyond physics and the overall great company at the institute or at other occasions. I would like to explicitly name Cristina Benso, Christian Döring, Thomas Hugle, Carlos Jaramillo, Christiane Klein, Moritz Platscher, Thomas Rink, Tobias Schierhuber, Oliver Scholer, Valentin Tenorth, and Susan van der Woude.

Furthermore, I would like to thank Britta Schwarz and Anja Berneiser for their accomodating and competent support which took a lot of weight from organizational matters including travel planning.

I cannot imagine that I could have ever reached this point without the consistent love and support from my parents Peter and Gaby, who have always encouraged me to pursue my interests and passions and who I knew unconditionally kept my back while I was going my own steps. Thank you. I would like to thank also my brother and my friends, especially the mates from Olphor, for all the great times we shared that made me feel like I belong and that kept me sane while diving into the abstract world of physics.

Finally I would like to thank Sandra. For your love, support and understanding, especially during the final stages of writing, as well as for your helpful tips and comments on the content and appearance of this thesis.

Contents

1. Introduction

1.1. Neutrino interactions as a pathway to new physics

Neutrinos are elusive. This statement is perhaps more vividly illustrated if one contrasts the history of these "little neutrons" with the spectacle of immensely energetic collisions and showers of strongly and electromagnetically interacting particles that makes up much of the story of the Standard Model of particle physics (SM). Indeed, the first sign of neutrinos was merely the absence of something else. They were hypothesized by W. Pauli in 1930 to explain what carried away the missing energy in nuclear beta decays. It was not until 1956 that the electron antineutrino was actually detected in the first reactor neutrino experiment [7]. In the meantime, neutron, positron, muon, and antiproton had been discovered, E. Fermi had set forth his theory of weak interactions, H. Yukawa had presented his theory of nuclear interactions postulating the pion, which was subsequently experimentally verified, C.N. Yang and R. Mills had introduced non-abelian gauge theories—and of course the nuclear chain reaction had been made usable and abusable [8–13]. Fast forwarding to 1995, the discovery of the top quark demonstrated the remarkable capabilities of accelerator and detector technology [14]. The procedure of colliding strongly accelerated particles and identifying the numerous remnants of such collisions was evidently advanced enough to deduce the masses and interactions of intermediate particles as heavy as 173 GeV produced for only split seconds. Yet, neutrinos created in such collisions were still only tractable in the form of missing energy. Nonetheless, one could conclude that there had to be neutrinos and antineutrinos of three flavors to provide a consistent picture of lepton number and lepton flavor conservation. However, the masses of neutrinos could or could not be zero while there were hints for actual non-conservation of neutrino flavor such as the missing electron neutrinos from the sun and missing atmospheric muon neutrinos. What followed was the success story of neutrino oscillations starting with Super-Kamiokande confirming the oscillation of atmospheric muon neutrinos in 1998 and the Sudbury Neutrino Observatory confirming that flavor transitions were responsible for the electron neutrino deficit from the sun [15,16]. Thanks to the work of these and numerous other experimental groups by now we have a solid understanding of the mixing of neutrinos of which at least two have to be massive in order to explain observations.

The detection of the Higgs boson by the CMS and ATLAS collaborations in 2012 was a spectacular confirmation of the SM and its mechanism for the generation of charged fermion masses. On the other hand, the SM cannot explain neutrino masses without extending the particle content, because the Higgs mechanism does not apply in the absence of right-handed neutrinos, and a Majorana mass cannot be generated through gauge-invariant and renormalizable interactions with SM particles either. For this reason

neutrino oscillations, which require neutrino masses, are arguably our most compelling evidence for physics beyond the Standard Model (BSM) to date. It is quite conceivable that the new particles needed to explain the neutrino masses involve neutral fermions which are uncharged under the SM gauge group and are therefore called sterile neutrinos, in contrast to the active neutrinos of the SM. Their masses could be anywhere between as light as the active neutrinos and much larger than all other SM particles [17]. These theoretical open questions about the neutrino sector are an excellent motivation to push neutrino physics even further in terms of precision on the experimental side and search for additional hints of new physics. The community has recognized this, as evidenced by the decisions to construct massive new experiments such as Hyper-Kamiokande [18] and the Deep Underground Neutrino Experiment (DUNE) [19]. Besides the immediate importance of these and other projects for fundamental physics, direction-sensitive neutrino detectors are a crucial component of the new era of multi-messenger astronomy—with neutrinos and gravitational waves complementing the traditional messengers, photons and cosmic rays. All of this calls for theorists to identify possible signals of new physics in the neutrino sector that can be tested in the present and upcoming experiments, which is the focus of this thesis.

Our approach is to study new interactions in a very general manner which means that we do not start from specific models and particular new particles. Rather, we use the framework of effective interactions in which we presuppose only our known elementary particles and symmetries such as spacetime and gauge symmetries. The only amendment to this is that we account for hypothetical sterile neutrinos. The theoretical framework of effective field theories (EFTs) [20] has become an important component of the experimental search for particle physics beyond the SM. The main reason for the ascent of EFTs compared to explicit ultraviolet (UV) complete models such as theoretically motivated extensions of the SM like the Minimal Supersymmetric Standard Model is that no compelling signs of any such theory have been observed so far. With powerful experimental machines like the Large Hadron Collider (LHC) in place, the question "if we do not observe these popular models, what else could we look for?" has called for an extensive investigation of possible observables relying on fewer theoretical assumptions. A model-independent framework of strong interest in the collider community is the Standard Model Effective Field Theory (SMEFT) [21], even though the assumptions of SMEFT can also lead to blind spots in potential signals and additionally so-called simplified models are being tested [22]. Another interesting possibility is the extension of SMEFT by right-handed SM-singlet neutrinos (SMNEFT or νSMNEFT) [3, 23] that would be expected to interact with the SM particles only through some new heavy mediator particles or through very weak mixing with the active neutrinos. This description is most suitable for collider scale energies. In the context of neutrino experiments which usually feature physics at significantly lower energies, effective interactions have been studied in a different EFT framework which reflects that the SM gauge symmetry is partially broken at these scales. A substantial amount of research has been pursued on the topic of such Non-Standard Interactions (NSI) [24, 25]. Dealing with massive neutrinos but applying the same EFT philosophy, these types of interactions can be extended to the General Neutrino Interactions (GNI). However, if new physics appears at a very high energy scale (particles with masses beyond the current reach of the LHC), then the same

new physics will induce both SMNEFT and GNI operators which are related by matching relations of the two EFT frameworks.

A strong advantage of the EFT treatment of new physics is that the results of experimental searches can be expressed as constraints on a finite number of Wilson coefficients at a given order in the expansion instead of constraints on various models. This allows us to easily compare bounds from different experiments in a model-independent way. Moreover, there may be some effective interactions discovered for which there does not yet exist a model and we could unnecessarily overlook these in the search for new physics if we neglect them. On the other hand, ultimately a consistent theory to explain the interactions is required to give meaning to the set of coefficients and to properly expand the SM. Therefore, in this thesis we consider both experimental constraints on the generic EFTs and concrete models which could realize various different interactions appearing therein.

The fact that we include sterile neutrinos in our EFT opens up an intriguing possible excursion. While we described neutrinos as elusive, we must admit that they have a worthy companion in this regard. Overwhelming astronomical and cosmological evidence implies the existence of dark matter. In fact, the majority of matter in the universe is found to be made up of this type of matter which is most likely not part of the SM. Like the neutrino, it was first postulated to explain something that was missing. In this case it was enormous amounts of mass to warrant the gravitational attraction observed from visible parts of galaxies and clusters [26–28]. Thanks to our understanding of the cosmic microwave background and the formation of structure in the universe, it is now evident that this dark matter must have been present for some time before photons decoupled from the primordial particle sea. It makes up about 85% of all matter, the other 15% consisting of SM particles which we call ordinary matter [29]. Observations so far show no signs of dark matter interacting through a force other than gravity. However, to explain its abundance in relation to ordinary matter it is often postulated that there is another coupling to the SM. For instance, a neutral weakly interacting massive particle (WIMP) of mass around 1-1000 GeV interacting about as weakly with the SM as the neutrinos could have been produced in the observed abundance. Such postulated non-gravitational interactions would make it possible to detect dark matter on Earth, since one would expect a large flux as the solar system moves in the galactic plane and therefore through the dark matter halo of the Milky Way. The obstacles to this detection are, depending on the precise assumptions, similar to neutrino detection: One expects a very small interaction cross section which requires a large detector volume and a low background in order to observe a decent number of events. Now since we are including sterile neutrinos of unknown mass in our EFTs, it is a an interesting possibility to identify such a sterile neutrino with the WIMP. This identification actually goes back to the initial proposals of WIMP dark matter [30–34]. Clearly, the mixing with active neutrinos must be extremely suppressed or absent in order for the dark matter to not quickly decay into active neutrinos, but this can be postulated to interpret the SMNEFT framework as a dark matter EFT.

This thesis is structured as follows. We complete the introduction in Section 1.2 by reviewing how neutrino masses can be introduced to the SM and what the current status of masses and mixing in the neutrino sector is. In Chapter 2 we introduce the EFT frame-

work for neutrino interactions above and below the weak scale. This is the conceptual toolbox from which we draw in the remaining chapters. These can be understood to a large extent independently of each other. Three types of explicit models extending the SM, which can be mapped to different types of neutrino interactions in the EFT, are presented in Chapter 3. This serves mainly to illustrate how the various types of interactions can realistically be generated from consistent models. In Chapter 4 we discuss a number of experiments and which constraints they pose on new neutrino interactions. As an excursion, we apply the EFT framework to dark matter in Chapter 5 and demonstrate that one can consistently explain observations with several scenarios of sterile neutrino dark matter coupling to the third generation SM fermions via four-fermion operators. We conclude the thesis in Chapter 6. It should be noted that some familiarity with quantum field theory (QFT) and the SM is presupposed.

In this work we draw to a significant extent from the contents of Reference [1–4]. Specifically, Section 3.3 is based on Reference [1] with a new discussion of the embedding into SMNEFT and experimental constraints. Section 4.4 is based on Reference [2] with an additional discussion of the scattering of electron neutrinos off electrons and current bounds on this process. Chapter 2, Section 4.2, and Section 4.3 are mostly based on Reference [3]. Finally, Section 3.1.2 and Chapter 5 feature the contents of Reference [4]. We will restate these connections at the beginning of the corresponding chapters. Additional publications completed by the author in collaboration with others during the doctoral studies, which were not included in this thesis, are References [5, 6].

1.2. Neutrinos beyond the Standard Model

To introduce our notation and approach our entry point to neutrino physics, we briefly sketch some basics of the SM. Our notational conventions follow Reference [35]. We will rely on the distinction of Weyl, Majorana and Dirac fermions and therefore briefly summarize these concepts in Appendix A.1. The SM is a gauge theory of the group $\mathrm{SU}(3)_\mathrm{C}\times\mathrm{SU}(2)_L\times\mathrm{U}(1)_Y$ made up by the elementary particles summarized in Table 1.1 in terms of their representation of the Lorentz group (spin) and gauge group. The fields Y_μ, W_μ, and G_μ are the gauge fields of the $\mathrm{U}(1)_Y$, $\mathrm{SU}(2)_L$, and $\mathrm{SU}(3)_\mathrm{C}$ subgroups, respectively, where μ (and later also ν) is a spacetime index. The generators of $\mathrm{SU}(2)_L$, the Pauli matrices, are denoted by τ^I, while the generators of $\mathrm{SU}(3)_\mathrm{C}$, the Gell-Mann matrices, are denoted by T^A. Additionally, there are five types of fermions with three generations each, and one complex scalar field, the Higgs doublet. For generation indices we use the letters $\alpha, \beta, \gamma, \delta$, while components of $\mathrm{SU}(2)_L$ doublets are indicated by a, b. The fermions are Weyl spinors which means that they have only one chiral component, but also that they are massless. Since this is in obvious conflict with our observation of massive fermions there has to be some explanation on how the masses of fermions are generated. This is of course the celebrated Higgs mechanism. To introduce our discussion of neutrino physics, we now first compare the origin of charged fermion masses to the possible mechanisms responsible for neutrino masses.

Table 1.1. Representations of the fields in the SM. In the last row, we show hypothetical sterile neutrinos which are not part of the SM and whose number is not fixed by theoretical requirements.

Field		Spin	$\mathrm{SU(3)_C}\times\mathrm{SU(2)}_L\times\mathrm{U(1)}_Y$ representation
Lepton doublets	$l_\alpha = \begin{pmatrix}\nu_{eL}\\ e_L\end{pmatrix}, \begin{pmatrix}\nu_{\mu L}\\ \mu_L\end{pmatrix}, \begin{pmatrix}\nu_{\tau L}\\ \tau_L\end{pmatrix}$	1/2	$(\mathbf{1},\mathbf{2},-1)$
Lepton singlets	$e_\alpha = e_R, \mu_R, \tau_R$	1/2	$(\mathbf{1},\mathbf{1},-2)$
Quark doublets	$q_\alpha = \begin{pmatrix}u_L\\ d_L\end{pmatrix}, \begin{pmatrix}c_L\\ s_L\end{pmatrix}, \begin{pmatrix}t_L\\ b_L\end{pmatrix}$	1/2	$(\mathbf{3},\mathbf{2},1/3)$
Quark singlets	$u_\alpha = u_R, c_R, t_R$	1/2	$(\mathbf{3},\mathbf{1},4/3)$
Quark singlets	$d_\alpha = d_R, s_R, b_R$	1/2	$(\mathbf{3},\mathbf{1},-2/3)$
Higgs doublet	H	0	$(\mathbf{1},\mathbf{2},1)$
Hypercharge boson	Y_μ	1	$(\mathbf{1},\mathbf{1},0)$
Weak gauge boson	W_μ	1	$(\mathbf{1},\mathbf{3},0)$
Gluon	G_μ	1	$(\mathbf{8},\mathbf{1},0)$
Neutrino singlets	N_α	1/2	$(\mathbf{1},\mathbf{1},0)$

1.2.1. Origin of neutrino masses

For our purposes it suffices to note that the Higgs mechanism generates Dirac masses for pairs of Weyl fermions through the Yukawa interaction terms,

$$\mathcal{L}_{\text{Yukawa}} = -y^e_{\alpha\beta}\,\overline{l_\alpha}\,H\,e_{\beta R} - y^d_{\alpha\beta}\,\overline{q_\alpha}\,H\,d_{\beta R} - y^u_{\alpha\beta}\,\overline{q_\alpha}\,\widetilde{H}\,u_{\beta R} + \text{H.c.} \tag{1.1}$$

where $y^f_{\alpha\beta}$ are 3-by-3 dimensionless Yukawa matrices for $f = e, d, u$. The Dirac mass terms are obtained when the Higgs field and its dual $\widetilde{H} = i\tau_2 H^*$, where τ_2 is the second Pauli matrix, are evaluated after spontaneous symmetry breaking (SSB) at the vacuum expectation value (vev), such that

$$\langle H\rangle = \frac{1}{\sqrt{2}}\begin{pmatrix}0\\ v\end{pmatrix}, \qquad \langle\widetilde{H}\rangle = \frac{1}{\sqrt{2}}\begin{pmatrix}v\\ 0\end{pmatrix}, \tag{1.2}$$

where $v \approx 246\,\text{GeV}$ [36]. They read

$$\mathcal{L}_{\text{mass}} = -\frac{v}{\sqrt{2}}y^e_{\alpha\beta}\,\overline{e_{\alpha L}}e_{\beta R} - \frac{v}{\sqrt{2}}y^d_{\alpha\beta}\,\overline{d_{\alpha L}}d_{\beta R} - \frac{v}{\sqrt{2}}y^u_{\alpha\beta}\,\overline{u_{\alpha L}}u_{\beta R} + \text{H.c.} \tag{1.3}$$

Obviously the two independent Weyl fields of left-handed and right-handed leptons and quarks with the symbols e, d, u have been combined to Dirac fermions with masses proportional to the Higgs vev. In this original Glashow-Weinberg-Salam model of electroweak

interactions, the neutrinos are considered to be massless. Indeed, with the particle content of Table 1.1, there are no renormalizable terms which could generate a neutrino mass through the Higgs mechanism due to the absence of right-handed neutrino singlets. Therefore, the electrically neutral upper components of the lepton doublets remain to be interpreted as Weyl fermions: There is a left-handed neutrino and a right-handed anti neutrino for each of the three generations. The discovery of neutrino oscillations which require at least two neutrino masses thus reveals a tension which can only be resolved by extending the SM. Unfortunately, the question how the SM needs to be extended to accommodate neutrino masses has no unique answer, not even in terms of a "minimal" extension. The two main avenues are tied to the immediate question that arises whenever a neutral Weyl fermion is promoted to a massive fermion: Is it a Dirac or a Majorana field? We now discuss the two options and try to answer what minimal changes to the SM can be made in order to realize them.

The simplest minimal way of providing the neutrinos with a Dirac mass term is by adding hypercharge-neutral right-handed neutrino singlets ν_R which generically leads to the "missing" Yukawa coupling term

$$\mathcal{L}_{\text{Yukawa},\nu} = -y^{\nu}_{\alpha\beta}\,\overline{l_\alpha}\,\widetilde{H}\,\nu_{\beta R} + \text{H.c.} \quad \overset{\text{SSB}}{\longrightarrow} \quad -\frac{v}{\sqrt{2}} y^{\nu}_{\alpha\beta}\,\overline{\nu_{\alpha L}}\nu_{\beta R} + \text{H.c.} \tag{1.4}$$

This way of mass generation is theoretically consistent while it poses a new theoretical question: Why would the eigenvalues of the Yukawa matrix y^ν be so small with respect to the other Yukawa couplings in the SM? In other words, why should neutrino masses be below at least 1 eV, while the charged fermions cover the range from 10^6 to 10^{11}eV? This relative smallness of the neutrino masses is perhaps the main reason why other explanations of the neutrino mass, which tie the smallness of the masses to the suppression by a high-energy scale, are very popular among theorists. These so-called seesaw mechanisms most often lead to Majorana neutrinos which we discuss next.

A Majorana mass term for the neutrinos would read

$$\mathcal{L}_{\text{mass}} = -\frac{1}{2} m_{\alpha\beta}\overline{\nu^c_{L\alpha}}\nu_{L\beta} + \text{H.c.}\,, \tag{1.5}$$

where

$$\nu^c_L = \mathcal{C}\overline{\nu_L}^T \tag{1.6}$$

denotes the particle-antiparticle conjugate of the chiral spinor ν_L, which is right-handed.[1] The properties of the matrix $\mathcal{C}$ are given in Appendix A.1. A mass term for the neutrinos as in Equation (1.5) cannot be generated from renormalizable gauge-invariant operators composed of the fields in Table 1.1. Indeed, it is obviously required for such an operator to be composed of one copy of each $\overline{l^c}$ and l which makes up for a total mass dimension three and hypercharge of -2. Then there is no single field of mass dimension one of opposite hypercharge to complete the operator at dimension four. If one assumes that there are some new particles which are too heavy to be detected so far, it could be that

[1] This operation on spinors is commonly identified with charge conjugation. However, as pointed out in Reference [37], charge conjugation only flips the charge-like quantum numbers, but not the chirality, whereas $P_R(\psi_L)^c = (\psi_L)^c$ for $P_R = (1+\gamma^5)/2$.

the masses generation can be accounted for by a non-renormalizable effective operator which encompasses the effect of heavier fields. The non-renormalizability would then not be a problem, since we would expect that the operator is replaced by renormalizable interactions at some higher scale. This framework is known as effective field theory and we introduce it in more detail in Chapter 2. The simplest such operator arises at mass dimension five and relies on two copies of the Higgs field to contribute the missing hypercharge +2. This is the Weinberg operator [38] defined as

$$\mathcal{L}^{(5)} = \frac{C_{\nu\nu}^{\alpha\beta}}{\Lambda} (\overline{l_\alpha^c} i\tau_2 H)(\widetilde{H}^\dagger l_\beta) \,, \tag{1.7}$$

where Λ is an unknown mass scale, and $C_{\nu\nu}^{\alpha\beta}$ is a dimensionless Wilson coefficient. Note that there is no distinction of upper and lower flavor indices–we will place them usually in the upper position for Wilson coefficients and lower position for fermion fields and imply sums over repeated indices. If the new-physics scale Λ is far above the weak scale, the neutrino masses are suppressed by v^2/Λ, which would give a compelling reason for their smallness.[2] The Weinberg operator is the only operator with mass dimension below seven that can generate Majorana masses for the neutrinos. However, there are numerous extensions of the SM which can lead to the Weinberg operator. Particularly attractive among those extensions are variations of the seesaw mechanism. They all have in common that they introduce heavy new particles and the smallness of neutrino masses is then tied to the inverse mass of these particles. Let us briefly comment on two of them.

It is straightforward to arrive at the Type-I seesaw scenario [39] following our discussion of Dirac masses. If SM-singlet (sterile) neutrinos are added to the SM, as we need to generate usual Dirac mass terms via the Higgs-Yukawa, they are generically allowed a Majorana mass term as well, since they are neutral under the SM gauge group. If we introduce these right-handed sterile neutrinos $N_{R\alpha}$ to the SM, the total addition to the Lagrangian, reads

$$\mathcal{L}_{4,N} = i\overline{N}_{R\alpha}\gamma^\mu \partial_\mu N_{R\alpha} - \left(\frac{1}{2}\overline{N_{R\alpha}^c} M_{\alpha\beta} N_{R\beta} + \text{H.c.}\right) - \left(y_{\alpha\beta}^\nu \, \bar{l}_\alpha N_{R\beta} \widetilde{H} + \text{H.c.}\right), \tag{1.8}$$

where the three terms are kinetic term, Majorana mass term and Yukawa term respectively. Here we describe the sterile neutrinos as a 4-component spinors

$$N = \begin{pmatrix} n_R^c \\ n_R \end{pmatrix} = N_R^c + N_R \,, \tag{1.9}$$

where N_R and N_R^c are 4-component chirality eigenstates. Since sterile neutrinos do not contribute to any gauge anomalies, their number is not restricted by theoretical necessities. In the limit of vanishing $M_{\alpha\beta}$ and for three sterile neutrinos, $N_{\alpha R}$ simply become the right-handed components of active Dirac neutrinos. This reflects the fact that two mass-degenerate Majorana neutrinos are equivalent to a Dirac neutrino [37]. If $M_{\alpha\beta} \neq 0$ on the other hand, all the mass eigenstates are Majorana neutrinos. Moreover, when the

[2] Identifying Λ with the scale of typical Grand Unification models 10^{15}, one finds the plausible mass scale $v^2/\Lambda \sim 10^{-2}$ eV [35].

typical Majorana mass scale $|M|$ is very large this leads to a scenario where the three mass eigenstates which are mostly composed of active neutrinos have masses proportional to $(y^\nu)^2 v^2/|M|$ while the mostly sterile neutrinos have masses proportional to $|M|$. The mixing between active and sterile sector is also suppressed by $(y^\nu)v/M$ which would explain the near-unitarity of the active-neutrino mixing matrix.

Another simple extension of the SM to accommodate neutrino masses is the type-II seesaw scenario [40]. In this case one adds a heavy scalar $\mathrm{SU}(2)_L$-triplet Δ with hypercharge 2, which allows for the Yukawa and scalar interactions

$$\mathcal{L}_{\text{type-II}} = -y^\nu_{\alpha\beta}\overline{l^c}_\alpha (i\tau_2)\Delta l_\beta - \lambda_{\Delta H}\widetilde{H}^\dagger \Delta^\dagger H + \text{H.c.} \tag{1.10}$$

The Yukawa interaction ties the neutrino bilinear $\overline{\nu_L^c}\nu_L$ to the neutral component Δ_0 of the triplet which in turn is coupled to the Higgs field. This leads, upon integrating out the heavy Δ_0, to a neutrino mass [41]

$$m_\nu^{\alpha\beta} = \frac{2y^\nu_{\alpha\beta}\lambda_{\Delta H}v^2}{m_\Delta^2}\,. \tag{1.11}$$

Again, neutrino masses are suppressed by the heavy scale m_Δ^2.

There are numerous details and further possibilities to the seesaw models which we do not elaborate on here. This short excursion was mainly designed to motivate the position on neutrino masses taken in this thesis. Our goal is to investigate new neutrino interactions with as few limiting assumptions in terms of extended particle content as possible. Therefore, we do not usually specify particular neutrino mass models. This has the consequence that we leave open both the number of sterile neutrinos and the Majorana or Dirac nature of any neutrinos. It is at the point when we start discussing experimental constraints that we have to make some explicit assumptions. Besides the active neutrinos, we then allow at most one sterile neutrino to play a role in the process at hand, all of which could be Dirac or Majorana. For the sterile neutrino this means that we have to assume that its mass is small enough to be kinematically accessible.

1.2.2. Flavor basis and mass basis

In order to consistently discuss interactions beyond the SM, we need to specify some details about flavor and mass bases, since some special properties of the SM interactions cannot generally be transferred to the new interactions. In the SM, the difference between flavor and mass basis manifests itself only through the charged-current interactions of fermions with the W boson. We briefly review the reasoning behind this to apply it to the more general case. The fermions appear in two kinds of interactions, the covariant derivative coupling to gauge bosons and the Yukawa coupling to the Higgs doublet leading to the mass term as discussed in Section 1.2.1. Therefore, one can diagonalize in flavor space only one of them at a time. We call the basis in which the interactions with the W boson are diagonal the flavor basis and the other one the mass basis. Starting in the mass basis (unprimed), for all the fields there is a unitary transformation to the flavor

basis (primed),

$$\begin{aligned} u'_{L\alpha} &= (V_L^{u\dagger})_{\alpha\beta}\, u_{L\beta}\,, \quad d'_{L\alpha} = (V_L^{d\dagger})_{\alpha\beta} d_{L\beta}\,, \quad e'_{L\alpha} = (V_L^{e\dagger})_{\alpha\beta} e_{L\beta}\,, \quad \nu'_{L\alpha} = (V_L^{\nu\dagger})_{\alpha\beta}\nu_{L\beta}\,, \\ u'_{R\alpha} &= (V_R^{u\dagger})_{\alpha\beta} u_{R\beta}\,, \quad d'_{R\alpha} = (V_R^{d\dagger})_{\alpha\beta} d_{R\beta}\,, \quad e'_{R\alpha} = (V_R^{e\dagger})_{\alpha\beta} e_{R\beta}\,, \end{aligned} \tag{1.12}$$

where in the SM the last equality is meaningless since for massless fields all bases are mass eigenbases, but with some mass term, e.g. induced by the Weinberg operator, the distinction becomes relevant. Now we consider the gauge boson interactions derived from the covariant derivatives after electroweak symmetry breaking (EWSB) which are diagonal in the flavor basis. For the quark charged-current interaction, the switch to the mass basis leads to a matrix factor,

$$\begin{aligned} \mathcal{L}^q_{\rm CC} &= -\frac{g}{\sqrt{8}} (\overline{u}'_\alpha \gamma^\mu (1-\gamma^5) d'_\alpha)\, W_\mu + \text{H.c.} \\ &= -\frac{g}{\sqrt{8}} \underbrace{\left[(V_L^u)(V_L^{d\dagger})\right]_{\beta\gamma}}_{\equiv V_{\beta\gamma}} (\overline{u}_\beta \gamma^\mu (1-\gamma^5) d_\gamma)\, W_\mu + \text{H.c.} \end{aligned} \tag{1.13}$$

where V denotes the Cabibbo-Kobayashi-Maskawa-Matrix (CKM matrix). The same happens in the lepton CC interaction if we consider massive neutrinos,

$$\begin{aligned} \mathcal{L}^l_{\rm CC} &= -\frac{g}{\sqrt{8}} (\overline{\nu}'_\alpha \gamma^\mu (1-\gamma^5) e'_\alpha)\, W_\mu + \text{H.c.} \\ &= -\frac{g}{\sqrt{8}} \underbrace{\left[(V_L^\nu)(V_L^{e\dagger})\right]_{j\gamma}}_{\equiv (U^\dagger)_{j\gamma}} (\overline{\nu}_j \gamma^\mu (1-\gamma^5) e_\gamma)\, W_\mu + \text{H.c.} \end{aligned} \tag{1.14}$$

with the Pontecorvo-Maki-Nakagawa-Sakata-Matrix (PMNS matrix) U whose known properties we summarize at the end of this section. In most cases the neutrino masses can be neglected and it is possible deal with neutrino flavor states here instead, such that one simply defines flavor states $\nu'_{L\alpha} = U_{\alpha j}\nu_{Lj}$ as the asymptotic in and out states, where we follow the usual convention to label neutrino mass eigenstates by Latin letters. For this reason we will in most cases consider new interactions in the neutrino flavor basis while charged leptons are in the mass basis. Note that the labeling of the three masses m_1, m_2 and m_3 is arbitrary. Conventionally, one defines ν_1, ν_2, ν_3 as the mass eigenstates with the largest, second largest and smallest admixture of ν_e. Turning to the neutral-current interactions it is important to appreciate the non-trivial particularity of the SM that basis changes of the right-handed matrices M_R are unphysical in the sense that they disappear from any interactions. The reason is the Glashow-Iliopoulos-Maiani (GIM) mechanism [42], which works when the interactions are neutral-current and flavor-universal due to the unitarity of the basis changes,

$$\begin{aligned} \mathcal{L}^f_{\rm NC} &= -\frac{g}{c_W} \left[g_L^f (\overline{f_L}'_\alpha \gamma^\mu f'_{L\alpha}) + g_R^f (\overline{f_R}'_\alpha \gamma^\mu f'_{R\alpha}) \right] Z_\mu \\ &= -\frac{g}{c_W} \left[g_L^f \underbrace{\left((M_L^f)(M_L^f)^\dagger\right)_{\beta\gamma}}_{=\delta_{\beta\gamma}} (\overline{f_L}_\beta \gamma^\mu f_{L\gamma}) + g_R^f \underbrace{\left((M_R^f)(M_R^f)^\dagger\right)_{\beta\gamma}}_{=\delta_{\beta\gamma}} (\overline{f_R}_\beta \gamma^\mu f_{R\gamma}) \right] Z_\mu\,, \end{aligned} \tag{1.15}$$

where the usual SM Z-charges for $f = \nu, e, u, d$ are given by

$$\begin{aligned} g_L^u &= \frac{1}{2} - \frac{2}{3}s_W^2\,, & g_L^d &= -\frac{1}{2} + \frac{1}{3}s_W^2\,, & g_L^e &= -\frac{1}{2} + s_W^2\,, & g_L^\nu &= \frac{1}{2}\,, \\ g_R^u &= -\frac{2}{3}s_W^2\,, & g_R^d &= \frac{1}{3}s_W^2\,, & g_R^e &= s_W^2\,, \end{aligned} \tag{1.16}$$

with $c_W = \cos(\theta_W)$ and $s_W = \sin(\theta_W)$ denoting the cosine and the sine of the Weinberg angle. Since all the interactions of right-handed fermions in the SM, i.e. with Z boson and photon, obey this condition, the right-handed basis transformations are unphysical.

If we move beyond the SM, flavor universality in neutral-current interactions could be violated and also there may be new flavor-violating charged-current interactions. In this case it becomes necessary to define an explicit convention for the flavor basis. Note that previously, our flavor basis (1.12) was not unique: Firstly, any U(3) flavor rotations simultaneous for u_L and d_L or for e_L and ν_L leave Equation (1.13) and Equation (1.14) as well as the CKM matrix V and the PMNS matrix U invariant. Secondly, due to the GIM mechanism any of the M_R can be rotated away. We may use these facts to conventionally fix

$$\begin{aligned} u'_{L\alpha} &= (V^\dagger)_{\alpha\beta}\, u_{L\beta}\,, & d'_{L\alpha} &= d_{L\alpha}\,, & e'_{L\alpha} &= e_{L\alpha}\,, & \nu'_{L\alpha} &= U_{\alpha j}\nu_{Lj}\,, \\ u'_{R\alpha} &= u_{R\alpha}\,, & d'_{R\alpha} &= d_{R\alpha}\,, & e'_{R\alpha} &= e_{R\alpha}\,. \end{aligned} \tag{1.17}$$

For any interaction operators defined in the flavor basis, we then have to follow this prescription to switch to the mass basis. This means that for each u_L appearing in new interaction terms, a factor of V has to be inserted when changing to the mass basis. In particular, now the CKM matrix generically appears also in neutral current operators. For instance, for a left-handed up-type quark neutral current, we obtain

$$C'_{\alpha\beta}\,(\overline{u}'_\alpha \gamma^\mu P_L u'_\beta) = (V_{\gamma\alpha} C'_{\alpha\beta} V^\dagger_{\beta\delta})\,(\overline{u}_\gamma \gamma^\mu P_L u_\delta)\,. \tag{1.18}$$

Here we can see the GIM mechanism working only in the case that the interaction matrix C is flavor-universal, $C_{\alpha\beta} \propto \delta_{\alpha\beta}$.

We close the summary of our excursion in masses and flavor mixing by comparing the quark and lepton mixing matrices and discussing why only mass-squared differences of neutrinos are known at present. Both mixing matrices have to be unitary and 3-by-3 in the case that there are precisely three generations of quarks and leptons. This makes the check for unitarity a test of the SM and the minimality of neutrino mass scenarios in the lepton case. Currently, both CKM matrix and PMNS matrix are consistent with three generations. Accounting for free phases of the fermion fields and unitarity, these 3-by-3 matrices can be reduced to four independent parameters, namely three angles and one phase. The usual parametrization with three Euler angles θ_{12}, θ_{13}, θ_{23} and a Dirac charge-parity phase δ_{13} is given by

$$U_{(D)} = \begin{pmatrix} c_{12}c_{13} & s_{12}c_{13} & s_{13}e^{-i\delta_{13}} \\ -s_{12}c_{23} - c_{12}s_{23}s_{13}e^{i\delta_{13}} & c_{12}c_{23} - s_{12}s_{23}s_{13}e^{i\delta_{13}} & s_{23}c_{13} \\ s_{12}s_{23} - c_{12}c_{23}s_{13}e^{i\delta_{13}} & -c_{12}s_{23} - s_{12}c_{23}s_{13}e^{i\delta_{13}} & c_{23}c_{13} \end{pmatrix}, \tag{1.19}$$

where $c_{ij} = \cos\theta_{ij}$ and $s_{ij} = \sin\theta_{ij}$. The charge-parity phase is named as such, because the interactions are invariant under charge-parity transformations precisely when $\delta_{13} =$

$0, \pi$. In the case of Majorana neutrinos, fewer phases can be absorbed in field redefinitions and therefore there are two more charge-parity-violating phases λ_2 and λ_3. The full mixing matrix is then given by $U_{(D)}$ times a second matrix,

$$U = U_{(D)}U_{(M)} = U_{(D)}\mathrm{diag}(1, e^{i\lambda_2}, e^{i\lambda_3})\,. \tag{1.20}$$

Besides the potential two additional phases, a striking difference between quark and lepton sector lies in the fact that the CKM matrix is hierarchical in the sense that the mixing among different generations is small, while the PMNS matrix encompasses large mixing. In numbers, the magnitudes of CKM matrix elements are currently measured to be [36]

$$|V| = \begin{pmatrix} 0.973\,70 \pm 0.000\,14 & 0.2245 \pm 0.0008 & 0.003\,82 \pm 0.000\,24 \\ 0.221 \pm 0.004 & 0.987 \pm 0.011 & 0.0410 \pm 0.0014 \\ 0.0080 \pm 0.0003 & 0.0388 \pm 0.0011 & 1.013 \pm 0.030 \end{pmatrix}, \tag{1.21}$$

and are mostly derived from decays of nuclei or heavy flavored mesons. In comparison, the current allowed ranges on the PMNS matrix entries at 3σ are according to the global fit of Reference [43]

$$|U| = \begin{pmatrix} 0.801 \to 0.845 & 0.513 \to 0.579 & 0.143 \to 0.155 \\ 0.234 \to 0.500 & 0.471 \to 0.689 & 0.637 \to 0.776 \\ 0.271 \to 0.525 & 0.477 \to 0.694 & 0.613 \to 0.756 \end{pmatrix}. \tag{1.22}$$

Here it is only possible to give parameter ranges, since the measurements of the matrix entries are not independent.

Neutrinos are so light that we can so far only state upper bounds on their masses. The strongest bound on the effective electron neutrino mass which we define in Section 4.5 is $m_{\nu_e} \leq 1.1\,\mathrm{eV}$ at 90% confidence level (CL), inferred from the endpoint of the electron spectrum in tritium beta decay [44]. Cosmological bounds on the sum of neutrino masses of around 0.1 eV exist, but their exact numbers are dependent on the cosmological model and the use of approximations [45]. Unfortunately, without a measurable effect of masses, there is also no access to mixing angles. Therefore, our only knowledge of the mixing is derived from neutrino oscillations which are sensitive to mass-squared differences of neutrinos. In these processes, the effect of non-degenerate masses and mixing can be made visible because the neutrino flavor eigenstate produced at a source is a superposition of coherent mass eigenstates. Due to the almost degenerate and very low masses, the coherence length of this neutrino state is long. During the propagation of the coherent state, the flavor composition oscillates because the Hamiltonian of free neutrino states is non-diagonal in the flavor basis. Therefore, if we can understand a sufficiently homogeneous source of neutrinos, such as the sun, cosmic ray scattering in the atmosphere, colliders and nuclear reactors, and can measure the statistical distribution of neutrino flavor eigenstates at some distance from the source, we can draw conclusions about the mixing angles and mass-squared differences $\Delta m^2_{ij} = m^2_i - m^2_j$. The measured values for

the latter are, also according to Reference [43],

$$\begin{aligned}\Delta m^2_{21} &= 7.42^{0.21}_{-0.20} \times 10^{-5}\,\mathrm{eV}^2\,,\\ \Delta m^2_{3\ell} &= \begin{cases}\Delta m^2_{31} = 2.517^{+0.026}_{-0.028} \times 10^{-3}\,\mathrm{eV}^2 & \text{Normal ordering } (m_1 < m_3)\,,\\ \Delta m^2_{32} = -2.498^{+0.028}_{-0.028} \times 10^{-3}\,\mathrm{eV}^2 & \text{Inverted ordering } (m_3 < m_1)\,.\end{cases}\end{aligned} \tag{1.23}$$

Why it is these parameters that are determining the flavor composition during the propagation is sketched in Section 4.1 and thoroughly derived in Reference [35].

2. Effective field theory of neutrino interactions

The contents of this chapter have been published to a large extent in Reference [3] and partially Reference [4].

2.1. Effective Field Theories

A well-defined QFT needs to be UV complete or in other words renormalizable. Therefore the ultimate goal of the search for new physics is to formulate a renormalizable extension of the SM that explains observations consistently. However, from the history of particle physics, in particular the weak interactions, we know that with limited energy ranges and limited accuracy to test our predictions, a non-renormalizable effective theory of interactions used at a certain energy scale may be an instrumental intermediate step in the development of the UV theory. In this section, we discuss the formalism of such an EFT. Let us first illustrate the concept with the classic example of Fermi's interaction and then generalize it. Electromagnetic interactions can be well-described by the U(1)-gauge theory of photons coupled to electrons and positrons. Its renormalizable Lagrangian reads

$$\mathcal{L}_{\text{em}} = -\frac{1}{4}F_{\mu\nu}F^{\mu\nu} + \sum_{\psi=e,p,n} \overline{\psi}\left(i\gamma^{\mu}(\partial_{\mu} + iq_{\psi}A_{\mu}) - m_{\psi}\right)\psi\,, \tag{2.1}$$

where $q_{\psi} = -1, 1, 0$ for $\psi = e, p, n$ denotes the electric charge of the spinor field ψ, A_{μ} the photon field, and $F_{\mu\nu}$ the field strength tensor. This theory works well to describe electromagnetic interactions, but does not account for nuclear beta decays (and clearly says nothing about why nuclei should exist in the first place). If one, however, adds a neutral Weyl spinor ν_L^e, the electron neutrino, and considers a non-renormalizable addition $\mathcal{L}_{\text{Fermi}}$ to $\mathcal{L}_{\text{em}}$ which conserves the U(1) gauge symmetry,

$$\mathcal{L} = \mathcal{L}_{\text{em}} + \mathcal{L}_{\text{Fermi}} \equiv \mathcal{L}_{\text{em}} - \left(\frac{G_F}{\sqrt{2}}V_{ud}\left(\overline{e}\,\gamma_{\mu}(1-\gamma^5)\nu_L^e\right)\left(\overline{p}\,\gamma^{\mu}(g_V - g_A\gamma^5)n\right) + \text{H.c.}\right), \tag{2.2}$$

where g_V and g_A are nucleon form factors, this interaction can describe neutron decay. Note that this is the only term up to (mass) dimension six which would satisfy charge conservation and Lorentz invariance while at the same time allowing kinematically the decay of a neutron or nuclei. Without the neutrino this would not be possible. The theoretical cost is that we have had to introduce the non-renormalizable dimension-six term $\mathcal{L}_{\text{Fermi}}$ along with an ad-hoc scale G_F of dimension inverse mass squared. This is not a problem as long as we do not consider the theory as fundamental. It turns out

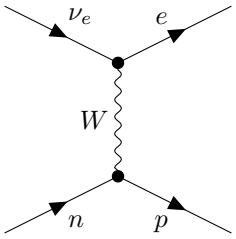

Figure 2.1. Virtual W boson exchange leading to the effective four-fermion interaction described by $\mathcal{L}_{\text{Fermi}}$ in Equation (2.2).

that the more fundamental theory of electroweak interactions ties the origin of the Fermi constant G_F to the mass scale of a mediator particle W which in turn is related to the scale of EWSB. Namely, the Fermi interaction $\mathcal{L}_{\text{Fermi}}$ can be understood as the exchange of a virtual W boson, as illustrated in Figure 2.1.[1]

This short history inspires the following general idea of model independent new physics search. Starting from a set of known particles $\mathbf{\Phi}$ and symmetries observed at an energy μ, we write down an expansion in mass scale of all possible operators constructed from the fields $\mathbf{\Phi}$ respecting the symmetries

$$\mathcal{L}_{\text{eff}} = \mathcal{L}_{\text{ren}}(\mathbf{\Phi}) + \sum_{n\geq 5} \sum_{i} \frac{1}{\Lambda^{n-4}} C_i^{(n)} \mathcal{O}_i^{(n)}(\mathbf{\Phi}) \,, \tag{2.3}$$

where $\mathcal{L}_{\text{ren}}$ describes the renormalizable part and the unknown mass scale Λ takes the role of $G_F^{-1/2}$, while $C_i^{(n)}$ are the dimensionless Wilson coefficients of the operators $\mathcal{O}_i^{(n)}$. The idea is that $\Lambda \gg \mu$ is the scale at which new particles can be generated on-shell. Similarly to the suppression with the W boson mass in the Fermi interaction, one expects that higher-order operators are suppressed by a larger inverse power of Λ, which suggests that cutting off the expansion at a fixed order n should give a reasonable approximation assuming the dimensionless coefficients are not extremely large. In this work, we are mainly concerned with four-fermion interactions like the Fermi interaction, since they naturally arise in many models where new heavy mediators are introduced and they are well-testable due to the abundance of machinery developed by the community to produce and detect the SM fermions. For these reasons we consider here the truncation of Eq. (2.3) after $n = 6$, i.e. at order Λ^{-2}. Since Λ is unknown we will usually parametrize the Wilson coefficients with respect to the Fermi constant such that they can be directly compared to the strength of the weak interactions, i.e. we assume $\Lambda^{-2} = \sqrt{8} G_F$. In Chapter 3 we discuss particular renormalizable models for which we can explicitly identify Λ, in which case we distinguish it from the weak scale.

Turning to the SM, we note that the answer to the question what the fields $\mathbf{\Phi}$ and symmetries are depends on the mass scale μ. Lorentz invariance is always required while the relevant gauge symmetry reduces from the full $\text{SU(3)}_\text{C}\times\text{SU(2)}_L\times\text{U(1)}_Y$ for $\mu \gtrsim m_W$ to $\text{SU(3)}_\text{C}\times\text{U(1)}_\text{em}$ for $\mu \lesssim m_W$. This implies that the fermions are defined in different representations above and below the weak scale and their interactions are described by

[1] All Feynman diagrams shown in this thesis have been produced using TikZ-Feynman [46].

different EFTs. In the remainder of this chapter, we discuss both regimes and how they are connected. In Section 2.2, we introduce SMNEFT as the high-energy ($\mu > m_W$) EFT of the SM extended with right-handed neutrinos. Subsequently, we discuss GNI as a low-energy ($\mu < m_W$) EFT in Section 2.3. Finally, we discuss the important case that occurs when we consider new physics beyond the weak scale which manifests itself in the form of SMNEFT operators. Namely, in this case we can match the low-energy EFT to the high-energy EFT at the weak scale which results in the interaction coefficients of the GNI not being completely independent from each other. The details and implications of this matching are discussed in Section 2.4.

2.2. Neutrino-extended Standard Model Effective Field Theory

The Standard Model EFT is, as the name suggests, precisely the EFT which arises if one takes the SM fields and gauge symmetry $\mathrm{SU}(3)_C \times \mathrm{SU}(2)_L \times \mathrm{U}(1)_Y$ along with Lorentz invariance and constructs all symmetry-compatible operators in addition to the SM Lagrangian, i.e.

$$\mathcal{L}_{\mathrm{SMEFT}}(\mathbf{\Phi}_{\mathrm{SM}}) = \mathcal{L}_{\mathrm{SM}}(\mathbf{\Phi}_{\mathrm{SM}}) + \sum_{n\geq 5} \sum_{i} \frac{1}{\Lambda^{n-4}} C_i^{(n)} \mathcal{O}_i^{(n)}(\mathbf{\Phi}_{\mathrm{SM}})\,. \tag{2.4}$$

The SM fields $\mathbf{\Phi}_{\mathrm{SM}}$ and their representations under Lorentz group (spin) and gauge group were summarized in Table 1.1.

2.2.1. Operators at dimension five and six

The only operator in SMEFT at dimension five is the Weinberg operator (1.7). At dimension six, there are 59 independent (inequivalent on-shell) baryon number conserving operators [47]. These operators can be classified by their field content. The largest class is constituted by the four-fermion operators which we already discussed in the context of Fermi's interaction in Section 2.1. We reproduce all of them in Table 2.1. The other operator types involving fermions are reproduced in Table 2.2 and are composed of two fermions contracted with either Higgs fields or gauge field-strength tensors. We leave out operators which do not involve any fermions, since we are focusing on neutrino interactions in this work.

Since the SMEFT expansion up to dimension six involves the Weinberg operator, it can accommodate Majorana masses for the three active neutrinos. However, in our investigation of new neutrino interactions we would like to be more general with the possible neutrino mass scenarios. In particular, we want to allow Dirac neutrinos, which means that the field content of our theory needs to be extended by right-handed sterile neutrinos. Sometimes we also consider the option of sterile Majorana neutrinos which could have a completely different mass than the mostly active neutrinos. In all cases, the number of possible operators increases and we use N_R as introduced in Section 1.2.1 as the symbol for right-handed neutrinos. At dimension five, the full Lagrangian including

Table 2.1. Four-fermion dimension-six operators in SMEFT (upper) and after adding right-handed neutrino singlets (lower) to generate SMNEFT, excluding baryon or lepton number violating operators. Regarding the operator $\mathcal{O}_{ff'}$, the index ff' runs over ee, uu, dd, eu, ed, and ud of all 3 generations. Flavor indices of the operator symbols are omitted to avoid cluttering.

$(\overline{L}L)(\overline{L}L)$ and $(\overline{R}R)(\overline{R}R)$		$(\overline{L}L)(\overline{R}R)$		$(\overline{L}R)(\overline{R}L)$ and $(\overline{L}R)(\overline{L}R)$	
$\mathcal{O}_{ll}$	$(\bar{l}_\alpha\gamma_\mu l_\beta)(\bar{l}_\gamma\gamma^\mu l_\delta)$	$\mathcal{O}_{le}$	$(\bar{l}_\alpha\gamma_\mu l_\beta)(\bar{e}_\gamma\gamma^\mu e_\delta)$	$\mathcal{O}_{elqd}$	$(\bar{e}_\alpha l^j_\beta)(\bar{q}^j_\gamma d_\delta)$
$\mathcal{O}^{(1)}_{lq}$	$(\bar{l}_\alpha\gamma_\mu l_\beta)(\bar{q}_\gamma\gamma^\mu q_\delta)$	$\mathcal{O}_{lu}$	$(\bar{l}_\alpha\gamma_\mu l_\beta)(\bar{u}_\gamma\gamma^\mu u_\delta)$	$\mathcal{O}_{eluq}$	$(\bar{e}_\alpha l^j_\beta)\epsilon_{jk}(\bar{u}_\gamma q^k_\delta)$
$\mathcal{O}^{(3)}_{lq}$	$(\bar{l}_\alpha\gamma_\mu\tau^I l_\beta)(\bar{q}_\gamma\gamma^\mu\tau^I q_\delta)$	$\mathcal{O}_{ld}$	$(\bar{l}_\alpha\gamma_\mu l_\beta)(\bar{d}_\gamma\gamma^\mu d_\delta)$	$\mathcal{O}'_{eluq}$	$(\bar{e}_\alpha\sigma_{\mu\nu} l^j_\beta)\epsilon_{jk}\times$
$\mathcal{O}^{(1)}_{qq}$	$(\bar{q}_\alpha\gamma_\mu q_\beta)(\bar{q}_\gamma\gamma^\mu q_\delta)$	$\mathcal{O}_{qe}$	$(\bar{q}_\alpha\gamma_\mu q_\beta)(\bar{e}_\gamma\gamma^\mu e_\delta)$		$(\bar{u}_\gamma\sigma^{\mu\nu} q^k_\delta)$
$\mathcal{O}^{(3)}_{qq}$	$(\bar{q}_\alpha\gamma_\mu\tau^I q_\beta)(\bar{q}_\gamma\gamma^\mu\tau^I q_\delta)$	$\mathcal{O}_{qu}$	$(\bar{q}_\alpha\gamma_\mu q_\beta)(\bar{u}_\gamma\gamma^\mu u_\delta)$	$\mathcal{O}^{(1)}_{quqd}$	$(\bar{q}^j_\alpha u_\beta)\epsilon_{jk}(\bar{q}^k_\gamma d_\delta)$
$\mathcal{O}_{ff'}$	$(\overline{f}_\alpha\gamma_\mu f_\beta)(\overline{f'}_\gamma\gamma^\mu f'_\delta)$	$\mathcal{O}_{qd}$	$(\bar{q}_\alpha\gamma_\mu q_\beta)(\bar{d}_\gamma\gamma^\mu d_\delta)$	$\mathcal{O}^{(8)}_{quqd}$	$(\bar{q}^j_\alpha T^A u_\beta)\epsilon_{jk}\times$
$\mathcal{O}^{(8)}_{ud}$	$(\overline{u}_\alpha\gamma_\mu T^A u_\beta)\times$	$\mathcal{O}^{(8)}_{qu}$	$(\bar{q}_\alpha\gamma_\mu T^A q_\beta)\times$		$(\bar{q}^k_\gamma T^A d_\delta)$
	$(\bar{d}_\gamma\gamma^\mu T^A d_\delta)$		$(\overline{u}_\gamma\gamma^\mu T^A u_\delta)$		
		$\mathcal{O}^{(8)}_{qd}$	$(\bar{q}_\alpha\gamma_\mu T^A q_\beta)\times$		
			$(\bar{d}_\gamma\gamma^\mu T^A d_\delta)$		
$\mathcal{O}_{Ne}$	$(\overline{N}_\alpha\gamma_\mu N_\beta)(\bar{e}_\gamma\gamma^\mu e_\delta)$	$\mathcal{O}_{Nl}$	$(\overline{N}_\alpha\gamma_\mu N_\beta)(\bar{l}_\gamma\gamma^\mu l_\delta)$	$\mathcal{O}_{Nlel}$	$(\overline{N}_\alpha l^j_\beta)\epsilon_{jk}(\bar{e}_\gamma l^k_\delta)$
$\mathcal{O}_{Nu}$	$(\overline{N}_\alpha\gamma_\mu N_\beta)(\overline{u}_\gamma\gamma^\mu u_\delta)$	$\mathcal{O}_{Nq}$	$(\overline{N}_\alpha\gamma_\mu N_\beta)(\bar{q}_\gamma\gamma^\mu q_\delta)$	$\mathcal{O}_{lNqd}$	$(\bar{l}^j_\alpha N_\beta)\epsilon_{jk}(\bar{q}^k_\gamma d_\delta)$
$\mathcal{O}_{Nd}$	$(\overline{N}_\alpha\gamma_\mu N_\beta)(\bar{d}_\gamma\gamma^\mu d_\delta)$			$\mathcal{O}'_{lNqd}$	$(\bar{l}^j_\alpha\sigma_{\mu\nu} N_\beta)\epsilon_{jk}\times$
$\mathcal{O}_{NN}$	$(\overline{N}_\alpha\gamma_\mu N_\beta)(\overline{N}_\gamma\gamma^\mu N_\delta)$				$(\bar{q}^k_\gamma\sigma^{\mu\nu} d_\delta)$
$\mathcal{O}_{eNud}$	$(\bar{e}_\alpha\gamma_\mu N_\beta)(\overline{u}_\gamma\gamma^\mu d_\delta)$			$\mathcal{O}_{lNuq}$	$(\bar{l}^j_\alpha N_\beta)(\overline{u}_\gamma q^j_\delta)$

the Weinberg operator (1.7) reads [48],

$$\begin{aligned}\mathcal{L}^{(5)}_N = &\frac{C^{\alpha\beta}_{\nu\nu}}{\Lambda}\,(\overline{l^c_\alpha} i\sigma_2 H)(\widetilde{H}^\dagger l_\beta) + \frac{C^{(5)\alpha\beta}_{NH}}{\Lambda}\,\overline{N^c_{R\alpha}} N_{R\beta}\, H^\dagger H \\ &+ \frac{C^{(5)\alpha\beta}_{NB}}{\Lambda}\,\overline{N^c_{R\alpha}}\sigma_{\mu\nu} N_{R\beta}\, B^{\mu\nu} + \text{H.c.}\,,\end{aligned} \tag{2.5}$$

where $B^{\mu\nu}$ denotes the $\mathrm{U}(1)_Y$ field strength tensor. The second operator is very interesting in terms of the detection of the sterile neutrino, since besides generating a weak-scale contribution to the Majorana mass it induces a Higgs portal coupling at dimension 5. As we will see in detail in Chapter 5, when N takes the role of WIMP dark matter, such a coupling can induce a strong direct detection signal. Moreover, it is hard to avoid, since whenever a theory can generate a dimension-six coupling like $\overline{N^c}N\overline{f}f$, the operator $\mathcal{O}^5_{NH}$ is usually generated through a fermion loop. The magnetic-dipole-like operator $\mathcal{O}^{(5)}_{NB}$ can only exist with $\alpha \neq \beta$ due to the antisymmetry of the tensor bilinear (see Appendix A.1 and Equation (A.35) in particular). Concerning the new dimension-six operators, we reproduce the non-redundant basis of Reference [23] in the lower sections of Tables 2.1 and 2.2 in a slightly rearranged fashion to be more suitable with respect to neutrino interactions.

To obtain a real Lagrangian we imply the addition of the Hermitian conjugate of each

Table 2.2. Mixed fermion-boson dimension-six operators giving rise to neutrino interactions, including only SM fields (upper) and including SM fields and right-handed sterile neutrino singlets (lower).

ψ^2H^3		ψ^2XH		ψ^2H^2	
$\mathcal{O}_{eH}$	$(H^\dagger H)(\bar{l}_\alpha e_\beta H)$	$\mathcal{O}_{eW}$	$(\bar{l}_\alpha\sigma^{\mu\nu}e_\beta)\tau^I H W^I_{\mu\nu}$	$\mathcal{O}^{(1)}_{Hl}$	$i\left(H^\dagger \vec{D}_\mu H\right)\left(\bar{l}_\alpha\gamma^\mu l_\beta\right)$
$\mathcal{O}_{uH}$	$(H^\dagger H)(\bar{q}_\alpha u_\beta \widetilde{H})$	$\mathcal{O}_{eB}$	$(\bar{l}_\alpha\sigma^{\mu\nu}e_\beta)H B_{\mu\nu}$	$\mathcal{O}^{(3)}_{Hl}$	$i\left(H^\dagger\tau^I \vec{D}_\mu H\right)\left(\bar{l}_\alpha\tau^I\gamma^\mu l_\beta\right)$
$\mathcal{O}_{dH}$	$(H^\dagger H)(\bar{q}_\alpha d_\beta H)$	$\mathcal{O}_{uW}$	$(\bar{q}_\alpha\sigma^{\mu\nu}u_\beta)\tau^I \widetilde{H} W^I_{\mu\nu}$	$\mathcal{O}^{(1)}_{Hq}$	$i\left(H^\dagger \vec{D}_\mu H\right)\left(\bar{q}_\alpha\gamma^\mu q_\beta\right)$
		$\mathcal{O}_{uB}$	$(\bar{q}_\alpha\sigma^{\mu\nu}u_\beta)\widetilde{H} B_{\mu\nu}$	$\mathcal{O}^{(3)}_{Hq}$	$i\left(H^\dagger\tau^I \vec{D}_\mu H\right)\left(\bar{q}_\alpha\tau^I\gamma^\mu q_\beta\right)$
		$\mathcal{O}_{dW}$	$(\bar{q}_\alpha\sigma^{\mu\nu}d_\beta)\tau^I H W^I_{\mu\nu}$	$\mathcal{O}_{He}$	$i\left(H^\dagger \vec{D}_\mu H\right)\left(\bar{e}_\alpha\gamma^\mu e_\beta\right)$
		$\mathcal{O}_{dB}$	$(\bar{q}_\alpha\sigma^{\mu\nu}d_\beta)H B_{\mu\nu}$	$\mathcal{O}_{Hu}$	$i\left(H^\dagger \vec{D}_\mu H\right)\left(\bar{u}_\alpha\gamma^\mu u_\beta\right)$
		$\mathcal{O}_{uG}$	$(\bar{q}_\alpha\sigma^{\mu\nu}T^A u_\beta)\widetilde{H} G^A_{\mu\nu}$	$\mathcal{O}_{Hd}$	$i\left(H^\dagger \vec{D}_\mu H\right)\left(\bar{d}_\alpha\gamma^\mu d_\beta\right)$
		$\mathcal{O}_{dG}$	$(\bar{q}_\alpha\sigma^{\mu\nu}T^A d_\beta)H G^A_{\mu\nu}$	$\mathcal{O}_{Hud}$	$i\left(\widetilde{H}^\dagger D_\mu H\right)\left(\bar{u}_\alpha\gamma^\mu d_\beta\right)$
$\mathcal{O}_{NlH}$	$(H^\dagger H)(\bar{l}_\alpha N_\beta \widetilde{H})$	$\mathcal{O}_{NW}$	$(\bar{l}_\alpha\sigma^{\mu\nu}N_\beta)\tau^I \widetilde{H} W^I_{\mu\nu}$	$\mathcal{O}_{HN}$	$i\left(H^\dagger \vec{D}_\mu H\right)\left(\overline{N}_\alpha\gamma^\mu N_\beta\right)$
		$\mathcal{O}_{NB}$	$(\bar{l}_\alpha\sigma^{\mu\nu}N_\beta)\widetilde{H} B_{\mu\nu}$	$\mathcal{O}_{HNe}$	$i\left(\widetilde{H}^\dagger D_\mu H\right)\left(\overline{N}_\alpha\gamma^\mu e_\beta\right)$

operator in Tables 2.1 and 2.2. The only exception are those operators for which taking the Hermitian conjugate simply results in a rearrangement of the Wilson coefficient's flavor indices, e.g.

$$\left[(\bar{l}_\alpha\gamma_\mu l_\beta)(\bar{q}_\gamma\gamma^\mu q_\delta)\right]^\dagger = (\bar{l}_\beta\gamma_\mu l_\alpha)(\bar{q}_\delta\gamma^\mu q_\gamma)\,. \tag{2.6}$$

In those cases, which are the four-fermion operators in the categories $(\overline{L}L)(\overline{L}L)$,$(\overline{R}R)(\overline{R}R)$, and $(\overline{L}L)(\overline{R}R)$ as well as ψ^2H^2 we omit adding the Hermitian conjugate and instead impose

$$C_X^{\alpha\beta\gamma\delta} = (C_X^{\beta\alpha\delta\gamma})^*\,, \qquad \text{or} \qquad C_Y^{\alpha\beta} = (C_Y^{\beta\alpha})^*\,. \tag{2.7}$$

To see why we can do this we write the Lagrangian with explicit Hermitian conjugate for one such operator,

$$\begin{aligned}\mathcal{L}^{(1)}_{lq} &= \frac{1}{\Lambda^2}\sum_{\alpha,\beta,\gamma,\delta}\left[C^{(1)\alpha\beta\gamma\delta}_{lq}(\bar{l}_\alpha\gamma_\mu l_\beta)(\bar{q}_\gamma\gamma^\mu q_\delta) + (C^{(1)\alpha\beta\gamma\delta}_{lq})^*(\bar{l}_\beta\gamma_\mu l_\alpha)(\bar{q}_\delta\gamma^\mu q_\gamma)\right] \\ &= \frac{1}{\Lambda^2}\sum_{\alpha,\beta,\gamma,\delta}\left[\left(C^{(1)\alpha\beta\gamma\delta}_{lq} + (C^{(1)\beta\alpha\delta\gamma}_{lq})^*\right)(\bar{l}_\alpha\gamma_\mu l_\beta)(\bar{q}_\gamma\gamma^\mu q_\delta)\right],\end{aligned} \tag{2.8}$$

where we made the sum over flavor indices explicit. So upon redefining the Wilson coefficients to $C'^{\alpha\beta\gamma\delta} = C^{\alpha\beta\gamma\delta} + (C^{\beta\alpha\delta\gamma})^*$ we can simply omit the Hermitian conjugate. Note that this also works for the ψ^2H^2 operators for which we introduced hermitian Higgs-derivative terms (following Reference [49])

$$\begin{aligned} i(H^\dagger \vec{D}_\mu H) &\equiv i\left(H^\dagger D_\mu H - (D_\mu H)^\dagger H\right), \\ i(H^\dagger \vec{D}^I_\mu H) &\equiv i\left(H^\dagger\tau^I D_\mu H - (D_\mu H)^\dagger\tau^I H\right). \end{aligned} \tag{2.9}$$

As a final remark we note that some flavor combinations of the operators $\mathcal{O}_{ll}$, $\mathcal{O}_{qq}^{(1)}$, $\mathcal{O}_{qq}^{(3)}$ and all $\mathcal{O}_{ff}$ with $f = e, u, d$, are redundant in the sense that

$$\mathcal{O}^{\alpha\beta\gamma\delta} = \mathcal{O}^{\gamma\delta\alpha\beta}\,. \tag{2.10}$$

While this can lead to some confusion, in this work we always consider only one of the two redundant forms and ignore the other. Another solution would be to use both and divide each by two.

2.3. General Neutrino Interactions

The EFT of the SM well below the weak scale, after decoupling the heavy particles t, the Higgs boson h, W, and Z, is usually referred to in the literature as low-energy effective field theory (LEFT) [50]. This EFT can be considered independently from SMEFT, or it can be connected to the latter via matching of Wilson coefficients at the weak scale and renormalization group (RG) evolution. This connection depends on whether there are some light (at most weak scale) new particles that induce new physics operators in LEFT which do not originate from SMEFT. In this case the new particles need to be added to the field content above the weak scale since SMEFT is incomplete. On the other hand, if new physics is heavy and can be described in SMEFT, it can be evolved down to LEFT. In this section we treat GNI, as a subset of LEFT, on its own right, but in Section 2.4 we will discuss the implications of the matching in case that the new physics is heavy.

The unbroken gauge group below the weak scale is $\mathrm{SU(3)_C}\times\mathrm{U(1)_{em}}$. Excitable fields are all the light fermions (the top quark being too heavy), photons and gluons in the representations as shown in Table 2.3. Since we consider different neutrino mass scenarios, sterile neutrinos N_α are included as well, as long as $m_N < m_W$. We will not list all the operators up to dimension six that can be constructed from the fields in Table 2.3 here. They can be found in Reference [50]. Instead, we consider only the subset of LEFT which is associated with neutrinos. The four-fermion interactions can be categorized into neutral-current and charged-current interactions which we write in terms of 10 operators

$$\mathcal{L}_{\mathrm{GNI}}^{\mathrm{NC}} = -\frac{G_F}{\sqrt{2}}\sum_{j=1}^{10}\left(\overset{(\sim)}{\epsilon}_{j,f}\right)^{\alpha\beta\gamma\delta}\left(\overline{\nu}_\alpha\mathcal{O}_j\nu_\beta\right)\left(\overline{f}_\gamma\mathcal{O}'_j f_\delta\right), \tag{2.11}$$

$$\mathcal{L}_{\mathrm{GNI}}^{\mathrm{CC}} = -\frac{G_F V_{\gamma\delta}}{\sqrt{2}}\sum_{j=1}^{10}\left(\overset{(\sim)}{\epsilon}_{j,ud}\right)^{\alpha\beta\gamma\delta}\left(\overline{e}_\alpha\mathcal{O}_j\nu_\beta\right)\left(\overline{u}_\gamma\mathcal{O}'_j d_\delta\right) + \mathrm{H.c.}\,, \tag{2.12}$$

where $f = e, u, d$, Greek indices run over flavor, V denotes the CKM matrix, and ϵ_j, $\widetilde{\epsilon}_j$, $\mathcal{O}_j$, and $\mathcal{O}'_j$ are given in Table 2.4. The entries of the flavor-space tensors ϵ_j, $\widetilde{\epsilon}_j$ are dimensionless and encode the strength of an interaction type j with respect to the SM Fermi interaction. We take the second fermionic bilinear of each line, (2.11) and (2.12), in the mass basis and therefore included the conventional mixing matrix factor $V_{\gamma\delta}$ in the charged-current Lagrangian. However, this tells us nothing about the flavor structure of the epsilon parameters which could deviate from the SM interactions.

Table 2.3. Representations of the fields defining the LEFT. Depending on the neutrino mass scenario, there could be any number of sterile Majorana or Dirac neutrinos N_α.

Field		Spin	$\mathrm{SU(3)_C}\times\mathrm{U(1)_{em}}$ representation
Charged leptons	e, μ, τ	1/2	$(\mathbf{1}, -1)$
Neutrinos	ν_1, ν_2, ν_3	1/2	$(\mathbf{1}, 0)$
Up-type quarks	u, c	1/2	$(\mathbf{3}, 2/3)$
Down-type quarks	d, s, b	1/2	$(\mathbf{3}, -1/3)$
Photon	A_μ	1	$(\mathbf{1}, 0)$
Gluon	G_μ	1	$(\mathbf{8}, 0)$
Sterile neutrinos	$N_1, N_2, \ldots$	1/2	$(\mathbf{1}, 0)$

Table 2.4. Coupling constants and operators appearing in generic neutral-current (2.11) and charged-current Lagrangians (2.12).

j	$\overset{(\sim)}{\epsilon}_j$	$\mathcal{O}_j$	$\mathcal{O}'_j$
1	ϵ_L	$\gamma_\mu(\mathbb{1} - \gamma^5)$	$\gamma^\mu(\mathbb{1} - \gamma^5)$
2	$\widetilde{\epsilon}_L$	$\gamma_\mu(\mathbb{1} + \gamma^5)$	$\gamma^\mu(\mathbb{1} - \gamma^5)$
3	ϵ_R	$\gamma_\mu(\mathbb{1} - \gamma^5)$	$\gamma^\mu(\mathbb{1} + \gamma^5)$
4	$\widetilde{\epsilon}_R$	$\gamma_\mu(\mathbb{1} + \gamma^5)$	$\gamma^\mu(\mathbb{1} + \gamma^5)$
5	ϵ_S	$(\mathbb{1} - \gamma^5)$	$\mathbb{1}$
6	$\widetilde{\epsilon}_S$	$(\mathbb{1} + \gamma^5)$	$\mathbb{1}$
7	$-\epsilon_P$	$(\mathbb{1} - \gamma^5)$	γ^5
8	$-\widetilde{\epsilon}_P$	$(\mathbb{1} + \gamma^5)$	γ^5
9	ϵ_T	$\sigma_{\mu\nu}(\mathbb{1} - \gamma^5)$	$\sigma^{\mu\nu}(\mathbb{1} - \gamma^5)$
10	$\widetilde{\epsilon}_T$	$\sigma_{\mu\nu}(\mathbb{1} + \gamma^5)$	$\sigma^{\mu\nu}(\mathbb{1} + \gamma^5)$

Instead of adding the Hermitian conjugate in (2.11) we impose relations like those in Equation (2.7),

$$\begin{gathered}\epsilon_L^{\alpha\beta\gamma\delta} = \left(\epsilon_L^{\beta\alpha\delta\gamma}\right)^*, \quad \widetilde{\epsilon}_L^{\alpha\beta\gamma\delta} = \left(\widetilde{\epsilon}_L^{\beta\alpha\delta\gamma}\right)^*, \quad \epsilon_R^{\alpha\beta\gamma\delta} = \left(\epsilon_R^{\beta\alpha\delta\gamma}\right)^*, \quad \widetilde{\epsilon}_R^{\alpha\beta\gamma\delta} = \left(\widetilde{\epsilon}_R^{\beta\alpha\delta\gamma}\right)^*, \\ \epsilon_S^{\alpha\beta\gamma\delta} = \left(\widetilde{\epsilon}_S^{\beta\alpha\delta\gamma}\right)^*, \quad \epsilon_P^{\alpha\beta\gamma\delta} = -\left(\widetilde{\epsilon}_P^{\beta\alpha\delta\gamma}\right)^*, \quad \epsilon_T^{\alpha\beta\gamma\delta} = \left(\widetilde{\epsilon}_T^{\beta\alpha\delta\gamma}\right)^*.\end{gathered} \tag{2.13}$$

We remark that there exists a different parametrization for such general four-fermion interactions introduced in Reference [51] which is sometimes used in GNI literature, e.g. References [52–54], and consists of coefficients named C and D instead of ϵ and $\widetilde{\epsilon}$. The mapping between the two different parametrizations can be found in Appendix A.4.

The interaction Lagrangians (2.11) and (2.12) encompass precisely what we earlier referred to as GNI.[2] The name *General* Neutrino Interactions is fitting, because they

[2]Besides GNI [2, 3, 55] they are sometimes called neutrino generalized interactions [54, 56].

include all possible Lorentz invariant operators which can be constructed out of four fermions (see Appendix A.2 for details) involving one or two neutrinos. As can be seen from the chiral structure in Table 2.4, the operators with even index j, i.e. those with an $\widetilde{\epsilon}$ coefficient involve a right-handed projection operator on the neutrino field. In the SM with only left-handed Weyl neutrinos (and right-handed Weyl antineutrinos) these operators vanish identically. The same is true for the neutral-current interactions ϵ_S, ϵ_P, and ϵ_T, since these require left-handed antineutrinos. This is due to the nature of the operators with $j \geq 5$ which require opposite-chirality fields, as demonstrated in Appendix A.2. The subset of GNI which is compatible with massless active neutrinos, the NSI, have accordingly been extensively investigated, as testified e.g. by the reviews [24,25] and numerous references therein. Within the last few years, there has been some stronger interest in the general interactions including right-handed neutrinos [2, 3, 52–57] which reflects the general broadening of the search for new physics to as many previously less considered channels as possible.

It is important to realize that the right-handed neutrinos in Equation (2.11) and Equation (2.12) could be any of the examples discussed in Section 1.2.1. Firstly, they could be right-handed Dirac partners of active neutrinos, which would mean that pairs of left-handed and right-handed neutrinos share a mass term. In this case, all of the operators could be present. Secondly, it could be that the active neutrinos are Majorana fermions and gain their mass through some BSM physics. In this case, the chirality-flipping neutral-current (pseudo)scalar and tensor operators are lepton number violating, as well as the right-handed ($\widetilde{\epsilon}$) charged-current operators. Furthermore, not all of the operators are allowed, since the right-handed neutrinos are the particle-antiparticle conjugates of the left-handed neutrinos $N_R = \nu_L^c = C\overline{\nu_L}^T$, as discussed in Section 1.2. This identification leads to the restrictions

$$\begin{aligned}
\epsilon_{L,f}^{\alpha\beta\gamma\delta} &= \epsilon_{L,f}^{\beta\alpha\delta\gamma*} = -\widetilde{\epsilon}_{L,f}^{\beta\alpha\gamma\delta} = -\widetilde{\epsilon}_{L,f}^{\alpha\beta\delta\gamma*}\,, \\
\epsilon_{R,f}^{\alpha\beta\gamma\delta} &= \epsilon_{R,f}^{\beta\alpha\delta\gamma*} = -\widetilde{\epsilon}_{R,f}^{\beta\alpha\gamma\delta} = -\widetilde{\epsilon}_{R,f}^{\alpha\beta\delta\gamma*}\,, \\
\epsilon_{S,f}^{\alpha\beta\gamma\delta} &= \epsilon_{S,f}^{\beta\alpha\gamma\delta} = \widetilde{\epsilon}_{S,f}^{\alpha\beta\delta\gamma*} = \widetilde{\epsilon}_{S,f}^{\beta\alpha\delta\gamma*}\,, \qquad \text{(Majorana neutrinos)} \\
\epsilon_{P,f}^{\alpha\beta\gamma\delta} &= \epsilon_{P,f}^{\beta\alpha\gamma\delta} = -\widetilde{\epsilon}_{P,f}^{\alpha\beta\delta\gamma*} = -\widetilde{\epsilon}_{P,f}^{\beta\alpha\delta\gamma*}\,, \\
\epsilon_{T,f}^{\alpha\beta\gamma\delta} &= -\epsilon_{T,f}^{\beta\alpha\gamma\delta} = -\widetilde{\epsilon}_{T,f}^{\alpha\beta\delta\gamma*} = \widetilde{\epsilon}_{T,f}^{\beta\alpha\delta\gamma*}\,.
\end{aligned} \tag{2.14}$$

We discuss the origin of these identities in Appendix A.5. This means, in particular, that all $\widetilde{\epsilon}$ can be reduced to their ϵ counterpart. Moreover, the left-handed and right-handed vector interactions are Hermitian, scalar and pseudoscalar interactions are symmetric, and tensor interactions are antisymmetric in flavor indices. Thirdly, the right-handed neutrinos in the interaction could be right-handed components of independent Majorana or Dirac sterile neutrinos in which case they could in principle have any mass different from the active neutrino mass. In the course of this thesis, we will encounter all three scenarios.

Similar restrictions to those in Equation (2.14) for Majorana neutrinos can be derived for assumptions like charge-parity or flavor conservation, which we also derive in Appendix A.5. Here we only show the result in terms of the number of free interaction parameters in Table 2.5. The detection of certain types of interactions which are only

Table 2.5. Number of free parameters in the general neutral-current Lagrangian (2.11) under different assumptions, for fixed charged fermion type f, either electron-type lepton, up-type quark or down-type quark. CP denotes charge-parity. By $\gamma = \delta =$ fixed, we mean that we take $\gamma = \delta$ and assign a definite generation number to it. By flavor-diagonal we mean that $\epsilon_{\alpha\beta\gamma\delta} \propto \delta_{\alpha\beta}$. Details are found in Appendix A.5. Strictly speaking, in the case of up-type quarks the top quark is too heavy to be part of the EFT below the weak scale and therefore the number of degrees of freedom would be smaller for $f = u$.

	Dirac	Majorana	CP-invariant	Majorana + CP-invariant
All indices free	810	432	423	225
$\gamma = \delta =$ fixed	90	48	51	27
flavor-diagonal and $\gamma = \delta =$ fixed	30	18	21	12

compatible with Dirac neutrinos, e.g. flavor-conserving tensor interactions, can therefore rule out the Majorana neutrino scenario, while the Dirac scenario cannot be ruled out in this way [52, 58, 59]. Note that in the charged-current case (2.12), since only one neutrino field is involved, relations such as (2.14) in general do not hold. While we do not discuss this in detail, we remark that a particularly interesting property of the scalar and tensor interactions is that they induce a large contribution to the magnetic moment of the neutrino [60]. It could be orders of magnitude larger than predicted by the SM and even within detector reach. This is again a consequence of the chirality flipping nature of the interaction. In the SM, the leading diagram couples two neutrino external lines to a photon line via a charged fermion loop. This requires a chirality flip in a neutrino line which implies a neutrino mass insertion. If the new interaction flips neutrino chirality, instead a charged fermion mass insertion is required. Therefore, compared to the SM amplitude the new contribution is enhanced by a large factor m_f/m_ν, where f is the charged fermion.

2.4. Matching relations

As already mentioned, LEFT or GNI and SMEFT can be treated independently. In the case that we want to describe new physics above the weak scale, however, it can be useful to connect the two. In this section, we discuss the matching of the Wilson coefficients at the weak scale which illuminates which GNI can be produced in a way that respects the electroweak symmetry. The matching is straightforward. One simply expands the SMNEFT operators in terms of their weak isospin components and identifies all the terms which contribute to a certain GNI operator. To perform the matching, it is necessary to specify in which bases with respect to flavor and mass the effective operators described in Section 2.2 and Section 2.3 are defined. Following the discussion in Section 1.2.2, we

specify the basis changes in Equation (1.17). This means that wherever a factor of u_L appears, a factor of V has to be inserted when changing to the mass basis. One needs to keep in mind that the matching relations given in this section and the bounds derived or cited in Chapter 4 depend on this choice of basis.

2.4.1. Four-fermion interactions

The complete matching relations between SMEFT and LEFT have been presented in Reference [50]. Adding the four-fermion matching relations of operators including right-handed neutrinos, the results expressed in terms of GNI coefficients are shown in Tables 2.6 and 2.7, where we assume $\Lambda^{-2} = \sqrt{8}G_F$ to obtain simple expressions. For generic Λ we have to divide the coefficients by $(\sqrt{8}G_F\Lambda^2)$. Recall that we defined GNI in the mass basis of quarks and charged leptons, while neutrinos are in the flavor basis such that their transformation into the mass basis can be performed depending on the specific assumptions that we make in Chapter 3 and Chapter 4. It is not surprising that many SMNEFT operators (which were defined in Table 2.1) containing lepton doublets l lead not only to GNI but also to new interactions among charged leptons and quarks. A simple example is $\mathcal{O}_{ll}$, for which we have

$$\begin{aligned} C_{ll}^{\alpha\beta\gamma\delta}(\bar{l}_\alpha\gamma^\mu l_\beta)(\bar{l}_\gamma\gamma_\mu l_\delta) = C_{ll}^{\alpha\beta\gamma\delta}\,[&\overline{\nu}_\alpha\gamma^\mu P_L\nu_\beta\,\overline{\nu}_\gamma\gamma_\mu P_L\nu_\delta + \overline{e}_\alpha\gamma^\mu P_L e_\beta\,\overline{e}_\gamma\gamma_\mu P_L e_\delta \\ &+\overline{\nu}_\alpha\gamma^\mu P_L\nu_\beta\,\overline{e}_\gamma\gamma_\mu P_L e_\delta + \overline{e}_\alpha\gamma^\mu P_L e_\beta\,\overline{\nu}_\gamma\gamma_\mu P_L\nu_\delta]\,, \end{aligned} \tag{2.15}$$

where $P_L = (1-\gamma^5)/2$ (and for later use $P_R = (1+\gamma^5)/2$). We see that one SMEFT operator implies a four-neutrino interaction, a type of interaction sometimes called secret neutrino interaction, a four-electron interaction and two contributions to the GNI operator parametrized by $\epsilon_{L,e}$. In total, all the four-charged-fermion interactions which are generated by SMNEFT operators in Table 2.1 which include lepton doublets and some other fields read (in the mass basis)

$$\begin{aligned} \mathcal{L} = \frac{1}{\Lambda^2}\Big\{&\left(C_{ll}^{\alpha\beta\gamma\delta} + C_{ll}^{\alpha\delta\gamma\beta}\right)(\overline{e}_\alpha\gamma_\mu P_L e_\beta)(\overline{e}_\gamma\gamma^\mu P_L e_\delta) + C_{le}^{\alpha\beta\gamma\delta}(\overline{e}_\alpha\gamma_\mu P_L e_\beta)(\overline{e}_\gamma\gamma^\mu P_R e_\delta) \\ &+ V_{\gamma\rho}V_{\sigma\delta}^\dagger(C_{lq(1)}^{\alpha\beta\rho\sigma} - C_{lq(3)}^{\alpha\beta\rho\sigma})(\overline{e}_\alpha\gamma_\mu P_L e_\beta)(\overline{u}_\gamma\gamma^\mu P_L u_\delta) + C_{lu}^{\alpha\beta\gamma\delta}(\overline{e}_\alpha\gamma_\mu P_L e_\beta)(\overline{u}_\gamma\gamma^\mu P_R u_\delta) \\ &+ (C_{lq(1)}^{\alpha\beta\gamma\delta} + C_{lq(3)}^{\alpha\beta\gamma\delta})(\overline{e}_\alpha\gamma_\mu P_L e_\beta)(\overline{d}_\gamma\gamma^\mu P_L d_\delta) + C_{ld}^{\alpha\beta\gamma\delta}(\overline{e}_\alpha\gamma_\mu P_L e_\beta)(\overline{d}_\gamma\gamma^\mu P_R d_\delta) \\ &- V_{\sigma\delta}^\dagger C_{eluq}^{\alpha\beta\gamma\sigma}(\overline{e}_\alpha P_L e_\beta)(\overline{u}_\gamma P_L u_\delta) - V_{\sigma\delta}^\dagger C_{eluq}^{\prime\alpha\beta\gamma\sigma}(\overline{e}_\alpha\sigma_{\mu\nu}P_L e_\beta)(\overline{u}_\gamma\sigma^{\mu\nu}P_L u_\delta) \\ &+ C_{elqd}^{\alpha\beta\gamma\delta}(\overline{e}_\alpha P_L e_\beta)(\overline{d}_\gamma P_R d_\delta)\Big\}\,. \end{aligned} \tag{2.16}$$

The constraints on these charged fermion interactions are typically much stronger than constraints on GNI. Therefore, this operator matching can be used to place strong indirect bounds on neutrino interactions from SMNEFT operators in the case that they have a common high-energy origin, as we will practice in Chapter 4, in particular in our study of charged lepton flavor violation in Section 4.2. For this reason we have printed all coefficients which are accompanied by strongly-constrained charged fermion interactions

Table 2.6. Neutral-current GNI coefficients appearing in Equation (2.11) and their contributions from dimensionless Wilson coefficients of SMNEFT four-fermion operators in Table 2.1 assuming $\Lambda^{-2} = \sqrt{8}G_F$. For general Λ, the GNI coefficients are given by the entries of the table divided by $\sqrt{8}G_F\Lambda^2$. The columns relate to $f = e, u, d$, respectively. The indices $\alpha, \beta = e, \mu, \tau$, and $\gamma, \delta, \mu, \nu = 1, 2, 3$ denote the generation numbers of leptons and quarks. Those SMNEFT coefficients which also lead to new interactions among four charged fermions described by Equation (2.16) are printed in red.

	e	u	d
$-\epsilon_{L,f}^{\alpha\beta\gamma\delta}$	$C_{ll}^{\alpha\beta\gamma\delta}$	$V_{\gamma\mu}V_{\nu\delta}^{\dagger}\left(C_{lq(1)}^{\alpha\beta\mu\nu} + C_{lq(3)}^{\alpha\beta\mu\nu}\right)$	$C_{lq(1)}^{\alpha\beta\gamma\delta} - C_{lq(3)}^{\alpha\beta\gamma\delta}$
$-\widetilde{\epsilon}_{L,f}^{\alpha\beta\gamma\delta}$	$C_{Nl}^{\alpha\beta\gamma\delta}$	$V_{\gamma\mu}V_{\nu\delta}^{\dagger}C_{Nq}^{\alpha\beta\mu\nu}$	$C_{Nq}^{\alpha\beta\gamma\delta}$
$-\epsilon_{R,f}^{\alpha\beta\gamma\delta}$	$C_{le}^{\alpha\beta\gamma\delta}$	$C_{lu}^{\alpha\beta\gamma\delta}$	$C_{ld}^{\alpha\beta\gamma\delta}$
$-\widetilde{\epsilon}_{R,f}^{\alpha\beta\gamma\delta}$	$C_{Ne}^{\alpha\beta\gamma\delta}$	$C_{Nu}^{\alpha\beta\gamma\delta}$	$C_{Nd}^{\alpha\beta\gamma\delta}$
$-\epsilon_{S,f}^{\alpha\beta\gamma\delta}$	$\frac{1}{2}C_{Nlel}^{\alpha\beta\gamma\delta} + \frac{1}{4}C_{Nlel}^{\gamma\beta\alpha\delta}$	$V_{\gamma\nu}(C_{lNuq}^{\beta\alpha\delta\nu})^*$	$(C_{lNqd}^{\beta\alpha\delta\gamma})^*$
$-\epsilon_{P,f}^{\alpha\beta\gamma\delta}$	$\frac{1}{2}C_{Nlel}^{\alpha\beta\gamma\delta} + \frac{1}{4}C_{Nlel}^{\gamma\beta\alpha\delta}$	$-V_{\gamma\nu}(C_{lNuq}^{\beta\alpha\delta\nu})^*$	$(C_{lNqd}^{\beta\alpha\delta\gamma})^*$
$-\epsilon_{T,f}^{\alpha\beta\gamma\delta}$	$\frac{1}{8}C_{Nlel}^{\gamma\beta\alpha\delta}$	0	$(C_{lNqd}^{\prime\beta\alpha\delta\gamma})^*$

in red in Tables 2.6 and 2.7. In total, the secret neutrino interactions induced by the operators in Table 2.1, still in the flavor basis, read

$$\begin{aligned}\mathcal{L}_{\text{secret}} = \frac{1}{\Lambda^2}\Big\{&\left(C_{ll}^{\alpha\beta\gamma\delta} + C_{ll}^{\alpha\delta\gamma\beta}\right)(\overline{\nu}_\alpha\gamma_\mu P_L\nu_\beta)(\overline{\nu}_\gamma\gamma^\mu P_L\nu_\delta)\\ &+C_{Nl}^{\alpha\beta\gamma\delta}(\overline{N}_\alpha\gamma_\mu P_R N_\beta)(\overline{\nu}_\gamma\gamma^\mu P_L\nu_\delta) + C_{NN}^{\alpha\beta\gamma\delta}(\overline{N}_\alpha\gamma_\mu P_R N_\beta)(\overline{N}_\gamma\gamma^\mu P_R N_\delta)\Big\}.\end{aligned} \tag{2.17}$$

These are naturally even harder to detect than GNI and we will only consider them in Section 3.3 where they give rise to NSI at loop-level through a modified coupling to the Z boson. However, they have been considered in the context of cosmology and astrophysics [61–66].

We conclude several points from the analysis of four-fermion matching. Firstly, some GNI coefficients, namely $\epsilon_{T,u}$, $\epsilon_{R,ud}$ and $\widetilde{\epsilon}_{L,ud}$ cannot be generated at all from operators up to dimension six in SMNEFT. If these GNI are detected, it poses a hint towards low-scale new physics, or towards higher order in the EFT expansion. Secondly, some operators (those printed in red in Tables 2.6 and 2.7) can be generated, but only at the cost of introducing equally strong charged fermion interactions, which should make them very constrained. The only remedy could be precise cancellations between Wilson coefficients. For instance, when we have in Equation (2.16)

$$C_{ll}^{\alpha\beta\gamma\delta} + C_{ll}^{\alpha\delta\gamma\beta} = 0 \tag{2.18}$$

we can still have sizable $\epsilon_{L,e}^{\alpha\beta\gamma\delta} \neq 0$ in Table 2.6. However, since the Wilson coefficients run with the interaction energy scale μ, a precise cancellation at one scale does not need to

Table 2.7. Charged-current GNI coefficients appearing in Equation (2.12) and their contributions from dimensionless Wilson coefficients of SMNEFT four-fermion operators in Table 2.1 assuming $\Lambda^{-2} = \sqrt{8}G_F$. For general Λ, the GNI coefficients are given by the entries of the table divided by $\sqrt{8}G_F\Lambda^2$. Indices and color coding are analogous to Table 2.6.

$-\epsilon^{\alpha\beta\gamma\delta}_{L,ud}$	$\frac{V_{\gamma\nu}}{V_{\gamma\delta}} 2C^{\alpha\beta\nu\delta}_{lq(3)}$	$-\widetilde{\epsilon}^{\alpha\beta\gamma\delta}_{L,ud}$	0
$-\epsilon^{\alpha\beta\gamma\delta}_{R,ud}$	0	$-\widetilde{\epsilon}^{\alpha\beta\gamma\delta}_{R,ud}$	$\frac{1}{V_{\gamma\delta}} C^{\alpha\beta\gamma\delta}_{eNud}$
$-\epsilon^{\alpha\beta\gamma\delta}_{S,ud}$	$\frac{1}{V_{\gamma\delta}} \left(V_{\gamma\nu} C^{\alpha\beta\nu\delta}_{elqd} + C^{\alpha\beta\gamma\delta}_{eluq} \right)$	$-\widetilde{\epsilon}^{\alpha\beta\gamma\delta}_{S,ud}$	$\frac{1}{V_{\gamma\delta}} \left(C^{\alpha\beta\gamma\delta}_{lNuq} - V_{\gamma\nu} C^{\alpha\beta\nu\delta}_{lNqd} \right)$
$-\epsilon^{\alpha\beta\gamma\delta}_{P,ud}$	$\frac{1}{V_{\gamma\delta}} \left(-V_{\gamma\nu} C^{\alpha\beta\nu\delta}_{elqd} + C^{\alpha\beta\gamma\delta}_{eluq} \right)$	$-\widetilde{\epsilon}^{\alpha\beta\gamma\delta}_{P,ud}$	$\frac{1}{V_{\gamma\delta}} \left(C^{\alpha\beta\gamma\delta}_{lNuq} + V_{\gamma\nu} C^{\alpha\beta\nu\delta}_{lNqd} \right)$
$-\epsilon^{\alpha\beta\gamma\delta}_{T,ud}$	$\frac{1}{V_{\gamma\delta}} C'^{\alpha\beta\gamma\delta}_{eluq}$	$-\widetilde{\epsilon}^{\alpha\beta\gamma\delta}_{T,ud}$	$-\frac{V_{\gamma\nu}}{V_{\gamma\delta}} C'^{\alpha\beta\nu\delta}_{lNqd}$

persist at another scale. Nonetheless, this kind of scenario is not too unrealistic to expect, as we will see in Section 3.3, where we present a model with new physics generating $\mathcal{O}_{ll}$ and the Wilson coefficients satisfy the relation (2.18) at tree-level. Thirdly, we observe that from the high-energy perspective, the assumption that up and down quark NSI are equal is unjustified, since they are generated by different operators. Fourthly, some single SMNEFT operators induce two different GNI coefficients. In particular, $\mathcal{O}_{lNuq}$, $\mathcal{O}_{lNqd}$ and $\mathcal{O}'_{lNqd}$ induce simultaneously scalar or tensor charged-current and neutral-current interactions. So it would be an attractive scenario to detect one of these interactions, say, in the neutral-current channel and then predict the corresponding interaction strength in the charge-current channel. Consistency of the two would give a strong hint towards the underlying SMNEFT operator. We discuss ways to test these connected operators through coherent elastic neutrino nucleus scattering and beta decays in Section 4.3.

As a final remark, we note that while we can map these operators according to Tables 2.6 and 2.7 at the weak scale, the RG running down to lower scales in general may mix those contributions. Throughout this work, we neglect the mixing as subleading, but there are some interesting insights from other publications. In Reference [67] it was found that the left-handed charged-current (pseudo)scalar and tensor NSI mix as one runs from 2 GeV to the weak scale, while the left and right vectors do not mix.

2.4.2. Boson-fermion mixed operators

Even though we will not consider the boson-fermion mixed operators of Table 2.2 in our phenomenological studies in Chapter 3 and Chapter 4, for completeness we comment here on the type of LEFT operators they generate below the weak scale. The leading effect of operators of the form $\psi^2 H^3$ is a correction to fermion masses and Yukawa couplings of h, since they are just the Yukawa terms of the Higgs doublet multiplied by a Higgs bilinear. This will lead to Yukawa couplings to h not being proportional to the fermion mass, unlike in the SM [68]. In the second column of Table 2.2 are the operators of type $\psi^2 XH$ which lead to dipole-like modified couplings of quarks and leptons to the W and

Z bosons, as well as the photon and gluon. We expect that these operators are strongly constrained by the electromagnetic properties of the fermions but do not consider them further here. Finally, the operators of type $\psi^2 H^2$ lead to modified couplings of fermion bilinears to W and Z. In the following, we calculate only those involving neutrinos, which are

$$\begin{aligned}
\left(\mathcal{O}_{Hl}^{(1)}\right)_{\alpha\beta} &= i\left(H^\dagger \overleftrightarrow{D}_\mu H\right)\left(\bar{l}_\alpha \gamma^\mu l_\beta\right), \qquad (\mathcal{O}_{HN})_{\alpha\beta} = i\left(H^\dagger \overleftrightarrow{D}_\mu H\right)\left(\overline{N}_\alpha \gamma^\mu N_\beta\right), \\
\left(\mathcal{O}_{Hl}^{(3)}\right)_{\alpha\beta} &= i\left(H^\dagger \tau^I \overleftrightarrow{D}_\mu H\right)\left(\bar{l}_\alpha \tau^I \gamma^\mu l_\beta\right), \quad (\mathcal{O}_{HNe})_{\alpha\beta} = i\left(\widetilde{H}^\dagger D_\mu H\right)\left(\overline{N}_\alpha \gamma^\mu e_\beta\right).
\end{aligned} \tag{2.19}$$

Evaluating the operators at the Higgs vacuum expectation value, one finds the usual structure of the weak interaction Lagrangians,

$$\begin{aligned}
\mathcal{L}_W &= -\frac{g}{2\sqrt{2}} W_\mu j_W^\mu + \text{H.c.}, \\
\mathcal{L}_Z &= -\frac{g}{2c_W} Z_\mu j_Z^\mu .
\end{aligned} \tag{2.20}$$

However, the leptonic fermion currents are modified and read,

$$\begin{aligned}
j^\mu_{W,\text{lepton}} &= (2\delta^{\alpha\beta} + 4C^{\alpha\beta}_{Hl(3)})\overline{\nu}_\alpha \gamma^\mu P_L e_\beta + 2C^{\alpha\beta}_{HNe}\overline{N}_\alpha \gamma^\mu P_R e_\beta , \\
j^\mu_{Z,\text{lepton}} &= 2(\widetilde{g}^\nu_L)_{\alpha\beta}(\overline{\nu}_\alpha \gamma^\mu P_L \nu_\beta) + 2(\widetilde{g}^e_L)_{\alpha\beta}(\overline{e}_\alpha \gamma^\mu P_L e_\beta) + 2g^e_R(\overline{e}_\alpha \gamma^\mu P_R e_\beta) \\
&\quad + 2(\widetilde{g}^N_R)_{\alpha\beta}(\overline{N}_\alpha \gamma^\mu P_R N_\beta) .
\end{aligned} \tag{2.21}$$

The SM leptonic charged current gets a contribution form $\mathcal{O}^{(3)}_{Hl}$. Moreover, there is a new right-handed leptonic charged current mediated by $\mathcal{O}_{HNe}$. Concerning the neutral currents, the modified couplings read

$$\begin{aligned}
(\widetilde{g}^\nu_L)_{\alpha\beta} &= g^\nu_L \delta^{\alpha\beta} - C^{\alpha\beta}_{Hl(1)} + C^{\alpha\beta}_{Hl(3)} , \\
(\widetilde{g}^e_L)_{\alpha\beta} &= g^e_L \delta^{\alpha\beta} - C^{\alpha\beta}_{Hl(1)} - C^{\alpha\beta}_{Hl(3)} , \\
(\widetilde{g}^N_R)_{\alpha\beta} &= -C^{\alpha\beta}_{HN} ,
\end{aligned} \tag{2.22}$$

with the SM contributions being the terms proportional to $\delta^{\alpha\beta}$ and where g^f_X are given in Equation (1.16). Besides the corrections to neutral-current SM couplings, there is a new right-handed neutrino coupling to the Z boson.

If we integrate out W and Z, which requires to compute the contractions $j^\mu_Z j_{Z,\mu}$ and $j^\mu_W j_{W,\mu}$, we arrive the following GNI coefficients to leading order in Wilson coefficients. First, we have

$$\begin{aligned}
\epsilon^{\alpha\beta\gamma\delta}_{L,e} &= 2\delta^{\alpha\delta} C^{\gamma\beta}_{Hl(3)} + 2C^{\alpha\delta}_{Hl(3)}\delta^{\gamma\beta} \\
&\quad - \delta^{\alpha\beta}\left(C^{\gamma\delta}_{Hl(1)} + C^{\gamma\delta}_{Hl(3)}\right) - 2g^e_L \delta^{\gamma\delta}\left(C^{\alpha\beta}_{Hl(1)} - C^{\alpha\beta}_{Hl(3)}\right),
\end{aligned} \tag{2.23}$$

From the contraction of the modified left-handed neutrino neutral-current with the standard neutral currents of u_L, u_R, d_L, d_R, e we find

$$\begin{aligned}
\epsilon^{\alpha\beta\gamma\delta}_{L,q} &= 2g^q_L \delta^{\gamma\delta}\left(C^{\alpha\beta}_{Hl(3)} - C^{\alpha\beta}_{Hl(1)}\right), \\
\epsilon^{\alpha\beta\gamma\delta}_{R,f} &= 2g^f_R \delta^{\gamma\delta}\left(C^{\alpha\beta}_{Hl(3)} - C^{\alpha\beta}_{Hl(1)}\right),
\end{aligned} \tag{2.24}$$

where $q = u, d$ and $f = u, d, e$. The contraction of the right-handed neutrino neutral current with the charged fermion neutral currents yields

$$\begin{aligned} \widetilde{\epsilon}^{\alpha\beta\gamma\delta}_{L,f} &= -2g^f_L \delta^{\gamma\delta} C^{\alpha\beta}_{HN}\,, \\ \widetilde{\epsilon}^{\alpha\beta\gamma\delta}_{R,f} &= -2g^f_R \delta^{\gamma\delta} C^{\alpha\beta}_{HN}\,. \end{aligned} \tag{2.25}$$

The right-handed W coupling induced by $\mathcal{O}_{HNe}$ implies

$$\begin{aligned} \epsilon^{\alpha\beta\gamma\delta}_{S,e} &= \epsilon^{\alpha\beta\gamma\delta}_{P,e} = 2\delta^{\beta\gamma} C^{\alpha\delta}_{HNe}\,, \\ \widetilde{\epsilon}^{\alpha\beta\gamma\delta}_{L,ud} &= (C^{\beta\alpha}_{HNe})^* \delta^{\gamma\delta}\,, \end{aligned} \tag{2.26}$$

and finally one finds,

$$\epsilon^{\alpha\beta\gamma\delta}_{L,ud} = 2\delta^{\gamma\delta}(C^{\beta\alpha}_{Hl(3)})^*\,. \tag{2.27}$$

These GNI are accompanied by a modified electron-Z coupling

$$\mathcal{L}_{Ze} = -\frac{g}{2c_W} Z_\mu j^\mu_{Ze} = -\frac{g}{2c_W} Z_\mu \left(2g^e_L \delta^{\alpha\beta} - 2C^{\alpha\beta}_{Hl(1)} - 2C^{\alpha\beta}_{Hl(3)}\right) \bar{e}_\alpha \gamma^\mu P_L e_\beta\,. \tag{2.28}$$

This coupling is of course again strongly constrained, such that relatively precise cancellations between $C_{Hl(1)}$ and $C_{Hl(3)}$ would be required to make these operators consistent with observations. Again all expressions of GNI coefficients are derived assuming $\Lambda^{-2} = \sqrt{8}G_F$. General expressions are found by the replacement rule

$$\epsilon_{\text{general}} = \frac{\epsilon}{\sqrt{8}G_F\Lambda^2}\,. \tag{2.29}$$

3. Theoretical origins of new neutrino interactions

In this chapter, we discuss several examples of UV complete models which at low energies leave traces in the form of GNI. The purpose of this discussion is mainly to demonstrate the versatility of different theoretical approaches, including gauge extensions, colored and uncolored scalar and vector bosons that all can give rise to different kinds of GNI. While this may inform us for which interactions we would have relatively straightforward theoretical explanations, we can only stress that experiments have to determine which, and if any at all, are realized. If anything, the versatility of these different models calls us to search for all possible traces of new physics including those considered exotic. This philosophy is reflected by our choice to analyze the most general Lorentz-invariant neutrino interactions in terms of their experimental probes in Chapter 4. Of course, detecting such new interactions is only the first step. After their detection, we may apply complete models that explain the observed interactions to make predictions about signals of new physics in other processes. Consistency or inconsistency of these results can then be used to distinguish which models are accurate and which ones fail.

The models we consider in this chapter are divided into three classes. In Section 3.1, we discuss U(1) gauge extensions of the SM and, in particular, a model with a gauged third-generation baryon number minus lepton number symmetry. This symmetry is broken at a high energy scale such that the massive gauge boson becomes a heavy mediator of new physics. Next, in Section 3.2, we discuss new scalars and vectors which carry both color and electroweak charges, the so-called leptoquarks. Both of these introduce GNI already at tree-level by integrating out heavy mediators. In Section 3.3 we investigate how new scalars, not necessarily very heavy, can introduce non-standard interactions at one-loop level. In this case, the loop suppression can be a reason for the smallness of new interactions.

This chapter partially relies on the content of References [1, 3, 4]. We comment on which parts specifically have been published at the appropriate places throughout the chapter.

3.1. Gauge extensions

The landscape of possible gauge extensions of the SM is of course far too vast to cover here. We choose to comment on selected phenomenologically inspired approaches with particular interest to neutrino interactions. A class of relatively economical gauge extensions can be denoted by $\mathrm{U}(1)_X$ models [69]. These are models in which the SM gauge group is extended by another U(1) gauge symmetry, i.e $\mathrm{SU}(3)_C \times \mathrm{SU}(2)_L \times \mathrm{U}(1)_Y \times \mathrm{U}(1)_X$.

Now, broadly speaking, the $\mathrm{U}(1)_X$ gauge boson can be light or massless, in which case it is usually referred to as a hidden photon. Or it can have a mass comparable to or larger than the Z boson, in which case it is usually referred to as a Z'. Due to loop diagrams, the dark photon will usually share a kinetic term with the regular photon and the Z' will mix with the Z boson through a mixed $\mathrm{U}(1)_Y$-$\mathrm{U}(1)_X$ kinetic term [70]. Therefore, these models are subject to strong constraints on this mixing, unless the mass of Z' is well above the weak scale. This is a remarkably generic fact, given that the charges of the SM fields or additional particles under the new U(1) do not need to be specified for these conclusions as long as there are particles carrying both $U(1)_X$ and SM charge. In this section, we first review the general dynamics of Z' models without specifying the charges of SM fields. Then we give a particularly attractive example, the gauged third-generation baryon number minus lepton number symmetry, in short $(B-L)_3$.

3.1.1. Z'-mixing and mass diagonalization

We will assume here a generic $\mathrm{U}(1)_X$ extension of the standard model, where the $\mathrm{U}(1)_X$ is already broken and the gauge boson X has acquired a mass $\hat{M}_X$. In the explicit model considered in Section 3.1.2, this mass is generated from the vev of a new scalar field. Without mention of the origin of $\hat{M}_X$, the $\mathrm{SU}(2)_L\times\mathrm{U}(1)_Y\times\mathrm{U}(1)_X$ gauge-fermionic component of the Lagrangian between the scale of $\mathrm{U}(1)_X$ breaking and EWSB reads

$$\begin{aligned}\mathcal{L}_{\text{g.f.}} = &-\frac{1}{4}W^{I,\mu\nu}W^I_{\mu\nu} - \frac{1}{4}\hat{B}^{\mu\nu}\hat{B}_{\mu\nu} - \frac{1}{4}\hat{X}^{\mu\nu}\hat{X}_{\mu\nu} - \frac{\epsilon}{2}\hat{X}^{\mu\nu}\hat{B}_{\mu\nu}\\ &+\frac{1}{2}\hat{M}_X^2\hat{X}^\mu\hat{X}_\mu - g\, j^{I,\mu}_W W^I_\mu - g' j^\mu_Y \hat{B}_\mu - g_X j^\mu_X \hat{X}_\mu\,,\end{aligned} \tag{3.1}$$

where the term proportional to ϵ is the kinetic mixing term which is always generated by loop processes, and a runs over $\mathrm{SU}(2)_L$-adjoint indices. Explicitly,

$$j^{I,\mu}_W = \sum_\psi \overline{\psi}\frac{\tau^I}{2}\gamma^\mu\psi\,, \qquad \psi = l, q\,, \tag{3.2}$$

$$j^\mu_B = \sum_\psi \frac{q^\psi_Y}{2}\overline{\psi}\gamma^\mu\psi\,, \qquad \psi = l, q, e, u, d\,, \tag{3.3}$$

$$j^\mu_X = \sum_\psi q^\psi_X\overline{\psi}\gamma^\mu\psi\,, \qquad \psi = l, q, e, N, u, d\,, \tag{3.4}$$

where q^ψ_Y denotes the hypercharge of the representation ψ, while q^ψ_X denotes the X-charge of the representation ψ. The hats are meant to indicate that the fields are not canonically normalized. To change this, one may perform the transformation

$$\begin{pmatrix}\hat{B}_\mu\\ \hat{X}_\mu\end{pmatrix} = \begin{pmatrix}1 & -\frac{\epsilon}{\sqrt{1-\epsilon^2}}\\ 0 & \frac{1}{\sqrt{1-\epsilon^2}}\end{pmatrix}\begin{pmatrix}B_\mu\\ X_\mu\end{pmatrix}\,, \tag{3.5}$$

which eliminates the kinetic mixing term, while establishing

$$m_X^2 = \frac{1}{1-\epsilon^2}\hat{M}_X^2\,. \tag{3.6}$$

How X_μ mixes with the other gauge fields now depends on whether the electroweak symmetry is broken or unbroken. Let us consider the two cases from high to low scale.

In the symmetric phase of $\mathrm{SU}(2)_L \times \mathrm{U}(1)_Y$, i.e. above the weak scale, there is no mass mixing between B and X, since B and W are strictly massless. The covariant derivative in terms of the canonically normalized fields then reads

$$D_\mu = \partial_\mu + igW_\mu^I \frac{\tau^I}{2} + ig' B_\mu \frac{Y}{2} + iX_\mu \frac{1}{\sqrt{1-\epsilon^2}} \left(g_X Y_X - \epsilon\, g' \frac{Y}{2} \right), \tag{3.7}$$

where Y denotes the hypercharge operator and Y_X the $\mathrm{U}(1)_X$ charge operator. Apart from the usual SM interactions, this leads to the fermionic neutral-current interactions with X,

$$\mathcal{L}_{X,\mathrm{NC}} = \frac{1}{\sqrt{1-\epsilon^2}} \left(-g_X j_X^\mu + \epsilon\, g' j_Y^\mu \right) X_\mu \,. \tag{3.8}$$

Considering a Higgs doublet H and its coupling to the gauge fields, we can derive the interaction with mass eigenfields,

$$(D^\mu H)^\dagger (D_\mu H) = (D^\mu H)^\dagger \left(\partial_\mu + igW_\mu^I \frac{\tau^I}{2} + i\frac{g'}{2} B_\mu - i\frac{g'}{2} \frac{\epsilon}{\sqrt{1-\epsilon^2}} X_\mu \right) H \,. \tag{3.9}$$

We conclude that the kinetic mixing introduces a small coupling to X for all fields carrying a hypercharge q_Y, even if they carry no $\mathrm{U}(1)_X$ charge.

Below the electroweak scale explicit masses for $\hat{B}$ and W are generated, giving rise to a combined mass matrix for the neutral component W^3 of W, B and X,

$$M^2 = \frac{v^2}{4} \begin{pmatrix} g^2 & -gg' & gg' \frac{\epsilon}{\sqrt{1-\epsilon^2}} \\ -gg' & g'^2 & -g'^2 \frac{\epsilon}{\sqrt{1-\epsilon^2}} \\ gg' \frac{\epsilon}{\sqrt{1-\epsilon^2}} & -g'^2 \frac{\epsilon}{\sqrt{1-\epsilon^2}} & \frac{4}{v^2} \hat{M}_X^2 (1-\epsilon^2)^{-1} + g'^2 \frac{\epsilon^2}{1-\epsilon^2} \end{pmatrix}. \tag{3.10}$$

Defining the Weinberg angle as usual, $\tan\theta_\mathrm{W} = g'/g$, with the rotation matrix

$$R_\theta = \begin{pmatrix} s_W & c_W & 0 \\ c_W & -s_W & 0 \\ 0 & 0 & 1 \end{pmatrix} \tag{3.11}$$

one obtains the partial diagonalization

$$R_\theta M^2 R_\theta^T = \begin{pmatrix} 0 & 0 & 0 \\ 0 & m_{Z,\mathrm{SM}}^2 & m_{Z,\mathrm{SM}}^2 s_W \frac{\epsilon}{\sqrt{1-\epsilon^2}} \\ 0 & m_{Z,\mathrm{SM}}^2 s_W \frac{\epsilon}{\sqrt{1-\epsilon^2}} & \mu_X^2 \end{pmatrix}, \tag{3.12}$$

where we used the SM tree-level relation $m_{Z,\mathrm{SM}} = gv/2c_W$ and the definition

$$\mu_X^2 = \hat{M}_X^2 (1-\epsilon^2)^{-1} + m_{Z,\mathrm{SM}}^2 s_W^2 \frac{\epsilon^2}{1-\epsilon^2} \,. \tag{3.13}$$

This can be diagonalized by another rotation to the mass eigenvalues m_Z^2 and $m_{Z'}^2$ with

$$m_Z^2 = \frac{m_{Z,\mathrm{SM}^2}}{2} + \frac{\mu_X^2}{2} + \frac{m_{Z,\mathrm{SM}}^2 - \mu_X^2}{2}\sqrt{1+\tan^2(2\xi)}\,, \tag{3.14}$$

$$m_{Z'}^2 = \frac{m_{Z,\mathrm{SM}^2}}{2} + \frac{\mu_X^2}{2} - \frac{m_{Z,\mathrm{SM}}^2 - \mu_X^2}{2}\sqrt{1+\tan^2(2\xi)}\,, \tag{3.15}$$

where the second mixing angle is defined by

$$\begin{aligned}\tan(2\xi) &= \frac{2m_{Z,\mathrm{SM}}^2 s_W}{m_{Z,\mathrm{SM}}^2 - \mu_X^2}\frac{\epsilon}{\sqrt{1-\epsilon^2}} \\ &= -\frac{m_{Z,\mathrm{SM}}^2}{\mu_X^2}\frac{2s_W}{1-\frac{m_{Z,\mathrm{SM}}^2}{\mu_X^2}}\frac{\epsilon}{\sqrt{1-\epsilon^2}}\,.\end{aligned} \tag{3.16}$$

This angle essentially depends on the kinetic mixing factor ϵ and the original mass parameter $\hat{M}_X$ set by the scale of $\mathrm{U}(1)_X$ breaking. To summarize, the diagonalization proceeds by

$$\mathrm{diag}(m_\gamma^2, m_Z^2, m_{Z'}^2) = R_\xi R_\theta M^2 R_\theta^T R_\xi^T, \tag{3.17}$$

where

$$R_\xi = \begin{pmatrix} 1 & 0 & 0 \\ 0 & \cos\xi & \sin\xi \\ 0 & -\sin\xi & \cos\xi \end{pmatrix}. \tag{3.18}$$

There are several phenomenologically relevant limits. If $\hat{M}_X^2 \gg m_{Z,\mathrm{SM}}^2$, then we may expand to first order in their ratio

$$\tan(2\xi) = -\frac{m_{Z,\mathrm{SM}}^2}{\hat{M}_X^2}\,2s_W\,\epsilon\sqrt{1-\epsilon^2} + \mathcal{O}\left(\frac{m_{Z,\mathrm{SM}}^4}{\hat{M}_X^4}\right). \tag{3.19}$$

Accordingly, the masses are given by

$$\begin{aligned} m_Z^2 &= m_{Z,\mathrm{SM}}^2\left(1 - \frac{m_{Z,\mathrm{SM}}^2}{\hat{M}_X^2}\epsilon^2 s_W^2\right) + \mathcal{O}\left(\frac{m_{Z,\mathrm{SM}}^4}{\hat{M}_X^4}\right), \\ m_{Z'}^2 &= \frac{\hat{M}_X^2}{1-\epsilon^2}\left(1 + \frac{m_{Z,\mathrm{SM}}^2}{\hat{M}_X^2}\epsilon^2 s_W^2\right) + \mathcal{O}\left(\frac{m_{Z,\mathrm{SM}}^4}{\hat{M}_X^4}\right) \\ &= \hat{M}_X^2\left(1 + \epsilon^2\left[1 + \frac{m_{Z,\mathrm{SM}}^2}{\hat{M}_X^2}s_W^2\right]\right) + \mathcal{O}(\epsilon^4)\,. \end{aligned} \tag{3.20}$$

Another approximation valid for all masses $\hat{M}_X^2$, but only for small ϵ reads

$$\tan(2\xi) = \frac{2s_W\,\epsilon}{1-\frac{\hat{M}_X^2}{m_{Z,\mathrm{SM}}^2}} + \mathcal{O}(\epsilon^2)\,. \tag{3.21}$$

This limit is most appropriate for dark photon theories with a light and weakly mixed Z'. We will not consider it further here.

Turning to the interactions with fermions, we note that the unnormalized states in Equation (3.1) are given in terms of mass eigenstates by

$$\begin{pmatrix} W^3 \\ \hat{B} \\ \hat{X} \end{pmatrix} = G R_\theta^T R_\xi^T \begin{pmatrix} A \\ Z \\ Z' \end{pmatrix}, \tag{3.22}$$

where

$$G = \begin{pmatrix} 1 & 0 & 0 \\ 0 & 1 & -\frac{\epsilon}{\sqrt{1-\epsilon^2}} \\ 0 & 0 & \frac{1}{\sqrt{1-\epsilon^2}} \end{pmatrix}. \tag{3.23}$$

Applying this, one may transform the vector-fermion interaction terms to the standard form

$$\begin{aligned} \mathcal{L}_{\mathrm{NC}} = \sum_f & -e\, q_f \overline{f}\gamma^\mu f A_\mu - \frac{g}{c_W}\left(g_L^f \overline{f}\gamma^\mu P_L f + g_R^f \overline{f}\gamma^\mu P_R f\right) Z_\mu \\ & - g_X \left(g_{L'}^f \overline{f}\gamma^\mu P_L f + g_{R'}^f \overline{f}\gamma^\mu P_R f\right) Z'_\mu , \end{aligned} \tag{3.24}$$

for $f = e, \nu, N, u, d$. Here q_f denotes the SM electric charge. For simplicity, we show the other couplings only up to linear order in ϵ. In general, one has

$$\begin{aligned} g_L^f &= g_{L,\mathrm{SM}}^f + \frac{g_X c_W}{g} q_X^f \xi , \\ g_{L'}^f &= q_X^f - I_3^f \frac{g}{g_X}\epsilon - \frac{g}{g_X c_W} g_{L,\mathrm{SM}} \xi , \\ g_R^f &= g_{R,\mathrm{SM}}^f + \frac{g_X c_W}{g} q_X^f \xi , \\ g_{R'}^f &= q_X^f - \frac{g}{g_X c_W} g_{R,\mathrm{SM}} \xi , \end{aligned} \tag{3.25}$$

where I_3^f denotes the weak isospin quantum number of f. Note that since $\xi \sim \epsilon + \mathcal{O}(\epsilon^2)$, we simplified $\cos\xi \approx 1$, $\sin\xi \approx \xi$.

3.1.2. Flavored baryon minus lepton number symmetry

When considering U(1) gauge extensions, it is advantageous for the simplicity of the particle content to gauge symmetries which are automatically free from gauge anomalies. In other cases, one frequently has to assume the existence of further new fermions which cancel such anomalies. Particular examples of anomaly free gauge extensions are lepton-flavor symmetries such as $L_\mu - L_\tau$, or baryon number minus lepton number symmetries $B - L$ which are anomaly free if one adds for each fermion generation a SM singlet neutrino with $B - L$ charge -1 [71, 72]. This cancellation, however, holds separately for each fermion generation. Therefore, it is possible to gauge only the third generation $B-L$

which relaxes experimental constraints. Moreover, the single sterile neutrino, which then carries L_3 charge -1, can serve as a dark matter candidate if it is sufficiently stable [73]. The model we present here has been proposed in Reference [73] to explain dark matter. We will first summarize it and then discuss the mapping to SMNEFT and subsequently GNI. The content of this section has been published in Reference [4].

The particle content of the model is a sterile Weyl neutrino N_R with $(B-L)_3$-charge -1, a SM singlet scalar Φ with $(B-L)_3$-charge $+2$ in addition to the SM particles of which the doublet l_τ and the singlet τ_R carry charge -1 while the doublet q_3 and singlets t_R and b_R carry charge $1/3$. The role of the scalar is to break the new U(1) symmetry at a scale $w \gg v$, thereby giving the Z' its mass $m_{Z'} \gg m_Z$. To see this, consider first the sterile neutrino part of the most general Lagrangian of this model

$$\mathcal{L}_N = i\overline{N}_R\gamma^\mu D_\mu N_R + \left(y_\alpha^\nu \bar{l}_\tau N_R \widetilde{H} + \text{H.c.}\right) - \left(\frac{y}{2}\overline{N_R^c} N_R \Phi + \text{H.c.}\right). \tag{3.26}$$

These are, in succession, the kinetic part including the covariant derivative

$$D_\mu = \partial_\mu + ig\frac{\tau^I}{2}W_\mu^I + ig'\frac{Y}{2}B_\mu + ig_X Y_{(B-L)_3}\hat{X}_\mu\,, \tag{3.27}$$

the neutrino Higgs Yukawa term discussed in Section 1.2.1, and a new Yukawa coupling to Φ. The final term will induce a large Majorana mass for N once Φ acquires a vev. The Higgs Yukawa, leading to a Dirac mass term and thereby to a mixing of ν_τ with N is not problematic by itself, since, as discussed in Section 1.2.1, the mass of the active neutrinos can still be small by virtue of the seesaw mechanism. However, this mixing leads to the possible decay of N into light neutrinos, which does pose a problem in the case that N is considered as a dark matter candidate. Since we investigate this option in Chapter 5, we assume a stabilizing $\mathbb{Z}_2$ symmetry under which only N is charged. This forbids the Higgs Yukawa term in Equation (3.26). We then find the complete Lagrangian

$$\begin{aligned}\mathcal{L} = {} & \mathcal{L}_{\text{SM}} + i\overline{N}_R\gamma^\mu\partial_\mu N_R + g_X\hat{X}_\mu\overline{N_R}\gamma^\mu N_R - g_X\sum_f q_X^f\hat{X}_\mu\bar{f}\gamma^\mu f \\ & - \left(\frac{y}{2}\overline{N_R^c}N_R\Phi + \text{H.c.}\right) - \frac{1}{4}\hat{X}^{\mu\nu}\hat{X}_{\mu\nu} - \frac{\epsilon}{2}\hat{X}^{\mu\nu}\hat{B}_{\mu\nu} \\ & + (D^\mu\Phi)^\dagger(D_\mu\Phi) + \mu_\Phi^2\Phi^\dagger\Phi - \lambda_\Phi\left(\Phi^\dagger\Phi\right)^2 - \lambda_{H\Phi}\left(H^\dagger H\right)\left(\Phi^\dagger\Phi\right),\end{aligned} \tag{3.28}$$

where μ_H^2 and μ_Φ^2 are chosen positive, and $f = l_\tau, \tau_R, q_3, t_R, b_R$. Again, 'hatted' fields denote non-canonically normalized gauge fields as in Equation (3.1).

We assume that Φ acquires a large vev $w \gg v$. Then in between the two energy scales, $\text{U}(1)_{(B-L)_3}$ is spontaneously broken and in unitary gauge we can define

$$\Phi = \frac{1}{\sqrt{2}}(w+\phi)\,, \tag{3.29}$$

from which we derive

$$\hat{M}_X^2 = 4g_X^2w^2\,, \qquad m_\phi^2 = 2\mu_\Phi^2\,, \qquad m_N = \frac{y}{\sqrt{2}}w\,. \tag{3.30}$$

The interactions of ϕ read

$$\mathcal{L} \supset \left(-\frac{y}{2\sqrt{2}}\overline{N_R^c}N_R\phi + \text{H.c.}\right) + 2g_X^2 X^\mu X_\mu \phi(\phi+2w) - \frac{\lambda_{H\Phi}}{2}H^\dagger H\phi(\phi+2w)\,. \quad (3.31)$$

The SM gauge symmetry remains intact and thus the Higgs remains massless and there is no scalar mass mixing. Now we concentrate on a certain parameter region of the model where we have $w, m_\phi \gg m_N$. In other words $w \sim \mu_\Phi$ and $y \ll g_X < 1$. In this region, the fields X_μ and ϕ appear only as virtual particles and the correct EFT in between the scale w and either v or m_N (depending which one is larger) is SMNEFT. Note that the situation is now analogous to the setup in Section 3.1.1. Hence, we know that the kinetic mixing leads to a coupling of all fermions to the canonically normalized massive vector field X_μ which is proportional to the mixing parameter ϵ, see Equation (3.8). The parameter ϵ itself has a calculable contribution at the one-loop level. However, this contribution is divergent and requires a renormalization to absorb the divergence. Therefore, ϵ cannot be predicted, but its physical value must be determined by experiment instead. The parameter ϵ can be constrained from electroweak precision data [74] which typically requires it to be below 0.03 for $m_{Z'} < m_Z$ and between approximately 0.05 and 0.3 for $m_{Z'}$ between 200 GeV and 1 TeV.

We now discuss the identification of Wilson coefficients from the fundamental theory. Any lepton-number violation is transmitted via Φ and thus requires an insertion of w. Considering first the dimension-five operators in Equation (2.5), this implies that the Weinberg operator cannot be generated since the lepton doublet does not couple to Φ and does not mix with N due to the $\mathbb{Z}_2$ symmetry. The third operator $\mathcal{O}_{NB}$ vanishes exactly for a single Majorana neutrino. What remains is $\mathcal{O}_{NH}^{(5)}$, which is generated by the tree-level exchange of a ϕ as shown in Figure 3.1a. We find

$$\frac{C_{NH}^{(5)}}{\Lambda} = -\frac{y}{2\sqrt{2}}\frac{1}{m_\phi^2}\lambda_{H\Phi}w = -\frac{m_N\lambda_{H\Phi}}{2\,m_\phi^2}\,. \quad (3.32)$$

The four-fermion operators $\mathcal{O}_{ff'}$ with $f, f' = l, e, N, q, u, d$ are generated by the tree-level exchange of an X boson as shown in Figure 3.1b. We find

$$\frac{C_{ff'}^{\alpha\alpha\beta\beta}}{\Lambda^2} = \frac{g_X^2}{m_X^2}\left[q_X^{f,\alpha}q_X^{f',\beta} - \frac{g'}{g_X}\frac{1}{2}\left(q_X^{f,\alpha}q_Y^{f'} + q_Y^f q_X^{f',\beta}\right)\epsilon + \left(q_X^{f,\alpha}q_X^{f',\beta} + \frac{g'^2}{g_X^2}\frac{1}{4}q_Y^f q_Y^{f'}\right)\epsilon^2\right]. \quad (3.33)$$

This can be understood from Equation (3.8). Notice the following hierarchy of coefficients. When $\alpha = \beta = 3$, $q_X \neq 0$ and the leading contribution is of order ϵ^0/m_X^2. When either α or β is 3 and the other is 1 or 2, the leading contribution is of order ϵ/m_X^2. When neither α nor β is 3, the leading contribution is of order ϵ^2/m_X^2. The lepton number violating operator $\mathcal{O}_{N^4}$ is generated by the exchange of a scalar ϕ but we will not be concerned with this sterile neutrino self-interaction. These are the only four-fermion operators which receive tree-level contributions of new physics. The operators $\mathcal{O}_{eNud}$, $\mathcal{O}_{Nlel}$, $\mathcal{O}_{lNqd}$, $\mathcal{O}'_{lNqd}$, and $\mathcal{O}_{lNuq}$ strictly vanish at any order, since they are forbidden by the $\mathbb{Z}_2$ symmetry.

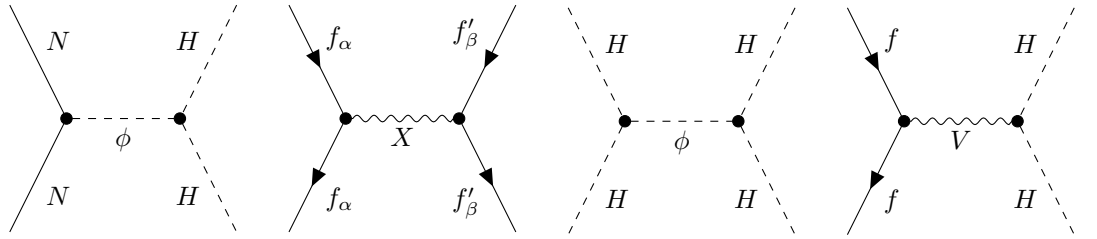

(a) $\mathcal{O}_{NH}^{(5)}$ **(b)** $\mathcal{O}_{ff'}^{\alpha\alpha\beta\beta}$ **(c)** λ_H **(d)** $\mathcal{O}_{Hf}, V = X, B, W$

Figure 3.1. Diagrams contributing to different SMNEFT operators and the effective quartic Higgs coupling at tree-level.

Now we turn to the operators of Table 2.2. The operators of type $\psi^2 H^3$ are generated in the SM via the quartic Higgs coupling. A new physics contribution is derived from the tree-level exchange of a ϕ shown in Figure 3.1c. This exchange amounts effectively to a modified quartic Higgs coupling

$$\lambda_H = \lambda_H^{\text{SM}} + \lambda_{H\phi}^2 \frac{w^2}{m_\phi^2} = \lambda_H^{\text{SM}} + \frac{\lambda_{H\phi}^2}{2} \frac{1}{\lambda_\Phi}\,, \tag{3.34}$$

which we expect to be the experimentally accessible SM Higgs coupling. Next we have the operators of type $\psi^2 H^2$ which are generated by the tree-level diagram shown in Figure 3.1d. The vector V can be B or X in the singlet operator case and is W in the case of triplet fermionic and Higgs bilinears which are signified by a superscript (3). The suppression of the X-exchange diagrams for these operators is always at least ϵ/m_X^2, since the Higgs coupling appears only through B-X-mixing.

If we assume both mixing parameters ϵ and $\lambda_{H\Phi}$ to be small, we can summarize the leading order ($\epsilon^0 \lambda_{H\Phi}^0$) Wilson coefficients as these three types of four-fermion operators

$$C_{LL} = g_X^2 \equiv c\,, \qquad C_{lq}^{(1)} = C_{LQ} = -\frac{g_X^2}{3} \equiv -\frac{c}{3}\,, \qquad C_{qq}^{(1)} = C_{QQ} = \frac{g_X^2}{9} \equiv \frac{c}{9}\,, \tag{3.35}$$

where $LL = ll, NN, ee, Nl, le, Ne$, $LQ = lu, ld, Nq, Nu, Nd, qe, eu, ed$, and $QQ = uu, dd$, qu, qd, ud, and flavor indices 3 are implicit. Consequently, it is a natural choice to define $\Lambda = m_{Z'}$. For matching these operators to LEFT we can use Table 2.6, Table 2.7 and the remaining SMEFT-LEFT-relations from Reference [50]. The neutrino interactions are accompanied by equally large charged fermion interactions. We hence expect the strongest constraints from the latter. Experimental constraints on the model will be discussed in Chapter 5, where besides the four-fermion operators we will also consider $\mathcal{O}_{NH}^{(5)}$ despite its strong suppression. The reason is that dark matter direct detection experiments are highly sensitive to this interaction when N constitutes dark matter.

As a final remark, we note that by itself this model cannot explain the flavor structure of the SM. The problem is that the $(B-L)_3$ symmetry separates the Higgs Yukawa interactions of the first and second generation from those of the third generation. This problem can be alleviated by introducing further particles. One example is to add scalars and vector-like fermions [75]. A second example is to add a scalar with mixed SM and $(B-L)_3$ charges [76].

3.2. Leptoquarks

Scalar extensions of the SM are not restricted by considerations of anomaly cancellation. Moreover, charged scalars are excellent candidates to search for at the LHC. The non-observation so far puts strong constraints on their coupling to the SM and their mass. Neutral scalars are typically less constrained, but consistency of the Higgs sector with the SM requires small mixing between the Higgs and the new scalar. An interesting class of scalar particles consists of the leptoquarks which carry both lepton and baryon number [77]. Traditionally discussed in the context of Grand Unified Theories [78, 79] and later R-parity violating Supersymmetry [80], there has recently been a renewed surge of interest in leptoquarks partially sparked by precision flavor observables like B meson decays that show some tension with SM expectations [81–85]. They are also interesting from the point of view of radiative neutrino mass generation [86–90]. In this thesis, our main interest is the generation of new neutrino interactions, in particular those with sterile neutrinos. Leptoquarks more generally also include vector bosons. In this case it is more intricate to generate the masses since it is required to make some assumptions about the embedding of leptoquarks in a larger new-physics sector. In this section we will first introduce leptoquarks rather generally in Section 3.2.1. Then, we will discuss some particular sets of leptoquarks in slightly more detail. Namely, a particular combination of leptoquarks can on the one hand generate radiative neutrino masses and on the other hand induce some interesting GNI phenomenology, which we discuss in Section 3.2.2. Finally, we discuss the phenomenology of two leptoquarks which can act as mediators between the SM and sterile neutrino dark matter in Section 3.2.3. This section is based mainly on Reference [3]. Whenever we go beyond these previously published results, we point this out in the text.

3.2.1. Heavy leptoquarks and their tree-level EFT matching

All the possible renormalizable couplings of a quark field and a lepton field to a scalar or vector have been labeled in Reference [91]. The list has been extended to include sterile neutrinos in Reference [3], from which we draw in this section. Keeping the distinction between leptoquarks with fermion number $F = 3B + L = 0$ and $F = 2$, the complete interaction Lagrangians read

$$\begin{aligned}\mathcal{L}_{F=2} = &\left(s_{1L}\,\overline{q^c} i\tau_2 l + s_{1e}\,\overline{u_R^c} e_R + s_{1N}\,\overline{d_R^c} N\right) S_1 \\ &+ s_1'\,\overline{d_R^c} e\, S_1' + s_1''\,\overline{u_R^c} N\, S_1'' + s_3 \overline{q^c} i\tau_2 \vec{\tau} l\, \vec{S}_3 \\ &+ \left(v_{2R}\,\overline{q^c}^a \gamma_\mu e_R + v_{2L}\,\overline{d_R^c}\gamma_\mu l^a\right)(i\tau_2)^{ab} V_2^{\mu,b} \\ &+ \left(v_{2R}'\,\overline{q^c}^a \gamma_\mu N + v_{2L}'\,\overline{u_R^c}\gamma_\mu l^a\right)(i\tau_2)^{ab} V_2^{\mu,b'} + \text{H.c.}\,,\end{aligned} \tag{3.36}$$

$$\begin{aligned}\mathcal{L}_{F=0} = &\left(r_{2R}\,\overline{q}^b e_R + r_{2L}\,\overline{u_R}\, l^a (i\tau_2)^{ab}\right) R_2^b \\ &+ \left(r_{2L}'\,\overline{d_R}\, l^a (i\tau_2)^{ab} + r_{2R}'\,\overline{q}^b N\right) R_2^{b'} \\ &+ \left(u_{1L}\,\overline{q}\gamma_\mu l + u_{1e}\,\overline{d_R}\gamma_\mu e_R + u_{1N}\,\overline{u_R}\gamma_\mu N\right) U_1^\mu \\ &+ u_1'\,\overline{u_R}\gamma_\mu e_R\, U_1^{\mu\prime} + u_1''\,\overline{d_R}\gamma_\mu N\, U_1^{\mu\prime\prime} + u_3\,\overline{q}\,\vec{\tau}\gamma_\mu\, l\,\vec{U}_3^\mu + \text{H.c.}\end{aligned} \tag{3.37}$$

Table 3.1. Leptoquarks that can couple to SM particles and right-handed neutrino singlets, together with the operators from Table 2.1 they can generate. Our convention is $Q = I_3 + Y/2$. Exact Wilson coefficients are found in Table 3.2. Operators which do not lead to neutrino interactions are printed in gray.

	F	Spin	$\mathrm{SU(3)_C}$	$\mathrm{SU(2)}_L$	$\mathrm{U(1)}_Y$	Operators
S_1	-2	0	$\overline{3}$	1	2/3	$\mathcal{O}_{lq}^{(1)}, \mathcal{O}_{Nd}, \mathcal{O}_{lNqd}, \mathcal{O}'_{lNqd}, \mathcal{O}_{eluq}, \mathcal{O}'_{eluq}, \mathcal{O}_{eNud}, \mathcal{O}_{eu}$
S_1'	-2	0	$\overline{3}$	1	8/3	$\mathcal{O}_{ed}$
S_1''	-2	0	$\overline{3}$	1	$-4/3$	$\mathcal{O}_{Nu}$
S_3	-2	0	$\overline{3}$	3	2/3	$\mathcal{O}_{lq}^{(3)}$
V_2	-2	1	$\overline{3}$	2	5/3	$\mathcal{O}_{ld}, \mathcal{O}_{elqd}, \mathcal{O}_{qe}$
V_2'	-2	1	$\overline{3}$	2	$-1/3$	$\mathcal{O}_{Nq}, \mathcal{O}_{lu}, \mathcal{O}_{lNuq}$
R_2	0	0	3	2	7/3	$\mathcal{O}_{lu}, \mathcal{O}_{eluq}, \mathcal{O}'_{eluq}, \mathcal{O}_{qe}$
R_2'	0	0	3	2	1/3	$\mathcal{O}_{ld}, \mathcal{O}_{Nq}, \mathcal{O}_{lNqd}, \mathcal{O}'_{lNqd}$
U_1	0	1	3	1	4/3	$\mathcal{O}_{lq}^{(1)}, \mathcal{O}_{Nu}, \mathcal{O}_{elqd}, \mathcal{O}_{lNuq}, \mathcal{O}_{eNud}, \mathcal{O}_{ed}$
U_1'	0	1	3	1	10/3	$\mathcal{O}_{eu}$
U_1''	0	1	3	1	$-2/3$	$\mathcal{O}_{Nd}$
U_3	0	1	3	3	4/3	$\mathcal{O}_{lq}^{(3)}$

The terminology is the same as in Reference [91], except that we replaced 'tilde' symbols with 'prime' symbols. This is because in addition to S_1 and S_1' the inclusion of sterile neutrinos allows for a third $\mathrm{SU(2)}_L$-singlet leptoquark with fermion number $F = 2$ which we call S_1''. Likewise, in addition to the $\mathrm{SU(2)}_L$-singlet vector leptoquarks U_1 and U_1', we introduce U_1''. The list of all scalar and vector leptoquarks and their quantum numbers is shown in Table 3.1. There are some further interactions possible for these leptoquarks, namely

$$\begin{aligned}\mathcal{L}_{F=2}^{\Delta B} = {} & s_{1B}\, l\bar{q} i\tau_2 q^c S_1 + s'_{1B}\, \bar{u}u^c S_1' + s''_{1B}\, \bar{d}d^c S_1'' \\ & + s_{3B}\, \bar{q}\vec{\tau} i\tau_2 q^c \vec{S}_3 + s_{2B}\, \bar{q}\gamma_\mu u^c V_2^\mu + s'_{2B}\, \bar{q}\gamma_\mu d^c V_2^{\mu'}.\end{aligned} \tag{3.38}$$

If these and the interactions in Equations (3.36) and (3.37) are present at the same time, baryon number is violated. In particular, a mixture of these interactions can lead to proton decay. Here we assume that baryon number is conserved, which rules out the operators of Equation (3.38) and avoids strong constraints from proton stability. Generically, the potential of the leptoquarks will include a coupling to the Higgs, i.e. the non-fermionic part of the leptoquark Lagrangian reads

$$\mathcal{L}_X = -m_X^2 X^\dagger X + (D_\mu X)^\dagger D^\mu X - \lambda_{XH} X^\dagger X H^\dagger H\,, \tag{3.39}$$

$$\mathcal{L}_Y = m_Y^2 Y_\mu^\dagger Y^\mu - \frac{1}{2}(Y_{\mu\nu})^\dagger (Y^{\mu\nu}) - \lambda_{YH} Y_\mu^\dagger Y^\mu H^\dagger H\,, \tag{3.40}$$

where X is a scalar leptoquark and Y_μ is a vector leptoquark with the definition

$$Y_{\mu\nu} = D_\mu Y_\nu - D_\nu Y_\mu\,. \tag{3.41}$$

(a) Leptoquark exchange leading to an effective four-fermion interaction $\mathcal{O}_{Nu}$. **(b)** Radiative neutrino mass through S_1 and R_2'.

Figure 3.2. Leptoquark diagrams

We will neglect the portal couplings $\lambda_{XH}, \lambda_{YH}$ for simplicity. If we assume that the leptoquarks are heavy, typically with masses around or above 1 TeV, they can be integrated out giving rise to effective four-fermion SMNEFT operators (or operators of LEFT extended by right-handed neutrinos below the weak scale). As an example consider the tree-level exchange of an S_1'' in Figure 3.2a. This allows us to identify the mass of the leptoquark with Λ and to relate the Wilson coefficients of the SMNEFT operators with the couplings in Equations (3.36) and (3.37). Going beyond our previously published results of Reference [3], we show the resulting Wilson coefficients in Table 3.2, while details of the calculation are delegated to Appendix B.1.

From the point of view of neutrino theory, some of these leptoquarks are particularly interesting. One criterion of interest is to select those leptoquarks which can generate the neutrino mass radiatively, i.e. by means of a loop diagram. These are the topic of Section 3.2.2. A second criterion is to focus on those leptoquarks whose quantum numbers dictate that they couple only to bilinears involving sterile neutrinos, namely S_1'' and U_1''. This opens the interesting possibility that they could be the mediators between thermal relic dark matter and the SM. The two candidates are discussed in Section 3.2.3 and later in the context of dark matter phenomenology in Chapter 5.

3.2.2. Radiative neutrino mass and chirality flipping GNI

Radiative neutrino masses at one loop can only be generated by two particular combinations of two leptoquarks, the scalar combination S_1 (or S_3) and R_2' or the vector combination U_1 (or U_3) and V_2' [90]. This holds for $\mathrm{SU(3)_C}$-triplet leptoquarks. Higher-dimensional representations open new possibilities, e.g. S_1 and a leptoquark in the (6,1,4/6) representation [88]. It is also possible to avoid this selection by considering double copies of some of the $\mathrm{SU(3)_C}$-triplet leptoquarks and introducing 3-leptoquark interactions [90]. We focus here on the simplest minimal scenario S_1 and R_2'. This combination works, because the quantum numbers allow for a scalar coupling of the form

$$\mathcal{L} = \lambda_{SHR}\, S_1 H^\dagger R_2' \,. \tag{3.42}$$

Therefore, one can connect the Higgs vev v to a neutrino propagator by a leptoquark loop, as shown in Figure 3.2b. This diagram results in a neutrino mass approximately

Table 3.2. Wilson coefficients of SMNEFT operators defined in Table 2.1 induced at tree-level by integrating out the leptoquarks in Equations (3.36) and (3.37) and assuming all leptoquark masses are equal to the EFT scale Λ.

Wilson Coefficient	Leptoquark contributions
$(C_{lq}^{(1)})^{\alpha\beta\gamma\delta}$	$-\frac{1}{2}(s_{1L})^*_{\gamma\alpha}(s_{1L})_{\delta\beta} + (u_{1L})^*_{\delta\alpha}(u_{1L})_{\gamma\beta}$
$(C_{lq}^{(3)})^{\alpha\beta\gamma\delta}$	$-\frac{1}{2}(s_3)^*_{\gamma\alpha}(s_3)_{\delta\beta} + (u_3)^*_{\delta\alpha}(u_3)_{\gamma\beta}$
$(C_{eu})^{\alpha\beta\gamma\delta}$	$-\frac{1}{2}(s_{1e})^*_{\gamma\alpha}(s_{1e})_{\delta\beta} + (u'_1)^*_{\delta\alpha}(u'_1)_{\gamma\beta}$
$(C_{ed})^{\alpha\beta\gamma\delta}$	$-\frac{1}{2}(s'_1)^*_{\gamma\alpha}(s'_1)_{\delta\beta} + (u_{1e})^*_{\delta\alpha}(u_{1e})_{\gamma\beta}$
$(C_{Nd})^{\alpha\beta\gamma\delta}$	$-\frac{1}{2}(s_{1N})^*_{\gamma\alpha}(s_{1N})_{\delta\beta} + (u''_1)^*_{\delta\alpha}(u''_1)_{\gamma\beta}$
$(C_{Nu})^{\alpha\beta\gamma\delta}$	$-\frac{1}{2}(s''_1)^*_{\gamma\alpha}(s''_1)_{\delta\beta} + (u_{1N})^*_{\delta\alpha}(u_{1N})_{\gamma\beta}$
$(C_{qe})^{\alpha\beta\gamma\delta}$	$\frac{1}{2}(r_{2R})_{\alpha\delta}(r_{2R})^*_{\beta\gamma} - (v_{2R})^*_{\alpha\gamma}(v_{2R})_{\beta\delta}$
$(C_{Nq})^{\alpha\beta\gamma\delta}$	$\frac{1}{2}(r'_{2R})_{\gamma\beta}(r'_{2R})^*_{\delta\alpha} - (v'_{2R})^*_{\gamma\alpha}(v'_{2R})_{\delta\beta}$
$(C_{lu})^{\alpha\beta\gamma\delta}$	$\frac{1}{2}(r_{2L})^*_{\delta\alpha}(r_{2L})_{\gamma\beta} - (v'_{2L})_{\gamma\alpha}(v'_{2L})^*_{\delta\beta}$
$(C_{ld})^{\alpha\beta\gamma\delta}$	$\frac{1}{2}(r'_{2L})^*_{\delta\alpha}(r'_{2L})_{\gamma\beta} - (v_{2L})_{\gamma\alpha}(v_{2L})^*_{\delta\beta}$
$(C_{eNud})^{\alpha\beta\gamma\delta}$	$-\frac{1}{2}(s_{1e})^*_{\gamma\alpha}(s_{1N})_{\delta\beta} + (u_{1e})^*_{\delta\alpha}(u_{1N})_{\gamma\beta}$
$(C_{elqd})^{\alpha\beta\gamma\delta}$	$-2(v_{2L})_{\delta\beta}(v_{2R})^*_{\gamma\alpha} - 2(u_{1L})_{\gamma\beta}(u_{1e})^*_{\delta\alpha}$
$(C_{eluq})^{\alpha\beta\gamma\delta}$	$\frac{1}{2}(s_{1L})_{\delta\beta}(s_{1e})^*_{\gamma\alpha} + \frac{1}{2}(r_{2R})^*_{\delta\alpha}(r_{2L})_{\gamma\beta}$
$(C'_{eluq})^{\alpha\beta\gamma\delta}$	$-\frac{1}{8}(s_{1L})_{\delta\beta}(s_{1e})^*_{\gamma\alpha} + \frac{1}{8}(r_{2R})^*_{\delta\alpha}(r_{2L})_{\gamma\beta}$
$(C_{lNqd})^{\alpha\beta\gamma\delta}$	$\frac{1}{2}(s_{1L})^*_{\gamma\alpha}(s_{1N})_{\delta\beta} + \frac{1}{2}(r'_{2R})_{\gamma\beta}(r'_{2L})^*_{\delta\alpha}$
$(C'_{lNqd})^{\alpha\beta\gamma\delta}$	$-\frac{1}{8}(s_{1L})^*_{\gamma\alpha}(s_{1N})_{\delta\beta} + \frac{1}{8}(r'_{2R})_{\gamma\beta}(r'_{2L})^*_{\delta\alpha}$
$(C_{lNuq})^{\alpha\beta\gamma\delta}$	$-2(v'_{2R})_{\delta\beta}(v'_{2L})^*_{\gamma\alpha} - 2(u_{1L})^*_{\delta\alpha}(u_{1N})_{\gamma\beta}$

given by [86, 92]

$$m_\nu^{\alpha\beta} \sim \frac{3}{\sqrt{2}} \frac{r_{2L}^{\alpha 3} s_{1L}^{3\beta}}{16\pi^2} m_b \frac{\lambda_{SHR} v}{m^2}\,, \tag{3.43}$$

where we assume the bottom quark to run in the loop and that $m_{S_1} \approx m_{R'_2} \approx m$. To explain the neutrino masses of order $m_\nu \sim 0.1\,\text{eV}$ for $\lambda_{SHR} \sim v$ and $m \sim 1\,\text{TeV}$ one needs couplings $r'_{2L}, s_{1L} \lesssim 10^{-2}$-$10^{-3}$.

On the other hand, these two leptoquarks can also generate the phenomenologically very interesting operators $\mathcal{O}_{lNqd}$ and $\mathcal{O}'_{lNqd}$ which induce simultaneously charged-current and neutral-current (pseudo)scalar and tensor GNI. In Section 4.3, we discuss how both of these can be detected by different experiments. Besides generating neutrino masses, these leptoquarks could be responsible for B physics anomalies at the same time [92], which we do not discuss further here. The vector combination for radiative neutrino masses U_1 and V'_2 is discussed in detail in Reference [87]. We note here only that these two leptoquarks can generate another very interesting operator $\mathcal{O}_{lNuq}$ which induces charged-current and neutral-current GNI at the same time. We summarize that it is precisely the leptoquarks generating radiative neutrino masses which generate the SMNEFT operators $\mathcal{O}_{eNud}$, $\mathcal{O}_{lNuq}$, $\mathcal{O}^{(\prime)}_{lNqd}$ which in turn induce the charged-current sterile neutrino GNI on the right-hand side of Table 2.7.

Let us slightly extend the discussion in Reference [3] on these operators. In Section 4.3.3

we show that current bounds from beta decay, pion decay and coherent elastic neutrino-nucleus scattering demand that if only one of the three operators is present at a time, we have

$$\begin{aligned} |C^{ee11}_{lNqd}| &\leq 4.0 \times 10^{-4} \cdot \sqrt{8} G_F \Lambda^2 \,, \\ |C'^{ee11}_{lNqd}| &\leq 2.4 \times 10^{-2} \cdot \sqrt{8} G_F \Lambda^2 \,. \end{aligned} \tag{3.44}$$

With the identification in Table 3.2 we thus have for S_1 and R_2

$$\begin{aligned} \frac{1}{2}(s_{1L})^*_{1e}(s_{1N})_{1e} + \frac{1}{2}(r'_{2R})_{1e}(r'_{2L})^*_{1e} &\leq 1.3 \times 10^{-2} \,, \\ -\frac{1}{8}(s_{1L})^*_{1e}(s_{1N})_{1e} + \frac{1}{8}(r'_{2R})_{1e}(r'_{2L})^*_{1e} &\leq 7.9 \times 10^{-1} \,, \end{aligned} \tag{3.45}$$

where we assumed for simplicity $\Lambda = m_{S_1} = m_{R_2} = 1\,\text{TeV}$ which as we mentioned fits the radiative neutrino mass scenario in Reference [92] when $s_{1L}, r'_{2L} \sim 10^{-2}$-$10^{-3}$. This gives us an idea of the coupling magnitude that would be needed for an effect that is close but below the current sensitivity, namely s_{1N} or r'_{2R} of order 1. This would be an example for a mixture of Scenario 1 and Scenario 3 in Section 4.3.3.[1] Depending on the signs of the couplings and potential cancellations in Equation (3.45) we could in principle even have tensor and (pseudo)scalar interactions close to the detection limit at the same time. Let us finally comment on Scenario 2 of Section 4.3.3. Here we need C_{lNqd} and C_{lNuq} to be of opposite sign and approximately equal magnitude. From Table 3.2 we conclude that we then need either S_1 or R'_2 and either V'_2 or U'_1 with appropriately matching couplings, which is possible but cannot generically be expected.

3.2.3. Two potential dark matter mediators

Our second focus is on S''_1 and U''_1, because these leptoquarks couple only to fermion bilinears involving a sterile neutrino. Besides the sterile neutrino, they couple to either u_R or d_R. The absence of any strongly-constrained four-charged-fermion interactions hence makes these leptoquarks attractive candidates to explain sizable new neutrino interactions. As a particular example, we consider S''_1 and U''_1 as the mediators between WIMP-like sterile neutrino dark matter N and the SM in Chapter 5. The remaining part of this section accordingly follows Reference [4] on which Chapter 5 is based. The corresponding Lagrangians of the two dark matter models we consider read

$$\begin{aligned} \mathcal{L}_{S\text{-LQ}} &= -m_S^2 S^\dagger S + (D^\mu S)^\dagger D_\mu S + x_t\, \overline{t^c_R} N\, S + x_t^*\, (S)^\dagger \overline{N} t^c_R \,, \\ \mathcal{L}_{U\text{-LQ}} &= m_U^2 U_\mu^\dagger U^\mu - \frac{1}{2}(U^{\mu\nu})^\dagger U_{\mu\nu} - i g_S \kappa\, U_\mu^\dagger T^A U_\nu G^A_{\mu\nu} \\ &\quad + x_b\, \overline{b_R} \gamma_\mu N_R\, U^\mu + x_b^*\, U^{\dagger\mu} \overline{N_R} \gamma_\mu b_R \,, \end{aligned} \tag{3.46}$$

where we renamed the leptoquarks to S and U and the couplings to x_t and x_b for compactness, and

$$U_{\mu\nu} = D_\mu U_\nu - D_\nu U_\mu \,, \qquad D_\mu = \partial_\mu + i g_s T^A G^A_\mu \,. \tag{3.47}$$

[1] Strictly speaking those bounds are obtained assuming only one Wilson coefficient at a time, but we assume here that the combined bounds are comparable.

The parameter κ is fixed by the UV origin of the vector leptoquark and is either one or zero, see e.g. Reference [93]. In these models the crucial SMNEFT operators responsible for the coupling of dark matter to the thermal bath until freeze-out are the tree-level generated $\mathcal{O}_{Nu}$ for the case of S_1'' and $\mathcal{O}_{Nd}$ for U_1''. Following Table 3.2, the effective interaction Lagrangians are given in terms of couplings and masses by

$$\begin{aligned}\mathcal{L}_{Nt} &= -\frac{|x_t|^2}{2m_{S_1''}^2}(\overline{N_R}\gamma_\mu N_R)(\overline{t_R}\gamma^\mu t_R)\,,\\ \mathcal{L}_{Nb} &= \frac{|x_b|^2}{m_U^2}(\overline{b_R}\gamma^\mu N_R)(\overline{N_R}\gamma_\mu b_R)\,.\end{aligned} \tag{3.48}$$

In the language of SMNEFT, we identify

$$C_{Nu}^{3333} = -\frac{1}{2}|x_t|^2 \qquad \text{for } \Lambda = m_S\,, \tag{3.49}$$

$$C_{Nd}^{3333} = |x_b|^2 \qquad \text{for } \Lambda = m_U\,. \tag{3.50}$$

Additionally, in the context of direct detection, the loop-induced operator $\mathcal{O}_{NH}^{(5)}$ becomes relevant, since it generates a Higgs portal between the sterile neutrino dark matter and the SM. The effective Higgs coupling for an S_1'' leptoquark which couples only to the top quark and Majorana dark matter has been calculated in Reference [94]. In our SMNEFT language[2] it reads

$$\frac{C_{NH}^{(5)}}{\Lambda} = -\frac{y_t^2|x_t|^2 m_N}{64\pi^2 m_t^2}\left(F(r) + \frac{s}{m_t^2}G(r) + \frac{m_N^2}{m_t^2}H(r)\right), \tag{3.51}$$

in the limit of $\sqrt{s}, m_N \ll m_S$, where y_t is the SM top Yukawa coupling, $r = m_S^2/m_t^2$ and the functions $F(r)$, $G(r)$, and $H(r)$ are given in Eq.(10) of Reference [95]. These are all the operators up to dimension six which play a role in our discussion of dark matter in Chapter 5.

3.3. Loop-induced interactions

Much like neutrino masses can be induced radiatively by some of the leptoquarks discussed in Section 3.2, it is possible that GNI are generated as a loop effect. In both cases there lies theoretical appeal in the fact that the observed smallness of both neutrino masses and GNI would be well-explained if they are loop-suppressed. Following Reference [1], we focus here on neutral-current NSI of the form $\epsilon_{L,f}$ and $\epsilon_{R,f}$, where $f = e, u, d$. As discussed in Section 4.1, these are most relevant to the coherent forward scattering of active neutrinos in matter which is important for the correct interpretation of neutrino oscillation experiments. When discussing experimental constraints, we will, however, deviate from Reference [1] and work based on the results of Chapter 4.

[2]Compared to Reference [95] we identify $g_{h\chi\chi}/v = 2C_{NH}^{(5)}/\Lambda$.

The approach taken in this section can be described as "bottom up" compared to the "top-down" explicit models of Section 3.1 and Section 3.2. This means that we start from the question which scalar interactions can induce the neutral-current NSI Lagrangian[3]

$$\mathcal{L} = \sqrt{8} G_F \sum_{f=e,u,d} \sum_{X=L,R} \epsilon^{\alpha\beta}_{X,f} (\overline{\nu}_\alpha \gamma_\mu P_L \nu_\beta)(\overline{f} \gamma^\mu P_X f) \,. \tag{3.52}$$

Noting that the fermionic currents in Equation (3.52) are all (axial) vector currents, we conclude that for a tree-level scalar exchange to induce this interaction there has to be a Fierz-transformation (see Appendix A.3) which translates from scalar currents to vector currents. Upon Fierz-transforming the Lagrangian in Equation (3.52) using Equations (A.26) and (A.27), one finds that only for $X = R$ the result involves scalar currents,

$$\mathcal{L} = -2(\overline{\nu}_\alpha P_R f)(\overline{f} P_L \nu_\beta) \,. \tag{3.53}$$

If this Lagrangian is induced by a scalar exchange, this scalar must carry the same charged as $(\overline{\nu}_\alpha P_R f)$. Moreover, if $f = u, d$, it needs to be colored, i.e. we recover the leptoquarks discussed in Section 3.2. An example of a model with a color-neutral scalar that induces the leptonic interaction of the type $\overline{\nu_L} e_R \overline{e_R} \nu_L$ is the type-II seesaw model as explained in Section 1.2. Recall that in these models neutrino masses are explained by a heavy $\mathrm{SU}(2)_L$-triplet scalar Δ, whose charge-1 component Δ^+ serves as the charged scalar to produce the leptonic NSI [41]. The fact that these charged scalars and leptoquarks are strongly constrained typically leads to very constrained matter NSI for the active neutrinos. It is therefore interesting to ask if larger NSI can be obtained by loop processes, in particular with neutral scalars, which we discuss next.

Two possible types of one-loop Feynman diagrams leading to NSI are shown in Figure 3.3. The first diagram, which we call the triangle diagram, relies on a modified coupling of neutrinos to the Z boson. This modified coupling is generated by a triangular loop involving a scalar and two mediator fermions ψ whose common charge is dictated by the charge of the scalar. Such a diagram is logarithmically divergent. In a UV complete theory it must either be possible to absorb this divergence in a counter term in the Lagrangian, or in the sum of all contributing diagrams the divergent parts must cancel. The second diagram, which we call the box diagram, involves two scalar propagators and two fermionic propagators which can again be different depending on the charge of the scalar. This diagram is UV finite, since in the loop there is an additional propagator compared to the triangle loop. In all cases, our notation is that the interaction Lagrangian of ϕ reads

$$\mathcal{L}_\phi = \sum_\alpha y_\alpha \, \overline{\psi} \nu_{L\alpha} \phi + y_f \, \overline{\psi'} f \phi + \text{H.c.} \,, \tag{3.54}$$

where the second Yukawa term is required only for the box diagram.

First we consider the triangle diagram. In the case that the divergences cancel, the effective Z coupling with the SM plus the loop contribution in the limit $m_\psi \ll m_Z, m_\phi$

[3]Note that we use here projection operators $P_L = (1-\gamma^5)/2$ and $P_R = (1+\gamma^5)/2$, while the original GNI operators in Table 2.4 were defined with $1-\gamma^5$ and $1+\gamma^5$ instead. To keep the definition consistent, we compensate for the two factors of $1/2$ by replacing the prefactor $G_F/\sqrt{2}$ with $\sqrt{8} G_F$.

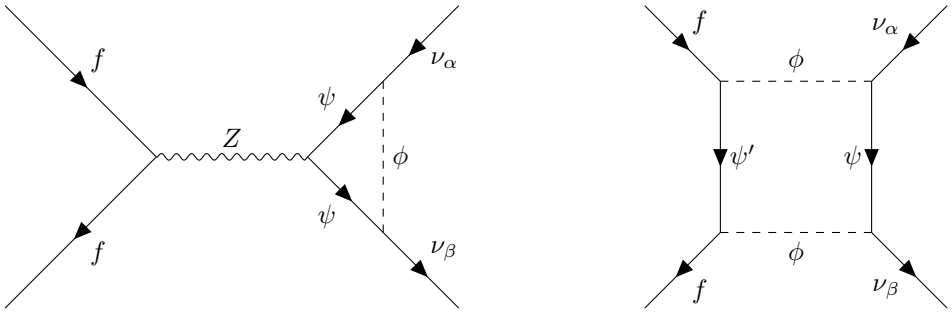

(a) Triangle diagram **(b)** Box diagram

Figure 3.3. One-loop diagrams inducing neutral-current matter NSI involving a new scalar ϕ. Which fermions ψ and ψ' are depends on the scalar's charge.

reads

$$\mathcal{L}_{Z,\nu} = -\frac{g}{2c_W} Z_\mu (g_L^\nu \delta_{\alpha\beta} + g_{\alpha\beta}^{(1)})(\overline{\nu}_\alpha \gamma_\mu (1-\gamma^5)\nu_\beta)\,, \tag{3.55}$$

where

$$g_{\alpha\beta}^{(1)} = \frac{y_\alpha^* y_\beta}{16\pi^2} \frac{m_Z^2}{m_\phi^2} \left[f(r) g_L^\nu + h(r) g_R^\psi \right]. \tag{3.56}$$

Here $g_L^\nu = \frac{1}{2}$ is the Z-charge of the left-handed neutrinos, $f(r)$ and $h(r)$ are finite complex functions of $r = m_Z^2/m_\phi^2$. The left and right Z-charges of e, u and d have been collected in Equation (1.16). The model is renormalizable, i.e. the divergences cancel, if ϕ carries a Z charge g^ϕ as well such that

$$g^\phi = g_R^\psi - g_L^\nu\,. \tag{3.57}$$

After integrating out the Z boson and calculating the finite box diagram, the induced NSI coefficients in the generic case read

$$\mathcal{L}_{\text{NSI}} = \sqrt{8} G_F \sum_{f=e,u,d} \sum_{X=L,R} \left(\left(\epsilon_{X,f}^{\triangleright}\right)^{\alpha\beta} + \left(\epsilon_{X,f}^{\square}\right)^{\alpha\beta} \right) (\overline{f}\gamma^\mu P_X f)(\overline{\nu_\alpha}\gamma_\mu P_L \nu_\beta)\,, \tag{3.58}$$

where

$$\left(\epsilon_{X,f}^{\triangleright}\right)^{\alpha\beta} = -2 g_{\alpha\beta}^{(1)} g_X^f \frac{c_W}{g} = -\frac{y_\alpha^* y_\beta}{8\pi^2} \frac{m_Z^2}{m_\phi^2} g_X^f \left[f(r) g_L^\nu + h(r) g_R^\psi \right], \tag{3.59}$$

$$\left(\epsilon_{X,f}^{\square}\right)^{\alpha\beta} = \frac{y_\alpha^* y_\beta |y_f|^2}{16\pi^2} \frac{\sqrt{2}}{G_F} \frac{1}{16 m_\phi^2} = \frac{y_\alpha^* y_\beta |y_f|^2}{32\pi^2} \frac{c_W^2}{g^2} \frac{m_Z^2}{m_\phi^2}, \tag{3.60}$$

again in the limit of all fermion masses including ψ' being negligible compared to m_ϕ and m_Z. We now review three example choices of scalars and which experimental constraints come into play for them.

3.3.1. The minimal charged Higgs model

The minimal charged Higgs model is our only example with a charged scalar and serves partially to demonstrate how the two diagrams are generated and how the strong constraints on charged scalars imply strongly constrained NSI. The scalar ϕ is an $\mathrm{SU}(2)_L$-singlet with hypercharge 2 and therefore the gauge-invariant Lagrangian reads

$$\mathcal{L}_\phi = \mathcal{L}_{\mathrm{SM}} + |D_\mu \phi|^2 - m_\phi^2 |\phi|^2 - V(\phi, H) + \left(\sum_{\alpha,\beta} y_{\alpha\beta} \overline{l_\alpha^c} (i\tau_2) l_\beta \phi + \mathrm{H.c.} \right), \tag{3.61}$$

where $V(\phi, H)$ denotes all quartic scalar interactions involving at least one factor of ϕ. This model has previously been studied in References [96–98], but we focus here on the loop-induced NSI. The important point is that there is only one Yukawa interaction term and it is antisymmetric in flavor space, because

$$\overline{l_\alpha^c}(i\tau_2) l_\beta = \overline{\nu_{L\alpha}^c} e_{L\beta} - \overline{e_{L\alpha}^c} \nu_{L\beta} = \overline{\nu_{L\alpha}^c} e_{L\beta} - \overline{\nu_{L\beta}^c} e_{L\alpha} = -\overline{l_\beta^c}(i\tau_2) l_\alpha \,, \tag{3.62}$$

and so $y_{\alpha\beta} = -y_{\beta\alpha}$. For convenience, we write out the Yukawa Lagrangian in components,

$$\begin{aligned} \mathcal{L}_{\mathrm{Yukawa}} = {} & 2y_{e\mu} \left(\overline{\nu_e^c} \mu_L - \overline{\nu_\mu^c} e_L \right) \phi + 2y_{\mu\tau} \left(\overline{\nu_\mu^c} \tau_L - \overline{\nu_\tau^c} \mu_L \right) \phi \\ & + 2y_{\tau e} \left(\overline{\nu_\tau^c} e_L - \overline{\nu_e^c} \tau_L \right) \phi + \mathrm{H.c.} \end{aligned} \tag{3.63}$$

We assume that $m_\phi \gg m_Z$ to avoid strong constraints on charged scalars. Therefore, it is instructive to apply the SMNEFT framework directly on Equation (3.61) and confirm the equivalence to the calculation on the basis of Equation (3.63) performed in Reference [1]. Integrating ϕ from Equation (3.61) while ignoring the scalar potential yields,

$$C_{ll}^{\alpha\beta\gamma\delta} = -C_{ll}^{\alpha\delta\gamma\beta} = -2 y_{\beta\delta} y_{\alpha\gamma}^* \,, \tag{3.64}$$

identifying $\Lambda^2 = m_\phi^2$ as we show in Appendix B.2. This relation also ensures that the four-neutrino and four-charged-lepton interaction terms generically implied by $\mathcal{O}_{ll}$ vanish, since their strength is proportional to $C^{\alpha\beta\gamma\delta} + C^{\alpha\delta\gamma\beta} = 0$, see Equation (2.16). Note that this definition also automatically ensures Hermiticity,

$$C_{ll}^{\alpha\beta\gamma\delta} = (C_{ll}^{\beta\alpha\delta\gamma})^* \,. \tag{3.65}$$

The leptonic NSI can then be read off from the first entry of Table 2.6 adjusted for generic Λ,

$$\epsilon_{L,e}^{\alpha\beta\gamma\delta} = -C_{ll}^{\alpha\beta\gamma\delta} = 2 y_{\beta\delta} y_{\alpha\gamma}^* \frac{1}{\sqrt{8} G_F \Lambda^2} \,. \tag{3.66}$$

These are the tree-level NSI. For the interactions with electrons, where $\gamma = \delta = e$, there are only NSI of neutrino flavors $\mu\mu$, $\mu\tau$ and $\tau\tau$. This changes once we proceed to the loop level.

Considering the diagrams in Figure 3.3, we can identify ψ with e_L^c, μ_L^c, τ_L^c for $(\alpha, \beta) = (\mu, \tau), (\tau, e), (e, \mu)$, respectively. In the triangle diagram, f can be a charged lepton or a quark, while in the box diagram the required direct coupling of f to ϕ requires f to be

a left-handed charged lepton. To ensure the correctness of applying Equation (3.59), we check for the correct Z charge of ϕ to ensure renormalizability of the triangle diagram. It can be read off the gauge-kinetic term in the Lagrangian after performing the Weinberg rotation,

$$D_\mu\phi = \partial_\mu - ig'B_\mu\frac{Y_\phi}{2}\,\phi = \partial_\mu - i\frac{g}{c_W}(-s_W^2)Z_\mu\phi - igs_W A_\mu\phi\,, \tag{3.67}$$

so that $g^\phi = -s_W^2$. We then have the renormalizability condition (3.57) satisfied, since

$$g_R^{(e^c)} - g_L^\nu = (-g_L^e) - g_L^\nu = \frac{1}{2} - s_W^2 - \frac{1}{2} = -s_W^2 = g^\phi\,. \tag{3.68}$$

Therefore we can use Equations (3.59) and (3.60) to conclude

$$\left(\epsilon^{\triangleright}_{X,f}\right)^{\alpha\beta\gamma\gamma} = -g_X^f\sum_\delta \frac{y^*_{\alpha\delta}y_{\beta\delta}}{2\pi^2}\frac{m_Z^2}{m_\phi^2}\left[f(r)g_L^\nu + h(r)(-g_L^e)\right] \tag{3.69}$$

$$\approx -g_X^f\sum_\delta \frac{y^*_{\alpha\delta}y_{\beta\delta}}{8\pi^2}\frac{m_Z^2}{m_\phi^2}\frac{2}{3}\left[\frac{c_W^2}{3} - (1-2s_W^2)\left(\log\frac{m_Z^2}{m_\phi^2} - i\pi\right)\right], \tag{3.70}$$

for $f = e, u, d$, $X = L, R$, and where we sum over δ corresponding to the internal fermion lines of $\psi = e^c_{L\delta}$ which has one contribution if $\alpha \neq \beta$ and two contributions if $\alpha = \beta$. The approximation follows the asymptotic limits of the functions $f(r)$ and $h(r)$ for $r = m_Z^2/m_\phi^2 \ll 1$ provided in Reference [1]. The factor of 2 in the identification of the couplings $y_\alpha = 2y_{\alpha\delta}$, $y_\beta = 2y_{\beta\delta}$ is due to the factor of 2 difference in Equation (3.63) and Equation (3.54).

In the box diagram, ψ' must be identified with the two neutrino species with flavors different from f. Explicitly, for $f = e_L, \mu_L, \tau_L$, there are contributions from ψ' being ν_μ and ν_τ, ν_e and ν_τ, or ν_e and ν_μ, respectively. Formula (3.60) then implies the matter NSI

$$\left(\epsilon^{\square}_{L,e}\right)^{\alpha\beta} = \frac{\sum_\delta y^*_{\alpha\delta}y_{\beta\delta}}{16\pi^2}\frac{\sqrt{2}}{G_F}\frac{1}{m_\phi^2}\left(|y_{e\mu}|^2 + |y_{e\tau}|^2\right). \tag{3.71}$$

More generally, we could have any flavor indices for the charged leptons, i.e.

$$\left(\epsilon^{\square}_{L,e}\right)^{\alpha\beta\gamma\delta} = \frac{\sum_\rho y^*_{\alpha\rho}y_{\beta\rho}}{16\pi^2}\frac{\sqrt{2}}{G_F}\frac{1}{m_\phi^2}\sum_{\rho\neq\gamma,\delta}\left(y_{\gamma\rho}y^*_{\delta\rho}\right). \tag{3.72}$$

We observe that there are a lot of NSI generated at the same time, depending on the flavor structure of the Yukawa couplings.

This model radiatively generates charged lepton flavor violation (CLFV) as can be seen, for instance, from the box diagram. Since CLFV is experimentally strongly constrained, it turns out that these are the strongest constraints on this model and therefore also on the NSI. This is a common feature which we will explore further in Chapter 4: When flavor-changing neutrino interactions are generated from new physics above the weak scale which is invariant under the SM gauge symmetry then usually also lepton flavor violating interactions between charged leptons are generated with couplings of similar magnitude.

Hence the strong CLFV constraints then also strongly constrain the neutrino interactions. In the case of the minimal charged Higgs model, the most important constraint comes from the radiative decays $e_\alpha \to e_\beta\gamma$ and $e_\alpha \to e_\beta e_{\beta'}\overline{e}_{\beta'}$ whose rates obey

$$\begin{aligned}\frac{\Gamma(e_\alpha \to e_\beta\gamma)}{\Gamma(e_\alpha \to e_\beta\nu_\alpha\overline{\nu}_\beta)} &= \frac{1}{16\pi^2}\frac{g^2 s_W^2}{12}\left|\frac{\sum_\delta y_{\alpha\delta}y^*_{\beta\delta}}{m_\phi^2 G_F}\right|^2,\\ \frac{\Gamma(e_\alpha \to e_\beta e_{\beta'}\overline{e}_{\beta'})}{\Gamma(e_\alpha \to e_\beta\nu_\alpha\overline{\nu}_\beta)} &= \frac{c_W^2}{g^2}\left|2g^{(1)}_{\alpha\beta}g^e_L\right|^2.\end{aligned} \tag{3.73}$$

We will discuss some more details about CLFV in Section 4.2, but here let us simply quote the current bounds on these processes for the different flavor combinations. These are [36]

$$\begin{aligned}&\mathrm{Br}(\mu \to \nu_\mu e\overline{\nu_e}) \approx 100\%\,,\\ &\mathrm{Br}(\tau \to \nu_\tau e\overline{\nu_e}) = (17.82 \pm 0.04)\%\,, \qquad \mathrm{Br}(\tau \to \nu_\tau \mu\overline{\nu_\mu}) = (17.39 \pm 0.04)\%\,,\end{aligned} \tag{3.74}$$

for the SM branching fractions, and for the lepton flavor violating ones[4]

$$\begin{aligned}&\mathrm{Br}(\mu \to e\gamma) < 4.2\times10^{-13}\,, \qquad &&\mathrm{Br}(\mu \to 3e) < 1.0\times10^{-12}\,,\\ &\mathrm{Br}(\tau \to e\gamma) < 3.3\times10^{-8}\,, \qquad &&\mathrm{Br}(\tau \to 3e) < 2.7\times10^{-8}\,,\\ &\mathrm{Br}(\tau \to \mu\gamma) < 4.4\times10^{-8}\,, \qquad &&\mathrm{Br}(\tau \to 3\mu) < 2.1\times10^{-8}\,.\end{aligned} \tag{3.75}$$

From these we can derive bounds on $g^{(1)}_{\alpha\beta}$ defined in Equation (3.56) of

$$\begin{aligned}&(\mu \to e\gamma):\ |g^{(1)}_{\mu e}| < 7.7\times10^{-8}\,, \qquad &&(\mu \to 3e):\ |g^{(1)}_{\mu e}| < 1.3\times10^{-6}\,,\\ &(\tau \to e\gamma):\ |g^{(1)}_{\tau e}| < 5.0\times10^{-5}\,, \qquad &&(\tau \to 3e):\ |g^{(1)}_{\tau e}| < 5.1\times10^{-4}\,,\\ &(\tau \to \mu\gamma):\ |g^{(1)}_{\tau \mu}| < 6.0\times10^{-5}\,, \qquad &&(\tau \to 3\mu):\ |g^{(1)}_{\tau \mu}| < 4.5\times10^{-4}\,.\end{aligned} \tag{3.76}$$

The values on the left-hand side depend logarithmically on m_Z^2/m_ϕ^2. For definiteness, we have fixed $m_\phi = 500\,\mathrm{GeV}$. Since the bounds from $e_\alpha \to e_\beta\gamma$ are generally stronger, we apply those bounds to the NSI coefficients of Equation (3.59)

$$\begin{aligned}&|(\epsilon^{\triangleright}_{X,f})^{\mu e}| < 2.2\times10^{-7}\,g_X^f\,, \qquad &&|(\epsilon^{\square}_{X,f})^{\mu e}| < 1.7\times10^{-6}\,,\\ &|(\epsilon^{\triangleright}_{X,f})^{\tau e}| < 1.4\times10^{-4}\,g_X^f\,, \qquad &&|(\epsilon^{\square}_{X,f})^{\tau e}| < 1.1\times10^{-3}\,,\\ &|(\epsilon^{\triangleright}_{X,f})^{\tau \mu}| < 1.6\times10^{-4}\,g_X^f\,, \qquad &&|(\epsilon^{\square}_{X,f})^{\tau \mu}| < 1.3\times10^{-3}\,,\end{aligned} \tag{3.77}$$

where for the box parameters on the right-hand side we assume $|y_{e\mu}|^2, |y_{e\tau}|^2 < 1$. These values confirm that even loop-induced NSI are very strongly constrained for a new charged mediator. Note that direct bounds on neutrino-flavor changing NSI are typically much less stringent, namely of the order 10^{-1}-10^{-2} as we discuss in Section 3.3.2 and more broadly in Chapter 4.

[4]The bound on $\mu \to e\gamma$ has mildly improved from the value of 3.7×10^{-13} used in Reference [1]. We present here the results for the updated value.

3.3.2. Neutral scalar bosons

For this model we introduce a neutral instead of a charged scalar singlet. The generic Yukawa interaction Lagrangian below the weak scale then reads

$$\mathcal{L}_\phi \supset y^\nu_{\alpha\beta}\overline{\nu_\alpha}\nu_\beta\phi + \sum_{\psi=e,u,d} y^f_{\alpha\beta}\overline{f}_\alpha f_\beta\phi + \text{H.c.} \tag{3.78}$$

This Lagrangian is defined in terms of the fields in the broken phase of the electroweak symmetry. As it stands, it is not gauge invariant under the full SM gauge group and therefore clearly not UV complete. Rather, it should be considered as part of a more complete model. Upon integrating out ϕ at tree level one obtains no matter NSI, but the chirality-flipping GNI of scalar type. Namely, the effective tree-level GNI Lagrangian reads

$$\mathcal{L}^0_{\text{GNI}} = -\frac{y^\nu_{\alpha\beta}y^{f*}_{\delta\gamma}}{m^2_\phi}\,\overline{\nu_\alpha}\nu_\beta\overline{f}_\gamma f_\delta\,, \tag{3.79}$$

from which we identify

$$\epsilon^{\alpha\beta\gamma\delta}_S = \widetilde{\epsilon}^{\alpha\beta\gamma\delta}_S = \frac{y^\nu_{\alpha\beta}y^{f*}_{\delta\gamma}}{2}\frac{\sqrt{2}}{G_F\,m^2_\phi}\,. \tag{3.80}$$

Of course there are similar scalar interactions induced for the charged fermions. For considering loop diagrams it is necessary to distinguish Majorana and Dirac neutrinos. Indeed, in the case of Dirac neutrinos the interaction term would be of the structure $\overline{\nu_R}\nu_L\phi$ and therefore in Figure 3.3a ψ would have to be ν_R which has no coupling to the Z boson. Therefore there are no NSI from the triangle diagram. In the Majorana case the interaction would be of the structure $\overline{\nu^c_L}\nu_L\phi$ where ν^c_L does couple to the Z boson. In this case one could even assign a lepton number to ϕ if the couplings to charged fermions vanish. Such new interactions which only affect the neutrino sector are called secret neutrino interactions. Let us first consider the case of secret neutrino interactions and Majorana neutrinos taking $y^f = 0$ and then the less secluded case with charged fermion interactions and Dirac neutrinos.

Secret neutrino interactions

In the case of secret neutrino interactions, the interaction Lagrangian (3.78) becomes

$$\mathcal{L}_\phi \supset y_{\alpha\beta}\overline{\nu^c_{L\alpha}}\nu_{L\beta}\phi + \text{H.c.} \tag{3.81}$$

The box diagram and the tree-level scalar GNI (3.80) are absent because the scalar does not couple to charged fermions. However, the triangle diagram gives a contribution which reads

$$\left(\epsilon^{\triangleright}_{X,f}\right)^{\alpha\beta\gamma\gamma} = -\frac{1}{16\pi^2}g^f_X\frac{m^2_Z}{m^2_\phi}\sum_\delta y^*_{\delta\alpha}y_{\delta\beta}\left[f(r)-h(r)\right], \tag{3.82}$$

where $\gamma = 1,2,3$ and the divergent part of the diagram is neglected. In a complete model, this divergent part must be canceled by other diagrams which should also influence the

final result for $\epsilon^{\triangleright}$. However, we can work with Equation (3.82) as an order-of-magnitude estimate. As we discuss below, this leads to the model being constrained by the invisible Z decay width and neutrino-electron scattering.

The only way to access the secret neutrino interactions directly is through the effective Z coupling from the triangle diagram. Consequently, two important channels to test this are the invisible Z decay width and neutrino electron scattering, which is mediated by W and Z bosons. We will discuss the latter in detail in Section 4.4 and only quote the results here. To calculate the invisible Z decay width $\Gamma_{Z,\text{inv}}$ we have to add to the SM coupling of neutrinos the loop-induced coupling, resulting in

$$\mathcal{L}_{Z,\nu} = \frac{g}{c_W} g_L^{\nu} \lambda_{\alpha\beta} Z_\mu (\overline{\nu_\alpha} \gamma^\mu P_L \nu_\beta) \,, \tag{3.83}$$

where

$$\lambda_{\alpha\beta} = \frac{c_W}{g} \frac{g^{(1)}_{\alpha\beta}}{g_L^{\nu}} + \delta_{\alpha\beta} \,. \tag{3.84}$$

The measured invisible decay width is [36]

$$\Gamma_{Z,\text{inv}} = N_\nu \Gamma_{Z\to\nu\overline{\nu}}, \quad N_\nu = 3.0026 \pm 0.0061 \,. \tag{3.85}$$

Since the decay width $\Gamma_{Z\to\nu\overline{\nu}}$ is proportional to the absolute square of the vertex coupling, in the generalized case we have $\Gamma_{Z,\text{ inv}} \propto \text{tr}[\lambda\lambda^\dagger]$, from which we can infer

$$N_\nu = \text{tr}[\lambda\lambda^\dagger] = \sum_{\alpha,\beta} |\lambda_{\alpha\beta}|^2 \,. \tag{3.86}$$

Due to this trace there can be cancellations of large $g^{(1)}_{\alpha\beta}$ even with $N_\nu = 3$. Therefore, a more precise test of the model are the tests of neutral current NSI at energies where the Z is integrated out. For instance, leptonic GNI are constrained by neutrino-electron scattering data from TEXONO [99] ($\overline{\nu_e} e \to \overline{\nu} e$) and CHARM-II [100, 101] ($\overline{\nu_\mu} e \to \overline{\nu} e$) and ($\nu_\mu e \to \nu e$). As we discuss in the dedicated section Section 4.4 and Appendix C.2, the strongest bounds from these experiments on flavor-off-diagonal leptonic NSI with electrons are

$$\begin{aligned} &\sqrt{|\epsilon^{e\mu}_{L,e}|^2 + |\epsilon^{\mu\tau}_{L,e}|^2} \leq 0.11 \,, \qquad &&\sqrt{|\epsilon^{e\mu}_{R,e}|^2 + |\epsilon^{\mu\tau}_{R,e}|^2} \leq 0.10 \,, \\ &\sqrt{|\epsilon^{e\mu}_{L,e}|^2 + |\epsilon^{e\tau}_{L,e}|^2} \leq 0.27 \,, \qquad &&\sqrt{|\epsilon^{e\mu}_{R,e}|^2 + |\epsilon^{e\tau}_{R,e}|^2} \leq 0.16 \,, \end{aligned} \tag{3.87}$$

and so these apply to the secret neutrino interactions. We do not quote here all explicit bounds on semi-leptonic neural current NSI, but they are typically of the order 10^{-2}, as collected in Reference [25].

Neutral scalar with charged fermion couplings

In the case of non-secluded interactions given by Equation (3.78) and Dirac neutrinos, the triangle diagram vanishes. However, triangle diagrams for the charged fermions do exist and lead to corrections to the Z boson couplings. By this we can constrain the

charged fermion Yukawas $y^f_{\alpha\beta}$ from the Z boson partial decay widths which we discuss below. Note that we have to assume a cancellation of divergences in the complete model here as well. We can safely state that the off-diagonal Yukawas $y^f_{\alpha\beta}$ will be much more strongly constrained since the measured Z-couplings are flavor-conserving to very high precision. Therefore, we consider now diagonal $y^f_{\alpha\alpha} = y^f$. The box NSI parameters read

$$\left(\epsilon^{\square}_{X,f}\right)^{\alpha\beta\gamma\gamma} = \frac{1}{16\pi^2}\frac{\sqrt{2}|y^f|^2}{4m^2_\phi G_F}\sum_{\delta=e,\mu,\tau} y^\nu_{\alpha\delta} y^\nu_{\delta\beta}\,. \tag{3.88}$$

Considering all experimental constraints for this rather broad class of models is beyond our scope. However, we make some estimates for the case that $f = e$. We can again use the bounds on neutrino electron scattering. In this case, the strongest bound on Yukawas is from the tree-level GNI of Equation (3.80),

$$|\epsilon^{\alpha\beta ee}_{S,e}| \lesssim 0.6\,, \tag{3.89}$$

see Equation (C.12) and (C.13). This implies that

$$\frac{m_\phi}{\sqrt{|y_{\alpha\beta}y^e|}} \gtrsim 318\,\text{GeV}\,. \tag{3.90}$$

With this, we check if the partial decay width of Z to e can be consistent with such a bound. Modifying Equation (3.56) to describe the correction to the left-handed coupling g^f_L to Z we have

$$\begin{aligned}
\mathcal{L}_{\text{eff}} &= g^{(1)}_{\psi_L} Z_\mu \overline{\psi}\gamma^\mu P_L \psi\,,\\
g^{e(1)}_L &= \frac{|y_e|^2}{16\pi^2}\frac{m_Z^2}{m_\phi^2}\left[f(r)g^e_L + h(r)g^e_R\right],\\
&\lesssim \frac{1}{16\pi^2}\frac{|y_e|}{|y_{\alpha\beta}|}\frac{m_Z^2}{(318\,\text{GeV})^2}\left[0.1\cdot g^e_R\right],
\end{aligned} \tag{3.91}$$

where we assume that all $y_{\alpha\beta}$ are all of the same order of magnitude. Further, we used that $|f(r)| \ll |h(r)|$ for $r \ll 1$ and $|h(r)| \leq 0.1$ for $m_\phi \gtrsim 300\,\text{GeV}$. A similar expression can be found for the right-handed coupling with g^e_L and g^e_R swapped. With this we estimate the effect on the partial decay width of electrons using $\Gamma_{ee} \sim (g^e_L)^2 + (g^e_R)^2$

$$\begin{aligned}
\frac{\Delta\Gamma_{ee}}{\Gamma_{ee}} &\sim \frac{\left(g^e_L + g^{e(1)}_L\right)^2 + \left(g^e_R + g^{e(1)}_R\right)^2 - \left((g^e_L)^2 + (g^e_R)^2\right)}{(g^e_L)^2 + (g^e_R)^2}\\
&\approx \frac{1}{16\pi^2}\frac{|y_e|}{|y_{\alpha\beta}|}\frac{m_Z^2}{(318\,\text{GeV})^2}\cdot 0.1\cdot\frac{4g^e_L g^e_R}{(g^e_L)^2 + (g^e_R)^2}\,.
\end{aligned} \tag{3.92}$$

This value is bounded by the relative error of the $Z \to ee$ branching fraction which reads 1.25×10^{-3} [36] such that we find

$$\frac{|y_e|}{|y_{\alpha\beta}|} \lesssim 12\,. \tag{3.93}$$

According to this estimation, the loop suppression would be strong enough e.g. for the configuration $y_{\alpha\beta} \sim y^e \sim 1$, $m_\phi \geq 318\,\text{GeV}$. As we noted before, if the loop calculations hold to this degree depends on the UV complete realization of the model.

4. Experimental tests of new neutrino interactions

In this chapter we discuss various experimental constraints on GNI arising from low-energy experiments. By this we mean experiments with interaction energies at or below a few GeV. Besides these analyses without assumptions on the origin of new interactions, we investigate what we can learn from the connections between different observables that are forged when one assumes that the new physics is of high-energy origin and manifests itself in the form of gauge-invariant operators of SMNEFT. The roadmap for these connections is constituted by the EFT matching relations between SMNEFT and GNI operators which we discussed in Section 2.4. From these we infer which combinations of GNI should occur simultaneously or which should not occur at all if they originate from SMNEFT at dimension six. In Table 4.1, we summarize the experimental channels discussed in this chapter, and which types of GNI parameters they are sensitive to. An overview of additional ways to constrain the subset of interactions categorized as NSI can be found in Reference [25].

Since they are of outstanding importance in the field of neutrino physics, we first very briefly discuss neutrino oscillations to the extend that we understand their sensitivity towards neutral-current GNI in Section 4.1. This discussion illustrates that complementary tests of GNI are valuable as cross-checks for the interpretation of flavor transitions in terms of mixing angles and the charge-parity phase. In the remaining sections, we discuss such complementary searches for GNI, not all of which are affecting neutrino oscillation experiments. We compare indirect and direct tests of lepton flavor violating GNI in Section 4.2. By indirect tests we mean searches for charged lepton flavor violation which imply bounds on neutrino flavor violation if we assume that both originate from the same SMNEFT operators. Most of the direct tests are either beta decays or neutrino scattering off leptons or nuclei. Therefore, the following sections are dedicated to investigating such processes. In Section 4.3 we briefly review and compare the constraints on (pseudo)scalar and tensor GNI involving right-handed neutrinos from coherent elastic neutrino-nucleus scattering (CEνNS), beta decays, and pion decays. Afterwards, we turn to two more detailed phenomenological analyses. In Section 4.4 we focus on neutrino-electron scattering which is an important direct probe of leptonic GNI. After reviewing the detectable influence of GNI on the cross section, we present the results of a sensitivity study for neutrino-electron scattering at the DUNE near detector which show that one can expect significant improvements to current bounds. Finally, we discuss the sensitivity of neutrino mass experiments to GNI in Section 4.5.

Throughout this chapter, we presuppose that the right-handed neutrinos are light. In particular, we assume that they are either particle-antiparticle conjugates of left-handed

Table 4.1. Classification of experiments discussed in this work which can probe different types of GNI. $X = L, R, S, P, T$, $Y = A, S, P, T$. CLFV refers to charged lepton flavor violation.

GNI type		Direct probes	Sec.	Indirect probes	Sec.
$\epsilon_{X,e}^{\alpha\beta ee}$		ν-osc., ν-e scattering	4.1, 4.4	CLFV	4.2
$\epsilon_{X,e}^{\alpha\beta\gamma\delta}$	$\gamma \neq e$			CLFV	4.2
$\epsilon_{V,u}^{\alpha\beta 11}$		ν-osc., ν-N scattering	4.1, 4.3	CLFV	4.2
$\epsilon_{V,d}^{\alpha\beta 11}$		ν-osc., ν-N scattering	4.1, 4.3	CLFV	4.2
$\epsilon_{Y,u}^{\alpha\beta 11}$		ν-N scattering	4.3	CLFV	4.2
$\epsilon_{Y,d}^{\alpha\beta 11}$		ν-N scattering	4.3	CLFV	4.2
$\epsilon_{X,ud}^{\alpha\beta 11}$		Beta and Pion decays	4.3, 4.5	CLFV	4.2

active neutrinos in the Majorana case or independent right-handed partners of active neutrinos in the Dirac case. In this way we have a clear notion of flavors e, μ and τ for the right-handed neutrinos. This choice is made for convenience of interpretation rather than out of necessity. Most results can also be interpreted as bounds on the interactions of hypothetical light sterile neutrinos. Only in Section 4.5, where we discuss neutrino mass experiments, do we consider an additional fourth neutrino of mass up to 40 eV besides the right-handed partners of active neutrinos.

This chapter partially relies on the contents of References [2,3]. Specifically, Section 4.2 and Section 4.3 are mostly based on Reference [3]. Moreover, the contents of Section 4.4 are published in Reference [2], except that we have added a discussion of the scattering cross sections and constraints in the case of electron neutrinos.

4.1. Neutrino oscillations

Neutrino oscillation experiments have been essential in understanding the neutrino sector of the SM as well as we do today. Currently, the three-neutrino picture with (compared to the CKM matrix) large mixing angles and tiny (compared to the other fermions and the weak scale) neutrino masses and mass-squared differences describes excellently the global data [43]. Here we would like to focus only on understanding how GNI can be probed by neutrino oscillations. For this we highlight some key points about the propagation of neutrinos in matter as compared to vacuum. Understanding this propagation is key in interpreting the results of oscillation experiments. In particular, the upcoming long-baseline experiments T2HK [18] and DUNE [19], which aim to measure the leptonic charge-parity phase, feature neutrino paths of up to 1300 kilometers through the Earth's crust from production to detection. Therefore they will be sensitive to matter interactions which can result in a misinterpretation in the presence of GNI [102–104].

We follow here loosely the discussion in Reference [35]. In a simplified quantum mechanical picture,[1] we consider a neutrino created at time $t = 0$ with momentum $\mathbf{p}$ in the flavor eigenstate

$$|\nu_\alpha\rangle = \sum_j U_{\alpha j} |\nu_j\rangle , \tag{4.1}$$

where $|\nu_j\rangle$ are mass eigenstates. The flavor evolution of this neutrino can be described by the Schrödinger equation

$$i\frac{\mathrm{d}}{\mathrm{d}t} |\nu_\alpha(t)\rangle = \mathscr{H} |\nu_\alpha(t)\rangle , \tag{4.2}$$

with $|\nu_\alpha(0)\rangle = |\nu_\alpha\rangle$ and where $\mathscr{H}$ denotes the Hamiltonian. Since $\mathscr{H}$ is not diagonal in flavor space, in general $|\nu_\beta(t)\rangle$ will be non-vanishing for $\beta \neq \alpha$. The transition probability from flavor α at $t = 0$ to flavor β at t is then given by

$$P_{\nu_\alpha \to \nu_\beta}(t) = |\, \langle \nu_\beta | \nu_\alpha(t) \rangle \,|^2 \equiv |\psi_{\alpha\beta}|^2 , \tag{4.3}$$

where we defined the amplitude $\psi_{\alpha\beta}(t)$. Using the Schrödinger equation (4.2) and assuming a constant Hamiltonian we find the evolution of the probability amplitude to follow

$$i\frac{\mathrm{d}}{\mathrm{d}t}\psi_{\alpha\beta} = i\frac{\mathrm{d}}{\mathrm{d}t}(\langle \nu_\beta | \nu_\alpha(t) \rangle) = \langle \nu_\beta | \mathscr{H} | \nu_\alpha(t) \rangle = \sum_\eta \mathcal{H}_{\beta\eta}\psi_{\alpha\eta}(t) , \tag{4.4}$$

or, as a matrix equation,

$$i\frac{\mathrm{d}}{\mathrm{d}x}\Psi_\alpha = \mathcal{H}\Psi_\alpha , \tag{4.5}$$

where $\Psi_\alpha = (\psi_{\alpha e}, \psi_{\alpha\mu}, \psi_{\alpha\tau})^T$ and $\mathcal{H}$ is the 3-by-3 Hamiltonian matrix whose form we discuss now. In the mass basis, the vacuum Hamiltonian matrix $\mathcal{H}'_0$ (the prime refers to mass basis) is diagonal and satisfies

$$(\mathcal{H}'_0)_{ij}\, \nu_j(\mathbf{p}) = \delta_{ij} E_j(\mathbf{p})\, \nu_j(\mathbf{p}) = \sqrt{\mathbf{p}^2 + m_j^2}\, \nu_j(p) . \tag{4.6}$$

Therefore we have in the flavor basis

$$(\mathcal{H}_0)_{\alpha\beta} = \sum_k U^*_{\alpha k} U_{\beta k} E_k . \tag{4.7}$$

If the flavor evolution takes place in matter (electrons, up, and down quarks), however, there is also an interaction Hamiltonian $\mathcal{H}_I$ to take into account. In the SM this Hamiltonian describing the coherent forward scattering of neutrinos in matter reads

$$(\mathcal{H}_I)_{\alpha\beta} = V_\alpha \delta_{\alpha\beta} , \tag{4.8}$$

including flavor-universal neutral current interactions and electron-neutrino exclusive charged current interactions

$$V_\alpha = V_{\mathrm{CC}}\delta_{\alpha e} + V_{\mathrm{NC}} = \sqrt{2} G_F (N_e \delta_{\alpha e} - \frac{1}{2} N_n) , \tag{4.9}$$

[1] A more accurate wave packet treatment is found in Reference [105].

with N_e and N_n the number density of electrons and neutrons respectively. This formula assumes neutral matter and therefore that the proton density N_p is equal to the electron density. Considering the ultra-relativistic limit, we approximate

$$E_j \approx E + \frac{m_j^2}{2E}, \qquad p \approx E, \qquad t \approx x\,. \tag{4.10}$$

This can be used to find

$$i\frac{\mathrm{d}}{\mathrm{d}x}\psi_{\alpha\beta}(x) = \left(p + \frac{m_1^2}{2E} + V_{\mathrm{NC}}\right)\psi_{\alpha\beta}(x) + \sum_\eta \frac{1}{2E}(U^*\mathbb{M}^2U^T + \mathbb{A})_{\beta\eta}\psi_{\alpha\eta}(x)\,, \tag{4.11}$$

where

$$\mathbb{M}^2 = \begin{pmatrix} 0 & 0 & 0 \\ 0 & \Delta m_{21}^2 & 0 \\ 0 & 0 & \Delta m_{31}^2 \end{pmatrix}, \qquad \mathbb{A} = \begin{pmatrix} A_{\mathrm{CC}} & 0 & 0 \\ 0 & 0 & 0 \\ 0 & 0 & 0 \end{pmatrix}, \tag{4.12}$$

with

$$A_{\mathrm{CC}} = 2EV_{\mathrm{CC}} = 2\sqrt{2}EG_FN_e\,. \tag{4.13}$$

The first term on the right-hand side of Equation (4.11) is irrelevant for the transition probability, since it generates a phase equal to all flavors. Hence the flavor-universal neutral-current interactions are irrelevant for the flavor evolution. If we consider now our more general interaction Lagrangian including new physics in Equation (2.11), there is a new contribution for each flavor combination which is governed by [25]

$$\epsilon_m^{\alpha\beta} \equiv \epsilon_{V,e}^{\alpha\beta ee} + \frac{N_u}{N_e}\epsilon_{V,u}^{\alpha\beta 11} + \frac{N_d}{N_e}\epsilon_{V,d}^{\alpha\beta 11}\,, \tag{4.14}$$

where $\epsilon_V = \epsilon_L + \epsilon_R$ and N_u and N_d denote the number densities of up and down quarks in the matter. Other types of GNI do not affect the propagation in unpolarized matter [106]. This implies that $\mathbb{A}$ becomes [107]

$$\mathbb{A} = A_{\mathrm{CC}}\begin{pmatrix} 1+\epsilon_m^{ee} & \epsilon_m^{e\mu} & \epsilon_m^{e\tau} \\ \epsilon_m^{\mu e} & \epsilon_m^{\mu\mu} & \epsilon_m^{\mu\tau} \\ \epsilon_m^{\tau e} & \epsilon_m^{\tau\mu} & \epsilon_m^{\tau\tau} \end{pmatrix}, \tag{4.15}$$

showing how the flavor evolution in matter is now distorted by new physics. Note that we have defined the coefficients to satisfy Equation (2.13) such that $\epsilon_m^{\alpha\beta} = (\epsilon_m^{\beta\alpha})^*$ which ensures that the Hamiltonian is Hermitian. Moreover, by the same argument which renders the SM neutral current interactions irrelevant, it is possible to subtract a diagonal element from $\mathbb{A}$, e.g. $\epsilon_m^{\mu\mu}$ such that from neutrino oscillations we can only constrain $\epsilon_m^{ee} - \epsilon_m^{\mu\mu}$ and $\epsilon_m^{\tau\tau} - \epsilon_m^{\mu\mu}$. More details about constraints from neutrino oscillations can be found in Reference [25].

The discussion to this point suffices to illustrate how neutrino oscillations are sensitive to GNI. Oscillation experiments are important tests of matter NSI, but suffer from some degeneracies, in particular between flavor-diagonal interactions. Moreover, they are not sensitive to the chirality-flipping (pseudo)scalar and tensor GNI. Since we derive our knowledge of neutrino mixing and leptonic charge-parity violation from those experiments it is imperative to perform complementary tests of GNI to ensure that these properties are inferred correctly. In the following sections we discuss such other test of GNI.

4.2. Charged lepton flavor violation

In this section we discuss implications of the assumption that lepton flavor violating GNI are induced by SMNEFT operators according to the matching discussed in Section 2.4. Recall that if we assume that GNI are generated by heavy new physics beyond the weak scale and that therefore SMNEFT at dimension six is the appropriate EFT to describe these new physics above the weak scale, then the mapping between SMNEFT and GNI is given in Tables 2.6 and 2.7. We can see that lepton-flavor off-diagonal leptonic and semi-leptonic[2] GNI of left-handed neutrinos are generated by the flavor off-diagonal Wilson coefficients of the operators involving the lepton doublet l. But as we have already discussed in Section 2.4, GNI are not the only interactions generated by these operators. Instead, the fact that neutrinos appear in lepton doublets generates the additional interaction terms among four charged fermions in Equation (2.16). Therefore, we can use tests of charged lepton flavor violation (CLFV) to constrain these SMNEFT Wilson coefficients, which in turn implies a constraint on neutrino interactions. As one would expect, it turns out that these bounds on CLFV are several orders of magnitude stronger than those on neutrino interactions. Before discussing the bounds we should note that they are generally obtained at low-energies ($\lesssim 2\,\mathrm{GeV}$), while our EFT matching is, strictly speaking, only valid at the weak scale. In between there is some extent of RG running which we do not calculate here. However, calculations in References [108, 109] indicate that typically the renormalization of individual coefficients amounts to an order-1 factor and that the mixing of Wilson coefficients is a subleading effect.

There are several experiments trying to detect flavor violation from μ to e, the main processes being $\mu \to eee$, $\mu \to e\gamma$, or $\mu \to e$ conversion in nuclei [110,111]. Similarly there are searches for $\tau \to \mu\mu\mu$ and $\tau \to eee$. We discuss in turn all these processes, which experiments currently yield the strongest bounds, and which SMNEFT and indirectly GNI coefficients are affected by this limit under our assumed EFT matching.

- $\mu \to eee$: This process is mediated in SMNEFT by $\mathcal{O}_{ll}^{\mu eee}$, $\mathcal{O}_{le}^{\mu eee}$ and $\mathcal{O}_{le}^{ee\mu e}$. The Wilson coefficients are constrained to be smaller than about 10^{-6} by the results of SINDRUM [111, 115].[3] We can expect an improvement of up to two orders of magnitude from the planned Mu3e experiment [116, 117]. This can be estimated from the fact that the branching ratio of this decay scales with C^2, where C is one of the corresponding Wilson coefficients and that phase two may reach an improvement of the upper bound on the branching fraction from 10^{-10} to 10^{-16} at 90% CL [116].

- $\mu \to e$ in nuclei: The SINDRUM-II collaboration [118] has measured an upper bound of the conversion $\mu^-\mathrm{Au} \to e^-\mathrm{Au}$ which has been evaluated in SMEFT language to constraints of the order 10^{-8} on the semi-leptonic coefficients $C_{ld,lu}^{e\mu 11}$ in Reference [119]. In their "Method 1" they have applied the formulas of Reference [120].

[2] By semi-leptonic operators, we mean operators with one lepton bilinear and one quark bilinear.

[3] Numerical values given in Reference [111] for C_a are normalized with respect to $\Lambda = 1\,\mathrm{TeV}$. To translate these to our convention of $\Lambda^{-2} = \sqrt{8}G_F$, one needs to multiply the numbers by $(\sqrt{8}G_F\mathrm{TeV}^2)^{-1} \approx 1/33$.

Table 4.2. Single-parameter bounds at 90% CL on general interaction parameters that are related to CLFV. The second column lists direct bounds from neutrino experiments, while the third column features bounds from CLFV searches under the assumption that the interactions are induced by one of the operators in the fourth column.

$\lvert\epsilon^{e\mu ee}\rvert$ or $\lvert\epsilon^{e\mu 11}\rvert$	Direct	CLFV	Operators
$\epsilon_{L,e}$	1.1×10^{-1} [52]	1.4×10^{-6}	$\mathcal{O}_{ll}$
$\epsilon_{R,e}$	1.0×10^{-1} [52]	1.0×10^{-6}	$\mathcal{O}_{le}$
$\epsilon_{L,u}$	2.3×10^{-2} [112]	3.3×10^{-7}	$\mathcal{O}_{lq(1)}, \mathcal{O}_{lq(3)}$
$\epsilon_{L,d}$	2.3×10^{-2} [112]	3.3×10^{-7}	$\mathcal{O}_{lq(1)}, \mathcal{O}_{lq(3)}$
$\epsilon_{R,u}$	3.6×10^{-2} [112]	6.0×10^{-8}	$\mathcal{O}_{lu}$
$\epsilon_{R,d}$	3.6×10^{-2} [112]	5.3×10^{-8}	$\mathcal{O}_{ld}$
$\epsilon_{L,ud}$	2.6×10^{-2} [113]	6.6×10^{-7}	$\mathcal{O}_{lq(3)}$
$\mathrm{Re}(\epsilon_{S,ud})$	8×10^{-3} [114]	3.0×10^{-8}	$\mathcal{O}_{elqd}, \mathcal{O}_{eluq}$
$\mathrm{Re}(\epsilon_{P,ud})$	4×10^{-4} [114]	3.0×10^{-8}	$\mathcal{O}_{elqd}, \mathcal{O}_{eluq}$
$\lvert\epsilon\rvert$	Direct	CLFV	Operators
$\epsilon_{L,e}^{\tau eee}$	2.7×10^{-1} [52]	2.8×10^{-4}	$\mathcal{O}_{ll}$
$\epsilon_{R,e}^{\tau eee}$	2.7×10^{-1} [52]	3.9×10^{-4}	$\mathcal{O}_{le}$
$\epsilon_{R,e}^{ee\tau e}$		3.9×10^{-4}	$\mathcal{O}_{le}$
$\epsilon_{R,e}^{\mu\mu\mu e}$		5.5×10^{-6}	$\mathcal{O}_{le}$
$\epsilon_{R,e}^{e\mu\mu\mu}$		5.5×10^{-6}	$\mathcal{O}_{le}$
$\epsilon_{R,e}^{\mu\tau\tau e}$		3.0×10^{-7}	$\mathcal{O}_{le}$
$\epsilon_{R,e}^{e\tau\tau\mu}$		3.0×10^{-7}	$\mathcal{O}_{le}$
$\epsilon_{L,e}^{\tau\mu\mu\mu}$		2.4×10^{-4}	$\mathcal{O}_{ll}$
$\epsilon_{R,e}^{\mu\tau\mu\mu}$		3.3×10^{-4}	$\mathcal{O}_{le}$
$\epsilon_{R,e}^{\mu\mu\mu\tau}$		3.3×10^{-4}	$\mathcal{O}_{le}$

By the same method, we can apply these formulas to constrain additionally the operators $C_{lq(1)}$, $C_{lq(3)}$, and the coefficients of scalar operators C_{elqd} and C_{eluq} with index structures $e\mu 11$. They all turn out to be bounded from above by 10^{-7}. Even stronger bounds can be expected from the future Mu2e experiment [121].

- $\mu \to e\gamma$: The strongest constraints on this process come from the MEG experiment [122]. According to Reference [111], they imply upper bounds on $C_{le}^{\mu\mu\mu e, e\mu\mu\mu}$ and $C_{le}^{\mu\tau\tau e, e\tau\tau\mu}$ which contribute to the decay at one-loop level at the order of 10^{-6}-10^{-7}.

- $\tau \to \mu\mu\mu$: Similarly to $\mu \to eee$, the contributing Wilson coefficients are $C_{ll}^{\tau\mu\mu\mu}$, $C_{le}^{\mu\tau\mu\mu}$, and $C_{le}^{\mu\mu\mu\tau}$, which are individually constrained to be at most of order 10^{-4} by the results of Belle [111, 123].

- $\tau \to eee$: Analogously to the previous cases, the contributing coefficients are $C_{ll}^{\tau eee}$, $C_{le}^{\tau eee}$, and $C_{le}^{ee\tau e}$, which are constrained to be at most of order 10^{-4} also by the

results of Belle [111, 123].

These quite strong constraints on SMNEFT coefficients can be compared to the directly measured bounds on neutrino interactions which we summarize next:

- $\epsilon^{\mu eee}_{L,e}$ and $\epsilon^{\mu eee}_{R,e}$: The strongest bounds come from neutrino-electron scattering. Current bounds from CHARM-II [124, 125] are at the order of 10^{-1}, while we expect significant improvement from the first phase of DUNE as we will discuss in Section 4.4. Bounds on NSI from CHARM-II have been calculated in References [52, 126] in differing parametrizations. Adapting the bounds from Reference [52] to our parametrization yields slightly stronger bounds as we discuss in Appendix C.2. In Table 4.2 we show the adapted bounds from Reference [52].

- $\epsilon^{e\mu 11}_{L,u}$, $\epsilon^{e\mu 11}_{R,u}$, $\epsilon^{e\mu 11}_{L,d}$, $\epsilon^{e\mu 11}_{R,d}$: These are bounded at the order of 10^{-2} by neutrino-nucleon scattering data from CHARM and CDHS [25, 100, 114, 127].

- $|\mathrm{Re}(\epsilon^{e\mu 11}_{S,ud})|$, $|\mathrm{Re}(\epsilon^{e\mu 11}_{P,ud})|$: The scalar and pseudoscalar coefficients are constrained at least at the order 10^{-3} from pion decay [114].

- $\epsilon^{\tau eee}_{L,e}$, $\epsilon^{\tau eee}_{R,e}$: The strongest direct bounds on these τ-e flavor violating neutrino interactions are at the order of 10^{-1} coming from $e^+e^- \to \overline{\nu}\nu\gamma$ data taken at LEP [126].

- For the other coefficients in Table 4.2 with rather exotic flavor combinations we are not aware of any analyses of direct bounds.

In Table 4.2 we summarize the directly measured bounds on GNI parameters together with the strongest upper bounds on them from CLFV. In conclusion, in all cases where direct bounds exist they are at least four orders of magnitude less stringent than the CLFV bounds. Therefore if lepton flavor violating GNI are generated by the SMEFT operators involving lepton doublets, there is practically no hope in detecting them. However, turning this argument around we can conclude that if any upcoming experiments detect such GNI, then they are not connected to dimension-six SMEFT and would therefore hint towards new physics below the weak scale. Another conclusion is that GNI with right-handed neutrinos are interesting from a high-energy physics perspective, since they are not connected to any strongly constrained charged fermion interactions. In the next sections, we therefore discuss some further experimental channels to trace neutral- and charged-current interactions of right-handed neutrinos.

4.3. Coherent scattering and beta decays

In this section we subsume two distinct topics, since from the point of view of neutrino interactions generated by SMNEFT they are partially sensitive to the same operators. As discussed in Section 2.4, three operators with right-handed neutrinos, $\mathcal{O}_{lNuq}$, $\mathcal{O}_{lNqd}$ and $\mathcal{O}'_{lNqd}$ induce simultaneously neutral- and charged-current semi-leptonic GNI. To

summarize here again, the matching in Tables 2.6 and 2.7 implies the following single-operator scenarios,

$$\mathcal{O}_{lNuq}: \quad \begin{aligned} \epsilon_{S,u}^{\alpha\beta\gamma\delta} &= -\epsilon_{P,u}^{\alpha\beta\gamma\delta} = -V_{\gamma\nu}(C_{lNuq}^{\beta\alpha\delta\nu})^*\,, \\ \widetilde{\epsilon}_{S,ud}^{\alpha\beta\gamma\delta} &= \widetilde{\epsilon}_{P,ud}^{\alpha\beta\gamma\delta} = -\frac{1}{V_{\gamma\delta}} C_{lNuq}^{\alpha\beta\gamma\delta}\,, \end{aligned} \tag{4.16}$$

$$\mathcal{O}_{lNqd}: \quad \begin{aligned} \epsilon_{S,d}^{\alpha\beta\gamma\delta} &= \epsilon_{P,d}^{\alpha\beta\gamma\delta} = -(C_{lNqd}^{\beta\alpha\delta\gamma})^*\,, \\ \widetilde{\epsilon}_{S,ud}^{\alpha\beta\gamma\delta} &= -\widetilde{\epsilon}_{P,ud}^{\alpha\beta\gamma\delta} = \frac{V_{\gamma\nu}}{V_{\gamma\delta}} C_{lNqd}^{\alpha\beta\nu\delta}\,, \end{aligned} \tag{4.17}$$

$$\mathcal{O}'_{lNqd}: \quad \begin{aligned} \epsilon_{T,d}^{\alpha\beta\gamma\delta} &= -(C_{lNqd}^{\prime\beta\alpha\delta\gamma})^*\,, \\ \widetilde{\epsilon}_{T,ud}^{\alpha\beta\gamma\delta} &= \frac{V_{\gamma\nu}}{V_{\gamma\delta}} C_{lNqd}^{\prime\alpha\beta\nu\delta}\,. \end{aligned} \tag{4.18}$$

Our main motivation for this section is to compare the bounds from CEνNS on the above neutral current GNI and beta decays on the above charged current GNI, even though they can of course constrain various other types of GNI as well. In this comparison we assume that the masses of the right-handed neutrinos that are produced in the scattering or decay can be neglected. Alternatively, one could consider sterile neutrinos of finite mass in CEνNS which is possible as long as the mass is below the initial neutrino energy [128,129]. For an evaluation of the constraints from CEνNS for all LEFT operators with right-handed neutrinos see Reference [55].

While we neglect the so far uncalculated RG running of these particular coefficients between the weak scale and low energies we try to find a very rough estimation. In Reference [109] the running of $\epsilon_{S,ud}$, $\epsilon_{P,ud}$ and $\epsilon_{T,ud}$ from the weak scale down to 2 GeV has been calculated. These coefficients are connected to the SMEFT operators $\mathcal{O}_{elqd}$, $\mathcal{O}_{eluq}$ and $\mathcal{O}'_{eluq}$ in a structure very similar to the right-handed neutrino counterparts in Equations (4.16)-(4.18). For the SMEFT operators it is found that the three epsilon coefficients mix, but the mixing can be neglected to leading order. Therefore, we expect such a situation also for $\widetilde{\epsilon}_{S,ud}$, $\widetilde{\epsilon}_{P,ud}$ and $\widetilde{\epsilon}_{T,ud}$. Another subject of caution is that the magnitude of individual coefficients is renormalized along the way, e.g. $\epsilon_{S,ud}^{2\,\mathrm{GeV}} \approx 1.72{\cdot}\epsilon_{S,ud}^{m_Z}$. However, in terms of order of magnitude our evaluation should still give a good indication. We now summarize the relevant aspects of CEνNS in Section 4.3.1, of beta decays in Section 4.3.2 and then compare the two in Section 4.3.3.

4.3.1. Coherent elastic neutrino nucleus scattering

CEνNS is a SM process which was first predicted decades ago [130], yet has not been observed until rather recently by the COHERENT collaboration [131]. Compared to inelastic neutrino nucleus scattering, this process takes place for relatively small neutrino energies which leads to an enhanced cross section due to the neutrino scattering coherently on all nucleons in the nucleus instead of individual nucleons. Concretely, the SM differential cross section reads [53]

$$\frac{\mathrm{d}\sigma}{\mathrm{d}T} = \frac{G_F^2 M}{4\pi}\left[N - (1-4s_W^2)Z\right]^2 F^2(Q^2)\left(1 - \frac{T}{T_{\max}}\right), \tag{4.19}$$

where T and M denote the kinetic energy and mass of the recoiled nucleus, N is the number of neutrons, Z the number of protons, and $F(q)$ denotes the nuclear form factor as a function of the energy transfer Q^2. Due to the $(1-4s_W^2) \approx 0.045$ suppression, the cross section is mostly controlled by N^2. This enhancement with respect to the scattering off individual nucleons is what makes the cross section relatively large. The largest cross sections are obtained for small Q^2 where $F^2(Q^2) \approx F^2(0) = 1$. What we mean by small depends on the nucleus, but for the typical detector materials argon, germanium or xenon the form factor becomes rapidly small for T in between a few tens of keV and 200 keV [132]. This immediately tells us the major challenge in detecting this process. The cross section is large, but it is required that we can detect a very small nuclear recoil in the order of keV which is why the process has not been detected until 2017 [131]. Besides COHERENT other experiments such as CONUS, CONNIE and many others [133–137] are running or planned with the aim to detect the process at other energies and with other target materials, which underlines that this process is considered an exciting new probe of neutrino interactions.

In Reference [53], the sensitivity of future reactor neutrino experiments such as CONUS towards general interactions has been studied. These have the advantage of a large flux of low-energetic reactor neutrinos for which $F(Q^2) \approx 1$ to great precision. The price to pay for this, however, is that a very low detection energy threshold is required. In Reference [54] this framework has been applied to the first COHERENT results [131] assuming neutrino flavor-universal GNI. Here we only focus on the (pseudo)scalar and tensor interactions described in Equations (4.16)-(4.18) and rely on References [53, 54] for details of the analyses.

If we consider nuclear reactors, which are a source of electron antineutrinos, the experiments are sensitive to epsilon coefficients of flavor $\beta e11$ and the (pseudo)scalar and tensor interactions are described by

$$\Delta\mathcal{L}_{S,P}^{\text{NC}} = -\frac{G_F}{\sqrt{2}} \sum_{\substack{\beta \\ \psi=u,d}} \left(\epsilon_{S,\psi}^{\beta e11} (\overline{N}_\beta (\mathbb{1} - \gamma^5)\nu_e)(\overline{\psi}\psi) - \epsilon_{P,\psi}^{\beta e11} (\overline{N}_\beta (\mathbb{1} - \gamma^5)\nu_e)(\overline{\psi}\gamma^5\psi) \right) + \text{H.c.} \tag{4.20}$$

$$\Delta\mathcal{L}_{T}^{\text{NC}} = -\frac{G_F}{\sqrt{2}} \sum_{\substack{\beta \\ \psi=u,d}} \left(\epsilon_{T,\psi}^{\beta e11} (\overline{N}_\beta \sigma_{\mu\nu} (\mathbb{1} - \gamma^5)\nu_e)(\overline{\psi}\sigma^{\mu\nu}(\mathbb{1} - \gamma^5)\psi) \right) + \text{H.c.} \tag{4.21}$$

Since we cannot distinguish the final neutrino flavor, we may set $\beta = e$ for simplicity. Note that we can only compare the reactor neutrino results with the bounds from COHERENT from Reference [54] if we assume that $\epsilon^{ee11} = \epsilon^{\mu\mu 11}$, because most neutrinos detected at COHERENT are of muon flavor.[4] Following Reference [53], the contribution to the CEνNS differential cross section of these scalar and tensor interactions read

$$\frac{\mathrm{d}\sigma}{\mathrm{d}T} = \frac{G_F^2 M}{4\pi} \left(\xi_S^2 \frac{MT}{2E_\nu^2} + \xi_T^2 \left(1 - \frac{T}{T_{\max}} + \frac{MT}{4E_\nu^2} \right) \right), \tag{4.22}$$

[4] If we assume this relation and tensor interactions, they are incompatible with Majorana neutrinos, see Appendix A.5. However, instead one could have $\epsilon_T^{\mu e11} = \epsilon_T^{e\mu 11}$ which would give the same results but would be compatible with Majorana neutrinos.

where E_ν denotes the neutrino energy and we neglected terms of higher order in T/E_ν. The effective parameters ξ_S and ξ_T are defined as follows.

$$\xi_S^2 = (C_S^2 + D_P^2)\,, \tag{4.23}$$
$$\xi_T^2 = 8(C_T^2 + D_T^2)\,, \tag{4.24}$$

with [54]

$$C_S = \sum_{q=u,d} C_S^{(q)} \left[N \frac{m_n}{m_q} f_{Tq}^n F_n(Q^2) + Z \frac{m_p}{m_q} f_{Tq}^p F_p(Q^2) \right], \tag{4.25}$$

$$D_P = \sum_{q=u,d} D_P^{(q)} \left[N \frac{m_n}{m_q} f_{Tq}^n F_n(Q^2) + Z \frac{m_p}{m_q} f_{Tq}^p F_p(Q^2) \right], \tag{4.26}$$

$$C_T = N(\delta_u^n C_T^u + \delta_d^n C_T^d) F_n(Q^2) + Z(\delta_u^p C_T^u + \delta_d^p C_T^d) F_p(Q^2)\,, \tag{4.27}$$

where F_n and F_p are the appropriate form factors of neutron and proton (typically assumed to be equal), and f_{Tq}^n and f_{Tq}^p parametrize the effective fraction of nucleon mass the given quark type contributes. These quantities are calculated in chiral perturbation theory [138]. Since we consider the results of Reference [54], we use the same values,

$$\begin{aligned} f_{Tu}^p &= 0.019\,, & f_{Td}^p &= 0.041\,, \\ f_{Tu}^n &= 0.023\,, & f_{Td}^n &= 0.034\,, \end{aligned} \tag{4.28}$$

which are taken from Reference [139]. For the tensor charges δ_q^n, δ_q^p we also take the same values as in Reference [54], namely

$$\begin{aligned} \delta_u^p &= 0.54\,, & \delta_d^p &= -0.23\,, \\ \delta_u^n &= -0.23\,, & \delta_d^n &= 0.54\,, \end{aligned} \tag{4.29}$$

taken from Reference [140]. We remark that there are relatively large uncertainties on these parameters, such that the values we extract below should be interpreted as estimates. The interaction parameters $C_j^{(q)}$, $D_j^{(q)}$ are equivalent to combinations of epsilon parameters,

$$\begin{aligned} C_S^{(q)} &= \epsilon_{S,q} + \widetilde{\epsilon}_{S,q}\,, & D_P^{(q)} &= i(\widetilde{\epsilon}_{S,q} - \epsilon_{S,q})\,, \\ C_T^{(q)} &= 2(\epsilon_{T,q} + \widetilde{\epsilon}_{T,q})\,, & D_T^{(q)} &= 2i(\epsilon_{T,q} - \widetilde{\epsilon}_{T,q})\,, \end{aligned} \tag{4.30}$$

where we suppressed flavor indices. The full mapping between the C and D parameters introduced by Lee and Yang [51] and our epsilon interaction coefficients is given in Appendix A.4. We neglect D_T in our calculations since it contributes only to the spin-dependent part of the cross section which is suppressed for heavy nuclei such as caesium iodide (CsI, COHERENT) and germanium (Ge, CONUS) [54]. For the same reason the pseudoscalar coefficients are absent from Equation (4.22).

We can use the bounds from the COHERENT experiment from Reference [54], if we adopt their assumption that electron and muon neutrino interactions with the nucleon are the same. We remark that these results are derived assuming equal Helm form factors for

proton and neutron which introduces some uncertainties for large momentum transfers $Q \geq 20\,\text{MeV}$ as is the case of COHERENT, but not for reactor neutrino experiments [56]. We quote

$$\begin{aligned} |\xi_S|/NF(Q^2) &\leq 0.62 \quad \text{at } 90\%\text{ CL}\,, \\ |\xi_S|/NF(Q^2) &\leq 1.065 \quad \text{at } 99\%\text{ CL}\,, \\ |\xi_T|/NF(Q^2) &\leq 0.591 \quad \text{at } 90\%\text{ CL}\,, \\ |\xi_T|/NF(Q^2) &\leq 1.072 \quad \text{at } 99\%\text{ CL}\,. \end{aligned} \tag{4.31}$$

If one relaxes the assumption $\epsilon_{S,q}^{ee11} = \epsilon_{S,q}^{\mu\mu 11}$ made in Reference [56], this bound gets weakened since the neutrinos at COHERENT are mostly muon flavor. This is not the case for the projected bounds from future reactor neutrino experiments calculated in [53] which are

$$\begin{aligned} |\xi_S|/NF(Q^2) &\leq 0.21 \quad \text{at } 3\sigma, \\ |\xi_T|/NF(Q^2) &\leq 0.25 \quad \text{at } 3\sigma. \end{aligned} \tag{4.32}$$

4.3.2. Beta decays

Beta decays in general are excellent processes to make precision tests of fundamental physics, since one can often prepare the parent particle in a controlled setup and detect decay products with high accuracy of direction and energy. This is also the reason why the current best terrestrial bound on the neutrino mass comes from the beta decay of tritium at the Karlsruhe Tritium Neutrino Experiment (KATRIN) [44], where from the very precise measurement of the endpoint of the electron spectrum an upper bound on the neutrino mass can be derived. We dedicate Section 4.5 to a discussion about the sensitivity of such an experiment to GNI. In this subsection, we only refer to Reference [109] for a detailed review on the subject of testing GNI with beta decays and quote the best limits on the (pseudo)scalar and tensor interactions. These are

$$\begin{aligned} |\text{Re}(\widetilde{\epsilon}_{P,ud}^{ee11})|, |\text{Im}(\widetilde{\epsilon}_{P,ud}^{ee11})| &\leq 2.8 \times 10^{-4} \quad [114]\,, \\ |\widetilde{\epsilon}_{S,ud}^{ee11}| &\leq 6.3 \times 10^{-2} \quad [109]\,, \\ 0.006 \leq |\widetilde{\epsilon}_{T,ud}^{ee11}| &\leq 0.024\,, \quad [109]\,, \end{aligned} \tag{4.33}$$

at 90% CL, where the first bound is obtained from the ratio between the rates of pion decay to electron and to muon [114], and the second and third bounds are taken from a global fit of nuclear and neutron beta decay data. Note that $\widetilde{\epsilon}_{T,ud}^{ee11}$ becomes compatible with zero at 2σ. A roughly two times stronger bound on $\widetilde{\epsilon}_{S,ud}$ can be derived from CKM unitarity tests [109].

4.3.3. Comparison

In this section, we compare the current and future bounds of tests of the (pseudo)scalar and tensor GNI in Equations (4.16)-(4.18) to see if there are any prospects of a complementary test of the SMNEFT operators $\mathcal{O}_{lNuq}$, $\mathcal{O}_{lNqd}$ and $\mathcal{O}'_{lNqd}$. We consider three scenarios:

1. Only one scalar operator $\mathcal{O}_{lNuq}$ or $\mathcal{O}_{lNqd}$ is present.
2. Both scalar operators $\mathcal{O}_{lNuq}$ and $\mathcal{O}_{lNqd}$ are present and correlated.
3. Only the tensor operator $\mathcal{O}'_{lNqd}$ is present.

Scenario 1

We take only C^{ee11}_{lNuq} to be non-vanishing. Then we can conclude from Equation (4.16)

$$\widetilde{\epsilon}^{ee11}_{S,ud} = \widetilde{\epsilon}^{ee11}_{P,ud} = -\frac{1}{V_{ud}} C^{ee11}_{lNuq} = \frac{1}{|V_{ud}|^2}(\epsilon^{ee11}_{S,u})^* = -\frac{1}{|V_{ud}|^2}(\epsilon^{ee11}_{P,u})^* \,. \tag{4.34}$$

Assuming $F_n = F_p = F$, Equation (4.25) can be simplified to

$$C_S = C_S^{(u)} F(Q^2) \left[N \frac{m_n}{m_u} f^n_{Tu} + Z \frac{m_p}{m_u} f^p_{Tu} \right], \tag{4.35}$$

and likewise for $D_P^{(u)}$. Since generally $\epsilon^{ee11}_{S,u} = (\widetilde{\epsilon}^{ee11}_{S,u})^*$, see Equation (2.13), we can use Equation (4.30) to identify

$$C_S^{(u)} = 2\,\mathrm{Re}(\epsilon^{ee11}_{S,u})\,, \qquad D_P^{(u)} = 2\,\mathrm{Im}(\epsilon^{ee11}_{S,u})\,. \tag{4.36}$$

For the case of CsI (COHERENT) we have $N = 78$, $Z = 55$ for caesium nuclei, and $N = 74$, $Z = 53$ for iodine nuclei, implying

$$\begin{aligned} \frac{\xi_S^2}{N^2 F^2(Q^2)} &= \sum_{i=\mathrm{Cs,I}} \frac{1}{N_i^2} \left((C_S^{(u)})^2 + (D_P^{(u)})^2 \right) \left[N_i \frac{m_n}{m_u} f^n_{Tu} + Z_i \frac{m_p}{m_u} f^p_{Tu} \right]^2 \\ &= 4|\epsilon^{ee11}_{S,u}|^2 \sum_{i=\mathrm{Cs,I}} \frac{1}{N_i^2} \left[N_i \frac{m_n}{m_u} f^n_{Tu} + Z_i \frac{m_p}{m_u} f^p_{Tu} \right]^2 . \end{aligned} \tag{4.37}$$

For the future reactor experiment we take $N = 40$, $Z = 32$ (germanium) as an average of stable isotopes, as well as $F^2(Q) = 1$, which is sufficiently accurate for reactor neutrino energies and keV-scale energy transfers. Thus we obtain

$$\xi_S^2 = 4|\epsilon^{ee11}_{S,u}|^2 \left[N \frac{m_n}{m_u} f^n_{Tu} + Z \frac{m_p}{m_u} f^p_{Tu} \right]^2 . \tag{4.38}$$

Using the bounds on ξ_S^2 from Equations (4.31) and (4.32) we deduce

$$\begin{aligned} &|\epsilon^{ee11}_{S,u}| \leq 1.5 \times 10^{-2} && 90\%\ \text{CL (COHERENT)}\,, \\ &|\epsilon^{ee11}_{S,u}| \leq 2.6 \times 10^{-2} && 99\%\ \text{CL (COHERENT)}\,, \\ &|\epsilon^{ee11}_{S,u}| \leq 6.4 \times 10^{-3} && 3\sigma\ \text{CL (future reactor-based exp.)}\,. \end{aligned} \tag{4.39}$$

These can be compared to present beta decay constraints given in Equation (4.33) to conclude that already now constraints from CEνNS are comparable to the traditional beta decay constraints, which underscores the value this experimental channel has for

probing new physics. If we consider, however, that our scenario is linked to the operator $\mathcal{O}_{lNuq}$, we have to compare this to even stronger constraints on $\widetilde{\epsilon}_{P,ud}$ from pion decay in Equation (4.33). Hence, applying Equation (4.34) with $|V_{ud}| = 0.97370$ [36] we conclude

$$\begin{aligned} |C_{lNuq}| &\leq 1.5 \times 10^{-2} \qquad 90\%\text{ CL from CE}\nu\text{NS}\,, \\ |C_{lNuq}| &\leq 3.9 \times 10^{-4} \qquad 90\%\text{ CL from pion decay}\,, \end{aligned} \tag{4.40}$$

where we quadratically added the bounds on real and imaginary parts of $\widetilde{\epsilon}_P$ for the second inequality. We conclude that Scenario 1 is experimentally disfavored and one cannot expect any signals soon at CEνNS experiments. This conclusion will also apply to the other single operator $\mathcal{O}_{lNqd}$ since it also leads to scalar and pseudoscalar interactions of equal magnitude. Namely, we have in this case

$$\widetilde{\epsilon}^{ee11}_{S,ud} = -\widetilde{\epsilon}^{ee11}_{P,ud} = C^{ee11}_{lNqd} = -(\epsilon^{ee11}_{S,d})^* = -(\epsilon^{ee11}_{P,d})^*\,. \tag{4.41}$$

Therefore Equation (4.37) is modified in the form of simply replacing u by d,

$$\frac{\xi_S^2}{N^2F^2(Q^2)} = 4|\epsilon^{ee11}_{S,d}|^2 \sum_{i=\text{Cs,I}} \frac{1}{N_i^2}\left[N_i \frac{m_n}{m_d} f^n_{Td} + Z_i \frac{m_p}{m_d} f^p_{Td}\right]^2. \tag{4.42}$$

and analogously for Equation (4.38). From this we can derive

$$\begin{aligned} |\epsilon^{ee11}_{S,d}| &\leq 1.7 \times 10^{-2} \qquad 90\%\text{ CL (COHERENT)}\,, \\ |\epsilon^{ee11}_{S,d}| &\leq 3.0 \times 10^{-2} \qquad 99\%\text{ CL (COHERENT)}\,, \\ |\epsilon^{ee11}_{S,d}| &\leq 7.9 \times 10^{-3} \qquad 3\sigma\text{ CL (future reactor-based exp.)}\,, \end{aligned} \tag{4.43}$$

and hence, using Equation (4.41),

$$\begin{aligned} |C_{lNqd}| &\leq 1.7 \times 10^{-2} \qquad 90\%\text{ CL from CE}\nu\text{NS}\,, \\ |C_{lNqd}| &\leq 4.0 \times 10^{-4} \qquad 90\%\text{ CL from pion decay}\,. \end{aligned} \tag{4.44}$$

One way to circumvent this would be if both SMNEFT operators are contributing such that together they cancel the contribution of $\widetilde{\epsilon}_P$, which leads us to Scenario 2.

Scenario 2

Observing that if we consider both operators from Table 2.7 contributing to $\widetilde{\epsilon}_{S,ud}$ and $\widetilde{\epsilon}_{P,ud}$ at the same time, the following scenario could be viable,

$$C_{lNuq} \approx -V_{ud} C_{lNqd} \quad \Rightarrow \quad \widetilde{\epsilon}_{P,ud} \approx 0\,, \qquad \widetilde{\epsilon}_{S,ud} \approx -\frac{2}{V_{ud}} C_{lNuq}\,. \tag{4.45}$$

Such a relation, however is not guaranteed to hold at all energies, even if true at some scale, due to RG running. Nonetheless let us consider this scenario briefly. We find

$$(\widetilde{\epsilon}^{ee11}_{S,ud})^* \approx -\frac{2}{V_{ud}^*}(C^{ee11}_{lNuq})^* = \frac{2}{|V_{ud}|^2}\epsilon^{ee11}_{S,u} = -\frac{2}{|V_{ud}|^2}\epsilon^{ee11}_{P,u} = -2\epsilon^{ee11}_{S,d} = -2\epsilon^{ee11}_{P,d}\,. \tag{4.46}$$

This time we identify, again with Equation (4.30),

$$\begin{aligned} C_S^{(u)} &= 2\,\mathrm{Re}(\epsilon_{S,u}^{ee11}) = -2\,\mathrm{Re}(V_{ud}C_{lNuq})\,, \quad D_P^{(u)} = 2\,\mathrm{Im}(\epsilon_{S,u}^{ee11}) = 2\,\mathrm{Im}(V_{ud}C_{lNuq})\,, \\ C_S^{(d)} &= 2\,\mathrm{Re}(\epsilon_{S,d}^{ee11}) = 2\,\mathrm{Re}(V_{ud}^{-1}C_{lNuq})\,, \quad D_P^{(d)} = 2\,\mathrm{Im}(\epsilon_{S,d}^{ee11}) = -2\,\mathrm{Im}(V_{ud}^{-1}C_{lNuq})\,. \end{aligned} \tag{4.47}$$

Using Equations (4.31) and (4.32) we obtain

$$\begin{aligned} |C_{lNuq}| &\leq 1.8 \times 10^{-2} \qquad 90\%\ \text{CL from CE}\nu\text{NS}\,, \\ |C_{lNuq}| &\leq 3.7 \times 10^{-2} \qquad 90\%\ \text{CL from beta decay}\,. \end{aligned} \tag{4.48}$$

Therefore, this scenario is still possible with Wilson coefficients around 10^{-2}, which corresponds to NP scales of around 1.7 TeV. Applying the projections from Reference [53] we conclude that it could be tested down to

$$|C_{lNuq}| = |V_{ud}^{-1}\epsilon_{S,u}^{ee11}| = |V_{ud}\,\epsilon_{S,d}^{ee11}| \leq 2.0 \times 10^{-4}\,. \tag{4.49}$$

by future CEνNS reactor neutrino experiments. If this interaction would be observed in both coherent scattering and beta decays, then it would constitute a clear hint towards the operator structure of $\mathcal{O}_{lNuq}$ and $\mathcal{O}_{lNqd}$.

Scenario 3

Here we consider $\mathcal{O}'^{ee11}_{lNqd}$ which is the only SMNEFT source of semi-leptonic tensor GNI to be non-vanishing, which implies

$$\epsilon_{T,d}^{ee11} = -(\widetilde{\epsilon}_{T,ud}^{ee11})^* = -(C'^{ee11}_{lNqd})^*. \tag{4.50}$$

Since there are now only neutral-current interactions with down quarks, Equation (4.24) is simplified to

$$\xi_T^2 = 8C_T^2 = 8F^2(Q^2)(C_T^d)^2(N\delta_d^n + Z\delta_d^p)^2\,. \tag{4.51}$$

With Equations (4.24) and (4.30), we conclude

$$\xi_T^2/N^2F^2(Q^2) = 128\,\mathrm{Re}\big(\epsilon_{T,d}^{ee11}\big)^2\left(\delta_d^n + \frac{Z}{N}\delta_d^p\right)^2\,. \tag{4.52}$$

From this form, we can again use the constraints on ξ_T^2 from Reference [54] given in Equation (4.31) and the projections from Reference [53] given in Equation (4.32) to find

$$\begin{aligned} |\mathrm{Re}\big(\epsilon_{T,d}^{ee11}\big)\,| = |C'^{ee11}_{lNqd}| &\leq 9.8 \times 10^{-2} \qquad 90\%\ \text{CL (COHERENT)}\,, \\ |\mathrm{Re}\big(\epsilon_{T,d}^{ee11}\big)\,| = |C'^{ee11}_{lNqd}| &\leq 1.8 \times 10^{-1} \qquad 99\%\ \text{CL (COHERENT)}\,, \\ |\mathrm{Re}\big(\epsilon_{T,d}^{ee11}\big)\,| = |C'^{ee11}_{lNqd}| &\leq 6.2 \times 10^{-2} \qquad 3\sigma\ \text{CL (future reactor-based exp.)}\,. \end{aligned} \tag{4.53}$$

The current bounds from beta decays in Equation (4.33) are stronger by a factor of 4 than the bounds from COHERENT. However, a future reactor-based CEνNS experiment will be competitive with beta decays. This makes the tensor interactions an interesting

candidate to check for GNI from a high energy origin expressing itself through the operator $\mathcal{O}'_{lNqd}$.

We conclude this section about CEνNS and beta decay by noting that we have identified two viable scenarios where SMNEFT operators give rise to detectable signals in both types of experiments in the form of neutral current and charged current scalar or tensor GNI. These sort of complementary measurements could be suitable to favor or disfavor a common high energy origin of both interaction types. In any case, both experimental channels continue to be, as we have seen, essential in future efforts to search for new neutrino interactions at the precision frontier not only for scalar and tensor interactions, but all types of GNI.

4.4. Neutrino-electron scattering

Neutrino electron scattering is mediated in the SM by the exchange of a Z or W boson. Therefore, at low energies, the process is suppressed by the Fermi constant G_F. It is relatively clean in the sense that at tree level no nuclear physics contributes. Therefore, it has been a crucial process in confirming the validity of electroweak interactions, for instance weak neutral currents and the electroweak mixing angle θ_W [141]. The currently strongest bounds on GNI in neutrino-electron scattering, judging from the precision of their determination of c_W, come from the TEXONO experiment [99] for $\overline{\nu}_e$-e-scattering and from the CHARM-II experiment [100,101] for ν_μ-e and $\overline{\nu}_\mu$-e-scattering [52,142]. More recently, constraints from solar neutrinos detected by the Borexino experiment [143], which involve all three flavors, have been derived [144,145]. We do not consider radiative corrections here, since our aim is merely to project the sensitivity, but they become important if one reaches percent-level precision [141,146]. Moreover, we assume that the mass of neutrinos in the final state can be neglected. Current constraints on the case of massive final states have been evaluated in [145].

In this section, we proceed as follows. In Section 4.4.1 we discuss the differential cross section of ν_μ-e scattering in the presence of GNI and identify the observable effective parameters. Then, in Section 4.4.2 we explain the setup of DUNE with focus on the near detector and discuss the projected sensitivity of the experiment to new physics. We note that other future possibilities to probe neutrino-electron scattering such as the nuSTORM facility [147] are being discussed, albeit at less concrete stages of planning.

4.4.1. The differential cross section

In the SM at tree level and at energies well below the weak scale the relevant Lagrangians induced by integrating out W and Z in Figure 4.1 read

$$\mathcal{L}_W = -\frac{g^2}{2m_W^2}(\overline{\nu}_\alpha\gamma_\mu P_L e_\alpha)(\overline{e}_\beta\gamma_\mu P_L\nu_\beta) = -\frac{g^2}{2m_W^2}(\overline{\nu}_\alpha\gamma_\mu P_L\nu_\beta)(\overline{e}_\beta\gamma_\mu P_L e_\alpha)\,, \tag{4.54}$$

$$\mathcal{L}_Z = -\frac{g^2}{4c_W^2 m_Z^2} g_L^\nu(\overline{\nu}_\alpha\gamma_\mu P_L\nu_\alpha)\left[g_L^e(\overline{e}_\beta\gamma_\mu P_L e_\beta) + g_R^e(\overline{e}_\beta\gamma_\mu P_R e_\beta)\right], \tag{4.55}$$

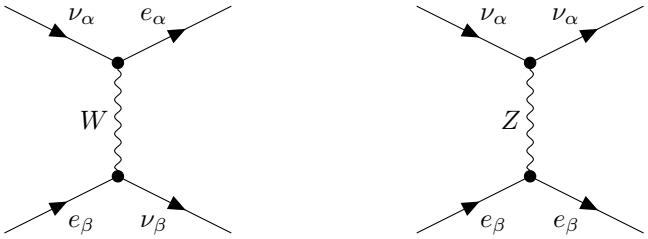

Figure 4.1. SM contributions to neutrino electron scattering at tree level.

where in the first line we used the Fierz transformation (A.27), and the Z charges were given in Equation (1.16). Using $m_Z^2 c_W^2 = m_W^2$ and $g^2/8m_W^2 = G_F/\sqrt{2}$ while fixing the charged leptons to be electrons, we can describe the full interaction by a Lagrangian similar to the neutral current GNI Lagrangian (2.11), where we identify SM values for ϵ_L and ϵ_R,

$$\epsilon^{\alpha\beta ee}_{L,e,\mathrm{SM}} = \delta_{\alpha e}\delta_{\beta e} + 2g_L^\nu g_L^e\,\delta_{\alpha\beta}\,, \qquad \epsilon^{\alpha\beta ee}_{R,e,\mathrm{SM}} = 2g_L^\nu g_R^e\,\delta_{\alpha\beta}\,. \tag{4.56}$$

For the numerical values of g_L^e and g_R^e, we use the value $s_W^2 = 0.22343$ (which is obtained in the on-shell scheme) [148]. We consider two scattering channels which play an important role at DUNE. These are, as we discuss in Section 4.4.2, $\nu_\mu e^- \to \nu_\beta e^-$ and $\overline{\nu}_\mu e^- \to \overline{\nu}_\beta e^-$, where β denotes any flavor. From inspecting Equation (4.56), we conclude that in the SM case only the Z-contribution is non-vanishing, and only for $\beta = \mu$. However, since the final neutrino flavor is not observed, we cannot exclude the presence of also ν_e and ν_τ final states if new physics plays a role. Effectively, we thus have to sum over the cross sections of all neutrino final states. For compactness of notation, we will henceforth drop the unnecessary indices and write

$$\epsilon_j^{\alpha\beta} = \epsilon_{j,e}^{\alpha\beta ee} \tag{4.57}$$

throughout this section. The differential cross sections for the general interaction Lagrangian (2.11) are derived in Appendix C.1 (see also References [2, 52]) and read

$$\begin{aligned}
\frac{\mathrm{d}\sigma_{\nu_\mu\to\nu_\beta}}{\mathrm{d}T} &= \frac{G_F^2 m_e}{\pi}\left[A + 2B\left(1-\frac{T}{E_\nu}\right) + C\left(1-\frac{T}{E_\nu}\right)^2 + D\frac{m_e T}{E_\nu^2}\right],\\
\frac{\mathrm{d}\sigma_{\overline{\nu}_\mu\to\overline{\nu}_\beta}}{\mathrm{d}T} &= \frac{G_F^2 m_e}{\pi}\left[C + 2B\left(1-\frac{T}{E_\nu}\right) + A\left(1-\frac{T}{E_\nu}\right)^2 + D\frac{m_e T}{E_\nu^2}\right],
\end{aligned} \tag{4.58}$$

where $E_\nu \gg m_e$ denotes the energy of the incoming (anti-)neutrino, $T < E_\nu$ the kinetic energy of the recoiled electron, and the coefficients are given by

$$\begin{aligned}
A &= 2|\epsilon_L^{\mu\beta}|^2 + \frac{1}{4}(|\epsilon_S^{\mu\beta}|^2 + |\epsilon_P^{\mu\beta}|^2) + 8|\epsilon_T^{\mu\beta}|^2 - 2\mathrm{Re}\left((\epsilon_S+\epsilon_P)^{\mu\beta}\epsilon_T^{\mu\beta *}\right),\\
B &= -\frac{1}{4}(|\epsilon_S^{\mu\beta}|^2 + |\epsilon_P^{\mu\beta}|^2) + 8|\epsilon_T^{\mu\beta}|^2,\\
C &= 2|\epsilon_R^{\mu\beta}|^2 + \frac{1}{4}(|\epsilon_S^{\mu\beta}|^2 + |\epsilon_P^{\mu\beta}|^2) + 8|\epsilon_T^{\mu\beta}|^2 + 2\mathrm{Re}\left((\epsilon_S+\epsilon_P)^{\mu\beta}\epsilon_T^{\mu\beta *}\right),\\
D &= -2\mathrm{Re}\left(\epsilon_L^{\mu\beta}\epsilon_R^{\mu\beta *}\right) + \frac{1}{2}|\epsilon_S^{\mu\beta}|^2 - 8|\epsilon_T^{\mu\beta}|^2.
\end{aligned} \tag{4.59}$$

In these expressions we have absorbed the SM contributions given in Equation (4.56) in the definition of ϵ_L and ϵ_R. Immediately, we see that most contributions are proportional to squares of the absolute values of epsilon parameters. There is one exception in the coefficients A and C, namely a term mixing ϵ_S and ϵ_P with ϵ_T which therefore vanishes unless there are both (pseudo)scalar and tensor interactions at the same time. In the definition of coefficient D there is furthermore a mixture of L and R coefficients. However, the contribution of D to the differential cross section is suppressed by a factor of m_e/E_ν which we discuss below to be of order 10^{-4}. This also shows us that ϵ_S and ϵ_P will be practically indistinguishable. This formula is consistent with the SM result

$$A_{\rm SM} = 2(g_L^e)^2\,, \quad B_{\rm SM} = 0\,, \quad C_{\rm SM} = 2(g_R^e)^2\,, \quad D_{\rm SM} = -2g_L^e g_R^e\,. \tag{4.60}$$

To see what the parameters determining the shape of the spectrum are, we sum over final states $\beta = e, \mu, \tau$. First we consider the chirality-flipping interactions S, P and T. Neglecting the (pseudo)scalar-tensor mixed term, it is clear that we are only sensitive to the effective parameters

$$|\epsilon_X^\mu|^2 \equiv \sum_{\beta=e,\mu,\tau} |\epsilon_X^{\mu\beta}|^2\,, \quad X = S, P, T\,, \tag{4.61}$$

and not to individual flavors. Therefore, we will use ϵ_μ^j with $j = S, P, T$ for fitting the spectrum and later translate bounds on this parameter to bounds on $|\epsilon_X^{\mu e}|$, $|\epsilon_X^{\mu\mu}|$, and $|\epsilon_X^{\mu\tau}|$ assuming only one of them contributes to ϵ_X^μ. Concerning the NSI-type interactions $j = L, R$, the fact that ϵ_L and ϵ_R can be split into SM plus new physics contributions,

$$\epsilon_L^{\mu\beta} = \epsilon_{L,\rm SM}^{\mu\beta} + \epsilon_{L,\rm NSI}^{\mu\beta}\,, \quad \epsilon_R^{\mu\beta} = \epsilon_{R,\rm SM}^{\mu\beta} + \epsilon_{R,\rm NSI}^{\mu\beta}\,, \tag{4.62}$$

leads to a contribution of new physics already at the linear order. Namely, when neglecting the suppressed D-term, taking the sum over β results in

$$\sum_\beta \left| g_X \delta_{\mu\beta} + \epsilon_{X,\rm NSI}^{\mu\beta} \right|^2 = \left(g_X + \epsilon_{X,\rm NSI}^{\mu\mu} \right)^2 + |\epsilon_{X,\rm NSI}^\mu|^2\,, \quad X = L, R\,, \tag{4.63}$$

where we used that $\epsilon_X^{\mu\mu}$ is real and defined the effective parameter analogue of ϵ_X^μ for $j = L, R$ as

$$|\epsilon_{j,\rm NSI}^\mu|^2 \equiv \sum_{\beta=e,\tau} |\epsilon_X^{\mu\beta}|^2\,, \quad X = L, R\,. \tag{4.64}$$

Notice that the flavor-diagonal contribution is left out of the sum on the right-hand side. Therefore, the flavor-diagonal coefficients $\epsilon_L^{\mu\mu}$ and $\epsilon_R^{\mu\mu}$ contribute to the cross section at linear order, while all others contribute at quadratic order. The contribution of D includes further superpositions of L and R parameters,

$$\sum_\beta \mathrm{Re}\left(\epsilon_L^{\alpha\beta} \epsilon_R^{\alpha\beta *} \right) = g_L g_R + g_L \epsilon_{R,\rm NSI}^{\alpha\alpha} + g_R \epsilon_{L,\rm NSI}^{\alpha\alpha} + \sum_\beta \mathrm{Re}\left(\epsilon_{L,\rm NSI}^{\mu\beta} \epsilon_{R,\rm NSI}^{\mu\beta *} \right). \tag{4.65}$$

However, these are subleading since the whole term is suppressed by m_e/E_ν as noted earlier. Therefore we set the new physics in this term to zero unless we consider explicitly

Table 4.3. Parameters that influence the scattering of electrons with muon (anti)neutrinos (first line) and the fundamental new interaction parameters that can be constrained from the respective measurements (second line).

Observable	$\epsilon^{\mu\mu}_{L/R,\mathrm{NSI}}$	$\lvert\epsilon^{\mu}_{L/R,\mathrm{NSI}}\rvert$	$\lvert\epsilon^{\mu}_{S/P/T}\rvert$
Bound on	$\epsilon^{\mu\mu}_{L/R,\mathrm{NSI}}$	$\lvert\epsilon^{\mu e}_{L/R,\mathrm{NSI}}\rvert$, $\lvert\epsilon^{\mu\tau}_{L/R,\mathrm{NSI}}\rvert$	$\lvert\epsilon^{\mu e}_{S/P/T}\rvert$, $\lvert\epsilon^{\mu\mu}_{S/P/T}\rvert$, $\lvert\epsilon^{\mu\tau}_{S/P/T}\rvert$

the simultaneous presence of flavor diagonal L and R coefficients in which case we use

$$\sum_{\beta} \mathrm{Re}\left(\epsilon_L^{\alpha\beta}\epsilon_R^{\alpha\beta *}\right) = g_L g_R + g_L \epsilon^{\alpha\alpha}_{R,\mathrm{NSI}} + g_R \epsilon^{\alpha\alpha}_{L,\mathrm{NSI}} + \epsilon^{\mu\mu}_{L,\mathrm{NSI}}\epsilon^{\mu\mu}_{R,\mathrm{NSI}}\,. \tag{4.66}$$

To summarize, we consider the seven parameters shown in Table 4.3. In the second line we show on which GNI parameters they depend. We note that, as shown in Appendix A.5, all seven parameters are allowed in both Dirac and Majorana neutrino case, unless one assumes flavor conservation in which case $|\epsilon^{\alpha}_T| = |\epsilon^{\alpha\alpha}_T| = 0$. We translate previous bounds on muon-neutrino GNI from CHARM-II to bounds on these seven parameters in Appendix C.2 [52]. The results are shown in Table 4.4 together with the new expected bounds from DUNE which we discuss in the next section.

For completeness, we comment on the neutrino-electron scattering of other flavors than muon. If we consider, as suitable for TEXONO [99], the scattering $\overline{\nu}_e e \to \overline{\nu}_\beta e$, we can still use the cross section (4.58) with μ replaced by e. However, according to Equation (4.56), the SM value of ϵ_L and ϵ_R are different due to the additional charged current interaction,

$$A_{\mathrm{SM}} = 2(1+g_L^e)^2\,, \quad B_{\mathrm{SM}} = 0\,, \quad C_{\mathrm{SM}} = 2(g_R^e)^2\,, \quad D_{\mathrm{SM}} = -2(1+g_L^e)g_R^e\,. \tag{4.67}$$

Besides this modified SM part, we have the same dependence of the cross section on seven parameters, namely

$$\epsilon^{ee}_{L,\mathrm{NSI}}\,, \quad |\epsilon^{e}_{L,\mathrm{NSI}}|\,, \quad \epsilon^{ee}_{R,\mathrm{NSI}}\,, \quad |\epsilon^{e}_{R,\mathrm{NSI}}|\,, \quad |\epsilon^{e}_{S}|\,, \quad |\epsilon^{e}_{P}|\,, \quad |\epsilon^{e}_{T}|\,, \tag{4.68}$$

where

$$\begin{aligned} |\epsilon^{e}_{X,\mathrm{NSI}}| &= \sqrt{|\epsilon^{e\mu}_{X,\mathrm{NSI}}|^2 + |\epsilon^{e\tau}_{X,\mathrm{NSI}}|^2}\,, & X &= L, R\,, \\ |\epsilon^{e}_{X}| &= \sqrt{|\epsilon^{ee}_{X}|^2 + |\epsilon^{e\mu}_{X}|^2 + |\epsilon^{e\tau}_{X}|^2}\,, & X &= S, P, T\,. \end{aligned} \tag{4.69}$$

In Appendix C.2 we derive constraints on these parameters from the previous GNI analysis in Reference [52].

4.4.2. Sensitivity of the DUNE near detector

The Deep Underground Neutrino Experiment (DUNE) is a planned experimental facility set to observe neutrino oscillations at a long baseline of 1300 km [149]. Its ambitious scale and versatile liquid argon detector design admits a rich physics programme both at

the near detector and far detector which includes besides neutrino oscillations and the test of leptonic charge-parity violation the possibility to observe supernova neutrinos and to probe the proton lifetime [19]. We have discussed some aspects of GNI in neutrino oscillations in Section 4.1. In this section, however, we focus on the opportunity to test neutrino-electron scattering at the near detector. The influence of NSI (embedded in SMEFT) on the total cross section has been considered in Reference [150] for the DUNE near detector. As in the corresponding publication (Reference [1]), we include here instead all types of GNI and apply the differential cross section. The tremendous advantage of using spectral information becomes clear when considering two important points. Firstly, the spectral shape (in contrast to the total event numbers) can be used to distinguish different types of new physics. Secondly, the neutrino-electron scattering channel is due to its theoretical simplicity one of the ingredients to determine the normalization of the beam intensity [19] which means that the neutrino-electron scattering spectrum itself is expected to have a large systematic uncertainty concerning the normalization. This is less of a problem if we fit the shape of the spectrum. We note that matter NSI will also be tested in the study of oscillation physics at DUNE [107, 151–153]. This concerns, however, only interactions of the type $\epsilon_V \equiv \epsilon_L + \epsilon_R$ and a sum of electron, up, and down quark interactions as defined in Equation (4.14), since other types of interaction play no role for the coherent forward scattering of neutrinos in (unpolarized) matter [154]. In this sense, our study is complementary to the oscillation tests, in particular since we can identify various types of GNI specific to electrons. Below we numerically compare the expected constraints from the oscillation analysis to our results.

To assess the sensitivity, we need besides the cross section mainly the expected neutrino flux and some properties of the detector. We take the simulated fluxes from Reference [155], which we plot in Figure 4.2. There are two beam modes corresponding to mainly muon neutrinos or muon antineutrinos, respectively. The composition in the neutrino mode is approximately 90-95% muon neutrinos, 5-10% muon antineutrinos and about 1% electron (anti)neutrinos. In the antineutrino mode, the fractions of muon neutrinos and antineutrinos are reversed, as shown in Figure 4.2. In Section 4.4.1 we stated that $\nu_\mu e \to \nu_\beta e$ and $\overline{\nu}_\mu e \to \overline{\nu}_\beta e$ scattering were most important, and here we can see the reasons: The electron and tau (anti)neutrino components are by design very small compared to the muon (anti)neutrinos and we therefore neglect them as initial particles in our study. In principle, we could also consider $\nu_\mu e \to \nu_\beta \mu$ scattering. However, the threshold energy of this process is $E_\nu = m_\mu^2/2m_e \approx 10.9\,\text{GeV}$ and the fraction of such high-energy neutrinos is very small. Therefore we consider the flux only up to energies of 10 GeV. Hence, the full energy range we consider is 0.125-10 GeV. Concerning the intensity we assume for the first phase of operation a 1.2 MW beam of 120 GeV protons [149]. For the second, later phase the plan is to double the beam power. Considering the first phase as operating for 5 years (2.5 in each beam mode) and assuming 1.8×10^7 seconds per year operating time we obtain 1.123×10^{21} POT/a (protons-on-target per year) or 2.809×10^{21} POT per channel in total.

At the time of this analysis, published in Reference [2], the near detector design was not yet determined. However, it was clear that the core part would be a liquid argon time projection chamber (LArTPC) akin to the far detector, although naturally significantly smaller in volume. This is still valid, even though it is now clear that the near detector

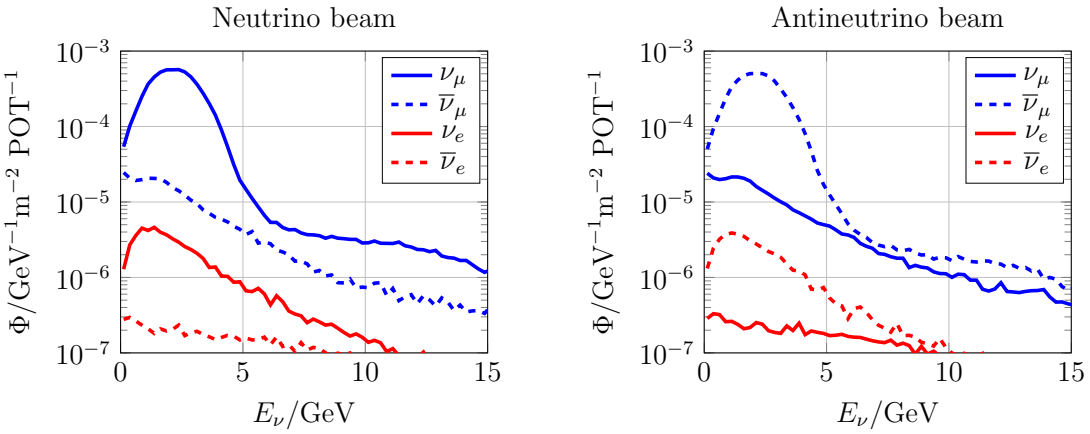

Figure 4.2. Simulated neutrino fluxes from the optimized design published in Reference [155] for both neutrino and antineutrino beam. Figure adapted from Reference [2].

design will be modular and also involve a high-pressure gaseous argon time projection chamber as well as the possibility to move the liquid and gaseous argon detectors off axis (DUNE PRISM) [19]. Our sensitivity study assumes a LArTPC with 84 tons of fiducial argon mass [156]. From this we estimate the number of target electrons as $18 \cdot 1.2663 \times 10^{30} = 2.2793 \times 10^{31}$. We assume full 4π solid angle coverage and for the energy resolution we take $0.06/\sqrt{E_e} \approx 0.06/\sqrt{T}$ (in GeV), which should be valid in our region of interest up to 10 GeV [157].

The expected number of events in a given energy bin $[T_i, T_i + \Delta T]$ of size ΔT for a given type of neutrino $X = \nu_\mu, \overline{\nu}_\mu$ reads

$$N_i(\vec{\epsilon}) = \Delta t N_e \int_{\Delta T\cdot(i-1)}^{\Delta T\cdot i} \mathrm{d}T \int_0^{E_{\max}} \mathrm{d}E_\nu\, \Theta(T - E_\nu) \frac{\mathrm{d}\sigma_X}{\mathrm{d}T}(E_\nu, T, \vec{\epsilon}) \frac{\mathrm{d}\Phi_X}{\mathrm{d}E_\nu}(E_\nu)\,, \tag{4.70}$$

where Δt is the time of data taking times the beam-specific POT (per time), N_e is the number of electron targets, $E_{\max} = 10\,\mathrm{GeV}$ is the maximal neutrino energy, $\mathrm{d}\Phi_X/\mathrm{d}E_\nu$ is the differential neutrino flux of type X in units of neutrinos/GeV/m^2/POT (i.e. as plotted in Figure 4.2). We require the Heaviside step function $\Theta(T - E_\nu)$ to assert the kinematic condition $T \leq E_\nu$. The differential cross sections $\mathrm{d}\sigma_X/\mathrm{d}T$ have been given in Equations (4.58). The dependence of the cross sections on the seven independent new physics parameters have been included in the form of the shorthand notation

$$\vec{\epsilon} = \left(\epsilon_{\mu\mu}^{L,\mathrm{NSI}},\, \epsilon_{\mu\mu}^{R,\mathrm{NSI}},\, |\epsilon_\mu^{L,\mathrm{NSI}}|,\, |\epsilon_\mu^{R,\mathrm{NSI}}|,\, |\epsilon_\mu^S|,\, |\epsilon_\mu^P|,\, |\epsilon_\mu^T|\right). \tag{4.71}$$

To account for imperfect resolution, this spectrum is further convolved with a Gaussian function,

$$N_i(\vec{\epsilon}) = \Delta t N_e \int_{\Delta T\cdot(i-1)}^{\Delta T\cdot i} \mathrm{d}T \int_0^{E_{\max}} \mathrm{d}E_\nu \int_0^{E} \mathrm{d}t\, f(T - t) \frac{\mathrm{d}\sigma_X}{\mathrm{d}T}(E_\nu, t, \vec{\epsilon}) \frac{\mathrm{d}\Phi_X}{\mathrm{d}E_\nu}(E_\nu)\,, \tag{4.72}$$

where

$$f(T - t) = \frac{1}{\sqrt{2\pi}\sigma(t)} e^{-\frac{(T-t)^2}{2\sigma^2(t)}}\,, \qquad \sigma(t) = 0.06\sqrt{t}/\sqrt{\mathrm{GeV}}\,. \tag{4.73}$$

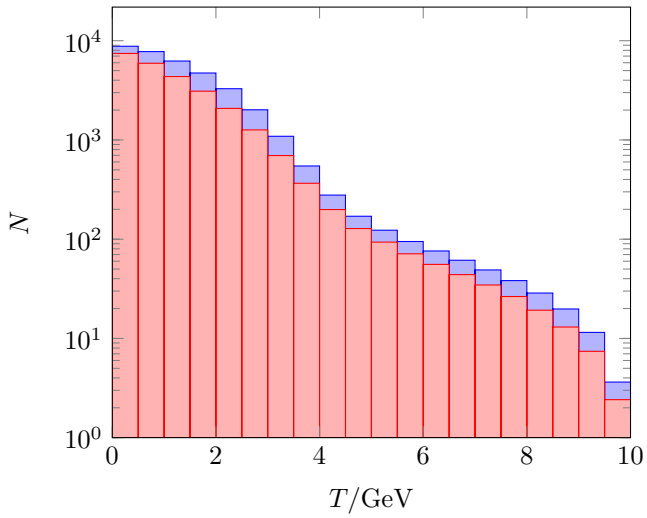

Figure 4.3. Expected electron event numbers from neutrino-electron scattering in neutrino channel (blue) and antineutrino channel (red) at each 2.5 years of exposure assuming SM parameters. Figure adapted from Reference [2].

Assuming SM $\vec{\epsilon} = 0$ and a bin size of $\Delta T = 0.5\,\text{GeV}$, we obtain the event numbers shown in Figure 4.3 from which we conclude that one expects good statistics. As an illustration of the effect of new physics on the shape of the spectrum, we show in Figure 4.4 the ratios of expected event numbers N/N_{SM}, where $N = N_{\text{NP+SM}}$ includes one of the parameters in $\vec{\epsilon}$. For these we take values approximately at the magnitude of current bounds. Figure 4.4 illustrates nicely why the shape information could prove to be crucial in distinguishing the source of new physics, if observed.

To quantify the sensitivity for new physics we perform a χ^2 test. Due to relatively low statistics ($\lesssim$ 100 Events) above $T = 5\,\text{GeV}$, we cut off the spectrum there. The obtained bounds do not sensitively depend on the precise choice of this "cutoff", as we have explicitly checked. Our χ^2 function is defined as

$$\chi^2(\vec{\epsilon}) = \frac{a^2}{\sigma_a^2} + \sum_{X=\nu_\mu,\overline{\nu}_\mu} \sum_{i=1}^{n_{\text{bins}}} \frac{\left((1+a)N_i^X(\vec{\epsilon}) - N_i^{X,\text{SM}}\right)^2}{(\sigma_i^X)^2(\vec{\epsilon})}\,, \tag{4.74}$$

where N_i^X denotes the number of events in the i-th bin of the channel X (either neutrino or antineutrino), and σ_i^X denotes the uncertainty, which we assume to be statistically dominated,

$$\sigma_i^X(\vec{\epsilon}) = \sqrt{N_i^X(\vec{\epsilon})}\,. \tag{4.75}$$

The parameter a is crucial in order to obtain realistic results since, as we previously discussed, the ν-e scattering is used to normalize the flux and therefore we need to take into account relatively large uncertainties σ_a on the normalization. To illustrate the dependence of the sensitivity on this normalization uncertainty, we consider three

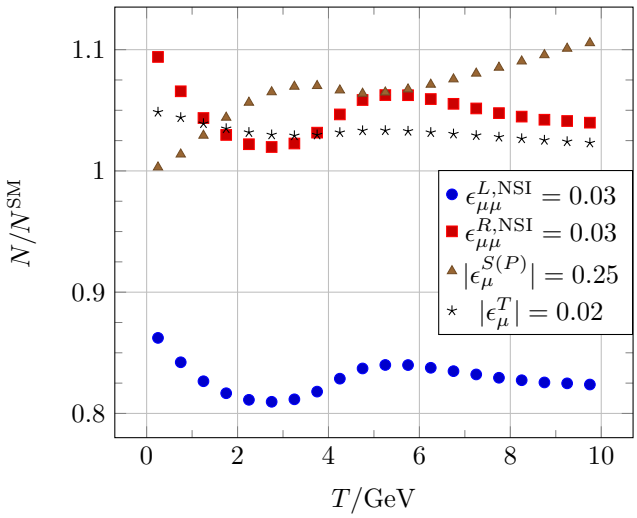

Figure 4.4. Expected event number spectrum $N = N_{\mathrm{SM+NP}}$ in the neutrino channel for different new physics parameters tuned away from zero compared to the SM spectrum N_{SM}. The sample values are of the order of magnitude of current bounds, see Table 4.4. Figure adapted from Reference [2].

scenarios, namely

$$\begin{aligned} &\text{A (“ideal”) :} && (\sigma_a, T_{\mathrm{th}}) = (0, 0)\,, \\ &\text{B (“optimistic”) :} && (\sigma_a, T_{\mathrm{th}}) = (1\%, 0)\,, \\ &\text{C (“conservative”) :} && (\sigma_a, T_{\mathrm{th}}) = (5\%, 500\,\mathrm{MeV})\,, \end{aligned} \tag{4.76}$$

where T_{th} denotes the threshold energy for detecting a recoil electron of this process.

Results

We investigate two kinds of configurations which are frequently used to express projected GNI bounds in the literature. The first is switching on a single one of the seven parameters in Equation (4.71) and compare the simulated event numbers N_i with the ones simulated for the SM case N_i^{SM} using the χ^2 function (4.74). From this we can deduce upper bounds at 90% CL which DUNE is expected to cast assuming the SM is the true theory. The results of this procedure are shown in Table 4.4, where they are also compared to present bounds from CHARM-II and TEXONO from Reference [52] whose adaptation is discussed in Appendix C.2. The second configuration we consider allows for two parameters at the same time. The resulting 90% and 95% confidence regions are shown in Figure 4.5. As discussed below Equation (4.58), ϵ_S and ϵ_P cannot be distinguished at the current precision and therefore we do not show the results for ϵ_P. The same holds true for off-diagonal L and R coefficients which is why we show only the more constrained $\epsilon_L^{\mu\mu}$ and $\epsilon_R^{\mu\mu}$. In the case of ϵ_μ^S or ϵ_μ^P and ϵ_μ^T non-zero, we assume real parameters for simplicity.

We conclude that the single parameter bounds on $\epsilon_L^{\mu\mu}$ and $\epsilon_R^{\mu\mu}$ can be expected to be improved after the first phase of DUNE by about an order of magnitude, even in the

Table 4.4. Expected bounds (90% CL) on electron GNI after 2.5+2.5 years of DUNE operation assuming three different experimental scenarios specified in (4.76), compared with current bounds from CHARM-II. For convenience, we list mass scales $\Lambda/\sqrt{C} = (\sqrt{2}/G_F\epsilon)^{1/2}$ associated withe the future bounds. In the lower section we show bounds on electron GNI from $\overline{\nu}_e$-e scattering at TEXONO. See Appendix C.2 for details.

Observable	NP Parameters	Scen.	Future DUNE	CHARM-II	$\Lambda/\sqrt{C}$ [TeV]
$\epsilon_{\mu\mu}^{L,\mathrm{NSI}}$	$\epsilon_{\mu\mu}^{L,\mathrm{NSI}}$	A	± 0.0014	$[-0.06, 0.02]$	9.3
		B	± 0.0028		6.7
		C	± 0.0038		5.7
$\epsilon_{\mu}^{L,\mathrm{NSI}}$	$\lvert\epsilon_{e\mu}^{L,\mathrm{NSI}}\rvert,\ \lvert\epsilon_{\mu\tau}^{L,\mathrm{NSI}}\rvert$	A	0.028	0.11	2.1
		B	0.039		1.8
		C	0.046		1.6
$\epsilon_{\mu\mu}^{R,\mathrm{NSI}}$	$\epsilon_{\mu\mu}^{R,\mathrm{NSI}}$	A	± 0.0017	$[-0.06, 0.02]$	8.6
		B	± 0.0027		6.8
		C	± 0.0031		6.3
$\epsilon_{\mu}^{R,\mathrm{NSI}}$	$\lvert\epsilon_{e\mu}^{R,\mathrm{NSI}}\rvert,\ \lvert\epsilon_{\mu\tau}^{R,\mathrm{NSI}}\rvert$	A	0.027	0.10	2.1
		B	0.035		1.9
		C	0.037		1.8
$\epsilon_{\mu}^{S}, \epsilon_{\mu}^{P}$	$\lvert\epsilon_{e\mu}^{S}\rvert,\ \lvert\epsilon_{\mu\mu}^{S}\rvert,\ \lvert\epsilon_{\mu\tau}^{S}\rvert,$	A	0.10	0.4	1.1
	$\lvert\epsilon_{e\mu}^{P}\rvert,\ \lvert\epsilon_{\mu\mu}^{P}\rvert,\ \lvert\epsilon_{\mu\tau}^{P}\rvert$	B	0.12		1.0
		C	0.14		0.9
ϵ_{μ}^{T}	$\lvert\epsilon_{e\mu}^{T}\rvert,\ \lvert\epsilon_{\mu\mu}^{T}\rvert,\ \lvert\epsilon_{\mu\tau}^{T}\rvert$	A	0.008	0.04	4.0
		B	0.012		3.1
		C	0.020		2.4
Observable	NP Parameters		TEXONO		
$\epsilon_{ee}^{L,\mathrm{NSI}}$	$\epsilon_{ee}^{L,\mathrm{NSI}}$		$[-0.31, 0.24]$		
$\epsilon_{e}^{L,\mathrm{NSI}}$	$\lvert\epsilon_{e\mu}^{L,\mathrm{NSI}}\rvert,\ \lvert\epsilon_{e\tau}^{L,\mathrm{NSI}}\rvert$		0.27		
$\epsilon_{ee}^{R,\mathrm{NSI}}$	$\epsilon_{ee}^{R,\mathrm{NSI}}$		$[-0.24, 0.31]$		
$\epsilon_{e}^{R,\mathrm{NSI}}$	$\lvert\epsilon_{e\mu}^{R,\mathrm{NSI}}\rvert,\ \lvert\epsilon_{e\tau}^{R,\mathrm{NSI}}\rvert$		0.16		
ϵ_{e}^{S}	$\lvert\epsilon_{ee}^{S}\rvert,\ \lvert\epsilon_{e\mu}^{S}\rvert,\ \lvert\epsilon_{e\tau}^{S}\rvert$		0.6		
ϵ_{e}^{P}	$\lvert\epsilon_{ee}^{P}\rvert,\ \lvert\epsilon_{e\mu}^{P}\rvert,\ \lvert\epsilon_{e\tau}^{P}\rvert$		0.7		
ϵ_{e}^{T}	$\lvert\epsilon_{ee}^{T}\rvert,\ \lvert\epsilon_{e\mu}^{T}\rvert,\ \lvert\epsilon_{e\tau}^{T}\rvert$		0.08		

conservative configuration. The bounds on chirality-flipping (pseudo)scalar and tensor interactions are expected to improve by at least a factor of 1/2. This corresponds to probing energy scales up to several TeV if we identify the interaction energy scale in an EFT-inspired way as $\Lambda/\sqrt{C} = (\sqrt{2}/G_F\epsilon)^{1/2}$. We can compare the bounds to the expected bounds on matter NSI from the neutrino oscillation analysis. Matter NSI have been defined in Equation (4.14). In the case when matter NSI are only constituted by interactions with electrons (and not quarks), we can compare results from Reference [107] with our conservative bound on the parameters contributing to matter NSI,

$$\begin{aligned} |\epsilon^V_{e\mu}| \leq 0.051\,, \quad |\epsilon^V_{\mu\tau}| \leq 0.031 \qquad & [107]\,, \\ |\epsilon^{L,\mathrm{NSI}}_{e\mu}|, |\epsilon^{L,\mathrm{NSI}}_{\mu\tau}|, |\epsilon^{R,\mathrm{NSI}}_{e\mu}|, |\epsilon^{R,\mathrm{NSI}}_{\mu\tau}| \leq 0.039 \qquad & \text{Table 4.4}\,. \end{aligned} \tag{4.77}$$

In this case the bounds are comparable in magnitude. However, the complementarity allows, for instance, to distinguish electron from quark matter interactions. Moreover, flavor-diagonal matter NSI of different flavors cannot be measured independently in the oscillation amplitudes and we see that ν-e scattering can help breaking this degeneracy,

$$\begin{aligned} \epsilon^V_{ee} - \epsilon^V_{\mu\mu} \in (-0.7, +0.8)\,, \quad \epsilon^V_{\tau\tau} - \epsilon^V_{\mu\mu} \in (-0.08, +0.08) \qquad & [107]\,, \\ |\epsilon^{L,\mathrm{NSI}}_{\mu\mu}|, |\epsilon^{R,\mathrm{NSI}}_{\mu\mu}| \in (-0.0027, 0.0027) \qquad & \text{Table 4.4}\,. \end{aligned} \tag{4.78}$$

In addition, constraints on neutrino-quark NSI are also expected to greatly improve on the one hand due to neutrino-nucleus scattering at the DUNE near detector [150], but on the other hand also from coherent elastic neutrino nucleus scattering experiments [53,54,158], as we discussed in Section 4.3. There are some interesting further insights to draw from the two-dimensional exclusion regions in Figure 4.5. In particular in the L-R plot we see the large degeneracy of the flux uncertainty with particular directions in parameter space. These are the directions for which the shape of the spectrum is nearly unchanged. It is worth noting that for the chirality-flipping interactions this effect is less pronounced due to the shift in shape with respect to the SM spectrum which we have shown in Figure 4.4.

In summary, we found that the spectral information of the differential cross section is suitable to reduce the vulnerability to flux normalization uncertainties. The expected bounds on GNI from the first phase of DUNE are summarized in Tables 4.4 and 4.5.

4.5. Neutrino mass experiments

Neutrino mass experiments like the Karlsruhe Tritium Neutrino Experiment (KATRIN) are of obvious interest and importance at a time when the absolute mass of neutrinos is still undetermined, making them the only SM particles for which this essential property is unknown. In this section, we consider the question if and how GNI can be tested as part of an extended physics programme at such experiments. This question has been previously addressed in Reference [57], where effects of GNI on the differential electron spectrum from the beta decay of tritium have been calculated. There are two major obstructions to actually detecting those modifications to the spectrum, as we will see explicitly in the following. Firstly, to reduce systematic errors and gain the best possible sensitivity from the data, on has to treat the normalization of the electron spectrum as a free fit parameter

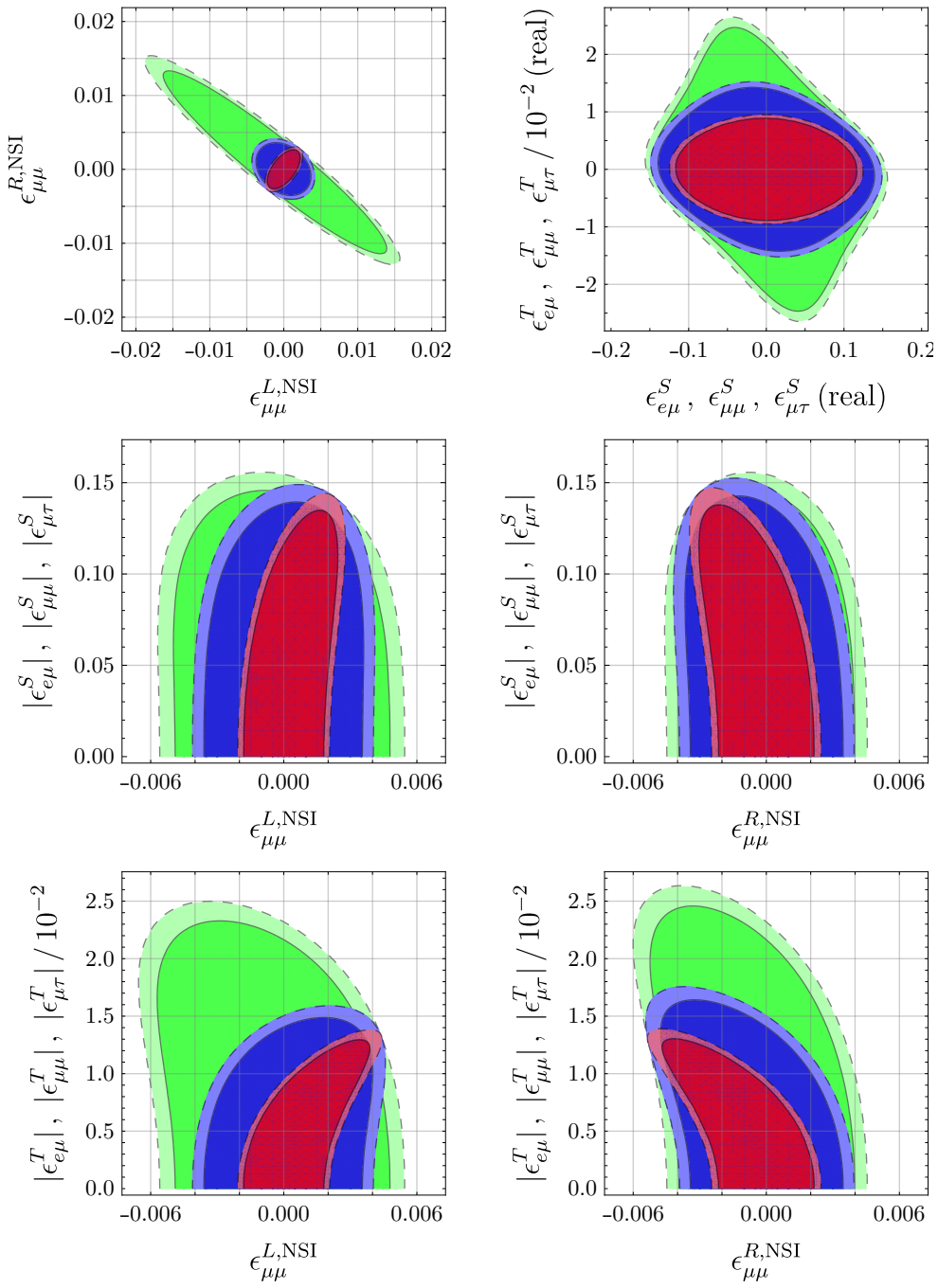

Figure 4.5. Projected two-parameter exclusion plots after 2.5+2.5 years of DUNE operation. Solid and dashed contour lines correspond to 90% and 95% CL, respectively. The red, blue, and green regions correspond to experimental scenarios A, B, and C specified in (4.76). We only show flavor-diagonal components of $\epsilon^{L,\mathrm{NSI}}$ and $\epsilon^{R,\mathrm{NSI}}$, single-parameter bounds on the off-diagonal parameters are given in Table 4.4. Figure adapted from Reference [2].

(shape-only fit) [44]. This implies that effects that mostly just increase or decrease the amplitude but not the shape of the spectrum are undetectable. Secondly, the main goal of KATRIN is to determine very precisely the endpoint of the electron spectrum and therefore the setup is optimized to detect only a small part of the spectrum, even though there are upgrade plans to make the entire spectrum accessible [159]. This means that even if new physics changes the shape of the spectrum it can only be seen if it changes the shape significantly close to the end point. For these reasons, neutrino mass experiments are not considered prime candidates for detecting GNI in beta decay [109]. Nonetheless, constraining new physics from as many channels as possible is valuable which is why we analyze here in detail which types of scenarios can be constrained by KATRIN. These considerations could also inform us which types of upgrades to the experiment would be fruitful in this endeavor. The section is structured as follows. In Section 4.5.1, we present and discuss the differential decay rate of tritium in the very general case of admitting both GNI and a sterile neutrino with a small mixing to the active neutrinos. In this setup there are in general right-handed partners of active neutrinos and a fourth, potentially heavier sterile neutrino. From this we identify the few parameters which determine the shape of the spectrum and how they depend on GNI and the mixing matrix. In Section 4.5.2, we then apply this to KATRIN and discuss which new physics scenarios can be constrained by the present experimental setup.

4.5.1. Tritium beta decay in the presence of new physics

In Appendix D.1 we derive the effective beta decay Lagrangian in the case of 3+1 neutrinos and in the presence of GNI, where we account for the fact that the measured CKM matrix prefactor $\widetilde{V}_{ud} = 0.97420 \pm 0.00021$ is measured in such a beta decay and therefore already contains some of the new physics. The effective Lagrangian reads

$$\begin{aligned}\mathcal{L}_{\text{eff}} = &-\frac{G_F \widetilde{V}_{ud}}{\sqrt{2}} \sum_{j=1}^{10} \widehat{\epsilon}_j \left(\overline{e}\mathcal{O}_j \nu_e\right) \left(\overline{u}\mathcal{O}'_j d\right) \\ &- \frac{G_F \widetilde{V}_{ud}}{\sqrt{2}} \sum_{j=1}^{10} \left(\delta_{1j} U_{e4} + \overset{(\sim)N}{\epsilon}_j\right) \left(\overline{e}\mathcal{O}_j N\right) \left(\overline{u}\mathcal{O}'_j d\right) + \text{H.c.}\,,\end{aligned} \tag{4.79}$$

where U denotes the (extended) PMNS matrix, N denotes a hypothetical sterile neutrino and

$$\begin{aligned}\widehat{\epsilon}_L &= 1 - \epsilon_R - \frac{1}{2}|U_{e4}|^2 - \frac{1}{2}K\,, \\ \widehat{\epsilon}_j &= \overset{(\sim)}{\epsilon}_j \quad (1 - \epsilon_L - \epsilon_R)\,, \qquad\qquad j \geq 2\,,\end{aligned} \tag{4.80}$$

with

$$K = 2\text{Re}\left(\epsilon_R(\epsilon_L + \epsilon_R)\right) + 2\text{Re}(U_{e4}(\epsilon_L^N + \epsilon_R^N)^*) + |\epsilon_L^N + \epsilon_R^N|^2\,. \tag{4.81}$$

We have suppressed indices $\epsilon_j = \epsilon^{ee11}_{j,ud}$ and introduced GNI parameters with the superscript N for the sterile neutrino mass eigenstate. The operators $\mathcal{O}_j$ and $\mathcal{O}'_j$ are as usual given by Table 2.4. Note that we assume here a 4-by-4 leptonic mixing matrix, where

the fourth neutrino is only weakly mixed, such that $|U_{e4}| \ll 1$. In this picture, the 3-by-3 submatrix mixing the first three mass eigenstates is the measured PMNS matrix and is unitary up to tiny corrections. Since both the epsilon parameters and $|U_{e4}|$ are small, we have chosen to write Equation (4.79) in a form that is valid up to quadratic order in these small parameters. Without going at least to quadratic order, we would not be able to describe the usual 3+1-mixing sterile neutrino search in the absence of GNI.

To calculate the decay rate, we follow the relativistic treatment of tritium decay in analogy to the neutron decay [160], i.e. we assume the nuclear matrix elements to be the same, just with nucleon-specific form factors. The nucleon-level form factors can be summarized as [109]

$$\begin{aligned}
\langle p(p_p)|\,\overline{u}\gamma_\mu d\,|n(p_n)\rangle &= \overline{u}_p(p_p)\left[g_V(Q^2)\,\gamma_\mu + i\frac{\tilde{g}_{T(V)}(Q^2)}{2M_N}\,\sigma_{\mu\nu}Q^\nu + \frac{\tilde{g}_S(Q^2)}{2M_N}\,Q_\mu\right]u_n(p_n)\,,\\
\langle p(p_p)|\,\overline{u}\gamma_\mu\gamma^5 d\,|n(p_n)\rangle &= \overline{u}_p(p_p)\left[g_A(Q^2)\gamma_\mu + i\frac{\tilde{g}_{T(A)}(Q^2)}{2M_N}\sigma_{\mu\nu}Q^\nu + \frac{\tilde{g}_P(Q^2)}{2M_N}Q_\mu\right]\gamma^5 u_n(p_n)\,,\\
\langle p(p_p)|\,\overline{u}\,d\,|n(p_n)\rangle &\approx g_S(0)\;\overline{u}_p(p_p)\,u_n(p_n) + \mathcal{O}(Q^2/M_N^2)\,,\\
\langle p(p_p)|\,\overline{u}\,\gamma^5\,d\,|n(p_n)\rangle &\approx g_P(0)\;\overline{u}_p(p_p)\,\gamma^5\,u_n(p_n) + \mathcal{O}(Q^2/M_N^2)\,,\\
\langle p(p_p)|\,\overline{u}\,\sigma_{\mu\nu}\,d\,|n(p_n)\rangle &\approx g_T(0)\,\overline{u}_p(p_p)\,\sigma_{\mu\nu}u_n(p_n) + \mathcal{O}(Q/M_N)\,,
\end{aligned} \tag{4.82}$$

where M_N denotes the approximately equal mass of the parent and daughter nucleus. In Reference [160], only the vector and axial nuclear matrix elements were considered, since new physics is required for the others to play a role. However, the form factors g_S, g_P, and g_T become relevant in the presence of exotic new physics. Only the zero-point values $g_X \equiv g_X(0)$ are required due to the low energy transfer in the decay. We leave those form factors as undetermined variables in all formulas, such that any future corrections to these values can be substituted. Whenever we calculate explicit numbers instead, we use the values from Table 4.5. The ratio g_A/g_V was explicitly calculated for tritium [161]. However, it is compatible with values from lattice QCD for the neutron g_A/g_V [109]. We neglect $\tilde{g}_S$ and $\tilde{g}_{T(A)}$, since they correspond to so-called second-class currents which vanish in the isospin limit.[5]

Details of the calculation of the differential decay rate are delegated to Appendix D.1. The following results are organized such that they are valid up to quadratic order in small interaction parameters $|U_{e4}|$ and $\epsilon_j^{(N)}$ and up to leading order in the following dimensionless kinematic parameters [57]

$$\epsilon = \frac{m_A - m_B}{m_A}\,, \quad \eta = \frac{E + m_e}{m_A}\,, \quad \delta = \frac{m_e}{m_A}\,, \quad \rho = \frac{m_k}{m_A}\,, \tag{4.83}$$

where m_A is the mass of the parent nucleus, m_B is the mass of the daughter nucleus, E is the kinetic energy of the electron, and m_k is the mass of the neutrino, either m_N or

[5] In the limit of vanishing mass difference between neutron and proton, and in analogy between tritium and its decay product helium-3, the pairs can be considered as the same particles in opposite isospin states in the context of strong interactions.

Table 4.5. Current best limits on nuclear form factors for $q \to 0$ of either tritium or neutron. CVC stands for the conserved vector current hypothesis.

Coupling	Value	Reference, Comments
g_V	1	[160], (assuming CVC), tritium
g_A/g_V	1.2646 ± 0.0035	[161], tritium
g_S	1.02 ± 0.11	[162], $\overline{\text{MS}}$, neutron
g_P	349 ± 9	[162], $\overline{\text{MS}}$, neutron
g_T	$0.987 \pm 0.051 \pm 0.020$	[163], lattice, $\overline{\text{MS}}$, neutron
$\tilde{g}_{T(V)}$	6.106	[160] (assuming CVC), tritium

the effective electron neutrino mass

$$m_\beta^2 = \sum_{k=1}^{3} \frac{|U_{ek}|^2}{1-|U_{e4}|^2} m_k^2 \,. \tag{4.84}$$

All the masses and momenta can be reduced to these four parameters and m_A. These are excellent expansion parameters, since they are all smaller than 2×10^{-4} for tritium. Furthermore, we introduce the symbol E_0 as the non-relativistic kinetic endpoint energy for $m_\beta = 0$ which is also used by the KATRIN collaboration. In contrast, the exact relativistic endpoint energy for $m_\beta = 0$ reads

$$E_0^{\text{rel}} = \frac{m_A^2 + m_e^2 - m_B^2}{2m_A} \,. \tag{4.85}$$

At leading order they are simply related by

$$E_0^{\text{rel}} - m_e = \frac{m_A^2 + m_e^2 - m_B^2}{2m_A} - m_e \approx (\epsilon - \delta)\, m_A = E_0 \,. \tag{4.86}$$

The neglected corrections of quadratic order in small parameters amount to a shift of the endpoint by approximately 3.4 eV. This is of course non-negligible if the experiment aims to reach a sensitivity of around or below 1 eV. However, it can be accounted for when treating E_0 not as a prediction but a fit parameter, as is the case for KATRIN. We discuss this further after presenting the formula for the differential decay rate.

We distinguish the separate decays of tritium into ν_e and N and give their rates individually, since we would like to entertain the possibility that the experiment may resolve the sterile neutrino. Variables associated with the ν_e decay are henceforth labeled by β for the standard beta decay, while variables associated with sterile neutrino decay are labeled by N. We find, to leading order in the small parameters, the differential decay rate for $k = \beta, N$

$$\begin{aligned} \frac{\mathrm{d}\Gamma_k}{\mathrm{d}E} = \frac{G_F^2 V_{ud}^2}{2\pi^3} &\sqrt{(E+m_e)^2 - m_e^2}(E+m_e)(E_0-E)\sqrt{(E_0-E)^2 - m_k^2} \\ &\times \xi_k \left[1 + b_k \frac{m_e}{E+m_e} - b_k' \frac{m_k}{E_0-E} - c_k \frac{m_e m_k}{(E+m_e)(E_0-E)}\right], \end{aligned} \tag{4.87}$$

where

$$\begin{aligned}\xi_\beta &= g_V^2\left(|\widehat{\epsilon}_L+\widehat{\epsilon}_R|^2+|\widetilde{\epsilon}_L+\widetilde{\epsilon}_R|^2\right)+g_S^2\left(|\epsilon_S|^2+|\widetilde{\epsilon}_S|^2\right)\\ &\quad+3g_A^2\left(|\widehat{\epsilon}_L-\widehat{\epsilon}_R|^2+|\widetilde{\epsilon}_L-\widetilde{\epsilon}_R|^2\right)+48g_T^2\left(|\epsilon_T|^2+|\widetilde{\epsilon}_T|^2\right),\end{aligned} \tag{4.88}$$

$$\begin{aligned}\xi_\beta b_\beta &= g_V g_S\,2\mathrm{Re}\left[(\widehat{\epsilon}_L+\widehat{\epsilon}_R)\widehat{\epsilon}_S+(\widetilde{\epsilon}_L+\widetilde{\epsilon}_R)(\widetilde{\epsilon}_S)^*\right]\\ &\quad-3g_Ag_T\,8\mathrm{Re}\left[(\widehat{\epsilon}_L-\widehat{\epsilon}_R)(\widehat{\epsilon}_T)^*-(\widetilde{\epsilon}_L-\widetilde{\epsilon}_R)(\widetilde{\epsilon}_T)^*\right],\end{aligned} \tag{4.89}$$

$$\begin{aligned}\xi_\beta b'_\beta &= g_V g_S\,2\mathrm{Re}\left[(\widehat{\epsilon}_L+\widehat{\epsilon}_R)\widehat{\widetilde{\epsilon}}_S+\epsilon_S(\widetilde{\epsilon}_L+\widetilde{\epsilon}_R)^*\right]\\ &\quad-3g_Ag_T\,8\mathrm{Re}\left[(\widehat{\epsilon}_L-\widehat{\epsilon}_R)\left(\widehat{\widetilde{\epsilon}}_T\right)^*-(\widetilde{\epsilon}_L-\widetilde{\epsilon}_R)(\epsilon_T)^*\right],\end{aligned} \tag{4.90}$$

$$\begin{aligned}\xi_\beta c_\beta &= 2\mathrm{Re}\left[g_V^2(\widehat{\epsilon}_L+\widehat{\epsilon}_R)\left(\widehat{\widetilde{\epsilon}}_L+\widehat{\widetilde{\epsilon}}_R\right)+g_S^2\,\epsilon_S(\widetilde{\epsilon}_S)^*\right]\\ &\quad+2\mathrm{Re}\left[-3g_A^2(\widehat{\epsilon}_L-\widehat{\epsilon}_R)\left(\widehat{\widetilde{\epsilon}}_L-\widehat{\widetilde{\epsilon}}_R\right)^*+48g_T^2\,\epsilon_T(\widetilde{\epsilon}_T)^*\right],\end{aligned} \tag{4.91}$$

and, similarly,

$$\begin{aligned}\xi_N &= g_V^2\left(|U_{e4}+\epsilon_L+\epsilon_R|^2+|\widetilde{\epsilon}_L+\widetilde{\epsilon}_R|^2\right)+g_S^2\left(|\epsilon_S|^2+|\widetilde{\epsilon}_S|^2\right)\\ &\quad+3g_A^2\left(|U_{e4}+\epsilon_L-\epsilon_R|^2+|\widetilde{\epsilon}_L-\widetilde{\epsilon}_R|^2\right)+48g_T^2\left(|\epsilon_T|^2+|\widetilde{\epsilon}_T|^2\right),\end{aligned} \tag{4.92}$$

$$\begin{aligned}\xi_N b_N &= g_V g_S\,2\mathrm{Re}\left[(U_{e4}+\epsilon_L+\epsilon_R)(\epsilon_S)^*+(\widetilde{\epsilon}_L+\widetilde{\epsilon}_R)(\widetilde{\epsilon}_S)^*\right]\\ &\quad-3g_Ag_T\,8\mathrm{Re}\left[(U_{e4}+\epsilon_L-\epsilon_R)(\epsilon_T)^*-(\widetilde{\epsilon}_L-\widetilde{\epsilon}_R)(\widetilde{\epsilon}_T)^*\right],\end{aligned} \tag{4.93}$$

$$\begin{aligned}\xi_N b'_N &= g_V g_S\,2\mathrm{Re}\left[(U_{e4}+\epsilon_L+\epsilon_R)(\widetilde{\epsilon}_S)^*+\epsilon_S(\widetilde{\epsilon}_L+\widetilde{\epsilon}_R)^*\right]\\ &\quad-3g_Ag_T\,8\mathrm{Re}\left[(U_{e4}+\epsilon_L-\epsilon_R)(\widetilde{\epsilon}_T)^*-(\widetilde{\epsilon}_L-\widetilde{\epsilon}_R)(\epsilon_T)^*\right],\end{aligned} \tag{4.94}$$

$$\begin{aligned}\xi_N c_N &= 2\mathrm{Re}\left[g_V^2(U_{e4}+\epsilon_L+\epsilon_R)(\widetilde{\epsilon}_L+\widetilde{\epsilon}_R)^*+g_S^2\,\epsilon_S(\widetilde{\epsilon}_S)^*\right]\\ &\quad+2\mathrm{Re}\left[-3g_A^2(U_{e4}+\epsilon_L-\epsilon_R)(\widetilde{\epsilon}_L-\widetilde{\epsilon}_R)^*+48g_T^2\,\epsilon_T(\widetilde{\epsilon}_T)^*\right].\end{aligned} \tag{4.95}$$

Here we omitted the indices N on the ϵ-coefficients to avoid cluttering. We remark that the definitions of ξ, b, b' and c are inspired by the literature of beta decays, see e.g. Reference [164]. However, we chose to define them as dimensionless. The first important point about Equation (4.87) is that the kinematic prefactors in the first line are the same as in the usual SM calculation. Therefore, in the absence of new physics, $b_k = b'_k = c_k = \xi_N = 0$ and we recover

$$\xi_\beta^{\mathrm{SM}} = g_V^2 + 3g_A^2\,, \tag{4.96}$$

with which Equation (4.87) becomes identical to the standard formula, see e.g. Reference [160]. As usual, it is the factor $((E_0-E)^2-m_k^2)^{1/2}$ which ensures that the rate drops to zero at the endpoint. Now let us discuss the new terms proportional to b_k, b'_k, and c_k in the second row of Equation (4.87). These involve couplings of electrons or neutrinos with opposing chiralities and are therefore proportional to either electron or neutrino masses, or both.[6] Therefore b' and c can only appear in the presence of right-handed neutrinos, e.g. Dirac partners of active neutrinos in the case of b'_β and c_β, or a

[6] Consider for instance $\widehat{\epsilon}_L\widehat{\epsilon}_S$ in the $\xi_\beta b_\beta$-term: The GNI proportional to $\widehat{\epsilon}_L$ involve left-handed neutrinos and left-handed electrons, while the GNI proportional to $\widehat{\epsilon}_S$ involve left-handed neutrinos and right-handed electrons. The opposite chiralities for the electron require an electron mass insertion.

sterile neutrino in the case of b'_N and c_N. This can be seen from the fact that b' and c vanish if all $\widetilde{\epsilon}$ vanish, which are precisely the GNI connected to right-handed neutrinos, see Table 2.4.

We can estimate what the effect of the new physics terms on the spectrum will be. The electron energy along the full spectrum varies within $E \in [0, E_0 + m_\beta]$. For $m_\beta \approx 0$ and $E_0 \approx 18\,575\,\mathrm{eV}$ the factor $m_e/(E + m_e)$ multiplying b_k varies between 1 and 0.965 and thus gives only a very small distortion of the spectrum. Along the currently accessible range $[E_0 - 40\,\mathrm{eV}, E_0]$ close to the endpoint, the variation is only on the level of 10^{-5}. Therefore, in summary the b-term increases or decreases the amplitude of the spectrum by an approximately constant factor of $(1 + 0.965 \cdot b_k)$ close to the endpoint. The second new term $m_k/(E_0 - E)$ proportional to b'_k can vary more strongly along the full spectrum, e.g. for $m_k = 1\,\mathrm{eV}$ between 5×10^{-5} and 1. In the 40 eV interval close to the end point the variation is still between 0.025 and 1. Therefore, this term has a significant energy-dependence and so changes the shape of the spectrum. However, in the case that m_k is very small it is still strongly suppressed. The third new term proportional to c_k is basically is just the product of the factors of b_k and b'_k. Therefore, the energy dependence is approximately the same as that of the b'_k term.

For completeness we can write down the total differential decay rate, which is simply the sum over the rates of decay into electron or sterile neutrino

$$\begin{aligned}\frac{\mathrm{d}\Gamma}{\mathrm{d}E} &= \frac{\mathrm{d}\Gamma_\beta}{\mathrm{d}E}\Theta(E_0 - m_\beta - E) + \frac{\mathrm{d}\Gamma_N}{\mathrm{d}E}\Theta(E_0 - m_N - E) \\ &= \frac{G_F^2 V_{ud}^2}{2\pi^3}\sqrt{(E+m_e)^2 - m_e^2}(E + m_e)(E_0 - E)\left\{\sum_{k=\beta,N}\sqrt{(E_0 - E)^2 - m_\beta^2}\right. \\ &\quad \left.\times\xi_k\left[1 + b_k\frac{m_e}{E + m_e} - b'_k\frac{m_k}{E_0 - E} - c_k\frac{m_e m_k}{(E + m_e)(E_0 - E)}\right]\Theta(E_0 - m_k - E)\right\},\end{aligned} \tag{4.97}$$

where we include explicit Heaviside theta functions to ensure that the total rate is well-defined up to energies $E = E_0 - \min(m_\beta, m_N)$.

4.5.2. Sensitivity of KATRIN to GNI

In this section we discuss the sensitivity of KATRIN to the new physics contributing to the tritium decay rate in Equation (4.97). In their usual fit, the KATRIN collaboration uses the SM limit of the leading-order result (4.97), i.e. $\xi_\beta = g_V^2 + 3g_A^2$ while $b_\beta = b'_\beta = c_\beta = \xi_N = 0$. The endpoint is left as a free parameter in order to reduce systematic errors. In this way the minuscule shift of the endpoint between the exact and non-relativistic endpoint is accounted for in the fit. Moreover, a Fermi function $F(E + m_e, 2)$ incorporates the electromagnetic interaction of the emitted electron with the daughter nucleus. Finally, one has to account for the fact that the tritium source is constituted by a several molecular states, which before and after the decay may be in an excited state. This is accounted for by modifying the available endpoint energy E_0, which is reduced by an excitation energy V_j. There are a number of further correction factors summarized in

Reference [165] which have to be accounted for but which we do not comment on here. Applying the above modifications to the decay rate (4.97), we arrive at the formula

$$\frac{\mathrm{d}\Gamma_{\mathrm{KA}}}{\mathrm{d}E} = \frac{G_F^2 V_{ud}^2}{2\pi^3} F(E+m_e,2)\sqrt{(E+m_e)^2-m_e^2}(E+m_e)\left\{\sum_j \sum_{k=\beta,N} \zeta_j \epsilon_j \sqrt{\epsilon_j^2-m_k^2}\right.$$
$$\left.\times\xi_k\left[1+b_k\frac{m_e}{E+m_e}-b_k'\frac{m_k}{\epsilon_j}-c_k\frac{m_e m_k}{(E+m_e)\epsilon_j}\right]\Theta(\epsilon_j-m_k)\right\}. \tag{4.98}$$

This assumes a set of probabilities ζ_j to produce the daughter molecular system in certain excited states with excitation energies V_j. Depending on these final states, the neutrino energy reads $\epsilon_j = E_0 - E - V_j$. Notice that if we ignore those different molecular systems and assume just one unexcited daughter nucleus, i.e. $V_j = 0$ with $\zeta_j = 1$, we reproduce Equation (4.97). Below we explore different new physics scenarios which all follow particular limits of this master formula.

The expected count rate is given by [44]

$$R_{\mathrm{calc}}(\langle qU\rangle) = R_{\mathrm{bg}} + A_s N_{\mathrm{T}} \int \frac{\mathrm{d}\Gamma_{\mathrm{KA}}}{\mathrm{d}E}(E)\cdot f_{\mathrm{calc}}(E-\langle qU\rangle)\mathrm{d}E\,, \tag{4.99}$$

where R_{bg} is the background rate, A_s is the signal amplitude, N_{T} is the effective number of tritium atoms in the source, and f_{calc} is the detector response function. In the absence of new physics, the fitting procedure has in total four parameters. Besides m_β^2 and E_0, also A_s and R_{bg} are fitted which corresponds to a shape-only fit. Due to these limitations it is important to analyze which types of new physics can be constrained from a fit of the endpoint of the spectrum. Since any effect on the signal amplitude A_s will be absorbed, we have to distinguish the effects of new physics on the amplitude and on the shape of the spectrum. In turn, we discuss ξ, b, b', and c for active and sterile neutrinos to see if they sufficiently modify the spectrum. Then we consider scenarios from the perspective of GNI parameters which is of course ultimately what we are after in this work. In the SM limit of the eight parameters ξ_β, b_β, b'_β, c_β, x_N, b_N, b'_N, and c_N only ξ_β is non-vanishing. Therefore we discuss now scenarios with select parameters besides ξ_β assumed as non-vanishing.

Without sterile neutrino

- Only ξ_β: A modification of ξ_β through GNI results only in a modification of the amplitude, not the shape. This can only be observed when A_s is not a completely free fit parameter.

- Only ξ_β and b_β: As already discussed above Equation (4.97), the effect of this term on the shape is negligible while the effect on the amplitude will be absorbed in A_s. Therefore this type of new physics is not observable with the current setup.

- Only ξ_β and b'_β: As already discussed, in this case the rate gets multiplied by an energy-dependent factor

$$\frac{\mathrm{d}\Gamma_{\mathrm{KA}}}{\mathrm{d}E} \to \frac{\mathrm{d}\Gamma_{\mathrm{KA}}}{\mathrm{d}E}\left(1 - b'_\beta \frac{m_\beta}{\epsilon_j}\right). \tag{4.100}$$

  Neglecting the molecular excitations, we have have discussed that this factor varies between $1 - b'_\beta \cdot 5 \times 10^{-5}$ and $1 - b'_\beta$ along the whole spectrum for $m_\beta = 1\,\mathrm{eV}$. Therefore in this case it would be very beneficial to measure the entire spectrum. However, even in the 40 eV-interval around the endpoint, the factor would still vary from $1 - b'_\beta \cdot 0.025$ to $1 - b'_\beta$. Unfortunately the neutrino mass must not be too small in order to detect this, because in the limit $m_\beta \to 0$ this shape modification vanishes. As long as no neutrino mass is observed, we can thus only obtain bounds on b'_β for given assumptions about m_β.

- Only ξ_β and c_β: This case is analogous to b'_β and the shape change of the spectrum is practically the same. This is because the spectrum gets modified by the factor

$$\frac{\mathrm{d}\Gamma_{\mathrm{KA}}}{\mathrm{d}E} \to \frac{\mathrm{d}\Gamma_{\mathrm{KA}}}{\mathrm{d}E}\left(1 - c_\beta \frac{m_e}{E + m_e}\frac{m_\beta}{\epsilon_j}\right), \tag{4.101}$$

  and we already discussed that $m_e/(E + m_e)$ changes only at the 10^{-5} level close to the endpoint. Therefore, the constraints on b'_β and c_β give the same effect on the shape.

- Mixed scenarios: As discussed above, b_β cannot be detected and b'_β and c_β are indistinguishable. So the only reasonable scenario to search for with the current KATRIN setup is assuming without loss of generality $b_\beta = 0$, $b'_\beta \neq 0$ and $c_\beta = 0$. Then one can constrain b'_β depending on the assumed real neutrino mass. The resulting bounds on b'_β are then equally valid for c_β.

With sterile neutrino

- Only ξ_β and ξ_N: This is the minimal scenario with a sterile neutrino. If $m_N > m_\beta$ can be resolved, the additional addend in the rate (4.97) deforms the spectrum. In particular, if the contribution of the sterile neutrino decay rate to the total rate is large enough, one would expect to observe a dent in the spectrum at the endpoint of the sterile neutrino subspectrum. Therefore, ξ_N can be constrained from the shape-only fit if the endpoint of the m_N spectrum lies within the fit range. If one could measure the whole spectrum, this would allow us to test up to keV-scale masses of sterile neutrinos which are interesting candidates of warm dark matter [166–168]. At present, however, the endpoint fit only allows to test masses up to about 40 eV. In this scenario, the shape-only fit effectively measures the ratio ξ_N/ξ_β for a given value of m_N. In these scenarios it is handy to set $m_\beta = 0$ since we already know that the data is consistent with this assumption. If we neglect GNI and consider the case of purely mixing-mediated decay, this is equivalent to the usual fit of $|U_{e4}|$

as can be seen from Equations (4.88) and (4.92) together with the definitions (4.80)

$$\frac{\xi_N}{\xi_\beta} = \frac{|U_{e4}|^2}{|\widehat{\epsilon}_L|^2} = \frac{|U_{e4}|^2}{1-|U_{e4}|^2}\,, \tag{4.102}$$

where in the last step we neglected higher orders of $|U_{e4}|$ since our definitions (4.80) are only valid at quadratic order in $|U_{e4}|$. Therefore, we may use immediately the usual sterile neutrino fit which constrains the parameter space m_N-$|U_{e4}|$ and generalize it to a constraint on the (m_N-ξ_N/ξ_β)-space.

- Only ξ_β, ξ_N, and b_N: In analogy to b_β, b_N also mostly affects the amplitude of the sterile neutrino decay rate. Its effect is therefore indistinguishable from the effect of ξ_N.

- Only ξ_β, ξ_N, and b'_N: If the sterile neutrino has a relatively large mass, e.g. 1 keV, m_N/ϵ_j could be very large close to the endpoint of the sterile neutrino part of the spectrum. This can, to some extend, compensate for a small value of b'_N. However, even for $m_N \lesssim 40\,\text{eV}$ there could be an interesting effect. The maximal effect is expected for $b'_N = -1$, as we show below. To constrain this scenario, one can fit, as in the previous scenario, m_N vs. ξ_N/ξ_β at a few fixed values $b'_N = -1, -0.75, -0.5, -0.25$.

- Only ξ_β, ξ_N, and c_N: The situation is analogous to ξ_β, ξ_N, and b'_N by the same reasoning as in the active neutrino case.

To summarize, there are two viable scenarios to constrain GNI with the current setup of KATRIN:

1. Constrain b'_β for fixed values of m_β.

2. Constrain the two parameters m_N and ξ_N/ξ_β for fixed values $m_\beta = 0$ and $b'_N = -1, -0.75, -0.5, -0.25, 0$. The assumption $b'_N = 0$ corresponds to the usual 3+1 fit but with generalized relative normalizations of the electron neutrino and sterile neutrino decay rates.

To interpret the results in terms of GNI, we construct scenarios with a minimal number of GNI coefficients. To produce b'_β, we need at least one GNI parameter, e.g. $\widetilde{\epsilon}_S$, which interferes with the SM vector interaction. In this case we have $\widehat{\epsilon}_L = 1$, $\widehat{\widetilde{\epsilon}}_S = \widetilde{\epsilon}_S$ and therefore

$$\xi_\beta = g_V^2 + 3g_A^2 + g_S^2|\widetilde{\epsilon}_S|^2\,, \qquad b'_\beta \approx \frac{g_V g_S}{g_V^2+3g_A^2} 2\mathrm{Re}\,\widetilde{\epsilon}_S \approx 0.35\,\mathrm{Re}\,\widetilde{\epsilon}_S\,. \tag{4.103}$$

Equivalently, we could produce c_β to which there is an equal sensitivity. In this case we need only $\widetilde{\epsilon}_V = \widetilde{\epsilon}_L + \widetilde{\epsilon}_R$, such that $\widehat{\epsilon}_L = 1$ and $\widehat{\widetilde{\epsilon}}_V = \widetilde{\epsilon}_V$ and therefore

$$\xi_\beta = g_V^2 + 3g_A^2 + g_V^2|\widetilde{\epsilon}_V|^2\,, \qquad c_\beta \approx \frac{g_V^2}{g_V^2+3g_A^2} 2\mathrm{Re}\,\widetilde{\epsilon}_V \approx 0.34\,\mathrm{Re}\,\widetilde{\epsilon}_V\,. \tag{4.104}$$

Turning to the sterile neutrino scenarios, the simplest way to generate ξ_N is by the mixing matrix. However, any GNI could also instead mediate the decay. Accordingly, a bound on ξ_N/ξ_β implies a bound on single GNI parameters. For these single parameter bounds we set U_{e4} and all other epsilons to zero. Then we find, from a constraint $\xi_N/\xi_\beta \leq q$

$$|\epsilon| \leq \sqrt{q/C}\,, \tag{4.105}$$

where

$$\begin{aligned} C = \frac{1}{1-\frac{1}{2}|\epsilon|^2} \approx 1 \qquad & \text{for } \epsilon_L^N \text{ or } \epsilon_R^N\,, \\ C = 1 \qquad & \text{for } \widetilde{\epsilon}_L^N \text{ or } \widetilde{\epsilon}_R^N\,, \\ C = \frac{g_S^2}{g_V^2+3g_A^2} \qquad & \text{for } \epsilon_S^N \text{ or } \widetilde{\epsilon}_S^N\,, \\ C = \frac{48 g_T^2}{g_V^2+3g_A^2} \qquad & \text{for } \epsilon_T^N \text{ or } \widetilde{\epsilon}_T^N\,. \end{aligned} \tag{4.106}$$

This shows that the bound on $|U_{e4}|$ implied by the 3+1 fit is immediately applicable to ϵ_L^N, ϵ_R^N, $\widetilde{\epsilon}_L^N$, and $\widetilde{\epsilon}_R^N$. For the others, a rescaling involving g_S and g_T is necessary. Finally let us discuss the minimal requirements for $b'_N \neq 0$ or $c_N \neq 0$. Clearly we need one ϵ or U_{e4} and one $\widetilde{\epsilon}$. All combinations are possible and we will now see that the largest possible value is $|b'_N| = 1$. An optimal scenario is ϵ_V^N together with $\widetilde{\epsilon}_S^N$. Then we have

$$\xi_N = g_V^2|\epsilon_V^N|^2 + g_S^2|\widetilde{\epsilon}_S^N|^2 = |w|^2 + |z|^2\,, \tag{4.107}$$

$$\xi_N b'_N = g_V g_S\, 2\mathrm{Re}\left[\epsilon_V^N(\widetilde{\epsilon}_S^N)^*\right] = 2\mathrm{Re}(wz^*)\,, \tag{4.108}$$

where we defined $w = g_V\,\epsilon_V^N$, and $z = g_S\,\widetilde{\epsilon}_S^N$. Consequently, we find

$$b'_N = \frac{wz^* + w^*z}{|w|^2+|z|^2}\,. \tag{4.109}$$

It turns out that this fraction can only take values in the range [-1,1]. Indeed, writing $w = r_1 \cdot \exp(\phi_1)$, $z = r_2 \cdot \exp(\phi_2)$, and assuming without loss of generality that $r_1 \leq r_2$, we obtain

$$\frac{|wz^* + w^*z|}{|w|^2+|z|^2} = \frac{|2r_1r_2\cos(\phi_1-\phi_2)|}{r_1^2+r_2^2} \leq \frac{2r_1r_2}{r_1^2+r_2^2} \leq \frac{2r_1^2}{r_1^2+r_2^2} = \frac{2}{1+r_2^2/r_1^2} \leq 1\,. \tag{4.110}$$

For illustration, we could use the case of real w and z to find the extremal values

$$b'_N = \frac{2wz}{w^2+z^2} \approx \begin{cases} \pm 1 & \text{if } w = \pm z\,, \\ 0 & \text{if } w \gg z\,. \end{cases} \tag{4.111}$$

Note that the conclusion is the same for other representatives. In less optimal cases $|b'_N|$ can only be smaller than 1 as we show in Appendix D.2. Hence, there are many scenarios in terms of ϵ-coefficients which we do not all discuss. However, the GNI framework informs us about the possible values b'_N can have.

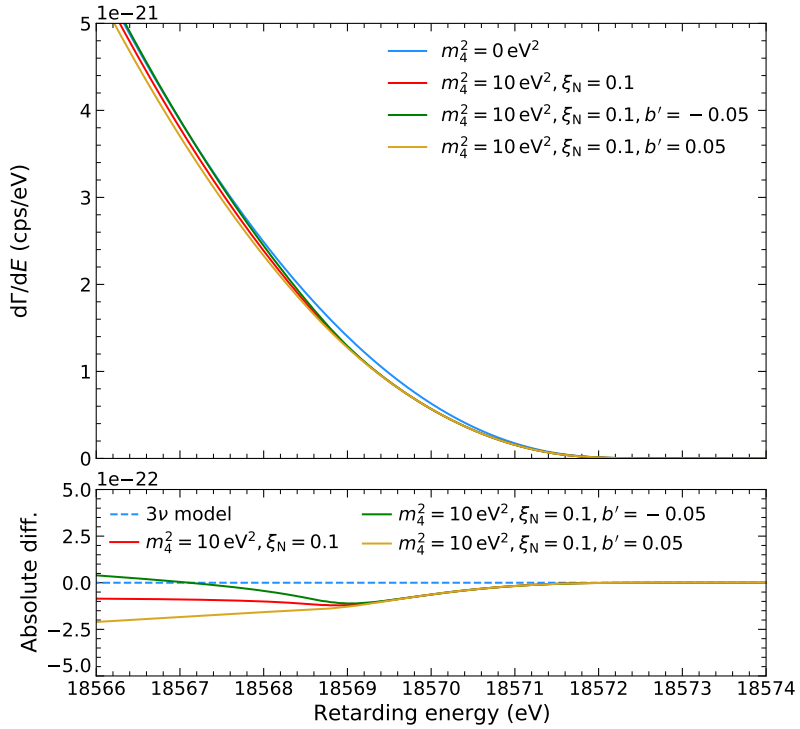

Figure 4.6. Expected count rate for the measurement of the endpoint of the tritium decay spectrum at KATRIN for the SM expectation and including sterile neutrino contributions. Figure adapted from Reference [169] at a preliminary stage.

4.5.3. Preliminary results

An analysis of the constraints on new interactions of a sterile neutrino from the KATRIN data is to be published in the near future. For illustration, we present some preliminary results from Reference [169]. In Figure 4.6 we show the expected differential decay rate around the endpoint region for a sterile neutrino of squared mass $m_N^2 \equiv m_4^2 = 10\,\mathrm{eV}^2$ and different values of ξ_N and b'_N compared to the SM expectation. The shape difference can be understood from our previous analysis of the spectrum. In the case of $b'_N = 0$, the spectrum agrees with the usual 3+1 scenario. The additional contribution of the sterile neutrino decay drops out at the endpoint of the sterile neutrino spectrum and therefore at higher electron energies there is no dependence on b'_N. At lower energies, the value of b'_N can enhance the count rate if $b'_N < 0$ or reduce it if $b'_N > 0$. As explained above, if one fits ξ_N/ξ_β and m_N for fixed values of b'_N, one can obtain bounds on pairs of epsilon parameters, for instance ϵ_V^N and $\widetilde{\epsilon}_S^N$. The results of such a fit can be illustrated as a two-dimensional exclusion plot for given values of m_N. Such a plot is shown in Figure 4.7 for $m_N^2 = 100\,\mathrm{eV}^2$. Details on the statistical inference of the exclusion regions will be found in Reference [169].

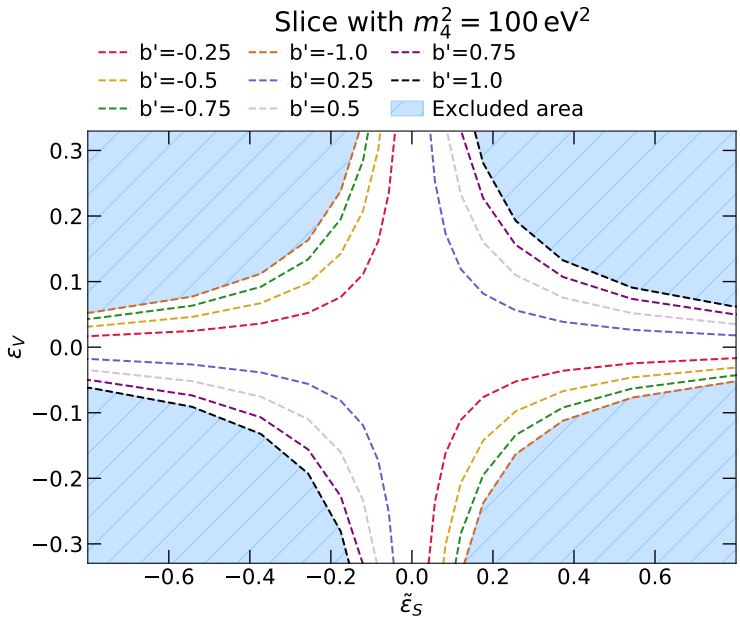

Figure 4.7. Exclusion plot for a fixed value $m_N^2 \equiv m_4^2 = 100\,\mathrm{eV}^2$, assuming that the decay into sterile neutrinos is mediated by the GNI parameters ϵ_V^N and $\widetilde{\epsilon}_S^N$. Figure adapted from Reference [169] at a preliminary stage.

4.6. Summary

We have discussed a number of direct and indirect experimental tests of GNI. The complementarity of different searches for such interactions is particularly valuable for resolving ambiguities in the extraction of fundamental neutrino parameters from neutrino oscillation data, as we have illustrated in Section 4.1. For convenience, we summarize in Table 4.6 the current constraints on leptonic single GNI parameters, and in Table 4.7 the constraints on semi-leptonic single GNI parameters. Concerning leptonic GNI, we find neutrino-electron scattering to provide the strongest direct bounds, see Section 4.4. Currently, these are drawn from the CHARM-II and TEXONO experiments. After the first phase of operation, significantly improved bounds can be expected from near detector data of DUNE. In the case that flavor-changing leptonic GNI are linked to SMNEFT operators, very stringent constraints can be deduced from the searches for charged lepton flavor violation, as discussed in Section 4.2. Turning to semi-leptonic interactions, we can distinguish charged-current and neutral-current GNI. The strongest direct bounds on flavor-conserving charged-current interactions are currently derived from nuclear beta decays and pion decay, see Reference [109] and Section 4.3.2. Direct bounds on flavor-conserving neutral-current interactions can be derived from coherent elastic neutrino nucleus scattering. The values given in Table 4.7 rely on the assumption $\epsilon^{ee11} = \epsilon^{\mu\mu 11}$ made in Reference [54], see Section 4.3.1. Following Reference [53], we additionally estimated that in future reactor neutrino experiments, significant improvements on these bounds can be expected. In the case that neutral-current interactions of (pseudo)scalar

or tensor type are connected to the SMNEFT operators $\mathcal{O}_{lNuq}, \mathcal{O}_{lNqd}, \mathcal{O}'_{lNqd}$, the bounds on charged-current interactions from beta and pion decay impose strong indirect limits on the neutral-current interactions. Direct bounds on flavor-changing semi-leptonic interactions are derived from a combination of different sources in References [112–114], while indirect bounds are implied by the non-observation of $\mu \to e$ conversion in nuclei and rely on the assumption that the GNI originate from SMNEFT operators, see Section 4.2. Investigating the suitability of KATRIN to test GNI in Section 4.5, we found that the main strength lies in the possibility to test the interactions of potential eV-scale sterile neutrinos which cannot usually be resolved in other beta decay experiments.

Table 4.6. Current direct and indirect bounds on leptonic GNI discussed in this chapter. A summary of their origins is provided in the main text. For convenience, we list associated mass scales $\Lambda/\sqrt{C} = (\sqrt{2}/G_F\epsilon)^{1/2}$.

NP Parameter	Direct	Indirect	$\Lambda/\sqrt{C}$ [TeV] direct	$\Lambda/\sqrt{C}$ [TeV] indirect
$\epsilon^{eeee}_{L,e}$	$[-0.31, 0.24]$		[0.6,0.7]	
$\epsilon^{\mu\mu ee}_{L,e}$	$[-0.06, 0.02]$		[1.4,2.5]	
$\lvert\epsilon^{e\mu ee}_{L,e}\rvert$	0.11	1.4×10^{-6}	1.0	294
$\lvert\epsilon^{\mu\tau ee}_{L,e}\rvert$	0.11		1.0	
$\lvert\epsilon^{e\tau ee}_{L,e}\rvert$	0.27	2.8×10^{-4}	0.7	21
$\epsilon^{eeee}_{R,e}$	$[-0.24, 0.31]$		[0.6,0.7]	
$\epsilon^{\mu\mu ee}_{R,e}$	$[-0.06, 0.02]$		[1.4,2.5]	
$\lvert\epsilon^{e\mu ee}_{R,e}\rvert$	0.10	1.0×10^{-6}	1.1	348
$\lvert\epsilon^{\mu\tau ee}_{R,e}\rvert$	0.10		1.1	
$\lvert\epsilon^{e\tau ee}_{R,e}\rvert$	0.27	3.9×10^{-4}	0.7	18
$\lvert\epsilon^{ee}_{S,e}\rvert$, $\lvert\epsilon^{e\tau}_{S,e}\rvert$	0.6		0.4	
$\lvert\epsilon^{e\mu}_{S,e}\rvert$, $\lvert\epsilon^{\mu\mu}_{S,e}\rvert$, $\lvert\epsilon^{\mu\tau}_{S,e}\rvert$	0.4		0.6	
$\lvert\epsilon^{ee}_{P,e}\rvert$, $\lvert\epsilon^{e\tau}_{P,e}\rvert$	0.7		0.4	
$\lvert\epsilon^{e\mu}_{P,e}\rvert$, $\lvert\epsilon^{\mu\mu}_{P,e}\rvert$, $\lvert\epsilon^{\mu\tau}_{P,e}\rvert$	0.4		0.6	
$\lvert\epsilon^{ee}_{T,e}\rvert$, $\lvert\epsilon^{e\tau}_{T,e}\rvert$	0.08		1.2	
$\lvert\epsilon^{e\mu}_{T,e}\rvert$, $\lvert\epsilon^{\mu\mu}_{T,e}\rvert$, $\lvert\epsilon^{\mu\tau}_{T,e}\rvert$	0.04		1.7	
$\lvert\epsilon^{ee\tau e}_{R,e}\rvert$		3.9×10^{-4}		18
$\lvert\epsilon^{\mu\mu\mu e}_{R,e}\rvert$		5.5×10^{-6}		148
$\lvert\epsilon^{e\mu\mu\mu}_{R,e}\rvert$		5.5×10^{-6}		148
$\lvert\epsilon^{\mu\tau\tau e}_{R,e}\rvert$		3.0×10^{-7}		636
$\lvert\epsilon^{e\tau\tau\mu}_{R,e}\rvert$		3.0×10^{-7}		636
$\lvert\epsilon^{\tau\mu\mu\mu}_{L,e}\rvert$		2.4×10^{-4}		22
$\lvert\epsilon^{\mu\tau\mu\mu}_{R,e}\rvert$		3.3×10^{-4}		19
$\lvert\epsilon^{\mu\mu\mu\tau}_{R,e}\rvert$		3.3×10^{-4}		19

Table 4.7. Current direct and indirect bounds on semi-leptonic GNI discussed in this chapter. A summary of their origins is provided in the main text. For convenience, we list associated mass scales $\Lambda/\sqrt{C} = (\sqrt{2}/G_F\epsilon)^{1/2}$.

NP Parameter	Direct	Indirect	$\Lambda/\sqrt{C}$ [TeV] direct	$\Lambda/\sqrt{C}$ [TeV] indirect
$\lvert\mathrm{Re}(\widetilde{\epsilon}^{ee11}_{P,ud})\rvert, \lvert\mathrm{Im}(\widetilde{\epsilon}^{ee11}_{P,ud})\rvert$	2.8×10^{-4}		21	
$\lvert\widetilde{\epsilon}^{ee11}_{S,ud}\rvert$	6.3×10^{-2}		1.4	
$\lvert\widetilde{\epsilon}^{ee11}_{T,ud}\rvert$	$0.006 \leq \lvert\epsilon\rvert \leq 0.024$		2.2	
$\lvert\epsilon^{ee11}_{S,u}\rvert$	1.5×10^{-2}	3.8×10^{-4}	2.8	18
$\lvert\epsilon^{ee11}_{P,u}\rvert$		3.8×10^{-4}		18
$\lvert\epsilon^{ee11}_{S,d}\rvert$	1.7×10^{-2}	4.0×10^{-4}	2.7	17
$\lvert\epsilon^{ee11}_{P,d}\rvert$		4.0×10^{-4}		17
$\lvert\mathrm{Re}(\epsilon^{ee11}_{T,d})\rvert$	9.8×10^{-2}	$0.006 \leq \lvert\epsilon\rvert \leq 0.024$	1.1	2.2
$\lvert\epsilon^{e\mu11}_{L,u}\rvert$	2.3×10^{-2}	3.3×10^{-7}	2.3	606
$\lvert\epsilon^{e\mu11}_{L,d}\rvert$	2.3×10^{-2}	3.3×10^{-7}	2.3	606
$\lvert\epsilon^{e\mu11}_{R,u}\rvert$	3.6×10^{-2}	6.0×10^{-8}	1.8	1422
$\lvert\epsilon^{e\mu11}_{R,d}\rvert$	3.6×10^{-2}	5.3×10^{-8}	1.8	1513
$\lvert\epsilon^{e\mu11}_{L,ud}\rvert$	2.6×10^{-2}	6.6×10^{-7}	2.2	429
$\lvert\mathrm{Re}(\epsilon^{e\mu11}_{S,ud})\rvert$	8×10^{-3}	3.0×10^{-8}	3.9	2010
$\lvert\mathrm{Re}(\epsilon^{e\mu11}_{P,ud})\rvert$	4×10^{-4}	3.0×10^{-8}	17	2010

5. Heavy sterile neutrinos as dark matter

In this chapter, we investigate how the framework of SMNEFT introduced in Chapter 2 can be applied to dark matter. To prepare this, we begin in Section 5.1 with an introduction to dark matter and the most important observables from a particle physics viewpoint. In Section 5.2, we then propose to identify dark matter as a sterile neutrino with a mass of at least a few GeV which interacts with the SM through dimension-five and dimension-six operators in SMNEFT. We demonstrate that viable scenarios exist which predict the observed amount of cold dark matter and are consistent with observational evidence from direct and indirect detection experiments. To validate the robustness of the EFT assumptions, we consider three example models which are represented by this EFT in Section 5.3 and show how they can be distinguished by producing the mediator at the LHC before concluding in Section 5.4. The contents of this chapter have been published in Reference [4].

5.1. Overview of dark matter observables

Identifying dark matter with a new particle requires that we can explain how it is produced in the observed abundance. The production mechanism usually implies ways to detect the dark matter directly or indirectly, or to even produce it artificially at a particle collider. Therefore we devote this section to a minimal overview of dark matter observables from the perspective of a particle physicist.

The energy content of the universe can be separated into dark energy, baryonic and dark matter, radiation and curvature. It is well-established by astronomical and cosmological evidence that the dark energy component dominates our universe, while radiation and curvature are negligible today [29]. We focus on the density of dark matter ρ_{DM}, which dominates the matter component over baryonic matter of density ρ_b. We follow the usual convention of expressing these quantities in terms of the density parameters defined by

$$\Omega_x h^2 = \frac{\rho_x}{\rho_c} h^2 = \frac{\rho_x}{3 M_{\mathrm{Pl}}^2 H_0^2} h^2 \,, \qquad \text{for } x = b, \mathrm{DM} \,, \tag{5.1}$$

where ρ_c denotes the critical density, M_{Pl} denotes the Planck mass and

$$H_0 = h \cdot (100\,\mathrm{km\,s^{-1}Mpc^{-1}}) \tag{5.2}$$

denotes the Hubble constant. The precise value of the dimensionless parameter h is not relevant to our discussion, but for completeness we quote the value obtained by the

Planck Collaboration [29] which is $h = 0.674 \pm 0.005$. The values of the density parameters identified in the same publication read

$$\Omega_b h^2 = \frac{\rho_b}{\rho_c} h^2 = 0.0224 \pm 0.0001\,, \qquad \Omega_{\rm DM} h^2 = \frac{\rho_{\rm DM}}{\rho_c} h^2 = 0.120 \pm 0.001\,. \tag{5.3}$$

The baseline requirement of a theory of dark matter is that it has to predict this observed dark matter density. A second requirement, however, is that dark matter should be cold, which means that whatever the production mechanism is, most of the dark matter particles must be non-relativistic during the era of structure formation. The degree to which this should hold is dictated by the observed large-scale structure of the universe, which can only form for sufficiently slow dark matter [170]. This requirement is also satisfied by warm dark matter which is not exactly but close-to non-relativistic and may even explain certain puzzling observations at smaller-scale structures [167]. Fermionic dark matter is affected by a third requirement known as the Tremaine-Gunn bound. The argument relies on the phase space distribution of a single species of fermionic dark matter in a galaxy and amounts to a lower limit $m_N \geq 0.4\,\text{keV}$ [167]. These requirements allow for two frequently considered scenarios of sterile neutrino dark matter. The first is realized by GeV-scale sterile neutrinos which are produced thermally. By this we mean that they are initially in thermal equilibrium with baryonic matter mediated by some new interaction, but freeze out once the temperature of the universe drops below a certain value $T_{\rm dec}$. In this scenario, the sterile neutrino appears essentially as a weakly-interacting massive particle (WIMP), one of the prime dark matter candidates from a theoretical perspective [171]. There must, however, be some mechanism to circumvent the decay of this type of dark matter. The second scenario is realized by keV-scale sterile neutrinos which cannot straightforwardly be produced via freeze-out. For new interactions analogous to the ones we introduce for GeV-scale neutrinos, the freeze-out would result in relativistic dark matter if we require the observed relic abundance to be obtained. Typical production mechanisms considered for this dark matter candidate are thermal freeze-in, warranted by a tiny mixing to active neutrinos, out-of-equilibrium decay of heavier new particles, and energy-dependent new interactions [166, 167].

We will consider only the thermal relic dark matter whose freeze-out is controlled by the dark matter annihilation cross-sections $\sigma \equiv \sigma_{NN\to X_1 X_2 \ldots}$ where X are SM particles. In this scenario, a balance of annihilation and creation processes in the thermal bath of the early universe holds the dark matter in thermal equilibrium. For a thermal distribution of particles, we can express the velocity-averaged dark matter annihilation rate as

$$\Gamma \sim \langle \sigma v \rangle \, n_N\,, \tag{5.4}$$

where $\langle v \rangle$ denotes the average velocity and n_N denotes the number density, both of which depend on temperature and mass. One can imagine that as the temperature in the early universe decreases, also the annihilation rate decreases. On the other hand, the Hubble rate H describing the expansion of the universe increases during this epoch, such that at some point the annihilation and creation processes are no longer frequent enough to keep the dark matter in thermal equilibrium. At this point the dark matter freezes out and is no longer coupled to the thermal bath. The distribution afterwards simply gets diluted

and redshifted along with the expansion of the universe. In practice, we will calculate this process using the computational tool micrOMEGAs [172–175] which numerically solves the required Boltzmann equations. In essence, the two quantities deciding about the successful freeze-out are the velocity-averaged annihilation cross section $\langle \sigma v \rangle$ and the dark matter mass. For a given mass, the coupling to the SM must be strong enough in order for the particles become non-relativistic before decoupling. If the coupling is too strong, however, the decoupling takes place too late and the dark matter density is too low. On the other hand, if the coupling is too weak, the decoupling takes place too early and dark matter is overproduced.

Predicting the correct relic density of non-relativistic dark matter is, however, not the only hurdle a successful theory needs to pass. We consider three important further consistency checks which concern direct detection, indirect detection, and collider production.

- **Direct detection:** If dark matter of a mass in the multi-GeV range interacts with quarks or gluons, the most promising channel to detect it is by the scattering off heavy nuclei which have a similar mass. This scattering of WIMP dark matter is being searched for at experiments such as XENON1T [176]. The dark-matter-nucleon interaction can be induced at tree-level or at loop level. For the models we consider below, we use the tool runDM [177] to calculate the RG running from our effective operators at high energies to the nuclear scale and to map coefficients to the nucleon-level EFT. Since no signal has been detected so far, usually the XENON collaboration releases upper limits on either the dark-matter-nucleus scattering cross section or on Wilson coefficients of the non-relativistic nucleon-level EFT. These bounds depend on the distribution of dark matter in our galaxy in order to predict the incident flux in the detector.

- **Indirect detection:** If two dark matter particles can annihilate in the early universe into SM particles, in principle the same can happen today where ever there is a sufficiently large concentration of dark matter. In particular, one can survey dwarf spheroidal galaxies (dSphs) for signs of such annihilations in the form of a gamma ray flux, since they combine a large dark matter density with a low background. Of course, the signal depends on the exact annihilation products, but can be simulated and compared to the data. If such a signal is detected consistently for several objects, one could claim the indirect detection of dark matter. The non-detection of an excess gamma ray flux enables us to exclude some dark matter models or parts of their parameter space. We note that the velocity-averaged annihilation cross section $\langle \sigma v \rangle$ which controls the freeze-out, is also responsible for the indirect detection signal. However, the average dark matter velocity today is much smaller than during freeze-out and so the averaged cross section may be different, as we discuss in Section 5.2.

- **Collider production:** For WIMP dark matter of a mass in the multi-GeV range, typically an interaction strength comparable to the electroweak scale or weaker is required to ensure that the freeze-out produces the observed relic abundance. Therefore, one would expect a mediator between dark matter and the SM to be of a mass in the 100 GeV to 1 TeV range. In this case it would be possible to produce

the mediator at the LHC. However, no new particles have been observed so far, which allows us to constrain models of dark matter. In our EFT approach, we will consider new-physics scales Λ which are comparable to LHC energies. Therefore, the assumption of a decoupled mediator, which works well for direct and indirect detection, breaks down at collider energies. There exist approaches to extend the application of an EFT framework into the collider regime by including mediator particles as additional degrees of freedom [178]. We choose to remain more general at the cost of being unable to apply the EFT at collider scales. However, we will show that if we pick concrete models which are represented by the EFT, the LHC searches are suitable for distinguishing these different models and mediators.

5.2. Third-generation νDMEFT

In this section we apply the framework of SMNEFT with one sterile neutrino N of super-GeV mass to explain dark matter. To ensure stability, we assume a $\mathbb{Z}_2$ symmetry under which only N is charged. Therefore, N cannot decay but pair-annihilate into SM particles. In particular, we consider the case when four-fermion interactions dominate and annihilations are given by $NN \to \overline{f}f$ with f some SM fermion. If we assume that N couples to the first or second generation of SM fermions, there are very strong constraints from direct detection. However, these can be less stringent if we assume that the four-fermion couplings are only present among dark matter and *third*-generation fermions. In this case, the coupling to nucleons is mainly generated by loops and therefore smaller. Hence, we decide to only consider couplings to the third generation in this chapter in order to reduce the pressure from direct detection constraints.

Let us list the relevant operators from Table 2.1. These are

$$\begin{aligned}
\mathcal{L}_{Nq} &= \frac{C_{Nq}}{\Lambda^2}(\overline{N}\gamma_\mu P_R N)(\bar{q}_3\gamma^\mu P_L q_3)\,, & \mathcal{L}_{Nl} &= \frac{C_{Nl}}{\Lambda^2}(\overline{N}\gamma_\mu P_R N)(\bar{l}_\tau\gamma^\mu P_L l_\tau)\,,\\
\mathcal{L}_{Nt} &= \frac{C_{Nt}}{\Lambda^2}(\overline{N}\gamma_\mu P_R N)(\bar{t}\gamma^\mu P_R t)\,, & \mathcal{L}_{N\tau} &= \frac{C_{N\tau}}{\Lambda^2}(\overline{N}\gamma_\mu P_R N)(\bar{\tau}\gamma^\mu P_R \tau)\,,\\
\mathcal{L}_{Nb} &= \frac{C_{Nb}}{\Lambda^2}(\overline{N}\gamma_\mu P_R N)(\bar{b}\gamma^\mu P_R b)\,,
\end{aligned} \tag{5.5}$$

where we omit the explicit flavor indices of the third generation and relabeled the Wilson coefficients for brevity. Due to the relevance to direct detection and the explicit models considered later, we also include the dimension-five operator

$$\mathcal{L}^{(5)}_{NH} = \frac{C^{(5)}_{NH}}{\Lambda}\,\overline{N^c_R}N_R\,H^\dagger H \qquad \text{(Majorana)}\,. \tag{5.6}$$

Generally we consider N as a Majorana fermion, but occasionally also discuss how the bounds are affected if we assume it is a Dirac fermion. In this case, the dimension-five operator must be replaced by

$$\mathcal{L}^{(5)}_{NH} = 2\frac{C^{(5)\alpha\beta}_{NH}}{\Lambda}\overline{N}NH^\dagger H \qquad \text{(Dirac)} \tag{5.7}$$

in order to have the same numerical bounds from direct detection on the Dirac and Majorana Wilson coefficients. Apart from this replacement, we consider the same dimension-six operators (5.5) even though in the Dirac case one could have additional couplings to the left-handed component of N.

We will consider energy scales $\Lambda/\sqrt{C}$, where C denotes one of the Wilson coefficients in Equation (5.5), in the range of 10^2–10^4GeV which is to a large extent accessible at the LHC. Therefore, we cannot treat collider constraints in the EFT framework. However, relic density, direct detection and indirect detection observables can be calculated entirely in the EFT framework. For this reason we now consider more explicitly the present constraints on the operators $\mathcal{O}_{N\tau(t,b)}$ under the assumption that one of them dominates the interaction of dark matter with the SM. We show the results in Figure 5.1 for the cases of Majorana and Dirac dark matter. These three operators are just chosen for simplicity, but in principle any combination of the operators in Equation (5.5) could be valid. One example with multiple operators is the $\mathrm{U}(1)_{(B-L)_3}$ model introduced in Section 3.1.2, which we discuss as one of the UV complete examples in Section 5.3.

As stated in Section 5.1, the dark matter mass m_N and the velocity-averaged annihilation cross section $\langle\sigma v\rangle$ are the two quantities which fix the relic abundance within the freeze-out mechanism. However, they also govern indirect detection signals. We note that the annihilation cross sections for Dirac and Majorana dark matter are different for the same operator $\mathcal{O}_{Nf}$. Namely, we find for Majorana dark matter

$$\langle\sigma v_{\mathrm{rel}}\rangle^{\mathrm{M}}_{Nf} = \frac{|C_{Nf}|^2}{8\pi\Lambda^4} N_{\mathrm{c}} \sqrt{1-\frac{m_f^2}{m_N^2}} \left(m_f^2 + \frac{16m_N^4 - 23m_N^2 m_f^2 + 10m_f^4}{24(m_N^2 - m_f^2)}\, v_{\mathrm{rel}}^2 \right) \tag{5.8}$$

up to first order in average squared relative DM velocity v_{rel}^2. For Dirac dark matter the annihilation rate for the same operator reads

$$\langle\sigma v_{\mathrm{rel}}\rangle^{\mathrm{D}}_{Nf} = \frac{|C_{Nf}|^2}{16\pi\Lambda^4} N_{\mathrm{c}}\, m_N^2 \sqrt{1-\frac{m_f^2}{m_N^2}}\,. \tag{5.9}$$

The color factor N_{c} is 1 for $f=\tau$ and 3 for $f=t,b$. To obtain the operators $\mathcal{O}_{Nf}$ with $f=l,q$, one can simply add the cross sections for t and b or for ν_τ and τ respectively. For instance, the Dirac annihilation cross section in this case reads

$$\langle\sigma v_{\mathrm{rel}}\rangle^{\mathrm{D}}_{Nq} = \frac{|C_{Nq}|^2}{16\pi\Lambda^4} N_{\mathrm{c}}\, m_N^2 \left(\sqrt{1-\frac{m_t^2}{m_N^2}} + \sqrt{1-\frac{m_b^2}{m_N^2}} \right). \tag{5.10}$$

In the lepton case $f=l$, we set $N_{\mathrm{c}}=1$ and replace the masses m_b with m_τ and m_t with $m_{\nu_\tau}=0$.

We should explain why we kept the first term of order v_{rel}^2 only in the Majorana case. Before the freeze-out of non-relativistic dark matter, the average velocity is determined by a thermal Boltzmann distribution and therefore we have approximately $v_{\mathrm{rel}} \sim \sqrt{T_f/m_f} \sim 10^{-1}$ for a WIMP-like scenario. In contrast, the typical velocity of dark matter in today's astrophysical structures is $v_{\mathrm{rel}} \sim 10^{-3}$ [178]. Now in the Dirac case, the leading order term is proportional to m_N^2, whereas in the Majorana case it is m_f^2 which is often much

smaller than m_N^2. Therefore, the second term proportional to $v_{\rm rel}^2$ becomes relevant in the Majorana case. Indeed, for $m_f^2 \ll m_N^2$ we obtain

$$\langle \sigma v_{\rm rel} \rangle_{Nf}^{\rm M} \approx \frac{|C_{Nf}|^2}{8\pi\Lambda^4} N_{\rm c} \sqrt{1-\frac{m_f^2}{m_N^2}} m_N^2 \left[\frac{2}{3} v_{\rm rel}^2 + \left(1 - \frac{7}{24} v_{\rm rel}^2\right) \frac{m_f^2}{m_N^2} + \mathcal{O}\left(\frac{m_f^4}{m_N^4}\right) \right] . \quad (5.11)$$

We conclude that the contribution proportional to $v_{\rm rel}^2$ is not always subleading in the Majorana case. This also shows that the Dirac annihilation cross section is practically always larger for the same value of C_{Nf}/Λ^2. For the relic density, which is controlled by $\langle \sigma v_{\rm rel} \rangle$, this means that in the Dirac case a larger value of $\Lambda/\sqrt{C_{Nf}}$ is required than in the Majorana case to obtain $\Omega_{\rm DM} h^2 = 0.12$.

Relic density

Implementing the models via FeynRules [179] and subsequently using micrOMEGAs, we can calculate the relic density for a given mass m_N and energy scale $\Lambda/\sqrt{C_{Nf}}$ for $f = \tau, b, t$ assuming $\Lambda \gg m_N$ to be consistent with the EFT framework. In Figure 5.1, we show the slice in parameter space for which the correct relic density is produced as a black line. Above (below) the black lines, dark matter is overproduced (underproduced). Note that a larger interaction scale leads to a weaker coupling and thus to an earlier decoupling of dark matter, resulting in a larger number density. Additionally, one can observe that the difference in the annihilation cross section between Dirac and Majorana dark matter indeed leads to larger scales $\Lambda/\sqrt{C_{Nf}}$ being required in the Dirac case.

Direct detection

As we noted before, the WIMP direct detection experiments search for dark matter scattering off nuclei. Thus, in order to compare the parameter space of our EFT scenarios with the regions excluded by direct detection experiments, we must find the effective couplings to nuclei. To do this, we use the tool runDM [177] which allows to calculate the RG running to the nuclear scale and maps the interaction to the nucleon-level EFT. Now there is a crucial difference between Majorana and Dirac dark matter. For the latter, the effective interactions involve a vector current,

$$(\overline{N}\gamma_\mu P_R N)(\overline{f}\gamma^\mu P_R f) = \frac{1}{2}(\overline{N}\gamma_\mu N + \overline{N}\gamma_\mu\gamma^5 N)(\overline{f}\gamma^\mu P_R f) . \quad (5.12)$$

This vector current induces a contribution to the operator $\mathcal{O}_1$ of the nucleon-level EFT [177]. The spin-independent scattering mediated by this operator is strongly constrained by XENON1T. Using [180]

$$\sigma_{\rm SI} = \frac{\mu_x^2}{\pi} (\mathcal{C}_{1,x})^2 , \quad (5.13)$$

with the reduced nucleon mass $\mu_x = m_N m_x/(m_N + m_x)$, we can translate the bounds on the spin-independent WIMP-nucleus cross section from XENON1T into constraints on the Wilson coefficients $\mathcal{C}_{1,x}$ of the relativistic nucleon-level EFT. These bounds can be compared to the results of runDM. We find that in the case of τ and b operators,

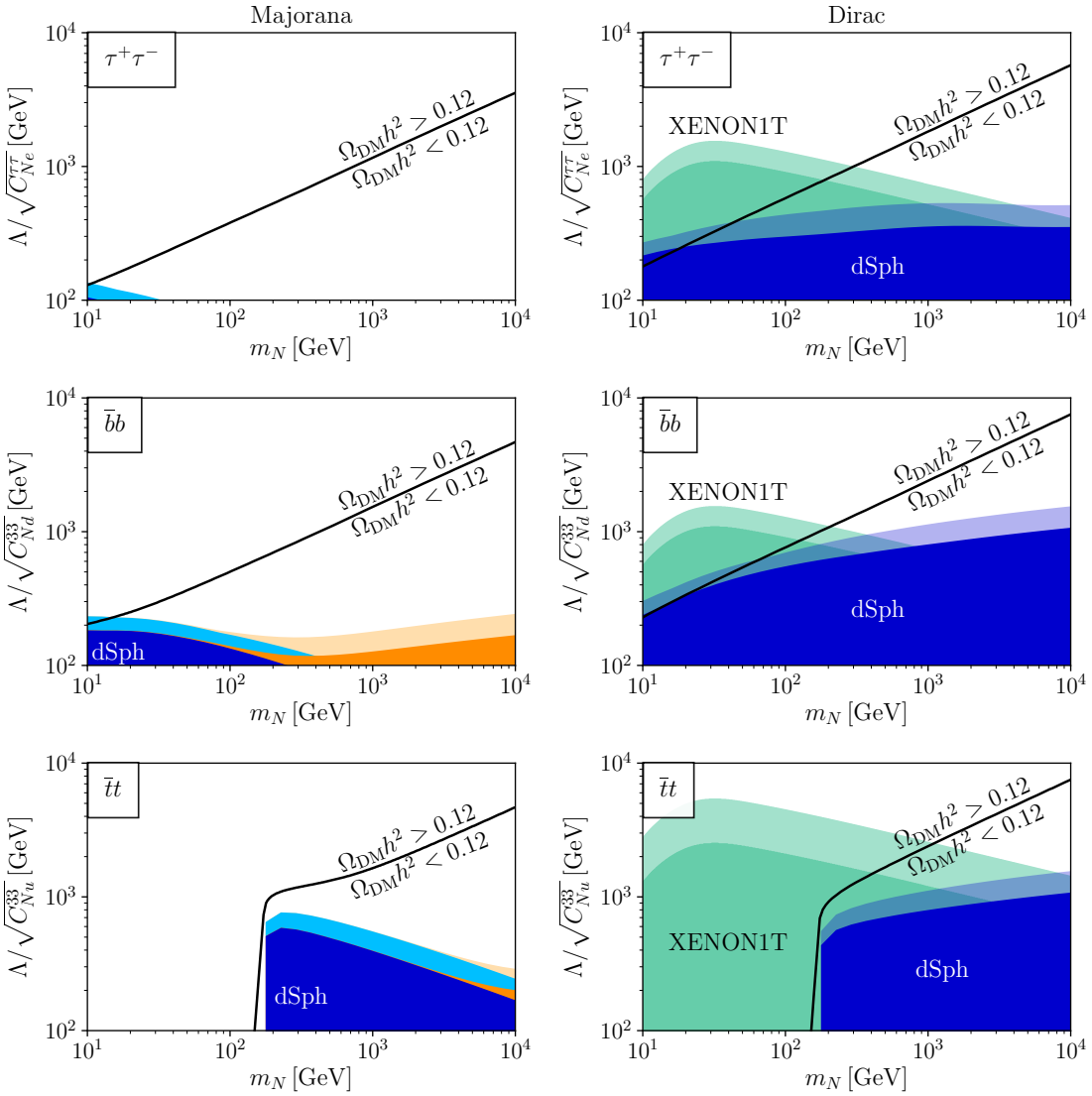

Figure 5.1. New physics scale required by the relic abundance for the third generation EFT scenarios dominated by $\mathcal{O}_{N\tau}$, $\mathcal{O}_{Nb}$, or $\mathcal{O}_{Nt}$ defined in Equation (5.5) (black line), assuming Majorana (left) and Dirac (right) sterile neutrinos. Regions excluded by indirect detection from dSphs are shown in blue. The light blue region corresponds to the variation of the J-factors within their 68% confidence bands. The orange bands show the indirect detection exclusion when we include the loop-induced annihilation into gluon pairs in a particular model. Direct detection limits from XENON1T (extrapolated between 1 TeV and 10 TeV) are shown in teal. The lighter-shaded band represents a realistic range of Λ. The weaker bounds correspond to $\Lambda = 100\,\text{GeV}$ (200 GeV in the $\bar{t}t$-case) and the stronger bounds to $\Lambda = 10\,\text{TeV}$. Direct and indirect detection constraints assume $\Omega_{\rm DM}h^2 = 0.12$ everywhere. Figure adapted from Reference [4].

the proton coupling with $x = p$ dominates, while for t the neutron coupling with $x = n$ dominates. However, the results of the running depend not only on $\Lambda/\sqrt{C}$ but also on the explicit scale of new physics Λ identified with the mediator mass because the running effect is smaller if one starts from a lower scale. To capture this dependence in Figure 5.1, we show the bounds on $\Lambda/\sqrt{C}$ in the range of 100(200) GeV $\leq \Lambda \leq$ 10 TeV, where the bracket refers to the $\bar{t}t$ case. For these bounds we assume $\Omega_{\rm DM}h^2 = 0.12$. Additionally, we calculate the lower bounds on m_N assuming $\Lambda > 100$ GeV. These read

$$m_N \geq \begin{cases} 185 \text{ GeV} & \text{for } \tau^+\tau^- , \\ 126 \text{ GeV} & \text{for } \bar{b}b , \\ 1002 \text{ GeV} & \text{for } \bar{t}t . \end{cases} \qquad \text{(Dirac case)} \tag{5.14}$$

We note that the bounds from XENON1T have been extrapolated between 1 TeV and 10 TeV which concerns only the bound on the $\bar{t}t$ case which is shifted from 1000 GeV to 1002 GeV. Returning to the Majorana case, the N-bilinear in the effective interaction reduces to an axial current, $\overline{N}\gamma^\mu\gamma^5 N$. Therefore, only relatively weakly constrained operators 4, 8, and 9 of non-relativistic scattering theory defined in Reference [181], which mediate spin-dependent interactions, are generated by the RG running. The numbers for our parameter space of m_N and $\Lambda/\sqrt{C}$ are well below current XENON limits [182]. Therefore, there is no excluded region for the Majorana case in Figure 5.1.

So far we have only considered four-fermion operators. Additionally, the dimension-five operator $\mathcal{O}^{(5)}_{NH}$ in Equation (5.6) leads to a Higgs portal coupling of the form NNh. This Higgs portal allows for a tree-level coupling between dark matter and nuclei and is therefore strongly constrained by XENON1T. The spin-independent elastic N-nucleus scattering cross section in the zero-momentum-transfer limit is given by [183]

$$\sigma_{\rm SI} = \frac{4}{\pi}\mu_x^2 f_x^2 , \tag{5.15}$$

where

$$f_x = m_x \frac{C^{(5)}_{NH}}{\Lambda m_h^2}\left(\sum_{q=u,d,s} f^x_{Tq} + \frac{2}{9} f^x_{TG}\right) \tag{5.16}$$

for $x = p, n$. To calculate explicit values, we take for f^x_{Tq} and f^x_{TG} the same values as Reference [184]. With this, we can derive 90% CL lower limits on $\Lambda/C^{(5)}_{NH}$ from the XENON1T bounds on the spin-independent cross section [176]. The result is shown in Figure 5.2. The constraints are quite strong such that $\Lambda/C^{(5)}_{NH}$ is required to be at least 2 TeV or larger. This also strongly constrains the role $NN \to h$ annihilation can play during freeze-out, unless m_N is close to the resonance $m_N \sim m_h/2$. We do not consider this sort of resonance here. This result implies that when we consider explicit models which have the sterile neutrino dark matter effective field theory (νDMEFT) as a limiting case, we have to check that this dimension-five operator is consistent with constraints. We note that the constraint in Figure 5.2 is the same for Dirac and Majorana dark matter by virtue of the factor of two in the definition (5.7).

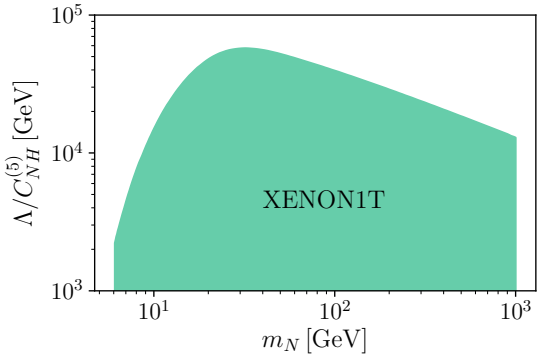

Figure 5.2. Direct detection constraints from XENON1T [176] on the operator $\mathcal{O}_{NH}^{(5)}$ introduced in Equation (5.6). The area is excluded at 90% CL. Figure adapted from Reference [4].

As a final remark on direct detection, we note that an effective dark-matter-gluon coupling can be present at dimension seven. Such a coupling is typically generated at loop level from interactions with quarks. In the leptoquark models discussed in Section 5.3 such a gluon-coupling is present in principle but turns out negligible for direct detection in the region of parameter space suitable for an EFT description.

Indirect detection

The most sensitive search for gamma rays from dark matter annihilation in dSphs was performed with Fermi-LAT [185]. We first discuss how we calculate a prediction for the expected gamma ray spectrum. Following Reference [185], the expected gamma ray flux in the energy range between $E_{\min}$ and $E_{\max}$ when allowing for multiple annihilation processes labeled by j reads

$$\phi = \frac{J}{8\pi m_N^2} \sum_j \langle \sigma v_{\text{rel}} \rangle_j \int_{E_{\min}}^{E_{\max}} \frac{\mathrm{d}N_{\gamma,j}}{\mathrm{d}E_\gamma} \mathrm{d}E_\gamma \,, \tag{5.17}$$

where $\langle \sigma v_{\text{rel}} \rangle_j$ are the velocity-averaged annihilation cross sections, which for our operators are given in Equations (5.8) and (5.9). For the Majorana cross section we assume $v_{\text{rel}} = 10^{-3}$ [178]. Furthermore, $\mathrm{d}N_{\gamma,j}/\mathrm{d}E_\gamma$ denotes the photon spectrum associated with the annihilation j, and J denotes the J-factors for the respective dSph. These J-factors are determined by the dark matter density in the dSph along the line of sight and the observed solid angle [186]. Since the precise astrophysical determination of the dark matter density is challenging, the J-factors are the main source of uncertainty in Equation (5.17). We consider the 19 dSphs with kinematically determined J-factors in Table 1 of Reference [185]. However, we employ for the J-factors the more recent results from Reference [187] and take as uncertainties their 68% confidence intervals. For the photon spectra we use those calculated in Reference [188] which include the relevant particle showers. To obtain limits, we compare the predictions from Equation (5.17) with the bin-by-bin likelihoods published by the Fermi-LAT and DES collaborations [185]. To assess

the uncertainty of the obtained limits, which are dominated by J-factor uncertainties, we choose to define an uncertainty band in the following way. For each value of m_N we define a best-case limit and a worst-case limit. The best-case limit is the strongest out of the 19 limits on $\langle \sigma v_{\mathrm{rel}} \rangle_j$ using the upper boundary of the 68% CL region, while the worst case limit is the strongest out of the 19 limits using the lower boundary of the 68% CL region. This gives us a relatively broad band between the two limits, in which the true exclusion curve should lie. We show the obtained exclusion areas obtained assuming $\Omega h^2 = 0.12$ in Figure 5.1. The blue areas correspond to the best-case and worst-case scenarios, i.e. J-factors at the upper or lower boundary of their 68% CL region. The Majorana case is more weakly constrained, as we understand from the comparison of the annihilation cross sections (5.8) and (5.9) which reveals the smaller cross section in the Majorana case. From the intersections with the lines representing $\Omega h^2 = 0.12$, we can derive for the different scenarios the lower limits on the DM mass

$$m_N \geq \begin{cases} 6 \text{ - } 10 \text{ GeV} & \text{for } \tau^+\tau^- \,, \\ 6 \text{ - } 14 \text{ GeV} & \text{for } \bar{b}b \,, \end{cases} \qquad \text{(Majorana case)} \tag{5.18}$$

and

$$m_N \geq \begin{cases} 18 \text{ - } 41 \text{ GeV} & \text{for } \tau^+\tau^- \,, \\ 11 \text{ - } 57 \text{ GeV} & \text{for } \bar{b}b \,. \end{cases} \qquad \text{(Dirac case)} \tag{5.19}$$

In the $\bar{t}t$ case, the indirect detection constraints are not yet strong enough to probe the parameter space for which the relic density constraint is satisfied. Therefore, here we obtain no lower bound.

We only briefly comment on the plausibility of assuming that models exist which can be mapped to the EFT scenarios where one operator like $\mathcal{O}_{Nb}$ or $\mathcal{O}_{Nt}$ dominates. Namely, one would expect a loop-induced coupling to gluons for those interactions with quarks, which would result in the possible annihilation $NN \to gg$. While we do not consider all the dimension-seven operators of SMNEFT which would describe such a coupling in general, we account for the contribution of this annihilation channel in a particular model which realizes the EFT scenario dominated by $\mathcal{O}_{Nt}$. This is the S_1'' leptoquark model introduced in Section 3.2.3 which will be discussed in more detail in Section 5.3. Here we only note that we can recalculate the indirect detection bounds including the $NN \to gg$ contribution for this model and analogously for the $\bar{b}b$ case, which results in the orange continuation of the blue exclusion regions in Figure 5.1. In the Dirac case, the annihilation cross sections into fermion pairs are significantly larger and therefore dominate, while for the $\tau^+\tau^-$ case one can expect a much smaller and hence negligible effective coupling to gluons. We conclude that the gluonic annihilation can be neglected for this model, which illustrates that our assumptions of an EFT dominated by the operators of dimension five and six in Equations (5.5)-(5.7) are realistic.

5.3. Models representing the νDMEFT

In this section we discuss three example models in order to demonstrate the viability of the third-generation νDMEFT. These are the gauged $(B-L)_3$ extension, and the S_1''

and U_1'' leptoquark scenarios discussed in Chapter 3. For each model, we will perform the following steps. First, we use the mapping of the full model to Wilson coefficients of the νDMEFT identified in Chapter 3 to calculate the constraints from relic density, direct detection and indirect detection and recast them in terms of the model parameter space. Second, we discuss potential additional constraints which we have to consider once we have identified the mediator. This concerns mainly the production of the mediator particle at the LHC. As a result we can constrain the model parameters space and identify those regions where a consistent explanation of dark matter is possible. Indeed, we find such consistent regions for all three models.

5.3.1. Flavored baryon minus lepton number symmetry

The gauged third-generation baryon number minus lepton number model has been introduced and mapped to SMNEFT in Section 3.1.2. In this case the heavy vector Z' is the mediator of four-fermion interactions. In Equations (3.32) and (3.35), we have summarized the arising Wilson coefficients when identifying $\Lambda = m_{Z'}$, which we reproduce here,

$$\begin{aligned} C_{NH}^{(5)} &= -\frac{m_{Z'} m_N}{2m_\phi^2}\lambda_{H\Phi}\,, & C_{lq}^{(1)} &= C_{LQ} = -\frac{g_X^2}{3} \equiv -\frac{c}{3}\,, \\ C_{LL} &= c\,, & C_{qq}^{(1)} &= C_{QQ} = \frac{g_X^2}{9} \equiv \frac{c}{9}\,, \end{aligned} \tag{5.20}$$

where $c = g_X^2$, $LL = ll, NN, ee, Nl, le, Ne$, $LQ = lu, ld, Nq, Nu, Nd, qe, eu, ed$, $QQ = uu, dd$, qu, qd, ud, and flavor indices 3 are implicit. Recall that all the operators were defined in Table 2.1. These are the only Wilson coefficients to leading order in ϵ, the kinetic mixing parameter.

EFT constraints

We proceed by calculating the constraints from relic density, direct detection, and indirect detection for this EFT scenario summarized in Equation (5.20). For small scalar mixing $\lambda_{H\Phi}$ and neglecting a possible resonant Higgs annihilation, the freeze-out is dominated by the four-fermion operators. We calculate the required scale $\Lambda/\sqrt{c}$ to produce the correct relic abundance with MICROMEGAs as before. The result is shown in Figure 5.3 in the same form as the plots in Figure 5.1. In this mixed-operator case, several annihilation channels contribute to the freeze-out. Their relative importance can be estimated when considering that $m_f \ll m_N$ and $v_{\text{rel}} \sim 0.1$ which leads to both the Majorana annihilation cross section in Equation (5.8) and the Dirac cross section in Equation (5.9) depending only weakly on the mass m_f. One can conclude that

$$\langle \sigma v_{\text{rel}} \rangle_{\tau^+\tau^-} \approx 2 \langle \sigma v_{\text{rel}} \rangle_{\overline{\nu}_\tau \nu_\tau} \approx 3 \langle \sigma v_{\text{rel}} \rangle_{\bar{b}b} \approx 3 \langle \sigma v_{\text{rel}} \rangle_{\bar{t}t} \tag{5.21}$$

if $m_N \gg m_t$, and without the last approximate equality when $m_b \ll m_N \ll m_t$. The factor of 2 stems from the absence of right-handed tau neutrinos and the factors of 3 are a result of the color factors and $(B-L)_3$-charges.

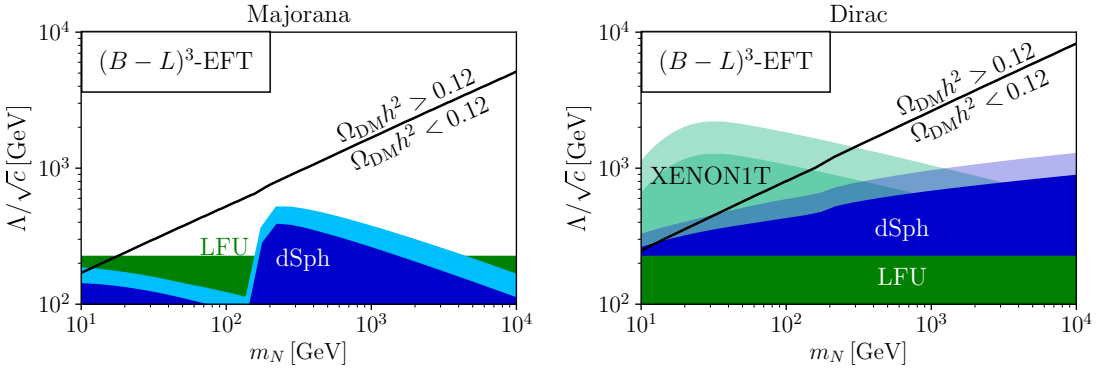

Figure 5.3. New-physics scale required by the relic abundance for the third generation EFT scenario defined by Equation (5.20) (black line) assuming Majorana (left) and Dirac (right) sterile neutrinos. Regions excluded by indirect detection from dSphs are shown in blue. The light blue region corresponds to the variation of the J-factors within their 68% confidence bands. The bound from lepton flavor universality tests is shown in green. Direct detection limits from XENON1T (extrapolated between 1 TeV and 10 TeV) are shown in teal. The lighter-shaded band represents a realistic range of Λ. The weaker bounds correspond to $\Lambda = 100\,\text{GeV}$ and the stronger bounds to $\Lambda = 10\,\text{TeV}$. Direct and indirect detection constraints assume $\Omega_{\rm DM}h^2 = 0.12$ everywhere. Figure adapted from Reference [4].

The direct detection constraints are evaluated as previously by running the interactions down to the nuclear scale using RUNDM. In the Majorana case, again only spin-dependent scattering operators are produced which are not sufficiently constrained to probe the parameter space. In the Dirac case, as for the single-operator scenarios, the vector current coupling to quarks leads to a contribution to spin-independent scattering which strongly constrains the model and leads to a lower bound on the dark matter mass of 146 GeV. In both cases, we need to consider that the Higgs operator is also constrained by direct detection. However, it depends on the scalar mixing $\lambda_{H\Phi}$ and the mass of the heavy scalar m_ϕ^2. Therefore, we recast the bounds on $C_{NH}^{(5)}$ as bounds on $m_\phi/\sqrt{\lambda_{H\Phi}}$ in Figure 5.4. In the following, we will assume that this bound is satisfied and concentrate on Z' as the relevant mediator. Concerning indirect detection constraints we can also repeat the procedure described in Section 5.2. The result is shown in Figure 5.3 in blue. The bounds are dominated by the rescaled sum of $\bar{t}t$ and $\bar{b}b$ annihilations, since the annihilations into $\overline{\nu}_\tau\nu_\tau$ and $\tau^+\tau^-$ produce a relatively weak gamma ray signal. In the Majorana case indirect detection leads to a lower limit on the dark matter mass of about $m_N \geq$ 7-11 GeV, and in the Dirac case $m_N \geq$ 11-29 GeV. These numbers are comparable to the limits for the single-operator scenarios in Figure 5.1.

In Section 5.2 we have presupposed an EFT scenario where only operators involving dark matter are present and therefore direct and indirect detection were the only constraints. In the present scenario defined by Equation (5.20) this is not the case since there are four-fermion operators involving only SM fermion representations. Interactions among third-generation fermions are not strongly constrained since they do not play a

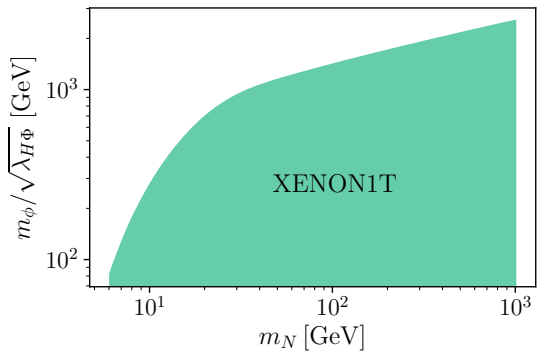

Figure 5.4. Direct detection constraints from XENON1T [176] on the mass scale $m_\phi/\sqrt{\lambda_{H\Phi}}$ which controls the Wilson coefficient of the operator $\mathcal{O}_{NH}^{(5)}$. The bounds have been obtained applying Equation (5.20) to the EFT results shown in Figure 5.2. Figure adapted from Reference [4].

role in most decays. However, we are able to constrain the model from lepton universality tests, as discussed in Reference [73]. Indeed, the operators $\mathcal{O}_{lq}$, $\mathcal{O}_{ld}$, $\mathcal{O}_{qe}$, $\mathcal{O}_{ed}$ coupling only to the third generation will affect the semi-leptonic b-meson branching ratios. We can calculate this effect by using the formula for $\Upsilon(1S)$ decay into leptonic final states [189, 190]

$$\Gamma_{\Upsilon(1S)\to\ell\ell} = 4\alpha^2 Q_b^2 \frac{|R_n(0)|^2}{m_\Upsilon^2} K_\ell \,, \tag{5.22}$$

where α denotes the fine-structure constant, $Q_b = -1/3$ the electric charge of the bottom quark, $R_n(0)$ the non-relativistic radial wave function at the origin, and

$$K_\ell = \left(1 + 2\frac{m_\ell^2}{m_\Upsilon^2}\right)\sqrt{1 - 4\frac{m_\ell^2}{m_\Upsilon^2}} \tag{5.23}$$

contains the kinematics which depends on the lepton mass. The SM expectation for the ratio $R_{\ell\ell'}$ then depends only on the lepton mass due to the flavor-universal coupling,

$$R_{\ell\ell'} \equiv \frac{\Gamma_{\Upsilon(1S)\to\ell\ell}}{\Gamma_{\Upsilon(1S)\to\ell'\ell'}} = \frac{K_\ell}{K_{\ell'}} \,. \tag{5.24}$$

This leads to the SM prediction $R_{\tau\mu} = 0.992$ which can be compared to the measured value $R_{\tau\mu} = 1.005 \pm 0.013(\text{stat.}) \pm 0.022(\text{syst.})$ from BaBar [190]. Adding statistical and systematic errors quadratically, for simplicity, results in $R_{\tau\mu} = 1.005 \pm 0.026$, which is consistent with the SM prediction. Now we can constrain the EFT by calculating the maximal value for c/Λ^2 which is consistent with the BaBar measurement at 68% CL. Adding all four mentioned operators with the Wilson coefficients dictated by Equation (5.20) results in the vector-current interaction

$$\mathcal{L}_{\text{LFV}(b\tau)} = -\frac{c}{3\Lambda^2}\bar{b}\gamma_\mu b\,\bar{\tau}\gamma^\mu\tau \,. \tag{5.25}$$

Therefore, we can add this contribution directly to the photon-mediated contribution, which results in

$$\Gamma_{\Upsilon(1S)\to\tau\tau} = 4\alpha^2 Q_b^2 \frac{|R_n(0)|^2}{m_\Upsilon^2} K_\tau \left(1 - \frac{m_\Upsilon^2}{4\pi\alpha Q_b} \frac{c}{3\Lambda^2}\right)^2 . \tag{5.26}$$

This contribution is limited to the decay of Υ into tau pairs and therefore violates flavor universality. Hence, we find the prediction

$$R_{\tau\mu} = \frac{K_\tau}{K_\mu} \left(1 + \frac{m_\Upsilon^2}{4\pi\alpha} \frac{c}{\Lambda^2}\right)^2 . \tag{5.27}$$

Since $c = g_X^2 > 0$, we conclude that $\Lambda/\sqrt{c} \geq 224\,\text{GeV}$ at 68% CL. This bound is shown in Figure 5.3 in green. From this we can extract that the lowest dark matter mass which is consistent with the measurements from BaBar and the observed relic density is $m_N \gtrsim 17\,\text{GeV}$ in the Majorana case.

Constraints on the full model

The EFT bounds shown in Figure 5.3 can be recast as bounds on the full model in the following way. If we identify $\Lambda = m_{Z'}$ and fix m_N, the value of $\Lambda/\sqrt{c}$ determined by the relic density can be translated into a required coupling $g_X = \sqrt{c}$. Then we can plot the parameter space spanned by m_N and $m_{Z'}$ such that at each point g_X is fixed by requiring the relic density constraint to be satisfied. In Figure 5.5 we show this parameter space and draw contour lines of constant g_X for two values of the kinetic mixing parameter ϵ. The dashed lines correspond to the EFT limit while the solid lines represent the required values of g_X calculated from the exact model. One can see that the EFT limit gives an excellent approximation. The validity of the EFT limit is ensured by excluding the orange region where $m_{Z'} < 3m_N$, since it would violate our assumption $m_{Z'} \gg m_N$. This region can be considered in the full model, but features annihilations $NN \to Z'$ and is therefore not suitable to represent the EFT approach taken in this work. We refer to Reference [73] for a discussion of this model beyond the EFT limit. We display in Figure 5.5 which regions of the parameter space are ruled out by the bounds from indirect detection and lepton flavor universality in the same color coding as used in Figure 5.3. These are essentially vertical lines, since they amount to a lower bound on the dark matter mass. Direct detection constraints are weak for Majorana dark matter such that they do not affect the parameter space of this model shown in Figure 5.3. Moreover, we include a gray region in the plots to signify where a non-perturbative coupling $g_X \gtrsim \sqrt{4\pi} \approx 3.5$ would be required to obtain the correct relic density. In this case, however, our EFT mapping breaks down because it relies on a perturbative gauge coupling. Therefore, we can make no statements about this case and visually exclude the region.

There are two more excluded regions in Figure 5.5 which we have not discussed before because they can only be evaluated assuming the full model. These are the constraints from collider production of the mediator Z' in red and from Z-Z'-mixing in purple which we discuss next.

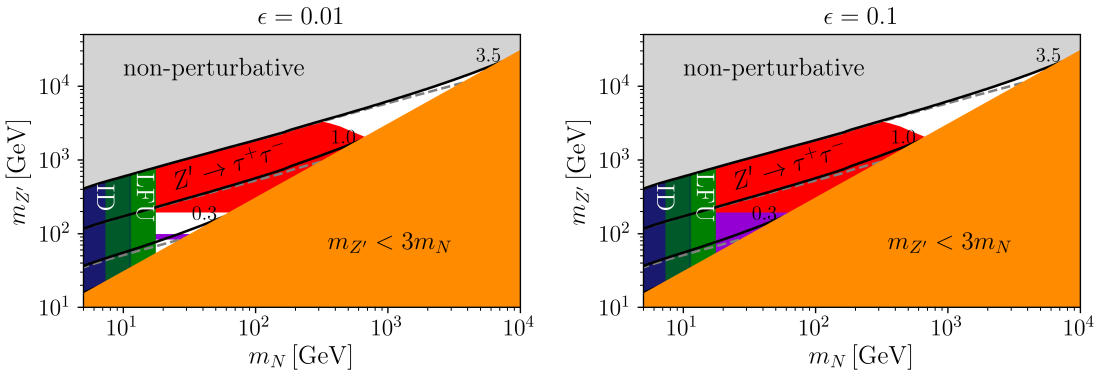

Figure 5.5. Parameter range of the gauged $(B-L)_3$ model introduced in Section 3.1.2 for Z-Z' mixing parameters $\epsilon = 0.01$ (left) and $\epsilon = 0.1$ (right). Contours of g_X producing the correct relic abundance are shown in black, while the dashed lines represent the EFT limit upon identifying $\Lambda = m_{Z'}$ and $c = g_X^2$ with c defined in Equation (5.20). For a given value of ϵ the purple areas are ruled out at 95% CL by electroweak precision data. The area with $m_{Z'} < 3m_N$ is drawn to signify where the EFT approach is valid, namely in the upper left corner. Above $g \simeq \sqrt{4\pi} \approx 3.5$ the theory ceases to be perturbative. Figure adapted from Reference [4].

Heavy vector bosons such as Z' have been searched for at the LHC through different decay channels. In the case of the third-generation couplings in our model, the most sensitive channel to a spin-1 resonance turns out to be $Z' \to \tau^+\tau^-$ [73, 191]. The currently strongest limits on the $pp \to Z' \to \tau^+\tau^-$ cross section come from the ATLAS collaboration [192]. To recast the bounds as limits on $m_{Z'}$ and m_N, we simulate the expected cross section using MadGraph [193]. More specifically, we apply 5-flavor parton distribution functions involving b quarks to simulate the leading-order production channel $\bar{b}b \to Z'$. The branching fraction of $Z' \to \tau^+\tau^-$ can be straightforwardly calculated from the interactions (5.20), see the appendix of Reference [4] for details. The result of the comparison of these simulations with the bounds on the cross section from ATLAS is a constraint on g_X for each value of $m_{Z'}$. Using the relic density bound, this can be translated into a lower limit on m_N for each value of $m_{Z'}$ which is shown in red in Figure 5.5.

Turning to kinetic mixing, we noted in Section 3.1.2 that ϵ must be determined by experiment and is constrained by electroweak precision data [74]. These constraints depend on the mass of Z' and become weak only in the limit $m_{Z'} \gg m_Z$. Therefore we can use the mass-dependent bounds from Reference [74] to determine which Z' masses are excluded for a fixed $\epsilon = 0.01$ or $\epsilon = 0.1$. For the weaker kinetic mixing $\epsilon = 0.01$, only a small band around $m_{Z'} \sim m_Z$ is ruled out, such that there remains a window below with $m_{Z'} < 200\,\text{GeV}$. This changes once the kinetic mixing is larger, since this window is closed entirely if we assume $\epsilon = 0.1$ which implies $m_{Z'} > 320\,\text{GeV}$. To lift all constraints from Z-Z'-mixing we would have to assume $\epsilon \lesssim 0.005$, see Reference [74].

Finally, let us comment on the influence of the interaction with the Higgs field. We explicitly accounted for the dimension five operator in Equation (5.6) leading to a Higgs portal coupling. This portal is expected to be the main coupling responsible for direct

detection and therefore in order for the plots in Figure 5.5 to be valid we have to assume that the constraint on $m_\phi/\sqrt{\lambda_{H\Phi}}$ in Figure 5.4 is satisfied.

We conclude that the EFT defined by the Wilson coefficients in Equation (5.20) can consistently represent the $\mathrm{U}(1)_{(B-L)_3}$ theory with small kinetic mixing. When considering the explicit model, LHC data can be used to probe the mediator and in this case rule out a large portion of the parameter space. However, there still remains room for which the model provides a consistent description of dark matter.

5.3.2. Scalar leptoquark

We have introduced the scalar leptoquark S_1'' model in Section 3.2.3. As discussed there, the tree-level EFT mapping up to dimension six produces only the two operators $\mathcal{O}_{Nt}$ and $\mathcal{O}_{NH}^{(5)}$ with coefficients

$$\begin{aligned} C_{Nt} &= -\frac{1}{2}|x_t|^2\,, \\ C_{NH}^{(5)} &= -\frac{y_t^2|x_t|^2 m_N m_S}{64\pi^2 m_t^2}\left(F(r)+\frac{s}{m_t^2}G(r)+\frac{m_N^2}{m_t^2}H(r)\right), \end{aligned} \tag{5.28}$$

for $\Lambda = m_S$, with $r = m_S^2/m_t^2$ and the functions $F(r)$, $G(r)$, and $H(r)$ given in Equation (10) of Reference [95]. Note that this model is studied in detail also outside the EFT region in this reference.

EFT constraints

The EFT constraints can mostly be carried over from the discussion of the single-operator $\mathcal{O}_{Nt}$ scenario in Section 5.2. An exception is direct detection. In the Dirac case, as previously discussed, spin-independent scattering is induced by the four-fermion operators and therefore the constraints are dominated by this fermion interaction. Hence the constraint from Figure 5.1 is carried over to the EFT of S_1''. In the Majorana case, the direct detection signal induced by $\mathcal{O}_{Nt}$ was negligible. However, we have to account for the Higgs portal coupling which is not independent from the mediator coupling x_t and mass m_S in this model, unlike in the $(B-L)_3$ model in Section 5.3.1 where it was independent of g_X and $m_{Z'}$. Therefore, the bound from XENON1T in Figure 5.2 holds with the identification of the operator coefficient according to Equation (5.28).

Constraints on the full model

We use the same reasoning as in Section 5.3.1 to recast the EFT constraints as constraints on the model parameter space spanned by m_N and m_S. Again for given m_N and m_S, we can fix the coupling $|x_t|$ such that the relic density constraint is satisfied. Then we can draw contour lines of constant $|x_t|$. The result is shown in Figure 5.6. We use again dashed lines for the EFT limit and solid lines for the exact model and observe that the EFT gives a good approximation. Again, we exclude the non-perturbative regime due to a breakdown of the tree-level EFT mapping. In Section 5.3.1, we considered an s-channel mediator Z' such that the resonant annihilation $NN \to Z'$ was possible. This forced us

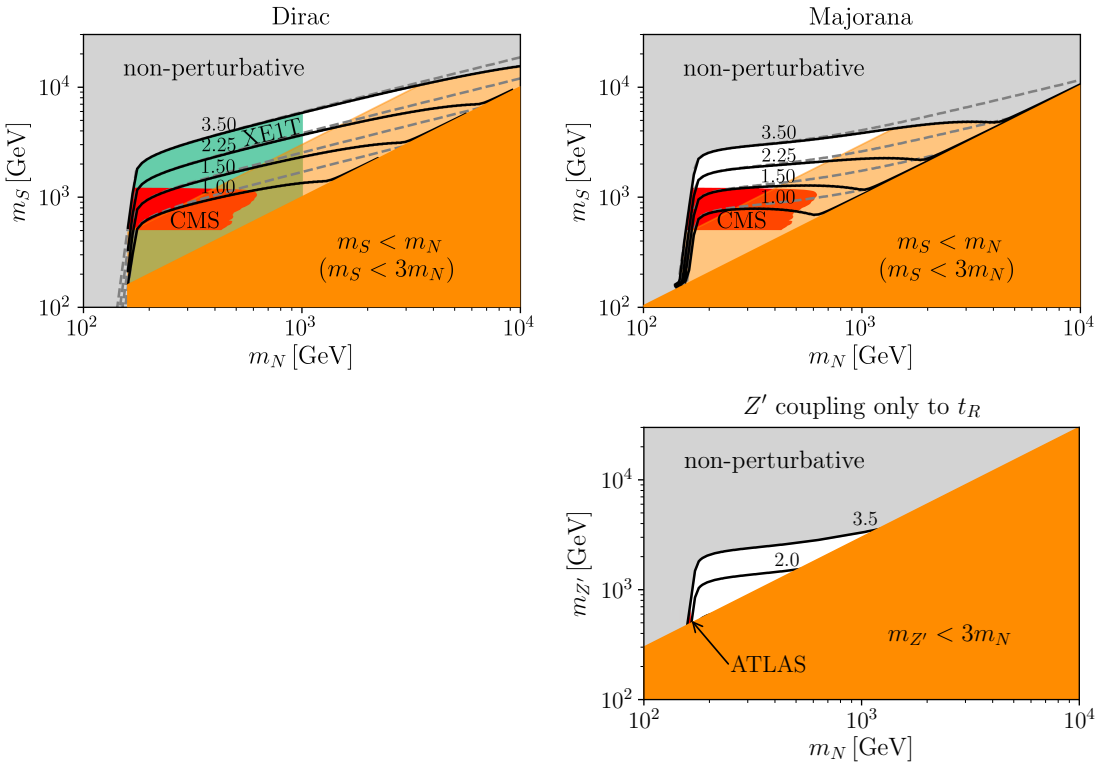

Figure 5.6. Upper: Contours of $|x_t|$ in the m_N-m_S-plane producing the correct relic abundance for the S_1'' leptoquark model. Dashed lines correspond to the EFT limit of the given coupling. Constraints from indirect and direct detection are very weak for Majorana neutrinos. In the case of Dirac neutrinos, direct detection limits from XENON1T are shown in teal. CMS limits are shown in red, perturbativity of the coupling and validity of the EFT description ($m_S < 3m_N$ in orange, $m_S < m_N$ in light orange) are also indicated. Lower: Analogous plot for a simplified Z' model coupling only to the $B - L$ charge of right-handed top quarks, see Equation (5.30). Contours of g_X producing the correct relic abundance are shown in black, the Z-Z' mixing parameter ϵ is zero. An almost invisible ATLAS constraint is included for the Z'. Figure adapted from Reference [4].

to make sure that $m_{Z'}$ was not too close to $2m_N$. Since S is a t-channel mediator, a pair of sterile neutrinos cannot annihilate into a single S, but instead into a leptoquark pair. Therefore, we can apply the EFT framework to a decent accuracy down to $m_S \gtrsim m_N$, as illustrated in Figure 5.6.

The direct detection limit from Figure 5.1 is carried over for the Dirac case and leads to a lower bound on the dark matter mass of $m_N \geq 1002\,\text{GeV}$. In the Majorana case we need to consider the constraint on $|x_t|$ and m_S through the Higgs portal coupling. As a second interaction one possibly needs to consider the effective coupling to quarks at dimension seven. It turns out that in the EFT region $m_S \gtrsim 3m_N$ the Higgs coupling dominates, and so we can neglect the gluon coupling [95]. Fixing the relic density and scanning through m_N and m_S, we find that the constraints are currently not strong enough to probe our

parameter space. We find that a substantial improvement of the current bounds on the WIMP-nucleon cross section would be necessary in order to constrain the parameter space, namely a factor of about 100. In order to rule out the model for masses below $m_N = 1\,\text{TeV}$ an improvement of about four orders of magnitude would be required. Accordingly, we conclude that future bounds from XENONnT will not be sufficient to probe this EFT region of the model further [194].

Now we turn to the constraints that only come into play once we consider the complete model instead of the EFT defined by Equation (5.28). Collider searches for leptoquarks are frequently performed. The possible signatures are classified in Reference [93]. The main production channel in our case is $gg \to SS^\dagger$ and is determined by the strong gauge coupling g_s instead of x_t. This is unavoidable due to the color charge of S and the covariant derivative coupling to gluons in Equation (3.46). The coupling x_t is only relevant to the decay width which must be small enough to ensure that the leptoquarks are produced on-shell. We can apply the bound from the search for a stop by the CMS collaboration [195]. This works because the signature for the decay into a neutral neutralino (i.e. an invisible massive fermion) and a top is equivalent to our signature. Roughly speaking, this search excludes $m_S \lesssim 1200\,\text{GeV}$ at 95% CL for $m_N \lesssim 400\,\text{GeV}$. We show the exact exclusion contours in in red in Figure 5.6. Clearly, above $m_S \approx 1200\,\text{GeV}$, this leaves some open parameter space for dark matter masses $m_N \gtrsim 200\,\text{GeV}$ in the Majorana case.

Concerning indirect detection, we have already hinted that the gluon coupling which is responsible for the collider pair production can also lead to the annihilation $NN \to gg$. From Reference [196], we know that this annihilation channel is relevant in the Majorana case for certain parameter configurations. We calculated the contribution to the gamma ray spectrum in our parameter range using the formulas from References [197, 198] for the annihilation of neutralinos into two gluons mediated by tops and stops, replacing stops by S. Comparing the gamma ray spectra with and without the gluonic channel, we find that the annihilation into top pairs always dominates in our parameter range where $m_N \leq 10\,\text{TeV}$, as visualized in Figure 5.1 as follows. We show the constraint from indirect detection without the gluonic channel in blue and with the gluonic channel in yellow. To translate the bound on $m_S/|x_t|$ into a bound on $\Lambda/\sqrt{C_{Nt}}$ we use the identification

$$\Lambda/\sqrt{C_{Nt}} = \sqrt{2} m_S/|x_t|\,. \tag{5.29}$$

In both cases, the constraint from indirect detection is by far not sufficient to probe the parameter space consistent with the relic density. The fact that the indirect detection constraints are dominated by the fermionic annihilation shows that the EFT limit at dimension six is valid for this model.

To illustrate how the collider constraints depend on the explicit mediator, we include in Figure 5.6 a plot with a Z'-like mediator for comparison. For this simplified model (which is not UV complete), we simply assume that instead of by the leptoquark S, the operator $\mathcal{O}_{Nt}$ is generated by a heavy vector boson coupling only to t_R and N_R according to

$$\mathcal{L} = g_X \left(-N_R \gamma^\mu N_R + \frac{1}{3} t_R \gamma^\mu t_R \right) Z'_\mu\,. \tag{5.30}$$

We try to estimate the limits on such a vector boson by applying ATLAS searches for resonant associated scalar production with a subsequent decay into t-pairs, $pp \to \bar{t}t\phi \to \bar{t}t\bar{t}t$ [199]. For details we refer to Reference [4]. We find a minuscule constraint only in the low-mass region, as displayed in Figure 5.6.

In conclusion, there is viable parameter space for the S_1'' leptoquark scenario for dark matter. In the Dirac case, strong direct detection constraints require $m_N \geq 1002\,\text{GeV}$, but in the Dirac case the strongest constraint comes from the collider search for leptoquark pair production and allows for WIMP masses of a few hundred GeV at mediator masses of 1-3 TeV. Again, the collider signal leads to a reduction of the parameter space allowed by pure EFT considerations, though not as strongly as in the previously discussed $(B-L)_3$-model. Compared to a simplified neutral vector mediator generating the same EFT limit, the collider bounds on the leptoquark are much more stringent.

5.3.3. Vector leptoquark

We have introduced the vector leptoquark U_1'' model in Section 3.2.3. As discussed there, the tree-level EFT mapping up to dimension six produces the operator $\mathcal{O}_{Nb}$ with the coefficient

$$C_{Nb} = |x_b|^2 \tag{5.31}$$

for $\Lambda = m_U$. For this model we cannot extract from the literature an explicit mapping to the dimension-five Higgs operator as we could in the scalar leptoquark case in Equation (5.28). However, it is plausible that the Higgs interaction is not orders-of-magnitude larger than in the scalar case and we therefore assume that it can be neglected in the EFT region also for this vector leptoquark.

EFT constraints

The EFT constraints can be carried over from the discussion of the single-operator $\mathcal{O}_{Nb}$ scenario in Section 5.2. Namely, we have the relatively strong constraint $m_N \geq 126\,\text{GeV}$ from direct detection in the Dirac case due to the contribution to spin-independent scattering, and no constraint from direct detection in the Majorana case.

Constraints on the full model

In Figure 5.7, we show the analogous plot to Figure 5.6 with m_S replaced by m_U. The plot features the usual contour lines of constant coupling $|x_b|$ with dashed lines for the EFT limit and solid lines for the exact model. The EFT is a good approximation as long as $m_U > m_N$ as for the scalar leptoquark, since again the annihilation into U-pairs becomes relevant during freeze-out when $m_U \sim m_N$. The direct detection limit in the Dirac case results in a vertical line at the minimal allowed dark matter mass $m_N = 126\,\text{GeV}$.

Now we turn to the additional model-dependent constraints. As in the scalar leptoquark case, the main collider production channel is pair production $gg \to UU^\dagger$ whose cross section depends on the strong gauge coupling and the leptoquark mass [200]. The value of x_b is again only relevant for the decay width, which should be sufficiently narrow to ensure on-shell production. Assuming on-shell production, we may use the limits from the

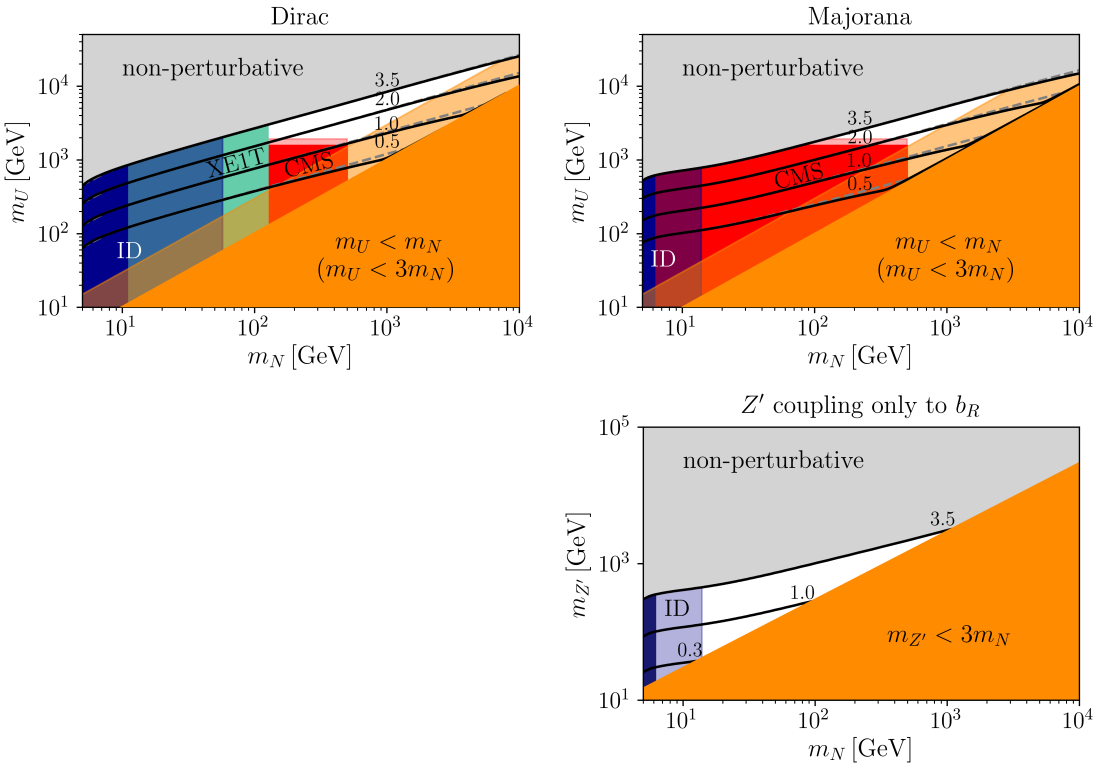

Figure 5.7. Upper: Contours of $|x_b|$ in the m_N-m_U-plane producing the correct relic abundance for the U_1'' leptoquark model are shown in black. Dashed lines correspond to the EFT limit of the given coupling. Constraints from indirect and direct detection are very weak for Majorana neutrinos. In the case of Dirac neutrinos, direct detection limits from XENON1T are shown in teal. CMS limits are shown in red, perturbativity of the coupling and validity of the EFT description ($m_S < 3m_N$ in orange, $m_S < m_N$ in light orange) are also indicated. Lower: Analogous plot for Z' models coupling only to the $B - L$ charge of right-handed bottom quarks, see Equation (5.33). Contours of g_X producing the correct relic abundance are shown in black, the Z-Z' mixing parameter ϵ is zero. Figure adapted from Reference [4].

CMS leptoquark search in Reference [201]. Unfortunately, the limit on the cross section for $pp \to UU^\dagger$ with subsequent respective decays into b or $\bar{b}$ and an invisible fermion like N is only available for $m_N = 0$. In this case, the exact bounds are $m_U \lesssim 1558\,\text{GeV}$ for $\kappa = 0$ and $m_U \lesssim 1927\,\text{GeV}$ for $\kappa = 1$ at 95% CL, where κ depends on the UV completion as discussed in Section 3.2.3. Therefore at the moment we have to project the bounds to non-zero dark matter masses. Comparing with the scalar leptoquark bounds from Reference [201] plotted in Figure 5.6 we conclude that the mass dependence begins around $m_N = 500\,\text{GeV}$ and so we only apply the bounds up to dark matter masses of this magnitude. The result is shown in red in Figure 5.7, where the light red region is only excluded when $\kappa = 1$. We stress again that this is just a projection and should only be considered as an estimate. A dedicated collider analysis of mass-dependent bounds in

analogy to the scalar leptoquark would be favorable.

Concerning indirect detection, the process $NN \to gg$ may play a role in the Majorana case. A precise evaluation of this annihilation cross section is unfortunately missing for this model. We can again try to estimate the effect by calculating the corresponding cross section for a scalar leptoquark coupling to b_R and N_R according to the formulas of References [197, 198] for the annihilation of neutralinos into two gluons mediated by bottoms and sbottoms. Comparing the gamma ray spectra with and without the gluonic channel, we find that the annihilation into bottom pairs dominates for $m_N \lesssim 200\,\text{GeV}$ and the annihilation into gluon pairs dominates for larger masses, as visualized in Figure 5.1. As before we show the constraint from indirect detection without the gluonic channel in blue and with the gluonic channel in yellow, translating the bound on $m_U/|x_b|$ into a bound on $\Lambda/\sqrt{C}$ by the identification

$$\Lambda/\sqrt{C} = m_U/|x_b|\,. \tag{5.32}$$

In the low-mass region of 10-20 GeV, where indirect detection actually probes the parameter space consistent with the observed relic density, the signal is dominated by the fermionic annihilation and therefore again the dimension-six EFT is valid for the evaluation of indirect detection constraints in this model.

As in the scalar case we include in Figure 5.6 a plot with a Z'-like mediator for comparison. For this simplified model (which is again not UV complete), we simply assume that instead of by the leptoquark U, the operator $\mathcal{O}_{Nb}$ is generated by a heavy vector boson coupling only to b_R and N according to

$$\mathcal{L} = g_X \left(-N_R \gamma^\mu N_R + \frac{1}{3} b_R \gamma^\mu b_R \right) Z'_\mu\,. \tag{5.33}$$

We try to estimate the bounds on such a vector boson by applying ATLAS searches for resonant associated scalar production with a subsequent decay into b-pairs, $pp \to \bar{b}b\phi \to \bar{b}b\bar{b}b$ [202]. For details we refer to Reference [4]. In this case we find the EFT parameter space to be unconstrained so far. During the final stages of completing this thesis, preliminary results for the resonant associated production of a heavy Z' with a b-pair subsequently decaying into a b-pair, $pp \to \bar{b}bZ' \to \bar{b}b\bar{b}b$ have been published by the ATLAS collaboration [203]. We expect that these would provide more stringent bounds on this simplified model.

We conclude that even when we extrapolate the collider constraint from CMS to large masses $m_N = 500\,\text{GeV}$, there is a range of parameter space which can consistently explain dark matter. Moreover, the EFT limit is sufficient to capture the physics of freeze-out, direct detection and indirect detection. For Dirac dark matter, the allowed masses are $m_N > 123\,\text{GeV}$ and $m_U \gtrsim 1\,\text{TeV}$. For Majorana dark matter the direct detection constraints from XENON1T do not apply and therefore dark matter masses can be as low as 77 GeV for $\kappa = 0$. Compared to a simplified neutral vector mediator generating the same EFT limit, the collider bounds on the leptoquark are much more stringent.

5.4. Summary

In this chapter, we have investigated the practical use of a dark matter EFT inspired by SMNEFT as a model-independent framework for dark matter physics. When making the assumption that only couplings of dark matter to the third generation SM fermions and to the Higgs boson are generated in the form of the operators in Equations (5.5)-(5.7), we could consistently treat the thermal production, direct detection and indirect detection constraints within the EFT framework. Three example models could be matched to the EFT which allowed for the application of the constraints calculated with effective interactions on the model parameter space. This demonstrates that the use of the third-generation νDMEFT to evaluate relic density, direct detection and indirect detection constraints is realistic from a theoretical point of view. To distinguish models which give the same hierarchy of Wilson coefficients, constraints on the collider production cross section of the mediator are very powerful. In particular, we found that due to the unavoidable coupling to gluons, leptoquark mediators can be efficiently tested at the LHC. In the case of the scalar leptoquark, constraints on the supersymmetric partner of the top quark can be applied directly, since it has the same coupling to gluons and the same decay signature. Of course, the are many more possibilities to arrange the four-fermion operators in Equation (5.5) than we could consider here. For instance, we have only discussed one EFT scenario including several operators, the gauged $(B-L)_3$ model in Section 5.3.1. An ideal use of the framework would be to identify which Wilson coefficients are important in the case of observation in direct or indirect detection. The matching of a given theory to the EFT then provides us with a straightforward check of its consistency with observations.

6. Conclusions

In this thesis, we have pursued a very general approach towards neutrino interactions beyond the Standard Model of particle physics (SM). Presupposing only the conservation of the SM gauge symmetry and Lorentz symmetry, a natural framework to consider effects of new physics associated with a large energy scale is constituted by effective field theories (EFTs). Discussing the possible operators composed of SM fields and sterile neutrinos up to mass-dimension six, we have identified General Neutrino Interactions (GNI) and a subset of the Standard Model Effective Field Theory extended by right-handed neutrinos (SMNEFT) as the suitable EFTs to describe new neutrino interactions with SM fermions below and above the weak scale. Assuming that the new physics originates from high energies, the two frameworks can be connected at the weak scale following a set of mapping prescriptions.

Moreover, we have identified several ultraviolet complete models which lead to such effective interactions when considering the exchange of off-shell heavy new mediator particles. One example featured an additional U(1) gauge symmetry broken at high energies, which led to a massive vector boson Z' as the mediator of new interactions. Other examples included colored, charged, and neutral scalar fields, demonstrating that various types of neutrino interactions are not only possible but realistic from a theoretical point of view. In fact, several of these models have been previously introduced to explain other open questions, for instance the origin of neutrino masses or dark matter, but involve new neutrino interactions as an additional effect.

In order to understand the implications of the mapping between GNI and SMNEFT, we have investigated connections between physical processes at energies below the weak scale, such as flavor-violating charged-lepton decays, coherent elastic neutrino-nucleus scattering, nuclear beta decays, pion decays, and neutrino-electron scattering. We found that these types of low-energy experiments probe interaction strengths comparable to TeV-scale new physics and are therefore excellent complements to collider searches. A consistent finding is that if GNI originate from SMNEFT operators, current experimental constraints on new interactions are significantly stronger. The reason for this is that the left-handed neutrinos appear in a weak doublet together with charged leptons in SMNEFT operators. Generically, this results in new neutrino interactions being accompanied by equally strong charged lepton interactions. The latter are, however, typically much more strongly constrained. In particular, extremely stringent bounds on charged lepton flavor violation then apply also for lepton flavor violating neutrino interactions. In other cases, the doublet structure leads to simultaneous neutral-current and charged-current GNI, such that the stronger charged-current constraint applies also to neutral-current interaction. This can be illustrated by our collection of direct and indirect experimental constraints on GNI parameters summarized in Table 4.6 and Table 4.7, where the in-

direct bounds rely on the SMNEFT-GNI mapping. Turning the argument around, this shows that if interactions violating the indirect bounds are detected, this would hint towards low-scale new physics which would render the SMNEFT approach incomplete. Considering the most general interactions, we investigated one running and one upcoming experiment (KATRIN and DUNE) in terms of their potential to test GNI.

As a further application of the framework, we have shown that SMNEFT provides an explanation of dark matter which is consistent with the observed abundance as well as direct and indirect detection constraints when we interpret a sterile neutrino as a weakly interacting massive particle and assume a stabilizing symmetry. We demonstrated that this EFT approach is realistic by identifying three possible models whose physics of production and detection is captured by the effective operators. For dark matter in the range of tens to hundreds of GeV, these models require mediators of masses around or below 1 TeV. Therefore, we find that the EFT description does not hold at the Large Hadron Collider and instead the explicit models can be constrained and distinguished by considering the direct collider production of the mediator.

In conclusion, we emphasize that neutrino observables are competitive probes of new physics at the precision frontier. This supports the current intensive efforts by the community to enhance the sensitivity and applicability of neutrino detectors and beam facilities to probe nuclear, particle, and astrophysics. Especially due to our limited present knowledge of how nature has realized neutrino mass generation and if there is leptonic charge-parity violation, we should be cautious about the interpretation of observations and account for potential new interactions in a global consideration. We have made the case that GNI are capable of capturing the low-energy effects of a vast landscape of theories beyond the SM and are therefore a valuable tool in our quest for the missing pieces in the puzzle of fundamental physics.

A. Properties of four-fermion interactions

A.1. Weyl, Majorana and Dirac fermions

In this section, we follow Reference [37] to introduce the notions of Weyl, Majorana and Dirac fermions. A free spin-1/2 fermion satisfies the Dirac equation

$$(i\gamma^\mu\partial_\mu - m)\psi(x) = 0\,, \tag{A.1}$$

where ψ is a four-component spinor field and m is the mass of the fermion. The four gamma matrices follow the usual relations

$$\{\gamma^\mu, \gamma^\nu\} = 2g^{\mu\nu}\cdot\mathbb{1}\,, \qquad \gamma^0\gamma^{\mu\dagger}\gamma^0 = \gamma^\mu\,. \tag{A.2}$$

An additional matrix γ^5 is defined by $\gamma^5 = i\gamma^0\gamma^1\gamma^2\gamma^3$ and satisfies

$$\{\gamma^5, \gamma^\mu\} = 0\,, \qquad \gamma^{5\dagger} = \gamma^5\,, \qquad (\gamma^5)^2 = \mathbb{1}\,. \tag{A.3}$$

With this matrix one can define the left-handed and right-handed projection operators

$$P_L = \frac{\mathbb{1}-\gamma^5}{2}\,, \qquad P_R = \frac{\mathbb{1}+\gamma^5}{2}\,, \tag{A.4}$$

abiding

$$P_L P_R = P_R P_L = 0\,, \qquad P_L + P_R = \mathbb{1}\,, \qquad P_L^2 = P_L\,, \qquad P_R^2 = P_R\,, \tag{A.5}$$

which enable us to project the spinor field ψ into left-handed and right-handed components

$$\psi = (P_L + P_R)\psi = P_L\psi + P_R\psi \equiv \psi_L + \psi_R\,. \tag{A.6}$$

Moreover, one can define a a particle-antiparticle conjugation, which exchanges the particle creation and annihilation operators with the antiparticle creation and annihilation operators in the mode expansion of ψ,

$$\psi \to \psi^c = \mathcal{C}\overline{\psi}^T\,, \qquad \overline{\psi^c} = -\psi^T C^\dagger\,, \tag{A.7}$$

where $\mathcal{C}$ can be defined as

$$\mathcal{C} = i\gamma^2\gamma^0 \tag{A.8}$$

and obeys

$$\mathcal{C}^{-1}\gamma^\mu\mathcal{C} = -\gamma^{\mu T}\,, \qquad \mathcal{C}^{-1}\gamma^5\mathcal{C} = \gamma^{5T}\,, \qquad \mathcal{C}^\dagger = \mathcal{C}^{-1} = -\mathcal{C}^* = -\mathcal{C}\,. \tag{A.9}$$

Crucially, this operation maps a left-chiral spinor onto a right-chiral spinor and vice versa,

$$P_R(\psi_L)^c = (\psi_L)^c\,, \qquad P_L(\psi_R)^c = (\psi_R)^c\,. \tag{A.10}$$

Two subsequent applications map back to the original field, $(\psi^c)^c = \psi$.

For distinguishing Weyl, Majorana, and Dirac fermions it is convenient to choose a particular representation for γ^μ called the Weyl representation given by

$$\gamma^0 = \begin{pmatrix} 0 & \mathbb{1}_2 \\ \mathbb{1}_2 & 0 \end{pmatrix}, \qquad \gamma^i = \begin{pmatrix} 0 & \sigma^i \\ -\sigma^i & 0 \end{pmatrix}, \qquad \gamma^5 = \begin{pmatrix} -\mathbb{1}_2 & 0 \\ 0 & \mathbb{1}_2 \end{pmatrix}, \tag{A.11}$$

where σ^i are the Pauli matrices. In this representation we can write

$$\psi = \begin{pmatrix} \phi \\ \xi \end{pmatrix} \quad \Rightarrow \quad P_L\psi = \begin{pmatrix} \phi \\ 0 \end{pmatrix}, \quad P_R\psi = \begin{pmatrix} 0 \\ \xi \end{pmatrix}, \tag{A.12}$$

where $\phi(x)$ and $\xi(x)$ are two-component (Weyl) spinors. Substituting them into the Dirac equation yields two equations coupled by the mass

$$\begin{aligned} (i\partial_0 - i\vec{\sigma}\cdot\vec{\nabla})\phi - m\xi = 0\,, \\ (i\partial_0 + i\vec{\sigma}\cdot\vec{\nabla})\xi - m\phi = 0\,. \end{aligned} \tag{A.13}$$

In the limit $m \to 0$ the two equations decouple and become the so-called Weyl equations which describe massless two-component spinors with negative (ϕ) or positive (ξ) helicity. If we consider now a massive fermion ψ, there are two options. ψ_L and ψ_R can be independent or they can be linked by $\psi_R = \psi_L^c$. In the latter case it immediately follows that

$$\psi^c = (\psi_L + \psi_L^c)^c = \psi_L^c + (\psi_L^c)^c = \psi\,, \tag{A.14}$$

i.e. particle and antiparticle are identical. If this is the case the field is called a Majorana fermion.

In this thesis we only consider four-component spinors. Therefore, when we say that ψ_L is a left-handed Weyl fermion, we mean that its free Lagrangian is given by

$$\mathcal{L}_\mathrm{W} = \overline{\psi_L}(i\gamma^\mu\partial_\mu)\psi_L\,, \tag{A.15}$$

and likewise for a right-handed Weyl fermion ψ_R. For a Majorana fermion, we instead have

$$\mathcal{L}_\mathrm{M} = \overline{\psi_L}(i\gamma^\mu\partial_\mu)\psi_L - \frac{m}{2}\left(\overline{\psi_L^c}\psi_L + \overline{\psi_L}\psi_L^c\right), \tag{A.16}$$

where the factor of $1/2$ is needed to compensate that the mass term is quadratic in ψ_L. For a Dirac fermion

$$\mathcal{L}_\mathrm{D} = \overline{\psi}(x)(i\gamma^\mu\partial_\mu - m)\psi(x)\,. \tag{A.17}$$

It is important to appreciate the following distinction concerning charges. If ψ conserves U(1) charges associated with the transformation $\psi \to \exp(i\alpha)\psi$, then the Lagrangian must be invariant under such transformations. This is clearly only the case for the Weyl and Dirac Lagrangians and thus Majorana fermions must be neutral. Another interesting fact is that when $m \to 0$ we can see that the Majorana Lagrangian reduces to a Weyl Lagrangian, while the Dirac Lagrangian reduces to a Lagrangian of two Weyl fermions, one for the left-handed, and one for the right-handed component. Therefore, all fermion types reduce to Weyl fermions in the limit of vanishing masses. Moreover, one can show that two Majorana fermions with the same mass are equivalent to a Dirac fermion.

A.2. General properties of four-fermion operators

Here we discuss how to obtain the most general Lorentz-scalar Lagrangians involving four fermions which explains the structure of the operators in Tables 2.1 and 2.4. The space of all 4-by-4 matrices in spinor space is generated by the following useful basis [35]

$$\{\Gamma_i\} = \{\mathbb{1}, \gamma^0, \gamma^1, \gamma^2, \gamma^3, \sigma^{01}, \sigma^{02}, \sigma^{03}, \sigma^{12}, \sigma^{13}, \sigma^{23}, \gamma^0\gamma^5, \gamma^1\gamma^5, \gamma^2\gamma^5, \gamma^3\gamma^5, \gamma^5\}\,, \quad \text{(A.18)}$$

where

$$\sigma^{\mu\nu} \equiv \frac{i}{2}[\gamma^\mu, \gamma^\nu]\,. \quad \text{(A.19)}$$

Hence, all matrices M in spinor space can be written as a sum of these 16 matrices. It is useful to classify the transformation properties under the Lorentz group of bilinears built of two four-component spinors ψ_a and ψ_b. Namely,

$$\begin{gathered} S_{ab} = \overline{\psi}_a\psi_b\,, \quad V^\mu_{ab} = \overline{\psi}_a\gamma^\mu\psi_b\,, \quad T^{\mu\nu}_{ab} = \overline{\psi}_a\sigma^{\mu\nu}\psi_b\,, \\ A^\mu_{ab} = \overline{\psi}_a\gamma^\mu\gamma^5\psi_b\,, \quad P_{ab} = \overline{\psi}_a\gamma^5\psi_b \end{gathered} \quad \text{(A.20)}$$

behave like a scalar, vector, rank-2 tensor, axial vector, and pseudoscalar, respectively. Knowing this, we can construct all possible Lorentz scalars involving four four-component fermions ψ_i, $i = 1, \ldots, 4$. When fixing that ψ_1 is contracted with ψ_2 and ψ_3 with ψ_4, the possible Lorentz scalars are given by

$$\begin{aligned} \mathcal{L}^S(\psi_1,\psi_2,\psi_3,\psi_4) &= \left(\overline{\psi_1}\psi_2\right)\left(\overline{\psi_3}\psi_4\right), \\ \mathcal{L}^V(\psi_1,\psi_2,\psi_3,\psi_4) &= \left(\overline{\psi_1}\gamma_\mu\psi_2\right)\left(\overline{\psi_3}\gamma^\mu\psi_4\right), \\ \mathcal{L}^T(\psi_1,\psi_2,\psi_3,\psi_4) &= \left(\overline{\psi_1}\sigma_{\mu\nu}\psi_2\right)\left(\overline{\psi_3}\sigma^{\mu\nu}\psi_4\right), \\ \mathcal{L}^A(\psi_1,\psi_2,\psi_3,\psi_4) &= \left(\overline{\psi_1}\gamma_\mu\gamma^5\psi_2\right)\left(\overline{\psi_3}\gamma^\mu\gamma^5\psi_4\right), \\ \mathcal{L}^P(\psi_1,\psi_2,\psi_3,\psi_4) &= \left(\overline{\psi_1}\gamma^5\psi_2\right)\left(\overline{\psi_3}\gamma^5\psi_4\right). \end{aligned} \quad \text{(A.21)}$$

In this thesis we are dealing with SM fermions whose chiral components ψ_L and ψ_R exist in different representations of the gauge group. Therefore, it is useful to consider the possible Lorentz scalars for chiral fields. To obtain these, we will apply a number of useful identities which are straightforwardly derived. Let ψ and χ denote two generic four-component spinors, then

$$\begin{aligned} \overline{\psi_R}\chi_R = \overline{\psi_L}\chi_L = \overline{\psi_R}\gamma^5\chi_R = \overline{\psi_L}\gamma^5\chi_L = 0\,, \\ \overline{\psi_R}\sigma^{\mu\nu}\chi_R = \overline{\psi_L}\sigma^{\mu\nu}\chi_L = \overline{\psi_R}\sigma^{\mu\nu}\gamma^5\chi_R = \overline{\psi_L}\sigma^{\mu\nu}\gamma^5\chi_L = 0\,, \\ \overline{\psi_R}\gamma^\mu\chi_L = \overline{\psi_L}\gamma^\mu\chi_R = \overline{\psi_L}\gamma^\mu\gamma^5\chi_R = \overline{\psi_R}\gamma^\mu\gamma^5\chi_L = 0\,. \end{aligned} \quad \text{(A.22)}$$

Therefore, the scalar, pseudoscalar, and tensor bilinears require combining spinors of opposite chirality, and the vector and axial vector bilinears require combining spinors of equal chirality. If we apply this to the Lorentz scalars in Equation (A.21), we find in total ten independent contractions in terms of chiral components L_i and R_i,

$$\begin{array}{lll} \mathcal{L}^S(L_1,R_2,L_3,R_4)\,, & \mathcal{L}^V(L_1,L_2,L_3,L_4)\,, & \\ \mathcal{L}^S(L_1,R_2,R_3,L_4)\,, & \mathcal{L}^V(L_1,L_2,R_3,R_4)\,, & \mathcal{L}^T(L_1,R_2,L_3,R_4)\,, \\ \mathcal{L}^S(R_1,L_2,L_3,R_4)\,, & \mathcal{L}^V(R_1,R_2,L_3,L_4)\,, & \mathcal{L}^T(R_1,L_2,R_3,L_4)\,, \\ \mathcal{L}^S(R_1,L_2,R_3,L_4)\,, & \mathcal{L}^V(R_1,R_2,R_3,R_4)\,, & \end{array} \quad \text{(A.23)}$$

Table A.1. Table of Fierz coefficients appearing in Equation (A.24).

		Y				
		S	V	T	A	P
	S	$-1/4$	$-1/4$	$-1/8$	$1/4$	$-1/4$
	V	-1	$1/2$	0	$1/2$	1
X	T	-3	0	$1/2$	0	-3
	A	1	$1/2$	0	$1/2$	-1
	P	$-1/4$	$1/4$	$-1/8$	$-1/4$	$-1/4$

which are equivalent to the ten types of GNI defined in Equations (2.11) and (2.12) together with Table 2.4. By applying the Fierz transformations, one can show that $\mathcal{L}^T(L_1, R_2, R_1, L_2) = \mathcal{L}^T(R_1, L_2, L_3, R_4) = 0$ and hence these two combinations do not appear. Moreover, $\mathcal{L}^A$ and $\mathcal{L}^P$ are redundant for chiral spinors since $\gamma^5 R = R$ and $\gamma^5 L = -L$.

A.3. Fierz transformations

The Fierz transformations are a set of identities concerning the Lorentz-scalar functions of four four-component spinors ψ_i, $i = 1, \ldots, 4$ in Equation (A.21). They are expressed as a set of coefficients C_{XY} summarized in Table A.1, such that

$$\mathcal{L}^X(\psi_1, \psi_2, \psi_3, \psi_4) = \sum_{Y=S,V,T,A,P} C_{XY} \mathcal{L}^Y(\psi_1, \psi_4, \psi_3, \psi_2)\,. \tag{A.24}$$

Notice that the positions of ψ_2 and ψ_4 are swapped from one side of the equation to the other. For the purpose of matching various four-fermion operators onto the precise form of the operator basis in Table 2.1 it is very convenient to know the transformation of chiral fields. Therefore we calculate them here once and can apply them to the chiral SM fields whenever needed. Again, we denote a left-chiral field by L_i and a right-chiral field by R_i.

$$\mathcal{L}^S(L_1, R_2, L_3, R_4) = -\frac{1}{2}\mathcal{L}^S(L_1, R_4, L_3, R_2) - \frac{1}{8}\mathcal{L}^T(L_1, R_4, L_3, R_2)\,, \tag{A.25}$$

$$\mathcal{L}^S(L_1, R_2, R_3, L_4) = -\frac{1}{2}\mathcal{L}^V(L_1, L_4, R_3, R_2)\,, \tag{A.26}$$

$$\mathcal{L}^V(L_1, L_2, L_3, L_4) = \mathcal{L}^V(L_1, L_4, L_3, L_2)\,, \tag{A.27}$$

$$\mathcal{L}^T(L_1, R_2, L_3, R_4) = -6\mathcal{L}^S(L_1, R_4, L_3, R_2) + \frac{1}{2}\mathcal{L}^T(L_1, R_4, L_3, R_2)\,. \tag{A.28}$$

The remaining identities are obtained by inverting all fields $L \leftrightarrow R$ on both sides of the equations.

A.4. Mapping between the Lee-Yang and epsilon parametrizations of GNI

We have noted in Section 2.3 that there is an alternative parametrization of the 10 independent GNI terms defined in Equations (2.11) and (2.12) which we call the Lee-Yang parametrization [204]. We define the alternative parametrization only for the neutral current case, but for the charged-current GNI the definitions are completely analogous. Recall that the epsilon parametrization is given by

$$\mathcal{L} = -\frac{G_F}{\sqrt{2}} \sum_{j=1}^{10} \begin{pmatrix} (\sim) \\ \epsilon_{j,f} \end{pmatrix}^{\alpha\beta\gamma\delta} (\overline{\nu}_\alpha \mathcal{O}_j \nu_\beta) \left(\overline{f}_\gamma \mathcal{O}'_j f_\delta\right), \tag{A.29}$$

with the operators $\mathcal{O}_j$, $\mathcal{O}'_j$ defined in Table 2.4. An alternative parametrization reads, see e.g. Reference [52],

$$\mathcal{L} = -\frac{G_F}{\sqrt{2}} \sum_{a=S,P,V,A,T} (\overline{\nu}_\alpha \, \Gamma_a \nu_\beta) \left(\overline{f_\gamma} \Gamma_a (C_a^{\alpha\beta\gamma\delta} + \overline{D}_a^{\alpha\beta\gamma\delta} i\gamma^5) f_\delta\right), \tag{A.30}$$

where the five possible independent combinations of Dirac matrices are defined as

$$\Gamma_a \in \left\{\mathbb{1}, i\gamma^5, \gamma^\mu, \gamma^\mu\gamma^5, \sigma^{\mu\nu}\right\}, \tag{A.31}$$

and the ten epsilon coefficients have the counterparts $C^a_{\alpha\beta\gamma\delta}$ and

$$D^a_{\alpha\beta\gamma\delta} \equiv \begin{cases} \overline{D}^a_{\alpha\beta\gamma\delta} & \text{for } a = S, P, T\,, \\ i\overline{D}^a_{\alpha\beta\gamma\delta} & \text{for } a = V, A\,. \end{cases} \tag{A.32}$$

Suppressing flavor indices, the mapping between the two parametrizations reads

$$\begin{aligned}
\epsilon_L &= \frac{1}{4}\left(C_V - D_V + C_A - D_A\right), & \widetilde{\epsilon}_L &= \frac{1}{4}\left(C_V - D_V - C_A + D_A\right), \\
\epsilon_R &= \frac{1}{4}\left(C_V + D_V - C_A - D_A\right), & \widetilde{\epsilon}_R &= \frac{1}{4}\left(C_V + D_V + C_A + D_A\right), \\
\epsilon_S &= \frac{1}{2}\left(C_S + iD_P\right), & \widetilde{\epsilon}_S &= \frac{1}{2}\left(C_S - iD_P\right), \\
-\epsilon_P &= \frac{1}{2}\left(C_P + iD_S\right), & -\widetilde{\epsilon}_P &= \frac{1}{2}\left(-C_P + iD_S\right), \\
\epsilon_T &= \frac{1}{4}\left(C_T - iD_T\right), & \widetilde{\epsilon}_T &= \frac{1}{4}\left(C_T + iD_T\right).
\end{aligned} \tag{A.33}$$

A.5. Number of degrees of freedom

Here we discuss how to obtain the contents of Table 2.5, i.e. the number of degrees of freedom of neutral-current GNI under different assumptions such as Majorana nature of the neutrinos, charge-parity (CP) invariance, and flavor conservation. We only explicitly prove how the first row of this table is obtained, since the other two rows follow the same

line of reasoning. There are a number of identities concerning Majorana neutrinos which are useful for the proofs. They read

$$\begin{aligned}
\overline{\nu}_\alpha \gamma^\mu \nu_\beta &= -\overline{\nu}_\beta \gamma^\mu \nu_\alpha \,, \\
\overline{\nu}_\alpha \gamma^\mu \gamma^5 \nu_\beta &= \overline{\nu}_\beta \gamma^\mu \gamma^5 \nu_\alpha \,, \\
\overline{\nu}_\alpha \nu_\beta &= \overline{\nu}_\beta \nu_\alpha \,, \\
\overline{\nu}_\alpha \gamma^5 \nu_\beta &= \overline{\nu}_\beta \gamma^5 \nu_\alpha \,, \\
\overline{\nu}_\alpha \sigma^{\mu\nu} \nu_\beta &= -\overline{\nu}_\beta \sigma^{\mu\nu} \nu_\alpha \,, \\
\overline{\nu}_\alpha \sigma^{\mu\nu} \gamma^5 \nu_\beta &= -\overline{\nu}_\beta \sigma^{\mu\nu} \gamma^5 \nu_\alpha \,.
\end{aligned} \tag{A.34}$$

These are straightforwardly proven as follows, applying $\overline{\nu^c} = -\nu^T C^\dagger = \nu^T C = \overline{\nu}$ and the definitions of the bilinears in Equation (A.20),

$$\begin{aligned}
V^\mu_{\alpha\beta} &= \nu^T_\alpha C \gamma^\mu \nu_\beta = -\nu^T_\alpha (\gamma^\mu)^T C \nu_\beta = -\overline{\nu^c_\beta} \gamma^\mu \nu_\alpha = -V^\mu_{\beta\alpha} \,, \\
A^\mu_{\alpha\beta} &= \nu^T_\alpha C \gamma^\mu \gamma^5 \nu_\beta = -\nu^T_\alpha (\gamma^\mu)^T (\gamma^5)^T C \nu_\beta = -\overline{\nu^c_\beta} \gamma^5 \gamma^\mu \nu_\alpha = +A^\mu_{\beta\alpha} \,, \\
S_{\alpha\beta} &= \nu^T_\alpha C \nu_\beta = \overline{\nu^c_\beta} \nu_\alpha = +S^\mu_{\beta\alpha} \,, \\
P_{\alpha\beta} &= \nu^T_\alpha C \gamma^5 \nu_\beta = \nu^T_\alpha (\gamma^5)^T C \nu_\beta = \overline{\nu^c_\beta} \gamma^5 \nu_\alpha = +P^\mu_{\beta\alpha} \,, \\
T^{\mu\nu}_{\alpha\beta} &= \nu^T_\alpha C \sigma^{\mu\nu} \nu_\beta = -\nu^T_\alpha (\sigma^{\mu\nu})^T C \nu_\beta = -\overline{\nu^c_\beta} \sigma^{\mu\nu} \nu_\alpha = -T^{\mu\nu}_{\beta\alpha} \,, \\
\widetilde{T}^{\mu\nu}_{\alpha\beta} &= \nu^T_\alpha C \sigma^{\mu\nu} \gamma^5 \nu_\beta = -\nu^T_\alpha (\sigma^{\mu\nu})^T (\gamma^5)^T C \nu_\beta = -\overline{\nu^c_\beta} \gamma^5 \sigma^{\mu\nu} \nu_\alpha = -\widetilde{T}^{\mu\nu}_{\beta\alpha} \,,
\end{aligned} \tag{A.35}$$

where we used

$$C\gamma^5 = (\gamma^5)^T C \,, \quad C\gamma^\mu = -(\gamma^\mu)^T C \,, \quad \left[\sigma^{\mu\nu}, \gamma^5\right] = 0 \tag{A.36}$$

and the anticommuting nature of the fermion fields. Now we state the identities that hold for the epsilon parametrization and for the Lee-Yang parametrization under different assumptions. Proofs are given subsequently in the epsilon parametrization.

1. **In general:** (810 real parameters)

$$\begin{aligned}
&\epsilon^j_{\alpha\beta\gamma\delta} = \epsilon^{j*}_{\beta\alpha\delta\gamma} \,, \quad j = 1,2,3,4 \,, \\
&\epsilon^S_{\alpha\beta\gamma\delta} = \widetilde{\epsilon}^{S*}_{\beta\alpha\delta\gamma} \,, && C^a_{\alpha\beta\gamma\delta} = C^{a*}_{\beta\alpha\delta\gamma} \,, \\
&\epsilon^P_{\alpha\beta\gamma\delta} = -\widetilde{\epsilon}^{P*}_{\beta\alpha\delta\gamma} \,, && D^a_{\alpha\beta\gamma\delta} = D^{a*}_{\beta\alpha\delta\gamma} \,. \\
&\epsilon^T_{\alpha\beta\gamma\delta} = \widetilde{\epsilon}^{T*}_{\beta\alpha\delta\gamma} \,,
\end{aligned} \tag{A.37}$$

2. **CP invariance:** (423 real parameters)

$$\begin{aligned}
&\epsilon^j_{\alpha\beta\gamma\delta} \in \mathbb{R} && \forall j, \\
&\epsilon^j_{\alpha\beta\gamma\delta} = \epsilon^j_{\beta\alpha\delta\gamma} && j = 1,2,3,4 \,,
\end{aligned} \qquad
\begin{aligned}
&C^a_{\alpha\beta\gamma\delta} \in \mathbb{R} && \forall a, \\
&D^a_{\alpha\beta\gamma\delta} \in \mathbb{R} \,, && a = V, A \,, \\
&D^a_{\alpha\beta\gamma\delta} \in i\mathbb{R} \,, && a = S, P, T \,.
\end{aligned} \tag{A.38}$$

Table A.2. Operators and their conjugates appearing in the Hermitian conjugate of Equation (A.29).

j	$\mathcal{O}_j$	$\gamma^0\mathcal{O}_j^\dagger\gamma^0$	$\mathcal{O}'_j$	$\gamma^0\mathcal{O}_j'^\dagger\gamma^0$
1	$\gamma_\mu(\mathbb{1}-\gamma^5)$	$\gamma_\mu(\mathbb{1}-\gamma^5)$	$\gamma^\mu(\mathbb{1}-\gamma^5)$	$\gamma_\mu(\mathbb{1}-\gamma^5)$
2	$\gamma_\mu(\mathbb{1}+\gamma^5)$	$\gamma_\mu(\mathbb{1}+\gamma^5)$	$\gamma^\mu(\mathbb{1}-\gamma^5)$	$\gamma_\mu(\mathbb{1}-\gamma^5)$
3	$\gamma_\mu(\mathbb{1}-\gamma^5)$	$\gamma_\mu(\mathbb{1}-\gamma^5)$	$\gamma^\mu(\mathbb{1}+\gamma^5)$	$\gamma_\mu(\mathbb{1}+\gamma^5)$
4	$\gamma_\mu(\mathbb{1}+\gamma^5)$	$\gamma_\mu(\mathbb{1}+\gamma^5)$	$\gamma^\mu(\mathbb{1}+\gamma^5)$	$\gamma_\mu(\mathbb{1}+\gamma^5)$
5	$(\mathbb{1}-\gamma^5)$	$(\mathbb{1}+\gamma^5)$	$\mathbb{1}$	$\mathbb{1}$
6	$(\mathbb{1}+\gamma^5)$	$(\mathbb{1}-\gamma^5)$	$\mathbb{1}$	$\mathbb{1}$
7	$(\mathbb{1}-\gamma^5)$	$(\mathbb{1}+\gamma^5)$	γ^5	$-\gamma^5$
8	$(\mathbb{1}+\gamma^5)$	$(\mathbb{1}-\gamma^5)$	γ^5	$-\gamma^5$
9	$\sigma_{\mu\nu}(\mathbb{1}-\gamma^5)$	$\sigma_{\mu\nu}(\mathbb{1}+\gamma^5)$	$\sigma^{\mu\nu}(\mathbb{1}-\gamma^5)$	$\sigma^{\mu\nu}(\mathbb{1}+\gamma^5)$
10	$\sigma_{\mu\nu}(\mathbb{1}+\gamma^5)$	$\sigma_{\mu\nu}(\mathbb{1}-\gamma^5)$	$\sigma^{\mu\nu}(\mathbb{1}+\gamma^5)$	$\sigma^{\mu\nu}(\mathbb{1}-\gamma^5)$

3. **Majorana neutrinos:** (432 real parameters)

$$\begin{aligned} &\epsilon^j_{\alpha\beta\gamma\delta} = -\widetilde{\epsilon}^j_{\beta\alpha\gamma\delta}\,, && j=L,R \\ &\epsilon^k_{\alpha\beta\gamma\delta} = \epsilon^k_{\beta\alpha\gamma\delta}\,, && k=S,P \\ &\epsilon^T_{\alpha\beta\gamma\delta} = -\epsilon^T_{\beta\alpha\gamma\delta}\,. \end{aligned} \qquad \begin{aligned} &C^a_{\alpha\beta\gamma\delta} = C^a_{\beta\alpha\gamma\delta}\,, \\ &D^a_{\alpha\beta\gamma\delta} = D^a_{\beta\alpha\gamma\delta}\,, && a=S,P,A\,, \\ &C^b_{\alpha\beta\gamma\delta} = -C^b_{\beta\alpha\gamma\delta}\,, \\ &D^b_{\alpha\beta\gamma\delta} = -D^b_{\beta\alpha\gamma\delta}\,, && b=V,T\,. \end{aligned} \tag{A.39}$$

4. **Majorana neutrinos + CP invariance:** (225 real parameters)

Proofs:

1. **In general:** The Hermitian conjugate of Equation (A.29) involves the expressions

$$(\overline{\nu}^\alpha\mathcal{O}_j\nu^\beta)^\dagger(\overline{f}^\gamma\mathcal{O}'_jf^\delta)^\dagger = (-\overline{\nu}^\beta\gamma^0\mathcal{O}_j^\dagger\gamma^0\nu^\alpha)(-\overline{f}^\delta\gamma^0\mathcal{O}_j'^\dagger\gamma^0f^\gamma)\,, \tag{A.40}$$

and therefore it is useful to determine $\gamma^0\mathcal{O}_j^\dagger\gamma^0$ and $\gamma^0\mathcal{O}_j'^\dagger\gamma^0$ in terms of the original operators. The results are shown in Table A.2. Applying these, we find the result

of taking the Lagrangian (A.29) and adding its Hermitian conjugate,

$$\begin{aligned}\mathcal{L} = -\frac{G_F}{\sqrt{2}} \sum_{\alpha,\beta,\gamma,\delta} \Bigg\{ & \sum_{j=1}^{4} \left(\begin{pmatrix} \overset{(\sim)j}{\epsilon} \end{pmatrix}_{\alpha\beta\gamma\delta} + \begin{pmatrix} \overset{(\sim)j}{\epsilon} \end{pmatrix}^*_{\beta\alpha\delta\gamma} \right) \left(\overline{\nu}^\alpha \mathcal{O}_j \nu^\beta\right) \left(\overline{f}^\gamma \mathcal{O}'_j f^\delta\right) \\ & + \left(\epsilon^S_{\alpha\beta\gamma\delta} + \widetilde{\epsilon}^{S*}_{\beta\alpha\delta\gamma}\right) \left(\overline{\nu}^\alpha \mathcal{O}_5 \nu^\beta\right) \left(\overline{f}^\gamma \mathcal{O}'_5 f^\delta\right) \\ & + \left(\widetilde{\epsilon}^S_{\alpha\beta\gamma\delta} + \epsilon^{S*}_{\beta\alpha\delta\gamma}\right) \left(\overline{\nu}^\alpha \mathcal{O}_6 \nu^\beta\right) \left(\overline{f}^\gamma \mathcal{O}'_6 f^\delta\right) \\ & + \left(-\epsilon^P_{\alpha\beta\gamma\delta} + \widetilde{\epsilon}^{P*}_{\beta\alpha\delta\gamma}\right) \left(\overline{\nu}^\alpha \mathcal{O}_7 \nu^\beta\right) \left(\overline{f}^\gamma \mathcal{O}'_7 f^\delta\right) \\ & + \left(-\widetilde{\epsilon}^P_{\alpha\beta\gamma\delta} + \epsilon^{P*}_{\beta\alpha\delta\gamma}\right) \left(\overline{\nu}^\alpha \mathcal{O}_8 \nu^\beta\right) \left(\overline{f}^\gamma \mathcal{O}'_8 f^\delta\right) \\ & + \left(\epsilon^T_{\alpha\beta\gamma\delta} + \widetilde{\epsilon}^{T*}_{\beta\alpha\delta\gamma}\right) \left(\overline{\nu}^\alpha \mathcal{O}_9 \nu^\beta\right) \left(\overline{f}^\gamma \mathcal{O}'_9 f^\delta\right) \\ & + \left(\widetilde{\epsilon}^T_{\alpha\beta\gamma\delta} + \epsilon^{T*}_{\beta\alpha\delta\gamma}\right) \left(\overline{\nu}^\alpha \mathcal{O}_{10} \nu^\beta\right) \left(\overline{f}^\gamma \mathcal{O}'_{10} f^\delta\right) \Bigg\} . \end{aligned} \tag{A.41}$$

From this, the identities in Equation (A.37) follow for redefined coefficients absorbing the Hermitian conjugates. Concerning the number of degrees of freedom we have for one epsilon coefficient with four flavor indices a priori $3^4 = 81$ complex degrees of freedom. For $j = 1, \ldots, 4$ we have $\epsilon_{\alpha\beta\gamma\delta} = \epsilon^*_{\beta\alpha\delta\gamma}$ which means the 9 coefficients which have $\alpha = \beta$ and $\gamma = \delta$ must be real. Of the remaining $81 - 9 = 72$ complex coefficients, half are determined by the other half such that we have to subtract 36 complex degrees of freedom. In total, we hence have 9 real plus 36 complex degrees of freedom, adding up to 81 real degrees of freedom for each ϵ^j with $j = 1, \ldots, 4$. For the S, P, and T coefficients it is simpler because the coefficients with the tilde are completely determined by the ones without, leaving ϵ^S, ϵ^P, and ϵ^T unconstrained which therefore each have 162 real degrees of freedom. In total we arrive at $4 \cdot 81 + 3 \cdot 162 = 810$ real degrees of freedom.

2. **CP invariance:** Under a CP transformation, the Dirac spinors transform according to [35]

$$\psi(x) \quad \xrightarrow{\text{CP}} \quad \gamma^0 \mathcal{C} \overline{\psi}^T(x) = -\mathcal{C}\psi^*(x)\,, \tag{A.42}$$

$$\overline{\psi}(x) \quad \xrightarrow{\text{CP}} \quad -\psi^T(x)\mathcal{C}^\dagger \gamma^0\,, \tag{A.43}$$

where $\mathcal{C}$ was defined in Equation (A.9) and the CP phase is set to one. The five

covariant bilinears transform as

$$\begin{aligned} V^{\mu}_{ab} = \overline{\psi}_a \gamma^{\mu} \psi_b \quad &\xrightarrow{\text{CP}} \quad -\overline{\psi}_b \gamma_{\mu} \psi_a \,, \\ A^{\mu}_{ab} = \overline{\psi}_a \gamma^{\mu} \gamma^5 \psi_b \quad &\xrightarrow{\text{CP}} \quad -\overline{\psi}_b \gamma_{\mu} \gamma^5 \psi_a \,, \\ S_{ab} = \overline{\psi}_a \psi_b \quad &\xrightarrow{\text{CP}} \quad +\overline{\psi}_b \psi_a \,, \\ P_{ab} = \overline{\psi}_a \gamma^5 \psi_b \quad &\xrightarrow{\text{CP}} \quad -\overline{\psi}_b \gamma^5 \psi_a \,, \\ T^{\mu\nu}_{ab} = \overline{\psi}_a \sigma^{\mu\nu} \psi_b \quad &\xrightarrow{\text{CP}} \quad -\overline{\psi}_b \sigma_{\mu\nu} \psi_a \,, \end{aligned} \tag{A.44}$$

where the lowering of indices indicates a change of sign of the spatial components. Let us express the Lagrangian in Equation (A.29) in terms of these bilinears to make use of these relations. For $j = 1, \ldots, 4$ the epsilon coefficients are contracted with

$$g_{\mu\nu} \left(V^{\mu}_{ab} \pm A^{\mu}_{ab}\right) \left(V^{\nu}_{cd} \pm A^{\nu}_{cd}\right) \quad \xrightarrow{\text{CP}} \quad g_{\mu\nu} \left(V^{\mu}_{ba} \pm A^{\mu}_{ba}\right) \left(V^{\nu}_{dc} \pm A^{\nu}_{dc}\right) \,, \tag{A.45}$$

where the left and right $\pm$ are independent of each other. Therefore $\epsilon_{\alpha\beta\gamma\delta} = \epsilon_{\beta\alpha\delta\gamma}$ which combined with (A.37) implies realness. For $j = 5, \ldots, 8$, we have

$$\left(S_{ab} \pm P_{ab}\right) S_{cd} \quad \xrightarrow{\text{CP}} \quad \left(S_{ba} \mp P_{ba}\right) S_{dc} \,, \tag{A.46}$$

$$\left(S_{ab} \pm P_{ab}\right) P_{cd} \quad \xrightarrow{\text{CP}} \quad -\left(S_{ba} \mp P_{ba}\right) P_{dc} \,, \tag{A.47}$$

and therefore $\epsilon^{S}_{\alpha\beta\gamma\delta} = \widetilde{\epsilon}^{S}_{\beta\alpha\delta\gamma} = \epsilon^{S*}_{\alpha\beta\gamma\delta}$ and $\epsilon^{P}_{\alpha\beta\gamma\delta} = -\widetilde{\epsilon}^{P}_{\beta\alpha\delta\gamma} = \epsilon^{P*}_{\alpha\beta\gamma\delta}$, using again (A.37). For the Tensor coefficients, we define

$$\widetilde{T}^{\mu\nu}_{ab} = \overline{\psi}_a \sigma^{\mu\nu} \gamma^5 \psi_b \quad \xrightarrow{\text{CP}} \quad \overline{\psi}_b \sigma_{\mu\nu} \gamma^5 \psi_a \tag{A.48}$$

to obtain

$$\left(T^{\mu\nu}_{ab} \pm \widetilde{T}^{\mu\nu}_{ab}\right) \left(T_{cd,\mu\nu} \pm \widetilde{T}_{cd,\mu\nu}\right) \quad \xrightarrow{\text{CP}} \quad \left(T^{\mu\nu}_{ba} \mp \widetilde{T}^{\mu\nu}_{ba}\right) \left(T_{dc,\mu\nu} \mp \widetilde{T}_{dc,\mu\nu}\right) \,, \tag{A.49}$$

such that $\epsilon^{T}_{\alpha\beta\gamma\delta} = \widetilde{\epsilon}^{T}_{\beta\alpha\delta\gamma} = \epsilon^{T*}_{\alpha\beta\gamma\delta}$ implying again realness. Counting degrees of freedom of the epsilon coefficients with $j = 1, \ldots, 4$, we had in the general case 36 complex entries and 9 real entries. Accordingly, from our CP invariance constraint we have now 36 real plus 9 real entries totaling 45. For the S, P, and T coefficients the previously 81 complex degrees of freedom reduce to 81 real degrees of freedom. In total we hence have $4 \cdot 45 + 3 \cdot 81 = 423$ real parameters.

3. **Majorana neutrinos:** Using Equation (A.34), we conclude that since S and P bilinears are all symmetric, while T bilinears are antisymmetric, so must be their epsilon coefficients. For V and A it is slightly more intricate. We have

$$\left(V^{\mu}_{\alpha\beta} \pm A^{\mu}_{\alpha\beta}\right) = -\left(V^{\mu}_{\beta\alpha} \mp A^{\mu}_{\beta\alpha}\right) \,, \tag{A.50}$$

such that the identities in Equation (A.39) follow. Turning to the degrees of freedom we note that compared to the general case the L and R coefficients with a tilde are

now completely determined by the ones without. Therefore, only half of the $4 \cdot 81$ real degrees of freedom for $j = 1, \ldots, 4$ are independent. The symmetry of the S and P coefficients in the first two entries render 3 of the 9 index configurations of $\alpha\beta$ dependent of the others, while leaving the $\gamma\delta$ index configurations unaffected. Therefore instead of $9 \cdot 9$ complex degrees of freedom in the Majorana case one has $6 \cdot 9 = 54$ complex degrees of freedom for S and P each. In the tensor case, the antisymmetry implies that entries diagonal in $\alpha\beta$ have to vanish, while 3 of the remaining 6 six configurations depend on the others. Hence, one only has $3 \cdot 9 = 27$ complex degrees of freedom. In terms of total real degrees of freedom in the Majorana case, we conclude that it is $2 \cdot 81 + 2 \cdot 2 \cdot 54 + 2 \cdot 27 = 432$.

4. **Majorana neutrinos + CP invariance:** The number of degrees of freedom can be counted starting from the Majorana case, where we have identified coefficients with $j = 1, \ldots, 4$ to have $2 \cdot (36\,\text{complex} + 9\,\text{real})$ degrees of freedom, those with $j = 5, \ldots, 8$ have $2 \cdot 54$ complex degrees of freedom, and those with $j = 9, 10$ have 27 complex degrees of freedom. Combining this with the CP requirement that all of them become real, we just reduce all complex degrees of freedom to real degrees of freedom and obtain in total $2 \cdot 45 + 2 \cdot 54 + 27 = 225$.

B. Matching of models to SMNEFT

B.1. Matching from leptoquarks onto SMNEFT operators

Here we derive the SMNEFT four-fermion operator coefficients shown in Table 2.1 obtained by integrating out the leptoquarks whose interactions are described by Equations (3.36) and (3.37). We assume for simplicity that all leptoquark masses are equal and identify the mass with the EFT scale Λ. Replacements for the case of unequal masses are immediate. First we note that each scalar propagator appears in the Feynman rules as

$$G_X^{(ab)}(p) = \frac{i(\delta_{ab})}{p^2 - m_X^2 + i\epsilon} \approx -\frac{i}{m_X^2}(\delta_{ab})\,, \tag{B.1}$$

where we used $p^2 \ll m_X^2$ and δ_{ab} stands symbolically for $\mathrm{SU}(3)_C$ and $\mathrm{SU}(2)_L$ color indices. The couplings in Equations (3.36) and (3.37) appear each with a prefactor of $(-i)$ in the Feynman rules. We therefore get, from integrating out X, an effective vertex factor

$$(-i)^2 G_X^{(ab)}(p) \approx (-i)\left(-\frac{1}{m_X^2}\right)(\delta_{ab})\,. \tag{B.2}$$

This leaves us with the following effective Lagrangians from scalar leptoquarks

$$\begin{aligned}
\mathcal{L}_{S_1} =& -\left(|s_{1L}|^2\ \bar{\widetilde{q}}\, l\ \bar{l}\widetilde{q} + |s_{1e}|^2\ \overline{u_R^c} e_R\, \overline{e_R} u_R^c + |s_{1N}|^2\ \overline{d_R^c} N\, \overline{N} d_R^c\right) \\
& -\left(s_{1L} s_{1e}^*\ \bar{\widetilde{q}}\, l\, \overline{e_R} u_R^c + s_{1L} s_{1N}^*\ \bar{\widetilde{q}}\, l\, \overline{N} d_R^c + s_{1e} s_{1N}^*\ \overline{u_R^c} e_R\, \overline{N} d_R^c + \text{H.c.}\right), && \text{(B.3)} \\
\mathcal{L}_{S_1'} =& -|s_1'|^2\ \overline{d_R^c} e_R\ \overline{e_R} d_R^c\,, && \text{(B.4)} \\
\mathcal{L}_{S_1''} =& -|s_1''|^2\ \overline{u_R^c} N\ \overline{N} u_R^c\,, && \text{(B.5)} \\
\mathcal{L}_{S_3} =& -|s_3|^2\ \bar{\widetilde{q}}\, \tau_a l\ \bar{l} \tau_a \widetilde{q}\,, && \text{(B.6)} \\
\mathcal{L}_{R_2} =& -\left(|r_{2R}|^2\ \bar{q}\, e_R\ \overline{e_R} q + |r_{2L}|^2\ \overline{u_R} l^a \bar{l}^a u_R\right) + \left(r_{2R} r_{2L}^*\ \bar{q}^a\, e_R\, (i\tau_2)_{ba} \bar{l}^b u_R + \text{H.c.}\right), && \text{(B.7)} \\
\mathcal{L}_{R_2'} =& -\left(|r_{2R}'|^2\ \bar{q} N\ \overline{N} q + |r_{2L}'|^2\ \overline{d_R} l^a\ \bar{l}^a d_R\right) + \left(r_{2R}' r_{2L}'^*\ \bar{q}^a\, N\, (i\tau_2)_{ba} \bar{l}^b d_R + \text{H.c.}\right), && \text{(B.8)}
\end{aligned}$$

where we absorbed a factor of Λ^{-1} in each coupling constant for brevity and introduced the notation of a quark doublet dual $\widetilde{q} = (i\tau_2) q^c$ in analogy to the Higgs dual $\widetilde{H}$. This ensures that $\widetilde{q}$ transforms like q under $\mathrm{SU}(2)_L$. Concerning the flavor structure we have ordered the fermion bilinears such that the first bilinear carries the flavors of the unconjugated coupling and the second bilinear carries the flavor of the conjugated coupling,

i.e.

$$\mathcal{L}_{S_1'} = -(s_1')_{\alpha\beta}(s_1')^*_{\gamma\delta}\ \overline{d^c_{R\alpha}} e_{R\beta}\ \overline{e_{R\delta}} d^c_{R\gamma}\,. \tag{B.9}$$

Let us turn to the vector leptoquarks. Their propagator appears in the Feynman rules as

$$G^{(ab)}_{Y,\mu\nu}(p) = i(\delta_{ab})\frac{-g_{\mu\nu} + \frac{p_\mu p_\nu}{m_Y^2}}{p^2 - m_Y^2 + i\epsilon} \approx \frac{i}{m_X^2} g_{\mu\nu}(\delta_{ab})\,. \tag{B.10}$$

Again, with the coupling prefactors of $(-i)$ the approximated propagator implies an effective vertex factor

$$(-i)^2 G^{(ab)}_{Y,\mu\nu}(p) \approx (-i)\frac{g_{\mu\nu}}{m_Y^2}(\delta_{ab})\,. \tag{B.11}$$

This leads us to the following effective Lagrangians

$$\begin{aligned}
\mathcal{L}_{V_2} =& \Big(|v_{2R}|^2\ \overline{q^c}\gamma_\mu e_R\ \overline{e_R}\gamma^\mu q^c + |v_{2L}|^2\ \overline{d^c_R}\gamma_\mu l^a\ \bar{l}^a\gamma^\mu d^c_R\Big) \\
&+ \Big(v_{2R}v^*_{2L}\ \overline{q^c}^a\gamma_\mu e_R\ \bar{l}^a\gamma^\mu d^c_R + \text{H.c.}\Big)\,, \qquad \text{(B.12)}\\
\mathcal{L}_{V_2'} =& \Big(|v'_{2R}|^2\ \overline{q^c}\gamma_\mu N\ \overline{N}\gamma^\mu q^c + |v'_{2L}|^2\ \overline{u^c_R}\gamma_\mu l^a\ \bar{l}^a\gamma^\mu u^c_R\Big) \\
&+ \Big(v'_{2R}v'^*_{2L}\ \overline{q^c}^a\gamma_\mu N\ \bar{l}^a\gamma^\mu u^c_R + \text{H.c.}\Big)\,, \qquad \text{(B.13)}\\
\mathcal{L}_{U_1} =& \big(|u_{1L}|^2\ \bar{q}\gamma_\mu l\ \bar{l}\gamma^\mu q + |u_{1e}|^2\ \overline{d_R}\gamma_\mu e_R\ \overline{e_R}\gamma^\mu d_R + |u_{1N}|^2\ \overline{u_R}\gamma_\mu N\ \overline{N}\gamma^\mu u_R\big) \\
&+ \big(u_{1L}u^*_{1e}\ \bar{q}\gamma_\mu l\ \overline{e_R}\gamma^\mu d_R + u_{1L}u^*_{1N}\ \bar{q}\gamma_\mu l\ \overline{N}\gamma^\mu u_R \qquad \text{(B.14)}\\
&\quad + u_{1e}u^*_{1N}\ \overline{d_R}\gamma_\mu e_R\ \overline{N}\gamma^\mu u_R + \text{H.c.}\big)\,, \\
\mathcal{L}_{U_1'} =& |u_1'|^2\ \overline{u_R}\gamma_\mu e_R\ \overline{e_R}\gamma^\mu u_R\,, \qquad \text{(B.15)}\\
\mathcal{L}_{U_1''} =& |u_1''|^2\ \overline{d_R}\gamma_\mu N\ \overline{N}\gamma^\mu d_R\,, \qquad \text{(B.16)}\\
\mathcal{L}_{U_3} =& |u_3|^2\ \bar{q}\,\vec{\tau}\gamma_\mu\, l\ \bar{l}\vec{\tau}\gamma^\mu q\,, \qquad \text{(B.17)}
\end{aligned}$$

where we again absorbed a factor of Λ^{-1} in each coupling and the bilinears are ordered such that the first one corresponds to the unconjugated coupling and second one corresponds to the conjugated coupling.

To get from these expressions to the SMNEFT operators, the remaining step is to apply Fierz transformations and subsequently use the following useful identities

$$\overline{\psi_1^c}\gamma_\mu\psi_2^c = -\overline{\psi_2}\gamma_\mu\psi_1\,, \tag{B.18}$$

$$\overline{\psi_1^c}\psi_2^c = \overline{\psi_2}\psi_1\,, \tag{B.19}$$

$$\widetilde{\bar{\psi}} = \overline{\psi^c}(-i\tau_2)\,, \tag{B.20}$$

to remove the particle-antiparticle conjugation symbols. The resulting Wilson coefficients are shown in Table 3.2.

B.2. Tree-level matching of the minimal charged Higgs model

Here we show that integrating out ϕ from the Lagrangian (3.61) leads to the set of SMNEFT Wilson coefficients given in Equation (3.64). When integrating out ϕ, we

obtain the effective Lagrangian

$$\begin{aligned}\mathcal{L}_{\text{eff}} &= \sum_{\alpha,\gamma}\sum_{\beta>\alpha,\,\delta>\gamma} -\frac{1}{m_\phi^2}\left(y_{\alpha\beta}\overline{\widetilde{l}_\alpha} l_\beta + y_{\beta\alpha}\overline{\widetilde{l}_\beta} l_\alpha\right)\left(y^*_{\gamma\delta}\bar{l}_\delta\widetilde{l}_\gamma + y^*_{\delta\gamma}\bar{l}_\gamma\widetilde{l}_\delta\right) \\ &= \sum_{\alpha,\gamma}\sum_{\beta>\alpha,\,\delta>\gamma} -\frac{1}{m_\phi^2}\left(y_{\alpha\beta} - y_{\beta\alpha}\right)\overline{\widetilde{l}_\alpha} l_\beta\,\left(y^*_{\gamma\delta} - y^*_{\delta\gamma}\right)\bar{l}_\delta\widetilde{l}_\gamma \\ &= \sum_{\alpha,\gamma}\sum_{\beta>\alpha,\,\delta>\gamma} -\frac{4y_{\alpha\beta}y^*_{\gamma\delta}}{m_\phi^2}\overline{\widetilde{l}_\alpha} l_\beta\,\bar{l}_\delta\widetilde{l}_\gamma\,,\end{aligned} \tag{B.21}$$

where we used the definition $\widetilde{l} = (-i\tau_2)l^c$. Now we can write a single addend with explicit $\mathrm{SU}(2)_L$ indices a, b and subsequently apply the Fierz transformation (A.26) and Equation (B.18) to find

$$\begin{aligned}-\frac{4y_{\alpha\beta}y^*_{\gamma\delta}}{m_\phi^2}(\overline{\widetilde{l}^a_\alpha} l^a_\beta)\,(\bar{l}^b_\delta\widetilde{l}^b_\gamma) &= \frac{4y_{\alpha\beta}y^*_{\gamma\delta}}{2m_\phi^2}(\overline{\widetilde{l}^a_\alpha}\gamma_\mu\widetilde{l}^b_\gamma)\,(\bar{l}^b_\delta\gamma^\mu l^a_\beta) \\ &= \frac{2y_{\alpha\beta}y^*_{\gamma\delta}}{m_\phi^2}(i\tau_2)_{ia}(-i\tau_2)_{bj}(\overline{(l^c_\alpha)^i}\gamma_\mu(l^c_\gamma)^j)\,(\bar{l}^b_\delta\gamma^\mu l^a_\beta) \\ &= -\frac{2y_{\alpha\beta}y^*_{\gamma\delta}}{m_\phi^2}\epsilon_{ia}\epsilon_{jb}(\overline{l^j_\gamma}\gamma_\mu l^i_\alpha)\,(\bar{l}^b_\delta\gamma^\mu l^a_\beta)\,.\end{aligned} \tag{B.22}$$

Therefore we have

$$\mathcal{L}_{\text{eff}} = \sum_{\alpha,\gamma}\sum_{\beta>\alpha,\,\delta>\gamma} -\frac{2y_{\alpha\beta}y^*_{\gamma\delta}}{m_\phi^2}\epsilon_{ia}\epsilon_{jb}(\overline{l^j_\gamma}\gamma_\mu l^i_\alpha)\,(\bar{l}^b_\delta\gamma^\mu l^a_\beta)\,. \tag{B.23}$$

The contraction with the antisymmetric tensors avoids a direct identification with a single $\mathcal{O}_{ll}^{\alpha'\beta'\gamma'\delta'}$ from Table 2.1. However, we note that the sum of two such operators with different flavor indices precisely yields the structure in Equation (B.23). Namely,

$$\begin{aligned}&\mathcal{O}_{ll}^{\gamma\beta\delta\alpha} - \mathcal{O}_{ll}^{\gamma\alpha\delta\beta} \\ &= (\overline{l^1_\gamma}\gamma_\mu l^1_\alpha)\,(\bar{l}^1_\delta\gamma^\mu l^1_\beta) + (\overline{l^2_\gamma}\gamma_\mu l^2_\alpha)\,(\bar{l}^2_\delta\gamma^\mu l^2_\beta) + (\overline{l^1_\gamma}\gamma_\mu l^1_\alpha)\,(\bar{l}^2_\delta\gamma^\mu l^2_\beta) + (\overline{l^2_\gamma}\gamma_\mu l^2_\alpha)\,(\bar{l}^1_\delta\gamma^\mu l^1_\beta) \\ &\quad - (\overline{l^1_\gamma}\gamma_\mu l^1_\beta)\,(\bar{l}^1_\delta\gamma^\mu l^1_\alpha) - (\overline{l^2_\gamma}\gamma_\mu l^2_\beta)\,(\bar{l}^2_\delta\gamma^\mu l^2_\alpha) - (\overline{l^1_\gamma}\gamma_\mu l^1_\beta)\,(\bar{l}^2_\delta\gamma^\mu l^2_\alpha) - (\overline{l^2_\gamma}\gamma_\mu l^2_\beta)\,(\bar{l}^1_\delta\gamma^\mu l^1_\alpha) \\ &= (\overline{l^1_\gamma}\gamma_\mu l^1_\alpha)\,(\bar{l}^2_\delta\gamma^\mu l^2_\beta) + (\overline{l^2_\gamma}\gamma_\mu l^2_\alpha)\,(\bar{l}^1_\delta\gamma^\mu l^1_\beta) - (\overline{l^1_\gamma}\gamma_\mu l^2_\beta)\,(\bar{l}^2_\delta\gamma^\mu l^1_\alpha) - (\overline{l^2_\gamma}\gamma_\mu l^1_\beta)\,(\bar{l}^1_\delta\gamma^\mu l^2_\alpha) \\ &= \epsilon_{ia}\epsilon_{jb}(\overline{l^j_\gamma}\gamma_\mu l^i_\alpha)\,(\bar{l}^b_\delta\gamma^\mu l^i_\beta)\,,\end{aligned} \tag{B.24}$$

where the first two terms of the second and third row cancel each other after applying the Fierz transformation (A.27). Defining

$$K^{\alpha\beta\gamma\delta} = -2y_{\beta\delta}y^*_{\alpha\gamma}\,, \tag{B.25}$$

we conclude

$$\mathcal{L}_{\text{eff}} = \sum_{\alpha,\delta}\sum_{\beta>\delta,\,\gamma>\alpha}\frac{K^{\alpha\beta\gamma\delta}}{m_\phi^2}(\mathcal{O}_{ll}^{\alpha\beta\gamma\delta} - \mathcal{O}_{ll}^{\alpha\delta\gamma\beta})\,, \tag{B.26}$$

such that

$$C_{ll}^{\alpha\beta\gamma\delta} = -C_{ll}^{\alpha\delta\gamma\beta} = K^{\alpha\beta\gamma\delta}\,. \tag{B.27}$$

C. Details of neutrino-electron scattering

C.1. Differential cross section

The differential cross sections of neutrino-electron scattering in the presence of GNI described by the effective Lagrangian Equation (2.11) can be derived as follows. We consider all neutrinos to be massless, such that their helicity coincides with their chirality. For the neutrino channel, the Feynman-rule quantity associated with an incoming massless neutrino of flavor α is $u_-(p_\nu)$ while the outgoing neutrino of flavor β can have any helicity s and is associated with $\overline{u_s}(k_\nu)$. For the antineutrino channel, the Feynman-rule quantity associated with an incoming massless antineutrino of flavor α is $\overline{v_+}(p_\nu)$ while the outgoing antineutrino of flavor β is associated with $v_s(k_\nu)$. Therefore, the amplitudes of the scattering $\nu_\alpha e_r \to \nu_{\beta,s} + e_{r'}$, and $\overline{\nu}_\alpha e_r \to \nu_{\beta,s} + e_{r'}$ read

$$\mathcal{A}^{srr'}_{\alpha\beta} = \frac{G_F}{\sqrt{2}} \sum_{j=1,3,5,7,9} \epsilon^{\alpha\beta ee}_{j,e} \left(\overline{u_s}(k_\nu)\mathcal{O}_j u_-(p_\nu)\right) \left(\overline{u_{r'}}(k_e)\mathcal{O}'_j u_r(p_e)\right), \tag{C.1}$$

$$\mathcal{A}^{srr'}_{\overline{\alpha}\overline{\beta}} = \frac{G_F}{\sqrt{2}} \sum_{j=1,3,6,8,10} \epsilon^{\beta\alpha ee}_{j,e} \left(\overline{v_+}(p_\nu)\mathcal{O}_j v_s(k_\nu)\right) \left(\overline{u_{r'}}(k_e)\mathcal{O}'_j u_r(p_e)\right), \tag{C.2}$$

where s, r, and r' denote helicities. The projection operators contained in the definition of $\mathcal{O}_j$ in Table 2.4 cancel half of the contributions. For instance, $\mathcal{O}_j$ with $j = 2, 4, 6, 8, 10$ contain right-handed projection operators acting on a left-handed neutrino in the first amplitude. The scattering amplitudes, averaging over initial electron helicities and summing over final state helicities are then given by

$$|\mathcal{A}_{\nu_\alpha e\to\nu_\beta e}|^2 = \frac{1}{2}\sum_{s,r,r'} |\mathcal{A}^{srr'}_{\alpha\beta}|^2, \tag{C.3}$$

$$|\mathcal{A}_{\overline{\nu}_\alpha e\to\overline{\nu}_\beta e}|^2 = \frac{1}{2}\sum_{s,r,r'} |\mathcal{A}^{srr'}_{\overline{\alpha}\overline{\beta}}|^2. \tag{C.4}$$

Since we have removed operators projecting incoming (anti)neutrinos on the wrong helicity in the definitions of the amplitudes, it is conveniently possible to sum also over initial neutrino helicities to apply the usual Dirac matrix trace identities. Finally, the differential cross sections are given by

$$\frac{\mathrm{d}\sigma}{\mathrm{d}T} = \frac{|\mathcal{A}|^2}{32\pi m_e E_\nu^2}. \tag{C.5}$$

To arrive at the final form of the cross section in Equation (4.58), we have to apply Equation (2.13) in order to replace any of the $\epsilon^{\beta\alpha ee}$ in the antineutrino scattering cross section by $(\epsilon^{\alpha\beta ee})^*$.

C.2. Adapting the existing bounds on neutrino-electron scattering

To adapt the bounds on GNI from neutrino-electron scattering calculated in Reference [52], we must first compare the cross section results. In this reference, only flavor-diagonal interactions are assumed and thus the formula for the cross section obtained therein is analogous to Equation (4.58), but with A, B, C, and D having only contributions from flavor-diagonal coefficients. We can identify A, B, C, and D in Reference [52] with $2A$, $2B$, $2C$ and $2D$ in Equation (4.59) after summing over final flavors β. The factor of 2 is a result of the differing prefactor in Equation (4.58) compared to Equations 9 and 10 in Reference [52]. It is then straightforward to arrive at the identifications

$$\begin{aligned} 4\sum_{\beta} |\epsilon_L^{\mu\beta}|^2 &= \frac{1}{4}\left(C_A - D_A + C_V - D_V\right)^2, \\ 4\sum_{\beta} |\epsilon_R^{\mu\beta}|^2 &= \frac{1}{4}\left(C_A + D_A - C_V - D_V\right)^2, \end{aligned} \tag{C.6}$$

where the coefficients C and D are simply the flavor-diagonal Lee-Yang parameters as presented in Appendix A.4. Separating the SM and BSM contributions to these parameters leads to the identities

$$\begin{aligned} (g_L + \epsilon_{L,\mathrm{NSI}}^{\mu\mu})^2 + \sum_{\beta=e,\tau} |\epsilon_{L,\mathrm{NSI}}^{\mu\beta}|^2 &= \left(g_L + \frac{1}{4}(C_A^{\mathrm{NSI}} - D_A^{\mathrm{NSI}} + C_V^{\mathrm{NSI}} - D_V^{\mathrm{NSI}})\right)^2, \\ (g_R + \epsilon_{R,\mathrm{NSI}}^{\mu\mu})^2 + \sum_{\beta=e,\tau} |\epsilon_{R,\mathrm{NSI}}^{\mu\beta}|^2 &= \left(g_R - \frac{1}{4}(C_A^{\mathrm{NSI}} + D_A^{\mathrm{NSI}} - C_V^{\mathrm{NSI}} - D_V^{\mathrm{NSI}})\right)^2. \end{aligned} \tag{C.7}$$

This allows us to transfer constraints on C or D parameters into constraints on $\epsilon_{L,\mathrm{NSI}}$ assuming only one to be non-vanishing at a time. Therefore, for the bound on $\epsilon_{L,\mathrm{NSI}}^{\mu\mu}$, $\epsilon_{R,\mathrm{NSI}}^{\mu\mu}$ we may use

$$\epsilon_{X,\mathrm{NSI}}^{\mu\mu} = 1/4 C_V^{\mathrm{NSI}} \in [-0.06, 0.02], \tag{C.8}$$

for $X = L, R$. Note that we always state bounds at 90% CL in this section. For the off-diagonal parameters the (equal) bounds on C_A^{NSI} and D_V^{NSI} are relevant,

$$|\epsilon_{X,\mathrm{NSI}}^{\mu}| = \sqrt{-\frac{1}{2}|g_X| C_A^{\mathrm{NSI}} + \frac{1}{16}(C_A^{\mathrm{NSI}})^2} \leq \begin{cases} 0.11 & \text{for } X = L, \\ 0.10 & \text{for } X = R, \end{cases} \tag{C.9}$$

where we take the bound on negative C_A^{NSI}, as it provides the strongest constraint. The (pseudo)scalar and tensor interactions are extracted analogously and we do not have to

consider a flavor-diagonal SM contribution, which simplifies the procedure. Using the definitions of Appendix A.4, we simply have

$$\begin{aligned} |\epsilon_S^\mu| &= \frac{1}{2}\sqrt{C_S^2 + D_P^2} \leq 0.4\,, \qquad |\epsilon_P^\mu| = \frac{1}{2}\sqrt{C_P^2 + D_S^2} \leq 0.4\,, \\ |\epsilon_T^\mu| &= \frac{1}{4}\sqrt{C_T^2 + D_T^2} \leq 0.04\,. \end{aligned} \tag{C.10}$$

Turning to the scattering of an electron neutrino instead of a muon neutrino, we have to account for the additional contribution from W boson exchange. Hence, the identification for the NSI reads

$$\begin{aligned} (g_L + 1 + \epsilon_{L,\mathrm{NSI}}^{ee})^2 + \sum_{\beta=\mu,\tau} |\epsilon_{L,\mathrm{NSI}}^{e\beta}|^2 &= \left(g_L + 1 + \frac{1}{4}(C_A^{\mathrm{NSI}} - D_A^{\mathrm{NSI}} + C_V^{\mathrm{NSI}} - D_V^{\mathrm{NSI}})\right)^2, \\ (g_R + \epsilon_{R,\mathrm{NSI}}^{ee})^2 + \sum_{\beta=\mu,\tau} |\epsilon_{R,\mathrm{NSI}}^{e\beta}|^2 &= \left(g_R - \frac{1}{4}(C_A^{\mathrm{NSI}} + D_A^{\mathrm{NSI}} - C_V^{\mathrm{NSI}} - D_V^{\mathrm{NSI}})\right)^2. \end{aligned} \tag{C.11}$$

Adapting from Reference [52] the bounds on individual Lee-Yang coefficients (and neglecting the minima not centered around zero), we find, in the notation of Equation (2.11),

$$\begin{aligned} \epsilon_{L,e}^{eeee} &\in [-0.31, 0.24]\,, \quad |\epsilon_{L,e}^{e\mu ee}|, |\epsilon_{L,e}^{e\tau ee}| \leq 0.27\,, \quad |\epsilon_{S,e}^{e\beta ee}| \leq 0.6\,, \quad |\epsilon_{T,e}^{e\beta ee}| \leq 0.08\,, \\ \epsilon_{R,e}^{eeee} &\in [-0.24, 0.31]\,, \quad |\epsilon_{R,e}^{e\mu ee}|, |\epsilon_{R,e}^{e\tau ee}| \leq 0.16\,, \quad |\epsilon_{P,e}^{e\beta ee}| \leq 0.7\,, \end{aligned} \tag{C.12}$$

at 90% CL, where $\beta = e, \mu, \tau$. For completeness, we also state the bounds on GNI of muon neutrinos from Equations (C.8)-(C.10) in the notation of Equation (2.11),

$$\begin{aligned} \epsilon_{L,e}^{\mu\mu ee} &\in [-0.06, 0.02]\,, \quad |\epsilon_{L,e}^{e\mu ee}|, |\epsilon_{L,e}^{\mu\tau ee}| \leq 0.11\,, \quad |\epsilon_{S,e}^{\mu\beta ee}| \leq 0.4\,, \quad |\epsilon_{T,e}^{\mu\beta ee}| \leq 0.04\,, \\ \epsilon_{R,e}^{\mu\mu ee} &\in [-0.06, 0.02]\,, \quad |\epsilon_{R,e}^{e\mu ee}|, |\epsilon_{R,e}^{\mu\tau ee}| \leq 0.10\,, \quad |\epsilon_{P,e}^{\mu\beta ee}| \leq 0.4\,, \end{aligned} \tag{C.13}$$

at 90% CL, where $\beta = e, \mu, \tau$. In Section 4.2, we noted that NSI constraints from CHARM-II were also calculated in Reference [126]. For comparison, we quote the results from this reference here,

$$\begin{aligned} |\epsilon_{L,e}^{\mu\mu ee}| &\leq 0.03\,, \qquad |\epsilon_{L,e}^{e\mu ee}|, \leq 0.13\,, \qquad |\epsilon_{L,e}^{\mu\tau ee}| \leq 0.1\,, \\ |\epsilon_{R,e}^{\mu\mu ee}| &\leq 0.03\,, \qquad |\epsilon_{R,e}^{e\mu ee}|, \leq 0.13\,, \qquad |\epsilon_{R,e}^{\mu\tau ee}| \leq 0.1\,. \end{aligned} \tag{C.14}$$

D. Details of neutrino mass experiments

D.1. Decay rate of tritium at leading order

In this section, we outline the derivation of the tritium decay rate at leading order including GNI and a sterile neutrino. To this end, we first have to reparametrize the effective Lagrangian. Subsequently, we give expressions for the differential decay rate in general and at leading-order.

D.1.1. Reparametrization of the effective Lagrangian

We consider the charged-current GNI Lagrangian (2.12) with four massive neutrinos ν_k and including the SM contribution to $j = 1$,

$$\mathcal{L}_{\text{eff}} = -\frac{G_F V_{ud}}{\sqrt{2}} \sum_{k=1}^{n_\nu} \sum_{j=1}^{10} \left(\delta_{1j}\, U_{ek} + {}^{(\sim)k}\epsilon_j \right) \left(\overline{e}\mathcal{O}_j \nu_k\right) \left(\overline{u}\mathcal{O}'_j d\right) + \text{H.c.}\,, \tag{D.1}$$

where U denotes the extended PMNS matrix. The coefficients $\epsilon_j^k, \widetilde{\epsilon}_j^k$ are defined in the neutrino mass basis, in contrast to Equation (2.12). Notice how we recover, for $U_{e4} = 0$ and in the absence of epsilon coefficients, the usual W-mediated charged-current interaction

$$\mathcal{L}_{\text{SM}} = -\frac{G_F V_{ud}}{\sqrt{2}} \left(\overline{e}(\mathbb{1} - \gamma^5)\nu_e\right) \left(\overline{u}(\mathbb{1} - \gamma^5)d\right) + \text{H.c.}\,, \tag{D.2}$$

due to

$$|\nu_e\rangle = \sum_k U_{ek}\, |\nu_k\rangle\,. \tag{D.3}$$

If we consider a sterile neutrino with $k = 4$, we know that the mixing matrix entry U_{e4} must be very small for a mass in the kinematically accessible range of nuclear beta decays. Therefore, to search for first signs of new physics it is reasonable to work only to leading order in small parameters $\epsilon, U_{\alpha 4}$ at the Lagrangian level. For simplicity, we introduce the symbol ω to denote the order of a given expression in any small parameters. For instance, expressions proportional to ϵ^2, $U_{\alpha 4}^2$, or $\epsilon\, U_{\alpha 4}$ are of order ω^2. As discussed in Section 1.2.2, the measured splittings between the mostly active neutrino mass eigenstates are at the level $\Delta m^2_{21} \approx 7 \times 10^{-5}\,\text{eV}^2$ and $\Delta m^2_{3\ell} \approx 2 \times 10^{-3}\,\text{eV}^2$. Hence, they cannot be resolved at KATRIN and it is convenient to consider the new interactions of the active neutrinos

in the electron flavor basis (as in Equation (2.12)), such that

$$\begin{aligned}\mathcal{L}_{\text{eff}} = &-\frac{G_F V_{ud}}{\sqrt{2}} \sum_{j=1}^{10} \left(\delta_{1j} \sqrt{1-|U_{e4}|^2} + \overset{(\sim)}{\epsilon}_j \right) (\bar{e}\mathcal{O}_j \nu_e) \left(\bar{u}\mathcal{O}'_j d\right) \\ &- \frac{G_F V_{ud}}{\sqrt{2}} \sum_{j=1}^{10} \left(\delta_{1j} U_{e4} + \overset{(\sim)N}{\epsilon}_j \right) (\bar{e}\mathcal{O}_j N) \left(\bar{u}\mathcal{O}'_j d\right) + \text{H.c.}\,,\end{aligned} \tag{D.4}$$

where $N = \nu_4$ denotes the sterile neutrino. For the electron neutrino we use the effective neutrino mass

$$m_\beta^2 = \sum_{k=1}^{3} \frac{|U_{ek}|^2}{1-|U_{e4}|^2} m_k^2\,, \tag{D.5}$$

while the sterile neutrino mass is symbolized by m_N. In Reference [109] it is pointed out that the CKM matrix element V_{ud} is measured through vector like nuclear decays. Therefore the measured value $|\widetilde{V}_{ud}| = 0.97370 \pm 0.00014$ already contains some new physics coefficients. In our case, when we consider that the sterile neutrino could not be resolved in these measurements, we must include all contributions to a vector-like interaction

$$\begin{aligned}|\widetilde{V}_{ud}|^2 &= |V_{ud}|^2 \left(|\sqrt{1-|U_{e4}|^2} + \epsilon_L + \epsilon_R|^2 + |U_{e4} + \epsilon_L^N + \epsilon_R^N|^2 \right) \\ &= |V_{ud}|^2 \left(1 + 2\text{Re}(\epsilon_L + \epsilon_R) + 2\text{Re}(U_{e4}(\epsilon_L^N + \epsilon_R^N)^*) \right. \\ &\qquad \left. + |\epsilon_L + \epsilon_R|^2 + |\epsilon_L^N + \epsilon_R^N|^2 \right) + \mathcal{O}\left(\omega^3\right),\end{aligned} \tag{D.6}$$

where V_{ud} denotes the actual CKM matrix element. Now we use this to rescale the Lagrangian such that the measured $|\widetilde{V}_{ud}|$ is the global prefactor in the following way. The effective couplings in Equation (D.4) can be written as

$$\begin{aligned}&\eta_1 \equiv \sqrt{1-|U_{e4}|^2} + \epsilon_L\,, \qquad && \eta_1^N \equiv U_{e4} + \epsilon_L^N\,, \\ &\eta_j \equiv \epsilon_j\,, && \eta_j^N \equiv \epsilon_j^N \qquad\qquad \text{for } j \geq 2\,.\end{aligned} \tag{D.7}$$

We would like to replace these by reparametrized coefficients $\widehat{\epsilon}_j$ which have a prefactor $\widetilde{V}_{ud}$ instead of V_{ud}. To do this consistently, we note that the decay rate is proportional to products of two effective couplings,

$$\frac{\mathrm{d}\Gamma}{\mathrm{d}E} \sim |V_{ud}|^2 \eta_i \eta_j^* \qquad \text{or} \qquad |V_{ud}|^2 \eta_i^N \eta_j^{N*}\,, \tag{D.8}$$

as shown below. Therefore, we aim to define $\widehat{\epsilon}_j$ such that

$$|V_{ud}|^2 \eta_i \eta_j^* = |\widetilde{V}_{ud}|^2 \widehat{\epsilon}_i \widehat{\epsilon}_j^*\,, \qquad |V_{ud}|^2 \eta_i^N \eta_j^{N*} = |\widetilde{V}_{ud}|^2 \widehat{\epsilon}_i^N \widehat{\epsilon}_j^{N*}\,. \tag{D.9}$$

If we were only interested in the leading order effects of GNI, we could work to linear order in small parameters and use

$$\widetilde{V}_{ud} = V_{ud}(1 + \epsilon_L + \epsilon_R)\,. \tag{D.10}$$

However, since we do not want to neglect the mixing matrix contribution, which contributes to the decay rate at quadratic order, we have to work consistently to quadratic order in small parameters ϵ and $|U_{\alpha 4}|$. Let us collect the products of $\eta_i \eta_j^*$ using Equation (D.6). For $|\eta_1|^2$ we have

$$\begin{aligned} |V_{ud}|^2 |\eta_1|^2 &= |V_{ud}|^2 \left(\sqrt{1-|U_{e4}|^2} + \epsilon_L\right) \left(\sqrt{1-|U_{e4}|^2} + \epsilon_L\right)^* \\ &= |\widetilde{V}_{ud}|^2 (1 - |U_{e4}|^2 - 2\mathrm{Re}\,\epsilon_R + |\epsilon_R|^2 + K) + \mathcal{O}(\omega^3)\,, \end{aligned} \tag{D.11}$$

where

$$K \equiv 2\mathrm{Re}\left(\epsilon_R(\epsilon_L + \epsilon_R)\right) + 2\mathrm{Re}(U_{e4}(\epsilon_L^N + \epsilon_R^N)^*) + |\epsilon_L^N + \epsilon_R^N|^2\,. \tag{D.12}$$

For the other combinations, we find

$$\begin{aligned} |V_{ud}|^2 \eta_1 \eta_j^* &= |V_{ud}|^2 (1+\epsilon_L)\,\epsilon_j^* + \mathcal{O}(\omega^3) \\ &= |\widetilde{V}_{ud}|^2 \epsilon_j^* (1 - \epsilon_L^* - 2\mathrm{Re}(\epsilon_R)) + \mathcal{O}(\omega^3)\,, \\ |V_{ud}|^2 \eta_i \eta_j^* &= |V_{ud}|^2 \epsilon_i \epsilon_j^* \\ &= |\widetilde{V}_{ud}|^2 \epsilon_i \epsilon_j^* + \mathcal{O}(\omega^3)\,, \\ |V_{ud}|^2 |\eta_1^N|^2 &= |V_{ud}|^2 \left|U_{e4} + \epsilon_L^N\right|^2 \\ &= |\widetilde{V}_{ud}|^2 \left|U_{e4} + \epsilon_L^N\right|^2 + \mathcal{O}(\omega^3)\,, \\ |V_{ud}|^2 \eta_1^N \eta_i^{N*} &= |V_{ud}|^2 (U_{e4} + \epsilon_L^N) \epsilon_j^{N*} \\ &= |\widetilde{V}_{ud}|^2 (U_{e4} + \epsilon_L^N) \epsilon_j^{N*} + \mathcal{O}(\omega^3)\,, \\ |V_{ud}|^2 \eta_i^N \eta_j^{N*} &= |V_{ud}|^2 \epsilon_i^N \epsilon_j^{N*} \\ &= |\widetilde{V}_{ud}|^2 \epsilon_i^N \epsilon_j^{N*} + \mathcal{O}(\omega^3)\,, \end{aligned} \tag{D.13}$$

where $i, j \geq 2$ and the tildes on epsilons with odd index have been omitted for simplicity. If we define

$$\begin{aligned} \widehat{\epsilon}_L &= 1 - \epsilon_R - \frac{1}{2}|U_{e4}| - \frac{1}{2}K\,, \\ \widehat{\epsilon}_j &= \epsilon_j (1 - \epsilon_L - \epsilon_R)\,, \qquad\qquad j \geq 2\,, \end{aligned} \tag{D.14}$$

these coefficients obey Equation (D.9), while the coefficients of the sterile neutrino do not need to be redefined. In summary, we can write the final effective Lagrangian as

$$\begin{aligned} \mathcal{L}_{\text{eff}} = &-\frac{G_F \widetilde{V}_{ud}}{\sqrt{2}} \sum_{j=1}^{10} \widehat{\epsilon}_j \left(\overline{e}\mathcal{O}_j \nu_e\right) \left(\overline{u}\mathcal{O}'_j d\right) \\ &- \frac{G_F \widetilde{V}_{ud}}{\sqrt{2}} \sum_{j=1}^{10} \left(\delta_{1j} U_{e4} + \overset{(\sim)N}{\epsilon}_j\right) \left(\overline{e}\mathcal{O}_j N\right) \left(\overline{u}\mathcal{O}'_j d\right) + \text{H.c.} \end{aligned} \tag{D.15}$$

There are two important limits here. In the case of no GNI parameters, one recovers the leading order approximation of the usual Lagrangian for the $3+1$ neutrino scheme,

$$\mathcal{L}_{\text{eff}} = -\frac{G_F V_{ud}}{\sqrt{2}} \left[\left(1 - \frac{1}{2}|U_{e4}|^2\right) \left(\overline{e}\mathcal{O}_1 \nu_e\right) \left(\overline{u}\mathcal{O}'_1 d\right) + \left(U_{e4}\right) \left(\overline{e}\mathcal{O}_1 N\right) \left(\overline{u}\mathcal{O}'_1 d\right)\right] + \text{H.c.} \tag{D.16}$$

If new physics is dominated by GNI coefficients, the leading order active neutrino Lagrangian reads

$$\begin{aligned}\mathcal{L}_{\text{eff}} = &-\frac{G_F V_{ud}}{\sqrt{2}}(1-\epsilon_R)\left(\overline{e}\mathcal{O}_1\nu_e\right)\left(\overline{u}\mathcal{O}_1' d\right) \\ &-\frac{G_F V_{ud}}{\sqrt{2}}\sum_{j=2}^{10}\overset{(\sim)}{\epsilon}_j\ \left(\overline{e}\mathcal{O}_j\nu_e\right)\left(\overline{u}\mathcal{O}_j' d\right),\end{aligned} \tag{D.17}$$

as for instance employed in Reference [109].

D.1.2. The exact decay rate

Let us first revisit the decay kinematics discussed in Reference [57]. It has been argued that the most general form of the matrix element of the decay $A \to B + e^- + \overline{\nu}_k$ in terms of the total relativistic energies of the electron E_{R} and the neutrino E_k, which are the variable quantities of the spectrum, reads

$$|\mathcal{M}|^2 = A + B_1 E_{\text{R}} + B_2 E_k + C E_{\text{R}} E_k + D_1 E_{\text{R}}^2 + D_2 E_k^2 . \tag{D.18}$$

This is true if none of the interaction matrices in Equation (4.82) are momentum-dependent. Therefore, the weak-magnetism term proportional to $\tilde{g}_{T(V)}\sigma_{\mu\nu}q^\nu$ is an exception. This term, however, contributes only at next-to-leading order, as we will see below. Nonetheless it is instructive to include potential momentum-dependent terms for sake of generality at this point. Then the general matrix element can be written as

$$\begin{aligned}|\mathcal{M}|^2 = A + B_1 E_{\text{R}} + B_2 E_k + C E_{\text{R}} E_k + D_1 E_{\text{R}}^2 + D_2 E_k^2 \\ + F_1 E_{\text{R}}^2 E_k + F_2 E_{\text{R}} E_k^2 + G_1 E_{\text{R}}^3 + G_2 E_k^3 .\end{aligned} \tag{D.19}$$

Following the procedure in Reference [57], we perform the integration over E_k. This leads to a straightforward general result of the differential decay rate which reads

$$\begin{aligned}\frac{\mathrm{d}\Gamma_k}{\mathrm{d}E_{\text{R}}} = \frac{Q(E_{\text{R}})}{32\pi^3 m_{\mathcal{A}}} \times \Bigg[&(A + B_1 E_{\text{R}} + D_1 E_{\text{R}}^2 + G_1 E_{\text{R}}^3) + (B_2 + C E_{\text{R}} + F_1 E_{\text{R}}^2) P(E_{\text{R}}) \\ &+ (D_2 + F_2 E_{\text{R}})\left(P^2(E_{\text{R}}) + \frac{1}{3}Q^2(E_{\text{R}})\right) + G_2 P(E_{\text{R}})\left(P^2(E_{\text{R}}) + Q^2(E_{\text{R}})\right)\Bigg] ,\end{aligned} \tag{D.20}$$

with the purely kinematic auxiliary functions [57]

$$\begin{aligned}P(E_{\text{R}}) &\equiv -\frac{(m_A - E_{\text{R}})(E_{\text{R}} m_A - \alpha)}{m_A^2 - 2 m_A E_{\text{R}} + m_e^2} , \\ Q(E_{\text{R}}) &\equiv \frac{|\vec{p}_e|\sqrt{(E_{\text{R}} m_A - \alpha + m_k^2)^2 - m_B^2 m_k^2}}{m_A^2 - 2 m_A E_{\text{R}} + m_e^2} , \\ \alpha &= \frac{1}{2}\left(m_A^2 - m_B^2 + m_e^2 + m_k^2\right) ,\end{aligned} \tag{D.21}$$

where m_A the mass of the parent nucleus, m_B the mass of the daughter nucleus, m_e the electron mass, and m_k the neutrino mass m_β or m_N. The dependence on epsilon parameters resides entirely in the polynomial coefficients of (D.19). They can be calculated exactly using e.g. PACKAGE-X [205] according to the prescription in Reference [57], and thus one finds the exact decay rate given by (D.20). The exact relativistic end-point energy reads

$$E_{\mathrm{R,max}} = \frac{m_A^2 + m_e^2 - (m_B - m_k)^2}{2m_A}\,. \tag{D.22}$$

D.1.3. Expansion in small parameters

The kinematic parameters remaining in the decay rate (D.20) are the masses and E_{R}. We may reexpress them in terms of m_A by defining

$$\epsilon = \frac{m_A - m_B}{m_A}\,, \quad \eta = \frac{E_{\mathrm{R}}}{m_A}\,, \quad \delta = \frac{m_e}{m_A}\,, \quad \rho = \frac{m_k}{m_A}\,. \tag{D.23}$$

These are excellent expansion parameters, since they are all smaller than 2×10^{-4} for tritium. If we expand the bracket in (D.20) in terms of these small parameters, the first non-vanishing order is quadratic in any combination of small parameters $\lambda = \epsilon, \eta, \delta, \rho$. Additionally, the prefactor $Q(E_{\mathrm{R}})/m_A$ is also of order λ^2. Hence, the leading order of the differential decay rate is λ^4. From inspecting (D.20), it is clear that we should therefore consider P and Q up to order λ^2. One can use

$$\alpha = \frac{1}{2} m_A^2 \left(2\epsilon - \epsilon^2 + \delta^2 + \rho^2\right) \tag{D.24}$$

to approximate

$$\begin{aligned} P(E_{\mathrm{R}})/m_A &= -\frac{(1-\eta)(\eta - \epsilon + \epsilon^2/2 - \delta^2/2 - \rho^2/2)}{1 - 2\eta + \delta^2} \\ &= \left[-(1-\eta)(\eta - \epsilon + \epsilon^2/2 - \delta^2/2 - \rho^2/2)\right] \cdot (1 + 2\eta) + \mathcal{O}(\lambda^3) \\ &= (\epsilon - \eta) + \eta(\epsilon - \eta) + \frac{1}{2}(\delta^2 + \rho^2 - \epsilon^2) + \mathcal{O}(\lambda^3)\,. \end{aligned} \tag{D.25}$$

For Q it is additionally useful to observe that

$$\eta_{\max} \equiv \frac{E_{\mathrm{R,max}}}{m_A} = \frac{\alpha}{m_A^2} - \rho^2 - \rho(1 - \epsilon)\,. \tag{D.26}$$

Therefore, we have

$$Q(E_{\mathrm{R}})/m_A = \sqrt{\eta^2 - \delta^2} \cdot \frac{\sqrt{(\eta_{\max} - \eta)^2 + 2(\eta_{\max} - \eta)\rho(1-\epsilon)}}{1 - 2\eta + \delta^2}\,. \tag{D.27}$$

Here we can observe that the rate indeed drops to zero as $\eta \to \eta_{\max}$. Moreover, we find the leading-order approximation

$$\begin{aligned} Q(E_{\mathrm{R}})/m_A &= \sqrt{\eta^2 - \delta^2} \cdot \sqrt{(\epsilon - \eta)^2 - \rho^2 + \mathcal{O}(\lambda^3)} \cdot (1 + \mathcal{O}(\lambda))\,, \\ &= \sqrt{\eta^2 - \delta^2} \cdot \sqrt{(\epsilon - \eta)^2 - \rho^2} + \mathcal{O}(\lambda^{5/2})\,, \\ &= \frac{1}{m_A^2} p_e \sqrt{(E_0 - E)^2 - m_k^2} + \mathcal{O}(\lambda^{5/2})\,, \end{aligned} \tag{D.28}$$

where E denotes the kinetic energy of the electron and E_0 its value at the endpoint for $m_k = 0$, i.e. $E_0 = m_A - m_B - m_e$. This approximation leads to a shift of the endpoint of the spectrum from its exact value to its value in the non-relativistic approximation, namely from $E_{\mathrm{R,max}}$ to $E_{\mathrm{NR,max}}$. For tritium and $m_k \lesssim 50\,\mathrm{eV}$, this amounts to

$$E_{\mathrm{R,max}} - E_{\mathrm{NR,max}} \approx 3.44\,\mathrm{eV}\,. \tag{D.29}$$

To retain the exact endpoint, Q must be taken at least up to order λ^3, such that the square root in the fraction of (D.27) remains exact. For KATRIN, however, this shift is unimportant because the endpoint is actually one of the fit parameters, as discussed in Section 4.5.

From the previous considerations, we can recover the usual non-relativistic rate in the SM limit, as used, for instance, by the KATRIN collaboration. Setting all new-physics couplings to zero, we find

$$A = \frac{\gamma}{2} m_A m_B\,(g_V^2 - g_A^2)(m_A^2 - m_B^2 + m_e^2 + m_k^2)\,, \tag{D.30}$$

$$B_1 = \frac{\gamma}{2} m_A\,\left\{(g_V - g_A)^2(m_A^2 - m_B^2 + m_e^2 - m_k^2) - 2m_A m_B(g_V^2 - g_A^2)\right\}\,, \tag{D.31}$$

$$B_2 = \frac{\gamma}{2} m_A\,\left\{(g_V + g_A)^2(m_A^2 - m_B^2 - m_e^2 + m_k^2) - 2m_A m_B(g_V^2 - g_A^2)\right\}\,, \tag{D.32}$$

$$C = 0\,, \tag{D.33}$$

$$D_1 = -\gamma m_A^2 (g_V - g_A)^2\,, \tag{D.34}$$

$$D_2 = -\gamma m_A^2 (g_V + g_A)^2\,, \tag{D.35}$$

where

$$\gamma = 16\,G_F^2 \widetilde{V}_{ud}^2\,. \tag{D.36}$$

Using the expansion of P and Q in small parameters and Equation (D.20), these coefficients can be combined to the leading order result

$$\begin{aligned} \frac{\mathrm{d}\Gamma_k}{\mathrm{d}E_{\mathrm{R}}} &= \frac{Q(E_{\mathrm{R}})}{2\pi^3} G_F^2 \widetilde{V}_{ud}^2 m_{\mathcal{A}}^3 \left[(g_V^2 + 3g_A^2)(\epsilon\eta - \eta^2) + \mathcal{O}(\lambda^3)\right] \\ &= \frac{G_F^2 \widetilde{V}_{ud}^2}{2\pi^3} \left(g_V^2 + 3g_A^2\right) p_e m_A^3 (\epsilon\eta - \eta^2)\sqrt{(\eta - \epsilon)^2 - \rho^2} \\ \Rightarrow \quad \frac{\mathrm{d}\Gamma_k}{\mathrm{d}E} &= \frac{G_F^2 \widetilde{V}_{ud}^2}{2\pi^3} \left(g_V^2 + 3g_A^2\right) p_e \sqrt{E + m_e}(E_0 - E)\sqrt{(E_0 - E)^2 - m_k^2}\,. \end{aligned} \tag{D.37}$$

This agrees with the usual leading-order result [160]. Notice how the rate is proportional to the factor $p_e((E_0 - E)^2 - m_k^2)^{1/2}$ coming from $Q(E_R)$. This prefactor is therefore universal to all interaction types. Now if we consider generic new physics instead, the polynomial coefficients $A, \ldots, D_2$ are too lengthy to reproduce here. However, the results can be summarized effectively when adding all terms proportional to the same kinematic parameters. Therefore, we present the result including new physics in the form given in Equation (4.87).

D.2. Proof that $|b'_N| \leq 1$

Here we would like to show that with one parameter of the set $U_{e4}, \epsilon_L^N, \epsilon_R^N, \epsilon_V^N, \epsilon_A^N, \epsilon_S^N, \epsilon_T^N$ and one parameter of the set $\widetilde{\epsilon}_L^N, \widetilde{\epsilon}_R^N, \widetilde{\epsilon}_V^N, \widetilde{\epsilon}_A^N \widetilde{\epsilon}_S^N, \widetilde{\epsilon}_T^N$ non-vanishing, the parameter b'_N in Equation (4.94) is in the range [-1,1]. Recall that

$$\begin{aligned} \epsilon_V^N &= \epsilon_L^N + \epsilon_R^N\,, \qquad & \epsilon_A^N &= \epsilon_L^N - \epsilon_R^N\,, \\ \widetilde{\epsilon}_V^N &= \widetilde{\epsilon}_L^N + \widetilde{\epsilon}_R^N\,, \qquad & \widetilde{\epsilon}_A^N &= \widetilde{\epsilon}_L^N - \widetilde{\epsilon}_R^N\,. \end{aligned} \tag{D.38}$$

We have already discussed in Section 4.5 the example scenario where ϵ_V^N and $\widetilde{\epsilon}_S^N$ were non-vanishing. This scenario was optimal in the sense that with $\epsilon_S^N = \pm\epsilon_V^N$ we have $b' = \pm 1$. For ϵ_A^N and $\widetilde{\epsilon}_T^N$ we have a very similar situation,

$$\xi_N = 3g_A^2|\epsilon_A^N|^2 + 48g_T^2|\widetilde{\epsilon}_T^N|^2 = |w|^2 + |z|^2\,, \tag{D.39}$$

$$\xi_N b'_N = 3g_A g_S\, 8\mathrm{Re}\left[\epsilon_A^N(\widetilde{\epsilon}_T^N)^*\right] = 2\mathrm{Re}(wz^*)\,, \tag{D.40}$$

where we defined $w = \sqrt{3}g_A\,\epsilon_A^N$ and $z = 4\sqrt{3}g_T\,\widetilde{\epsilon}_T^N$, leading to the same conclusion. One can check that the same identification is possible for any combination of one parameter of the set $\epsilon_V^N, \epsilon_A^N, \epsilon_S^N, \epsilon_T^N$ with one parameter of the set $\widetilde{\epsilon}_L^N, \widetilde{\epsilon}_R^N, \widetilde{\epsilon}_S^N, \widetilde{\epsilon}_T^N$, each of which would give rise to a contribution to b'_N or c_N.

Now we show that if we combine non-vanishing U_{e4}, ϵ_L^N, or ϵ_R^N instead of ϵ_V^N or ϵ_A^N with one non-vanishing $\widetilde{\epsilon}$, then $|b'_N| < 1$ or $|c_N| < 1$. For instance, picking U_{e4} and $\widetilde{\epsilon}_S$ leads to

$$\xi_N = (g_V^2 + 3g_A^2)|U_{e4}|^2 + g_S^2|\widetilde{\epsilon}_S^N|^2 = |w|^2 + |z|^2 + 3g_A^2|U_{e4}|^2\,, \tag{D.41}$$

$$\xi_N b'_N = g_V g_S\, 2\mathrm{Re}\left[\epsilon_V^N(\widetilde{\epsilon}_S^N)^*\right] = 2\mathrm{Re}(wz^*)\,, \tag{D.42}$$

where $w = g_V\,\epsilon_V^N$ and $z = g_S\,\widetilde{\epsilon}_S^N$. Therefore,

$$|b'_N| = \left|\frac{wz^* + w^*z}{|w|^2 + |z|^2 + 3g_A^2|U_{e4}|^2}\right| < \frac{wz^* + w^*z}{|w|^2 + |z|^2} \leq 1\,. \tag{D.43}$$

The same reasoning holds for other combinations with L or R instead of V and A coefficients, since additional positive contributions to ξ_N can only decrease the absolute value of b'_N or c_N.

List of abbreviations

νDMEFT sterile neutrino dark matter effective field theory

BSM beyond the Standard Model

CEνNS coherent elastic neutrino-nucleus scattering

CKM Cabibbo-Kobayashi-Maskawa

CL confidence level

CLFV charged lepton flavor violation

CP charge-parity

dSph dwarf spheroidal galaxy

DUNE Deep Underground Neutrino Experiment

EFT effective field theory

EWSB electroweak symmetry breaking

GIM Glashow-Iliopoulos-Maiani

GNI General Neutrino Interactions

KATRIN Karlsruhe Tritium Neutrino Experiment

LArTPC liquid argon time projection chamber

LEFT low-energy effective field theory

LHC Large Hadron Collider

NSI Non-Standard Interactions

PMNS Pontecorvo-Maki-Nakagawa-Sakata

QFT quantum field theory

RG renormalization group

SM Standard Model of particle physics

SMEFT Standard Model Effective Field Theory

SMNEFT SMEFT extended by right-handed neutrinos

SSB spontaneous symmetry breaking

UV ultraviolet

vev vacuum expectation value

WIMP weakly interacting massive particle

List of publications

References [1–6] have been published in peer-reviewed journals by the author in collaboration with others during the doctoral studies. In this thesis, we have relied on results from References [1–4] to the extend specified in Section 1.1 and at the beginning of the relevant sections. The contents of References [5, 6] have not been discussed.

[1] I. Bischer, W. Rodejohann, and X.-J. Xu, "Loop-induced Neutrino Non-Standard Interactions," *JHEP* **10** (2018) 096, arXiv:1807.08102 [hep-ph].

[2] I. Bischer, and W. Rodejohann, "General Neutrino Interactions at the DUNE Near Detector," *Phys. Rev.* **D99** no. 3, (2019) 036006, arXiv:1810.02220 [hep-ph].

[3] I. Bischer and W. Rodejohann, "General neutrino interactions from an effective field theory perspective," *Nucl. Phys.* **B947** (2019) 114746, arXiv:1905.08699 [hep-ph].

[4] I. Bischer, T. Plehn, and W. Rodejohann, "Dark Matter EFT, the Third – Neutrino WIMPs," *SciPost Phys.* **10** (2021) 039, arXiv:2008.04718 [hep-ph].

[5] I. Bischer, C. Döring, and A. Trautner, "Simultaneous Block Diagonalization of Matrices of Finite Order," *J. Phys. A* **54** no. 8, (2021) 085203, arXiv:2012.14440 [hep-ph].

[6] I. Bischer, T. Grandou, and R. Hofmann, "Perturbative Pecularities of Quantum Field Theories at High Temperatures," *Universe* **5** no. 3, (2019) 81.

Bibliography

[1] I. Bischer, W. Rodejohann, and X.-J. Xu, "Loop-induced Neutrino Non-Standard Interactions," *JHEP* **10** (2018) 096, arXiv:1807.08102 [hep-ph].

[2] I. Bischer and W. Rodejohann, "General Neutrino Interactions at the DUNE Near Detector," *Phys. Rev.* **D99** no. 3, (2019) 036006, arXiv:1810.02220 [hep-ph].

[3] I. Bischer and W. Rodejohann, "General neutrino interactions from an effective field theory perspective," *Nucl. Phys.* **B947** (2019) 114746, arXiv:1905.08699 [hep-ph].

[4] I. Bischer, T. Plehn, and W. Rodejohann, "Dark Matter EFT, the Third – Neutrino WIMPs," *SciPost Phys.* **10** (2021) 039, arXiv:2008.04718 [hep-ph].

[5] I. Bischer, C. Döring, and A. Trautner, "Simultaneous Block Diagonalization of Matrices of Finite Order," *J. Phys. A* **54** no. 8, (2021) 085203, arXiv:2012.14440 [math-ph].

[6] I. Bischer, T. Grandou, and R. Hofmann, "Perturbative Peculiarities of Quantum Field Theories at High Temperatures," *Universe* **5** no. 3, (2019) 81.

[7] C. L. Cowan, F. Reines, F. B. Harrison, H. W. Kruse, and A. D. McGuire, "Detection of the free neutrino: A Confirmation," *Science* **124** (1956) 103–104.

[8] J. Chadwick, "Possible Existence of a Neutron," *Nature* **129** (1932) 312.

[9] C. D. Anderson, "The positive electron," *Phys. Rev.* **43** (Mar, 1933) 491–494. https://link.aps.org/doi/10.1103/PhysRev.43.491.

[10] J. C. Street and E. C. Stevenson, "New evidence for the existence of a particle of mass intermediate between the proton and electron," *Phys. Rev.* **52** (Nov, 1937) 1003–1004. https://link.aps.org/doi/10.1103/PhysRev.52.1003.

[11] E. Fermi, "An attempt of a theory of beta radiation. 1.," *Z. Phys.* **88** (1934) 161–177.

[12] C. M. G. Lattes, H. Muirhead, G. P. S. Occhialini, and C. F. Powell, "PROCESSES INVOLVING CHARGED MESONS," *Nature* **159** (1947) 694–697.

[13] C. N. Yang and R. L. Mills, "Conservation of isotopic spin and isotopic gauge invariance," *Phys. Rev.* **96** (Oct, 1954) 191–195. https://link.aps.org/doi/10.1103/PhysRev.96.191.

[14] **CDF Collaboration** Collaboration, F. Abe *et al.*, "Observation of top quark production in $\overline{p}p$ collisions with the collider detector at fermilab," *Phys. Rev. Lett.* **74** (Apr, 1995) 2626–2631. https://link.aps.org/doi/10.1103/PhysRevLett.74.2626.

[15] **Super-Kamiokande** Collaboration, Y. Fukuda *et al.*, "Evidence for oscillation of atmospheric neutrinos," *Phys. Rev. Lett.* **81** (1998) 1562–1567, arXiv:hep-ex/9807003.

[16] **SNO** Collaboration, Q. R. Ahmad *et al.*, "Measurement of the rate of $\nu_e + d \to p + p + e^-$ interactions produced by ^{8}B solar neutrinos at the Sudbury Neutrino Observatory," *Phys. Rev. Lett.* **87** (2001) 071301, arXiv:nucl-ex/0106015.

[17] M. Drewes, "The Phenomenology of Right Handed Neutrinos," *Int. J. Mod. Phys. E* **22** (2013) 1330019, arXiv:1303.6912 [hep-ph].

[18] **Hyper-Kamiokande** Collaboration, K. Abe *et al.*, "Hyper-Kamiokande Design Report," arXiv:1805.04163 [physics.ins-det].

[19] **DUNE** Collaboration, B. Abi *et al.*, "Volume I. Introduction to DUNE," *JINST* **15** no. 08, (2020) T08008, arXiv:2002.02967 [physics.ins-det].

[20] A. V. Manohar, "Introduction to Effective Field Theories," arXiv:1804.05863 [hep-ph].

[21] I. Brivio and M. Trott, "The Standard Model as an Effective Field Theory," *Phys. Rept.* **793** (2019) 1–98, arXiv:1706.08945 [hep-ph].

[22] **LHC New Physics Working Group** Collaboration, D. Alves, "Simplified Models for LHC New Physics Searches," *J. Phys. G* **39** (2012) 105005, arXiv:1105.2838 [hep-ph].

[23] Y. Liao and X.-D. Ma, "Operators up to Dimension Seven in Standard Model Effective Field Theory Extended with Sterile Neutrinos," *Phys. Rev.* **D96** no. 1, (2017) 015012, arXiv:1612.04527 [hep-ph].

[24] T. Ohlsson, "Status of non-standard neutrino interactions," *Rept. Prog. Phys.* **76** (2013) 044201, arXiv:1209.2710 [hep-ph].

[25] Y. Farzan and M. Tortola, "Neutrino oscillations and Non-Standard Interactions," *Front.in Phys.* **6** (2018) 10, arXiv:1710.09360 [hep-ph].

[26] F. Zwicky, "Die Rotverschiebung von extragalaktischen Nebeln," *Helvetica Physica Acta* **6** (Jan., 1933) 110–127.

[27] K. C. Freeman, "On the disks of spiral and SO Galaxies," *Astrophys. J.* **160** (1970) 811.

[28] V. C. Rubin and W. K. Ford, Jr., "Rotation of the Andromeda Nebula from a Spectroscopic Survey of Emission Regions," *Astrophys. J.* **159** (1970) 379–403.

[29] **Planck** Collaboration, N. Aghanim *et al.*, "Planck 2018 results. VI. Cosmological parameters," *Astron. Astrophys.* **641** (2020) A6, arXiv:1807.06209 [astro-ph.CO].

[30] B. W. Lee and S. Weinberg, "Cosmological Lower Bound on Heavy Neutrino Masses," *Phys. Rev. Lett.* **39** (1977) 165–168.

[31] P. Hut, "Limits on Masses and Number of Neutral Weakly Interacting Particles," *Phys. Lett. B* **69** (1977) 85.

[32] K. Sato and M. Kobayashi, "Cosmological Constraints on the Mass and the Number of Heavy Lepton Neutrinos," *Prog. Theor. Phys.* **58** (1977) 1775.

[33] D. A. Dicus, E. W. Kolb, and V. L. Teplitz, "Cosmological Upper Bound on Heavy Neutrino Lifetimes," *Phys. Rev. Lett.* **39** (1977) 168. [Erratum: Phys.Rev.Lett. 39, 973 (1977)].

[34] M. Vysotsky, A. Dolgov, and Y. Zeldovich, "Cosmological Restriction on Neutral Lepton Masses," *JETP Lett.* **26** (1977) 188–190.

[35] C. Giunti and C. W. Kim, *Fundamentals of Neutrino Physics and Astrophysics*. Oxford University Press, 2007.

[36] **Particle Data Group** Collaboration, P. A. Zyla *et al.*, "Review of Particle Physics," *PTEP* **2020** no. 8, (2020) 083C01.

[37] E. Akhmedov, *Majorana neutrinos and other Majorana particles:Theory and experiment*. 12, 2014. arXiv:1412.3320 [hep-ph].

[38] S. Weinberg, "Baryon- and lepton-nonconserving processes," *Phys. Rev. Lett.* **43** (Nov, 1979) 1566–1570. https://link.aps.org/doi/10.1103/PhysRevLett.43.1566.

[39] P. Minkowski, "$\mu \to e\gamma$ at a Rate of One Out of 10^9 Muon Decays?," *Phys. Lett. B* **67** (1977) 421–428.

[40] J. Schechter and J. W. F. Valle, "Neutrino Masses in SU(2) x U(1) Theories," *Phys. Rev. D* **22** (1980) 2227.

[41] M. Malinsky, T. Ohlsson, and H. Zhang, "Non-Standard Neutrino Interactions from a Triplet Seesaw Model," *Phys. Rev. D* **79** (2009) 011301, arXiv:0811.3346 [hep-ph].

[42] S. L. Glashow, J. Iliopoulos, and L. Maiani, "Weak Interactions with Lepton-Hadron Symmetry," *Phys. Rev. D* **2** (1970) 1285–1292.

[43] I. Esteban, M. C. Gonzalez-Garcia, M. Maltoni, T. Schwetz, and A. Zhou, "The fate of hints: updated global analysis of three-flavor neutrino oscillations," *JHEP* **09** (2020) 178, arXiv:2007.14792 [hep-ph].

[44] **KATRIN** Collaboration, M. Aker *et al.*, "Improved Upper Limit on the Neutrino Mass from a Direct Kinematic Method by KATRIN," *Phys. Rev. Lett.* **123** no. 22, (2019) 221802, arXiv:1909.06048 [hep-ex].

[45] A. Loureiro *et al.*, "On The Upper Bound of Neutrino Masses from Combined Cosmological Observations and Particle Physics Experiments," *Phys. Rev. Lett.* **123** no. 8, (2019) 081301, arXiv:1811.02578 [astro-ph.CO].

[46] J. Ellis, "TikZ-Feynman: Feynman diagrams with TikZ," *Comput. Phys. Commun.* **210** (2017) 103–123, arXiv:1601.05437 [hep-ph].

[47] B. Grzadkowski, M. Iskrzynski, M. Misiak, and J. Rosiek, "Dimension-Six Terms in the Standard Model Lagrangian," *JHEP* **10** (2010) 085, arXiv:1008.4884 [hep-ph].

[48] A. Aparici, K. Kim, A. Santamaria, and J. Wudka, "Right-handed neutrino magnetic moments," *Phys. Rev.* **D80** (2009) 013010, arXiv:0904.3244 [hep-ph].

[49] B. Grzadkowski, M. Iskrzynski, M. Misiak, and J. Rosiek, "Dimension-Six Terms in the Standard Model Lagrangian," *JHEP* **10** (2010) 085, arXiv:1008.4884 [hep-ph].

[50] E. E. Jenkins, A. V. Manohar, and P. Stoffer, "Low-Energy Effective Field Theory below the Electroweak Scale: Operators and Matching," *JHEP* **03** (2018) 016, arXiv:1709.04486 [hep-ph].

[51] T. D. Lee and C. N. Yang, "Question of parity conservation in weak interactions," *Phys. Rev.* **104** (Oct, 1956) 254–258. https://link.aps.org/doi/10.1103/PhysRev.104.254.

[52] W. Rodejohann, X.-J. Xu, and C. E. Yaguna, "Distinguishing between Dirac and Majorana neutrinos in the presence of general interactions," *JHEP* **05** (2017) 024, arXiv:1702.05721 [hep-ph].

[53] M. Lindner, W. Rodejohann, and X.-J. Xu, "Coherent Neutrino-Nucleus Scattering and new Neutrino Interactions," *JHEP* **03** (2017) 097, arXiv:1612.04150 [hep-ph].

[54] D. Aristizabal Sierra, V. De Romeri, and N. Rojas, "COHERENT analysis of neutrino generalized interactions," *Phys. Rev.* **D98** (2018) 075018, arXiv:1806.07424 [hep-ph].

[55] T. Li, X.-D. Ma, and M. A. Schmidt, "General neutrino interactions with sterile neutrinos in light of coherent neutrino-nucleus scattering and meson invisible decays," *JHEP* **07** (2020) 152, arXiv:2005.01543 [hep-ph].

[56] D. Aristizabal Sierra, J. Liao, and D. Marfatia, "Impact of form factor uncertainties on interpretations of coherent elastic neutrino-nucleus scattering data," *JHEP* **06** (2019) 141, arXiv:1902.07398 [hep-ph].

[57] P. O. Ludl and W. Rodejohann, "Direct Neutrino Mass Experiments and Exotic Charged Current Interactions," *JHEP* **06** (2016) 040, arXiv:1603.08690 [hep-ph].

[58] S. P. Rosen, "Analog of the Michel Parameter for Neutrino - Electron Scattering: A Test for Majorana Neutrinos," *Phys. Rev. Lett.* **48** (1982) 842.

[59] B. Kayser and R. E. Shrock, "Distinguishing Between Dirac and Majorana Neutrinos in Neutral Current Reactions," *Phys. Lett.* **112B** (1982) 137–142.

[60] X.-J. Xu, "Tensor and scalar interactions of neutrinos may lead to observable neutrino magnetic moments," *Phys. Rev.* **D99** no. 7, (2019) 075003, arXiv:1901.00482 [hep-ph].

[61] E. W. Kolb and M. S. Turner, "Supernova SN 1987a and the Secret Interactions of Neutrinos," *Phys. Rev.* **D36** (1987) 2895.

[62] M. S. Bilenky, S. M. Bilenky, and A. Santamaria, "Invisible width of the Z boson and 'secret' neutrino-neutrino interactions," *Phys. Lett.* **B301** (1993) 287–291.

[63] S. Hannestad, R. S. Hansen, and T. Tram, "How Self-Interactions can Reconcile Sterile Neutrinos with Cosmology," *Phys. Rev. Lett.* **112** no. 3, (2014) 031802, arXiv:1310.5926 [astro-ph.CO].

[64] K. C. Y. Ng and J. F. Beacom, "Cosmic neutrino cascades from secret neutrino interactions," *Phys. Rev.* **D90** no. 6, (2014) 065035, arXiv:1404.2288 [astro-ph.HE]. [Erratum: Phys. Rev.D90,no.8,089904(2014)].

[65] F. Forastieri, M. Lattanzi, and P. Natoli, "Constraints on secret neutrino interactions after Planck," *JCAP* **1507** no. 07, (2015) 014, arXiv:1504.04999 [astro-ph.CO].

[66] G.-y. Huang, T. Ohlsson, and S. Zhou, "Observational Constraints on Secret Neutrino Interactions from Big Bang Nucleosynthesis," *Phys. Rev.* **D97** no. 7, (2018) 075009, arXiv:1712.04792 [hep-ph].

[67] M. González-Alonso, J. Martin Camalich, and K. Mimouni, "Renormalization-group evolution of new physics contributions to (semi)leptonic meson decays," *Phys. Lett.* **B772** (2017) 777–785, arXiv:1706.00410 [hep-ph].

[68] R. Alonso, E. E. Jenkins, A. V. Manohar, and M. Trott, "Renormalization Group Evolution of the Standard Model Dimension Six Operators III: Gauge Coupling Dependence and Phenomenology," *JHEP* **04** (2014) 159, arXiv:1312.2014 [hep-ph].

[69] P. Langacker, "The Physics of Heavy Z' Gauge Bosons," *Rev. Mod. Phys.* **81** (2009) 1199–1228, arXiv:0801.1345 [hep-ph].

[70] B. Holdom, "Two U(1)'s and Epsilon Charge Shifts," *Phys. Lett. B* **166** (1986) 196–198.

[71] J. Heeck and W. Rodejohann, "Gauged $L_\mu - L_\tau$ Symmetry at the Electroweak Scale," *Phys. Rev. D* **84** (2011) 075007, arXiv:1107.5238 [hep-ph].

[72] M. Bauer, S. Diefenbacher, T. Plehn, M. Russell, and D. A. Camargo, "Dark Matter in Anomaly-Free Gauge Extensions," *SciPost Phys.* **5** no. 4, (2018) 036, arXiv:1805.01904 [hep-ph].

[73] P. Cox, C. Han, and T. T. Yanagida, "Right-handed Neutrino Dark Matter in a U(1) Extension of the Standard Model," *JCAP* **1801** no. 01, (2018) 029, arXiv:1710.01585 [hep-ph].

[74] A. Hook, E. Izaguirre, and J. G. Wacker, "Model Independent Bounds on Kinetic Mixing," *Adv. High Energy Phys.* **2011** (2011) 859762, arXiv:1006.0973 [hep-ph].

[75] R. Alonso, P. Cox, C. Han, and T. T. Yanagida, "Flavoured $B - L$ local symmetry and anomalous rare B decays," *Phys. Lett. B* **774** (2017) 643–648, arXiv:1705.03858 [hep-ph].

[76] K. S. Babu, A. Friedland, P. A. N. Machado, and I. Mocioiu, "Flavor Gauge Models Below the Fermi Scale," *JHEP* **12** (2017) 096, arXiv:1705.01822 [hep-ph].

[77] I. Doršner, S. Fajfer, A. Greljo, J. Kamenik, and N. Košnik, "Physics of leptoquarks in precision experiments and at particle colliders," *Phys. Rept.* **641** (2016) 1–68, arXiv:1603.04993 [hep-ph].

[78] J. C. Pati and A. Salam, "Unified Lepton-Hadron Symmetry and a Gauge Theory of the Basic Interactions," *Phys. Rev. D* **8** (1973) 1240–1251.

[79] J. C. Pati and A. Salam, "Lepton Number as the Fourth Color," *Phys. Rev. D* **10** (1974) 275–289. [Erratum: Phys.Rev.D 11, 703–703 (1975)].

[80] R. Barbier *et al.*, "R-parity violating supersymmetry," *Phys. Rept.* **420** (2005) 1–202, arXiv:hep-ph/0406039.

[81] M. Bauer and M. Neubert, "Minimal Leptoquark Explanation for the $\mathrm{R}_{D^{(*)}}$, R_K, and $(g-2)_g$ Anomalies," *Phys. Rev. Lett.* **116** no. 14, (2016) 141802, arXiv:1511.01900 [hep-ph].

[82] D. Bečirević, S. Fajfer, N. Košnik, and O. Sumensari, "Leptoquark model to explain the B-physics anomalies, R_K and R_D," *Phys. Rev.* **D94** no. 11, (2016) 115021, arXiv:1608.08501 [hep-ph].

[83] D. Buttazzo, A. Greljo, G. Isidori, and D. Marzocca, "B-physics anomalies: a guide to combined explanations," *JHEP* **11** (2017) 044, arXiv:1706.07808 [hep-ph].

[84] A. Angelescu, D. Bečirević, D. A. Faroughy, and O. Sumensari, "Closing the window on single leptoquark solutions to the B-physics anomalies," *JHEP* **10** (2018) 183, arXiv:1808.08179 [hep-ph].

[85] J. Heeck and D. Teresi, "Pati-Salam explanations of the B-meson anomalies," *JHEP* **12** (2018) 103, arXiv:1808.07492 [hep-ph].

[86] K. S. Babu and C. N. Leung, "Classification of effective neutrino mass operators," *Nucl. Phys. B* **619** (2001) 667–689, arXiv:hep-ph/0106054.

[87] F. F. Deppisch, S. Kulkarni, H. Päs, and E. Schumacher, "Leptoquark patterns unifying neutrino masses, flavor anomalies, and the diphoton excess," *Phys. Rev.* **D94** no. 1, (2016) 013003, arXiv:1603.07672 [hep-ph].

[88] W.-F. Chang, S.-C. Liou, C.-F. Wong, and F. Xu, "Charged Lepton Flavor Violating Processes and Scalar Leptoquark Decay Branching Ratios in the Colored Zee-Babu Model," *JHEP* **10** (2016) 106, arXiv:1608.05511 [hep-ph].

[89] C. Hati, G. Kumar, J. Orloff, and A. M. Teixeira, "Reconciling B-meson decay anomalies with neutrino masses, dark matter and constraints from flavour violation," *JHEP* **11** (2018) 011, arXiv:1806.10146 [hep-ph].

[90] C. Klein, M. Lindner, and S. Ohmer, "Minimal Radiative Neutrino Masses," *JHEP* **03** (2019) 018, arXiv:1901.03225 [hep-ph].

[91] W. Buchmüller, R. Rückl, and D. Wyler, "Leptoquarks in Lepton - Quark Collisions," *Phys. Lett.* **B191** (1987) 442–448. [Erratum: Phys. Lett.B448,320(1999)].

[92] O. Cata and T. Mannel, "Linking lepton number violation with B anomalies," arXiv:1903.01799 [hep-ph].

[93] B. Diaz, M. Schmaltz, and Y.-M. Zhong, "The leptoquark hunter's guide: Pair production," *JHEP* **10** (2017) 097, arXiv:1706.05033 [hep-ph].

[94] A. Ibarra, A. Pierce, N. Shah, and S. Vogl, "Anatomy of Coannihilation with a Scalar Top Partner," *Phys. Rev. D* **91** no. 9, (2015) 095018, arXiv:1501.03164 [hep-ph].

[95] M. Garny, J. Heisig, M. Hufnagel, and B. Lülf, "Top-philic dark matter within and beyond the WIMP paradigm," *Phys. Rev.* **D97** no. 7, (2018) 075002, arXiv:1802.00814 [hep-ph].

[96] M. S. Bilenky and A. Santamaria, "One loop effective Lagrangian for a standard model with a heavy charged scalar singlet," *Nucl. Phys.* **B420** (1994) 47–93, arXiv:hep-ph/9310302 [hep-ph].

[97] S. Antusch, J. P. Baumann, and E. Fernandez-Martinez, "Non-Standard Neutrino Interactions with Matter from Physics Beyond the Standard Model," *Nucl. Phys. B* **810** (2009) 369–388, arXiv:0807.1003 [hep-ph].

[98] M. B. Wise and Y. Zhang, "Effective Theory and Simple Completions for Neutrino Interactions," *Phys. Rev.* **D90** no. 5, (2014) 053005, arXiv:1404.4663 [hep-ph].

[99] **TEXONO** Collaboration, M. Deniz *et al.*, "Measurement of Nu(e)-bar -Electron Scattering Cross-Section with a CsI(Tl) Scintillating Crystal Array at the Kuo-Sheng Nuclear Power Reactor," *Phys. Rev. D* **81** (2010) 072001, arXiv:0911.1597 [hep-ex].

[100] **CHARM-II** Collaboration, P. Vilain *et al.*, "Measurement of differential cross-sections for muon-neutrino electron scattering," *Phys. Lett.* **B302** (1993) 351–355.

[101] **CHARM-II** Collaboration, P. Vilain *et al.*, "Precision measurement of electroweak parameters from the scattering of muon-neutrinos on electrons," *Phys. Lett.* **B335** (1994) 246–252.

[102] J. Liao, D. Marfatia, and K. Whisnant, "Degeneracies in long-baseline neutrino experiments from nonstandard interactions," *Phys. Rev.* **D93** no. 9, (2016) 093016, arXiv:1601.00927 [hep-ph].

[103] J. Liao, D. Marfatia, and K. Whisnant, "Nonstandard neutrino interactions at DUNE, T2HK and T2HKK," *JHEP* **01** (2017) 071, arXiv:1612.01443 [hep-ph].

[104] J. M. Hyde, "Biprobability approach to CP phase degeneracy from non-standard neutrino interactions," *Nucl. Phys. B* **949** (2019) 114804, arXiv:1806.09221 [hep-ph].

[105] C. Giunti, C. W. Kim, and U. W. Lee, "Coherence of neutrino oscillations in vacuum and matter in the wave packet treatment," *Phys. Lett. B* **274** (1992) 87–94.

[106] S. Bergmann, Y. Grossman, and E. Nardi, "Neutrino propagation in matter with general interactions," *Phys. Rev.* **D60** (1999) 093008, arXiv:hep-ph/9903517 [hep-ph].

[107] M. Blennow, S. Choubey, T. Ohlsson, D. Pramanik, and S. K. Raut, "A combined study of source, detector and matter non-standard neutrino interactions at DUNE," *JHEP* **08** (2016) 090, arXiv:1606.08851 [hep-ph].

[108] A. Falkowski, M. González-Alonso, and K. Mimouni, "Compilation of low-energy constraints on 4-fermion operators in the SMEFT," *JHEP* **08** (2017) 123, arXiv:1706.03783 [hep-ph].

[109] M. Gonzalez-Alonso, O. Naviliat-Cuncic, and N. Severijns, "New physics searches in nuclear and neutron β decay," *Prog. Part. Nucl. Phys.* **104** (2019) 165–223, arXiv:1803.08732 [hep-ph].

[110] A. de Gouvea and P. Vogel, "Lepton Flavor and Number Conservation, and Physics Beyond the Standard Model," *Prog. Part. Nucl. Phys.* **71** (2013) 75–92, arXiv:1303.4097 [hep-ph].

[111] L. Calibbi and G. Signorelli, "Charged Lepton Flavour Violation: An Experimental and Theoretical Introduction," *Riv. Nuovo Cim.* **41** no. 2, (2018) 71–174, arXiv:1709.00294 [hep-ph].

[112] F. J. Escrihuela, M. Tortola, J. W. F. Valle, and O. G. Miranda, "Global constraints on muon-neutrino non-standard interactions," *Phys. Rev.* **D83** (2011) 093002, arXiv:1103.1366 [hep-ph].

[113] C. Biggio, M. Blennow, and E. Fernandez-Martinez, "General bounds on non-standard neutrino interactions," *JHEP* **08** (2009) 090, arXiv:0907.0097 [hep-ph].

[114] V. Cirigliano, S. Gardner, and B. Holstein, "Beta Decays and Non-Standard Interactions in the LHC Era," *Prog. Part. Nucl. Phys.* **71** (2013) 93–118, arXiv:1303.6953 [hep-ph].

[115] **SINDRUM** Collaboration, U. Bellgardt *et al.*, "Search for the Decay $\mu^+ \to e^+e^+e^-$," *Nucl. Phys.* **B299** (1988) 1–6.

[116] A. Blondel *et al.*, "Research Proposal for an Experiment to Search for the Decay $\mu \to eee$," arXiv:1301.6113 [physics.ins-det].

[117] **Mu3e** Collaboration, A.-K. Perrevoort, "The Rare and Forbidden: Testing Physics Beyond the Standard Model with Mu3e," in *15th International Workshop on Tau Lepton Physics (TAU2018) Amsterdam, Netherlands, September 24-28, 2018*. arXiv:1812.00741 [hep-ex].

[118] **SINDRUM II** Collaboration, W. H. Bertl *et al.*, "A Search for muon to electron conversion in muonic gold," *Eur. Phys. J.* **C47** (2006) 337–346.

[119] F. Feruglio, P. Paradisi, and A. Pattori, "Lepton Flavour Violation in Composite Higgs Models," *Eur. Phys. J.* **C75** no. 12, (2015) 579, arXiv:1509.03241 [hep-ph].

[120] R. Kitano, M. Koike, and Y. Okada, "Detailed calculation of lepton flavor violating muon electron conversion rate for various nuclei," *Phys. Rev.* **D66** (2002) 096002, arXiv:hep-ph/0203110 [hep-ph]. [Erratum: Phys. Rev.D76,059902(2007)].

[121] **Mu2e** Collaboration, L. Bartoszek *et al.*, "Mu2e Technical Design Report," arXiv:1501.05241 [physics.ins-det].

[122] **MEG** Collaboration, A. M. Baldini *et al.*, "Search for the lepton flavour violating decay $\mu^+ \to e^+\gamma$ with the full dataset of the MEG experiment," *Eur. Phys. J.* **C76** no. 8, (2016) 434, arXiv:1605.05081 [hep-ex].

[123] K. Hayasaka *et al.*, "Search for Lepton Flavor Violating Tau Decays into Three Leptons with 719 Million Produced Tau+Tau- Pairs," *Phys. Lett.* **B687** (2010) 139–143, arXiv:1001.3221 [hep-ex].

[124] **CHARM-II** Collaboration, P. Vilain *et al.*, "Measurement of differential cross-sections for muon-neutrino electron scattering," *Phys. Lett.* **B302** (1993) 351–355.

[125] **CHARM-II** Collaboration, P. Vilain *et al.*, "Precision measurement of electroweak parameters from the scattering of muon-neutrinos on electrons," *Phys. Lett.* **B335** (1994) 246–252.

[126] J. Barranco, O. G. Miranda, C. A. Moura, and J. W. F. Valle, "Constraining non-standard neutrino-electron interactions," *Phys. Rev.* **D77** (2008) 093014, arXiv:0711.0698 [hep-ph].

[127] A. Blondel *et al.*, "Electroweak Parameters From a High Statistics Neutrino Nucleon Scattering Experiment," *Z. Phys.* **C45** (1990) 361–379.

[128] V. Brdar, W. Rodejohann, and X.-J. Xu, "Producing a new Fermion in Coherent Elastic Neutrino-Nucleus Scattering: from Neutrino Mass to Dark Matter," *JHEP* **12** (2018) 024, arXiv:1810.03626 [hep-ph].

[129] W.-F. Chang and J. Liao, "Constraints on light singlet fermion interactions from coherent elastic neutrino-nucleus scattering," *Phys. Rev. D* **102** no. 7, (2020) 075004, arXiv:2002.10275 [hep-ph].

[130] D. Z. Freedman, "Coherent Neutrino Nucleus Scattering as a Probe of the Weak Neutral Current," *Phys. Rev.* **D9** (1974) 1389–1392.

[131] **COHERENT** Collaboration, D. Akimov *et al.*, "Observation of Coherent Elastic Neutrino-Nucleus Scattering," *Science* **357** no. 6356, (2017) 1123–1126, arXiv:1708.01294 [nucl-ex].

[132] **TEXONO** Collaboration, S. Kerman, V. Sharma, M. Deniz, H. T. Wong, J. W. Chen, H. B. Li, S. T. Lin, C. P. Liu, and Q. Yue, "Coherency in Neutrino-Nucleus Elastic Scattering," *Phys. Rev. D* **93** no. 11, (2016) 113006, arXiv:1603.08786 [hep-ph].

[133] **CONUS** Collaboration, H. Bonet *et al.*, "Constraints on Elastic Neutrino Nucleus Scattering in the Fully Coherent Regime from the CONUS Experiment," *Phys. Rev. Lett.* **126** no. 4, (2021) 041804, arXiv:2011.00210 [hep-ex].

[134] **TEXONO** Collaboration, L. Singh and H. T. Wong, "Low Energy Neutrino Physics with sub-keV Ge-Detectors at Kuo-Sheng Neutrino Laboratory," *J. Phys. Conf. Ser.* **888** no. 1, (2017) 012124.

[135] **CONNIE** Collaboration, A. Aguilar-Arevalo *et al.*, "Search for light mediators in the low-energy data of the CONNIE reactor neutrino experiment," *JHEP* **04** (2020) 054, arXiv:1910.04951 [hep-ex].

[136] R. Strauss, J. Rothe, F. Petricca, and S. Schönert, "The ν-cleus experiment: Gram-scale cryogenic calorimeters for a discovery of coherent neutrino scattering," *J. Phys. Conf. Ser.* **1342** no. 1, (2020) 012132.

[137] **MINER** Collaboration, G. Agnolet *et al.*, "Background Studies for the MINER Coherent Neutrino Scattering Reactor Experiment," *Nucl. Instrum. Meth. A* **853** (2017) 53–60, arXiv:1609.02066 [physics.ins-det].

[138] H.-Y. Cheng, "Low-energy interactions of scalar and pseudoscalar higgs bosons with baryons," *Physics Letters B* **219** no. 2, (1989) 347 – 353.

[139] G. Jungman, M. Kamionkowski, and K. Griest, "Supersymmetric dark matter," *Phys. Rept.* **267** (1996) 195–373, arXiv:hep-ph/9506380 [hep-ph].

[140] M. Anselmino, M. Boglione, U. D'Alesio, A. Kotzinian, F. Murgia, A. Prokudin, and S. Melis, "Update on transversity and Collins functions from SIDIS and e+ e- data," *Nucl. Phys. Proc. Suppl.* **191** (2009) 98–107, arXiv:0812.4366 [hep-ph].

[141] W. J. Marciano and Z. Parsa, "Neutrino electron scattering theory," *J. Phys. G* **29** (2003) 2629–2645, arXiv:hep-ph/0403168.

[142] J. Barranco, O. G. Miranda, C. A. Moura, and J. W. F. Valle, "Constraining non-standard neutrino-electron interactions," *Phys. Rev.* **D77** (2008) 093014, arXiv:0711.0698 [hep-ph].

[143] **Borexino** Collaboration, M. Agostini *et al.*, "First Simultaneous Precision Spectroscopy of *pp*, ^{7}Be, and *pep* Solar Neutrinos with Borexino Phase-II," *Phys. Rev. D* **100** no. 8, (2019) 082004, arXiv:1707.09279 [hep-ex].

[144] A. N. Khan, W. Rodejohann, and X.-J. Xu, "Borexino and general neutrino interactions," *Phys. Rev. D* **101** no. 5, (2020) 055047, arXiv:1906.12102 [hep-ph].

[145] Z. Chen, T. Li, and J. Liao, "Constraints on general neutrino interactions with exotic fermion from neutrino-electron scattering experiments," arXiv:2102.09784 [hep-ph].

[146] O. Tomalak and R. J. Hill, "Theory of elastic neutrino-electron scattering," *Phys. Rev. D* **101** no. 3, (2020) 033006, arXiv:1907.03379 [hep-ph].

[147] K. Long, "The nuSTORM experiment," *J. Phys. Conf. Ser.* **1056** no. 1, (2018) 012033.

[148] **ParticleDataGroup** Collaboration, M. Tanabashi *et al.*, "Review of Particle Physics," *Phys. Rev.* **D98** no. 3, (2018) 030001.

[149] **DUNE** Collaboration, R. Acciarri *et al.*, "LBNF and DUNE: Conceptual Design Report, Volume 1: The LBNF and DUNE Projects," arXiv:1601.05471 [physics.ins-det].

[150] A. Falkowski, G. Grilli di Cortona, and Z. Tabrizi, "Future DUNE constraints on EFT," *JHEP* **04** (2018) 101, arXiv:1802.08296 [hep-ph].

[151] A. de Gouvêa and K. J. Kelly, "Non-standard Neutrino Interactions at DUNE," *Nucl. Phys.* **B908** (2016) 318–335, arXiv:1511.05562 [hep-ph].

[152] P. Coloma, "Non-Standard Interactions in propagation at the Deep Underground Neutrino Experiment," *JHEP* **03** (2016) 016, arXiv:1511.06357 [hep-ph].

[153] K. N. Deepthi, S. Goswami, and N. Nath, "Challenges posed by non-standard neutrino interactions in the determination of δ_{CP} at DUNE," *Nucl. Phys.* **B936** (2018) 91–105, arXiv:1711.04840 [hep-ph].

[154] S. Bergmann, Y. Grossman, and E. Nardi, "Neutrino propagation in matter with general interactions," *Phys. Rev.* **D60** (1999) 093008, arXiv:hep-ph/9903517 [hep-ph].

[155] **DUNE** Collaboration, T. Alion *et al.*, "Experiment Simulation Configurations Used in DUNE CDR," arXiv:1606.09550 [physics.ins-det].

[156] A. Sousa, "Searching for Beyond the Standard Model Physics with the DUNE Experiment," 2018. Poster presented at NEUTRINO 2018; Heidelberg, Germany.

[157] **DUNE** Collaboration, R. Acciarri *et al.*, "LBNF and DUNE: Conceptual Design Report, Volume 4: The DUNE Detectors at LBNF," arXiv:1601.02984 [physics.ins-det].

[158] D. K. Papoulias and T. S. Kosmas, "COHERENT constraints to conventional and exotic neutrino physics," *Phys. Rev. D* **97** no. 3, (2018) 033003, arXiv:1711.09773 [hep-ph].

[159] T. Houdy *et al.*, "Hunting keV sterile neutrinos with KATRIN: building the first TRISTAN module," *J. Phys. Conf. Ser.* **1468** no. 1, (2020) 012177, arXiv:2004.07693 [physics.ins-det].

[160] F. Simkovic, R. Dvornicky, and A. Faessler, "Exact relativistic tritium beta-decay endpoint spectrum in a hadron model," *Phys. Rev. C* **77** (2008) 055502, arXiv:0712.3926 [hep-ph].

[161] Y. Akulov and B. Mamyrin, "Determination of the ratio of the axial-vector to the vector coupling constant for weak interaction in triton beta decay," *Phys. Atom. Nucl.* **65** (2002) 1795–1797.

[162] M. González-Alonso and J. Martin Camalich, "Isospin breaking in the nucleon mass and the sensitivity of β decays to new physics," *Phys. Rev. Lett.* **112** no. 4, (2014) 042501, arXiv:1309.4434 [hep-ph].

[163] T. Bhattacharya, V. Cirigliano, S. Cohen, R. Gupta, H.-W. Lin, and B. Yoon, "Axial, Scalar and Tensor Charges of the Nucleon from 2+1+1-flavor Lattice QCD," *Phys. Rev. D* **94** no. 5, (2016) 054508, arXiv:1606.07049 [hep-lat].

[164] C. Enz, "Fermi interaction with non-conservation of ≪lepton charge≫ and of parity," *Nuovo Cim* **6** (1957) 250–254.

[165] M. Kleesiek *et al.*, "β-Decay Spectrum, Response Function and Statistical Model for Neutrino Mass Measurements with the KATRIN Experiment," *Eur. Phys. J. C* **79** no. 3, (2019) 204, arXiv:1806.00369 [physics.data-an].

[166] A. Boyarsky, M. Drewes, T. Lasserre, S. Mertens, and O. Ruchayskiy, "Sterile neutrino Dark Matter," *Prog. Part. Nucl. Phys.* **104** (2019) 1–45, arXiv:1807.07938 [hep-ph].

[167] M. Drewes *et al.*, "A White Paper on keV Sterile Neutrino Dark Matter," *JCAP* **1701** no. 01, (2017) 025, arXiv:1602.04816 [hep-ph].

[168] S. Mertens, T. Lasserre, S. Groh, G. Drexlin, F. Glueck, A. Huber, A. W. P. Poon, M. Steidl, N. Steinbrink, and C. Weinheimer, "Sensitivity of Next-Generation Tritium Beta-Decay Experiments for keV-Scale Sterile Neutrinos," *JCAP* **02** (2015) 020, arXiv:1409.0920 [physics.ins-det].

[169] M. S. Wetter, "Search for Exotic Particles with the KATRIN Experiment," Master's thesis, Karlsruher Institut für Technologie, 2021.

[170] M. Davis, G. Efstathiou, C. S. Frenk, and S. D. M. White, "The Evolution of Large Scale Structure in a Universe Dominated by Cold Dark Matter," *Astrophys. J.* **292** (1985) 371–394.

[171] G. Arcadi, M. Dutra, P. Ghosh, M. Lindner, Y. Mambrini, M. Pierre, S. Profumo, and F. S. Queiroz, "The waning of the WIMP? A review of models, searches, and constraints," *Eur. Phys. J. C* **78** no. 3, (2018) 203, arXiv:1703.07364 [hep-ph].

[172] G. Belanger, F. Boudjema, A. Pukhov, and A. Semenov, "micrOMEGAs_3: A program for calculating dark matter observables," *Comput. Phys. Commun.* **185** (2014) 960–985, arXiv:1305.0237 [hep-ph].

[173] G. Belanger, F. Boudjema, A. Pukhov, and A. Semenov, "micrOMEGAs: A Tool for dark matter studies," *Nuovo Cim. C* **033N2** (2010) 111–116, arXiv:1005.4133 [hep-ph].

[174] G. Belanger, F. Boudjema, A. Pukhov, and A. Semenov, "Dark matter direct detection rate in a generic model with micrOMEGAs 2.2," *Comput. Phys. Commun.* **180** (2009) 747–767, arXiv:0803.2360 [hep-ph].

[175] G. Belanger, F. Boudjema, A. Pukhov, and A. Semenov, "MicrOMEGAs 2.0: A Program to calculate the relic density of dark matter in a generic model," *Comput. Phys. Commun.* **176** (2007) 367–382, arXiv:hep-ph/0607059.

[176] **XENON** Collaboration, E. Aprile *et al.*, "Dark Matter Search Results from a One Ton-Year Exposure of XENON1T," *Phys. Rev. Lett.* **121** no. 11, (2018) 111302, arXiv:1805.12562 [astro-ph.CO].

[177] F. D'Eramo, B. J. Kavanagh, and P. Panci, "You can hide but you have to run: direct detection with vector mediators," *JHEP* **08** (2016) 111, arXiv:1605.04917 [hep-ph].

[178] T. Alanne, G. Arcadi, F. Goertz, V. Tenorth, and S. Vogl, "Model-independent constraints with extended dark matter EFT," *JHEP* **10** (2020) 172, arXiv:2006.07174 [hep-ph].

[179] A. Alloul, N. D. Christensen, C. Degrande, C. Duhr, and B. Fuks, "FeynRules 2.0 - A complete toolbox for tree-level phenomenology," *Comput. Phys. Commun.* **185** (2014) 2250–2300, arXiv:1310.1921 [hep-ph].

[180] A. De Simone and T. Jacques, "Simplified models vs. effective field theory approaches in dark matter searches," *Eur. Phys. J. C* **76** no. 7, (2016) 367, arXiv:1603.08002 [hep-ph].

[181] N. Anand, A. L. Fitzpatrick, and W. Haxton, "Weakly interacting massive particle-nucleus elastic scattering response," *Phys. Rev. C* **89** no. 6, (2014) 065501, arXiv:1308.6288 [hep-ph].

[182] **XENON** Collaboration, E. Aprile *et al.*, "Effective field theory search for high-energy nuclear recoils using the XENON100 dark matter detector," *Phys. Rev.* **D96** no. 4, (2017) 042004, arXiv:1705.02614 [astro-ph.CO].

[183] J. R. Ellis, K. A. Olive, and C. Savage, "Hadronic Uncertainties in the Elastic Scattering of Supersymmetric Dark Matter," *Phys. Rev. D* **77** (2008) 065026, arXiv:0801.3656 [hep-ph].

[184] G. Arcadi, A. Djouadi, and M. Raidal, "Dark Matter through the Higgs portal," *Phys. Rept.* **842** (2020) 1–180, arXiv:1903.03616 [hep-ph].

[185] **Fermi-LAT, DES** Collaboration, A. Albert *et al.*, "Searching for Dark Matter Annihilation in Recently Discovered Milky Way Satellites with Fermi-LAT," *Astrophys. J.* **834** no. 2, (2017) 110, arXiv:1611.03184 [astro-ph.HE].

[186] N. W. Evans, J. L. Sanders, and A. Geringer-Sameth, "Simple J-Factors and D-Factors for Indirect Dark Matter Detection," *Phys. Rev. D* **93** no. 10, (2016) 103512, arXiv:1604.05599 [astro-ph.GA].

[187] S. Ando, A. Geringer-Sameth, N. Hiroshima, S. Hoof, R. Trotta, and M. G. Walker, "Structure formation models weaken limits on WIMP dark matter from dwarf spheroidal galaxies," *Phys. Rev. D* **102** no. 6, (2020) 061302, arXiv:2002.11956 [astro-ph.CO].

[188] M. Cirelli, G. Corcella, A. Hektor, G. Hutsi, M. Kadastik, P. Panci, M. Raidal, F. Sala, and A. Strumia, "PPPC 4 DM ID: A Poor Particle Physicist Cookbook for Dark Matter Indirect Detection," *JCAP* **03** (2011) 051, arXiv:1012.4515 [hep-ph]. [Erratum: JCAP 10, E01 (2012)].

[189] M. A. Sanchis-Lozano, "Leptonic universality breaking in upsilon decays as a probe of new physics," *Int. J. Mod. Phys. A* **19** (2004) 2183, arXiv:hep-ph/0307313.

[190] **BaBar** Collaboration, P. del Amo Sanchez *et al.*, "Test of lepton universality in Upsilon(1S) decays at BaBar," *Phys. Rev. Lett.* **104** (2010) 191801, arXiv:1002.4358 [hep-ex].

[191] A. Hayreter, X.-G. He, and G. Valencia, "LHC constraints on W', Z' that couple mainly to third generation fermions," *Eur. Phys. J. C* **80** no. 10, (2020) 912, arXiv:1912.06344 [hep-ph].

[192] **ATLAS** Collaboration, M. Aaboud *et al.*, "Search for additional heavy neutral Higgs and gauge bosons in the ditau final state produced in 36 inverse fb of pp collisions at $\sqrt{s} = 13$ TeV with the ATLAS detector," *JHEP* **01** (2018) 055, arXiv:1709.07242 [hep-ex].

[193] J. Alwall, R. Frederix, S. Frixione, V. Hirschi, F. Maltoni, O. Mattelaer, H. S. Shao, T. Stelzer, P. Torrielli, and M. Zaro, "The automated computation of tree-level and next-to-leading order differential cross sections, and their matching to parton shower simulations," *JHEP* **07** (2014) 079, arXiv:1405.0301 [hep-ph].

[194] **XENON** Collaboration, E. Aprile *et al.*, "Projected WIMP sensitivity of the XENONnT dark matter experiment," *JCAP* **11** (2020) 031, arXiv:2007.08796 [physics.ins-det].

[195] **CMS** Collaboration, A. M. Sirunyan *et al.*, "Search for direct top squark pair production in events with one lepton, jets, and missing transverse momentum at 13 TeV with the CMS experiment," *JHEP* **05** (2020) 032, arXiv:1912.08887 [hep-ex].

[196] M. Garny, A. Ibarra, M. Pato, and S. Vogl, "Internal bremsstrahlung signatures in light of direct dark matter searches," *JCAP* **12** (2013) 046, arXiv:1306.6342 [hep-ph].

[197] Z. Bern, P. Gondolo, and M. Perelstein, "Neutralino annihilation into two photons," *Phys. Lett. B* **411** (1997) 86–96, arXiv:hep-ph/9706538.

[198] L. Bergstrom and P. Ullio, "Full one loop calculation of neutralino annihilation into two photons," *Nucl. Phys. B* **504** (1997) 27–44, arXiv:hep-ph/9706232.

[199] **ATLAS** Collaboration, M. Aaboud *et al.*, "Search for new phenomena in events with same-charge leptons and b-jets in pp collisions at $\sqrt{s} = 13$ TeV with the ATLAS detector," *JHEP* **12** (2018) 039, arXiv:1807.11883 [hep-ex].

[200] M. Kramer, T. Plehn, M. Spira, and P. Zerwas, "Pair production of scalar leptoquarks at the CERN LHC," *Phys. Rev. D* **71** (2005) 057503, arXiv:hep-ph/0411038.

[201] **CMS** Collaboration, A. M. Sirunyan *et al.*, "Searches for physics beyond the standard model with the M_{T2} variable in hadronic final states with and without disappearing tracks in proton-proton collisions at $\sqrt{s} = 13$ TeV," *Eur. Phys. J. C* **80** no. 1, (2020) 3, arXiv:1909.03460 [hep-ex].

[202] **ATLAS** Collaboration, G. Aad *et al.*, "Search for heavy neutral Higgs bosons produced in association with b-quarks and decaying to b-quarks at $\sqrt{s} = 13$ TeV with the ATLAS detector," arXiv:1907.02749 [hep-ex].

[203] **ATLAS** Collaboration, "Search for heavy particles in the b-tagged di-jet mass distribution with additional b-tagged jets in proton-proton collisions at $\sqrt{s}$ =13 TeV with the ATLAS experiment,". https://atlas.web.cern.ch/Atlas/GROUPS/PHYSICS/CONFNOTES/ATLAS-CONF-2021-019/ATLAS-CONF-2021-019.pdf.

[204] T. D. Lee and C.-N. Yang, "Question of Parity Conservation in Weak Interactions," *Phys. Rev.* **104** (1956) 254–258.

[205] H. H. Patel, "Package-X: A Mathematica package for the analytic calculation of one-loop integrals," *Comput. Phys. Commun.* **197** (2015) 276–290, arXiv:1503.01469 [hep-ph].